An integrated approach to perforation analysis and design for corrugated drainage pipes

By

Naresh Gaj

Department of Bioresource Engineering

McGill University, Montréal

Submitted April 2021

A thesis submitted to McGill University in partial fulfillment of the requirements of the degree of Doctor of Philosophy

Abstract

Subsurface drainage systems, consisting of buried pipes with perforations for water entry, can be designed to function under both drainage and subsurface irrigation modes. There has been a growing interest in the use of large circular holes as perforations to increase the flowrate from corrugated pipes under drainage conditions. However, the entrance resistance (α_e) of corrugated pipes with holes of variable size and configuration has not been established. Pipe manufacturers also advertise larger opening areas with wide rectangular slots, but it is not known how perforation shape and size affect the local stress concentration in buried corrugated pipes that can lead to structural failure. Consequently, perforation characteristics such as shape, size, and configuration have not been fully incorporated into the analysis and design of corrugated pipes used in subsurface drainage systems. Questions on whether holes are better than slots from both hydraulic and structural perspectives have been raised. Furthermore, the influence of perforation on subsurface irrigation has not been thoroughly investigated. This research focused on the effects of variable perforation characteristics on the hydraulic and structural responses of corrugated pipes subjected to soil, water table, and field traffic conditions present on agricultural water management systems.

The first study in this thesis investigated the effects of perforation geometry on the α_e and delivery ratio (Q/Q_0) of corrugated pipes operated under drainage mode. A three-dimensional (3D) finite-element-based model of the radial flow region around buried pipes was used to simulate the effects of perforation characteristics on α_e and Q/Q_0. The model was calibrated with data from sand tank experiments and corrugated pipes perforated with holes and slots. The anticipated effect of perforation shapes on water table drawdown was also assessed. The results showed that corrugated pipes with holes had twice the α_e of those with slots having the same surface area. The use of slots was determined to be hydraulically more advantageous than holes for corrugated pipes.

The second study investigated the structural response of non-perforated and perforated corrugated high-density polyethylene (HDPE) pipes. A structural mechanics finite-element-based model was developed for 100-mm-diameter corrugated HDPE pipes in order to simulate wall stress and vertical deflection under variable loading conditions, which included 12 agricultural soil textures, two water table positions, and three agri-machinery wheel loads representative of field traffic on agricultural lands. The impact of variable perforation characteristics on stress concentration and deformation of corrugated pipes were evaluated. The results showed that pipes perforated with 0.56-cm diameter holes produced stresses that exceeded the yield strength at buried depths shallower than 0.9 m. In contrast, slots had a lower risk of failure against ductile yielding compared to holes, provided that the slot width was less than half of the corrugation valley width.

The third study investigated the exit resistance (α_x) of corrugated pipes with variable perforation characteristics under subsurface irrigation conditions. The 3D radial flow model was modified in order to simulate upward soil-water flow from the perforated pipe. The results showed that α_x was larger and statistically different from its counterpart α_e (drainage mode). Generally, the configuration of slots on the pipe wall had the largest impact on α_x.

The fourth study investigated the impact of perforations on the water table rise into the unsaturated zone for subsurface irrigation systems with four soil textures, three lateral drain spacings, and three buried depths. Soil-water fluxes were also computed for the system when operated under steady-state conditions. The findings show that increasing the number and length of slots can reduce the water table response time to reach the target level by 15 hours in a silt loam soil and 25 hrs in a clay soil. Computations for perforated pipes under steady-state conditions showed that the optimum drain spacing needed to maintain a soil-water flux of 6mm/day can be increased by using densely perforated pipes in coarse-grained soils (loamy sand and silt loam).

This thesis concludes that slots are both hydraulically and structurally advantageous over holes when selecting perforations for buried corrugated HDPE pipes to improve the performance of subsurface drainage and irrigation systems.

Résumé

Les systèmes de drainage souterrains, constitués de tuyaux enterrés avec des perforations pour l'entrée de l'eau, peuvent être conçus pour fonctionner à la fois en mode drainage et en mode irrigation souterraine. L'utilisation de grands trous circulaires comme perforations pour augmenter le débit des tuyaux ondulés dans des conditions de drainage a suscité un intérêt croissant. Cependant, la résistance à l'entrée (αe) des tuyaux ondulés avec des trous de taille et de configuration variables n'a pas été établie. Les fabricants de tuyaux annoncent également des zones d'ouverture plus grandes avec de larges fentes rectangulaires, mais on ne sait pas comment la forme et la taille des perforations affectent la concentration locale des contraintes dans les tuyaux ondulés enterrés qui peuvent conduire à une défaillance structurelle. Par conséquent, les caractéristiques des perforations telles que la forme, la taille et la configuration n'ont pas été entièrement intégrées dans l'analyse et la conception des tuyaux ondulés utilisés dans les systèmes de drainage souterrains. La question de savoir si les trous sont meilleurs que les fentes, tant du point de vue hydraulique que structurel, a été soulevée. En outre, l'influence de la perforation sur l'irrigation souterraine n'a pas été étudiée en profondeur. Cette recherche s'est concentrée sur les effets des caractéristiques variables de la perforation sur les réponses hydrauliques et structurelles des tuyaux ondulés soumis aux conditions du sol, de la nappe phréatique et de la circulation sur le terrain présentes sur les systèmes de gestion des eaux agricoles.

La première étude de cette thèse a examiné les effets de la géométrie de la perforation sur l'αe et le rapport de débit (Q/Q0) des tuyaux ondulés exploités en mode drainage. Un modèle tridimensionnel (3D) par éléments finis de la région d'écoulement radial autour des tuyaux enterrés a été utilisé pour simuler les effets des caractéristiques de perforation sur αe et Q/Q0. Le modèle a été calibré avec des données provenant d'expériences en bac à sable et de tuyaux ondulés perforés avec des trous et des fentes. L'effet anticipé des formes de perforation sur le

rabattement de la nappe phréatique a également été évalué. Les résultats ont montré que les tuyaux ondulés avec des trous avaient deux fois l'αe de ceux avec des fentes ayant la même surface. L'utilisation de fentes a été déterminée comme étant hydrauliquement plus avantageuse que les trous pour les tuyaux ondulés.

La deuxième étude a examiné la réponse structurelle de tuyaux en polyéthylène haute densité (PEHD) ondulés non perforés et perforés. Un modèle de mécanique structurelle par éléments finis a été développé pour des tuyaux PEHD ondulés de 100 mm de diamètre afin de simuler la contrainte de paroi et la déflexion verticale dans des conditions de charge variables, comprenant 12 textures de sol agricole, deux positions de nappe phréatique et trois charges de roues de machines agricoles représentatives du trafic sur les terres agricoles. L'impact des caractéristiques variables de perforation sur la concentration des contraintes et la déformation des tuyaux ondulés a été évalué. Les résultats ont montré que les tuyaux perforés avec des trous de 0,56 cm de diamètre produisaient des contraintes qui dépassaient la limite d'élasticité à des profondeurs d'enfouissement inférieures à 0,9 m. En revanche, les fentes présentaient un risque de rupture plus faible en cas d'élasticité ductile que les trous, à condition que la largeur de la fente soit inférieure à la moitié de la largeur de la vallée de l'ondulation.

La troisième étude a examiné la résistance à la sortie (αx) des tuyaux ondulés avec des caractéristiques de perforation variables dans des conditions d'irrigation souterraine. Le modèle d'écoulement radial 3D a été modifié afin de simuler l'écoulement ascendant de l'eau du sol à partir du tuyau perforé. Les résultats ont montré que αx était plus grand et statistiquement différent de sa contrepartie αe (mode de drainage). En général, la configuration des fentes sur la paroi du tuyau avait le plus grand impact sur αx.

La quatrième étude a examiné l'impact des perforations sur la montée de la nappe phréatique dans la zone non saturée pour des systèmes d'irrigation souterrains avec quatre textures de sol, trois espacements de drain latéral et trois profondeurs d'enfouissement. Les flux d'eau

dans le sol ont également été calculés pour le système lorsqu'il fonctionne dans des conditions stables. Les résultats montrent que l'augmentation du nombre et de la longueur des fentes peut réduire le temps de réponse de la nappe phréatique pour atteindre le niveau cible de 15 heures dans un sol limoneux et de 25 heures dans un sol argileux. Les calculs pour les tuyaux perforés dans des conditions stables ont montré que l'espacement optimal des drains nécessaire pour maintenir un flux d'eau du sol de 6 mm/jour peut être augmenté en utilisant des tuyaux densément perforés dans des sols à gros grains (sable limoneux et loam limoneux).

Cette thèse conclut que les fentes sont à la fois hydrauliquement et structurellement plus avantageuses que les trous lors du choix des perforations pour les tuyaux ondulés enterrés en PEHD afin d'améliorer les performances des systèmes de drainage et d'irrigation souterrains.

Dedication

To my late father, *Captain Lakeram Gaj* (1953-2017) and my dear mother, *Rajkumarie Gaj*. Your sacrifices will forever be cherished.

To my extraordinary wife, Sophia. Your support and patience throughout my graduate studies have been unwavering. This thesis is just as much yours as it is mine.

Acknowledgements

First and foremost, I am very thankful to my supervisor, Prof. Chandra A. Madramootoo, who has been a great mentor and supporter throughout my graduate studies. Prof. Madramootoo has been an excellent advisor, always challenging me to go the extra step and always pushing me to aim high. He leads by example as demonstrated by his ever increasing knowledge and experience that are never limited by international borders. I am grateful to Prof. Madramootoo for his training, funding, and continued guidance throughout this PhD.

Special thanks to Kenton Ollivierre who assisted me with the fabrication of the sand tank and all supporting laboratory facilities. Many thanks to Wendy Ouellette for helping with all the administrative tasks, especially expense reports. Thanks to Scott Manktelow for the great tips and do-it-yourself techniques that were much needed in the machine shop. Thanks Dinesh, Jafaun, and Kai for the many hands needed in the swine complex and lab. You all know what it took to get the sand tank to cooperate. Thanks to Eric St-Onge of Advanced Drainage System (ADS) Inc. for providing corrugated pipe samples and for answering my many questions about drainage pipes and perforation specifications.

I would like to acknowledge my peers from the Water Innovation Lab, McGill University, who has supported me on this journey from the very beginning. Thank you to Divya Gupta, Aghil Yari, Naeem Abbasi, Genevieve Grenon, Samuel Ihouma, Bhesram Singh, Mfon Essien, Aidan De Sena, Kosoluchukwu Ekwunife, Naresh Kumar, Anshika Jain, and Harsimar Sidana.

Thanks to members of the Graphos peer writing group at Macdonald campus: Marieve, Kate, Christopher, Edris, Deasy, Duminda, Karolin, and Mi. Special thanks to Dr. Yvonne Hung from the McGill Writing Centre for bringing the much needed writing workshops to Mac campus. Thanks to my TA partners Lizzette (Physics) and Christopher (Hydrology) for the

valuable time shared teaching and demonstrating lab experiments to all those ever curious undergraduates.

Finally, I thank my wife Sophia, who has proofread my manuscripts and listened to my long talks about drainage pipes and hydraulic conductivity of sands, but most of all for being my bedrock and beacon during this journey. Thanks to my family and siblings (Rajesh, Seema, and Semone) for always supporting me, especially my elder sister Seema, who has invested her time and interest in my education since primary school. It's been a long and fulfilling journey.

Contributions of Authors

Naresh Gaj is the author of this thesis, which is written in the manuscript-based format. All manuscripts were prepared, revised, and formatted by Mr. N. Gaj for submission to academic journals for peer review. Mr. Gaj was also responsible for the design of experiments, collection of laboratory data, development of numerical models, and analysis of all results as reported in the thesis. Dr. Chandra A. Madramootoo, James McGill Professor, Department of Bioresource Engineering was the primary supervisor of this thesis and provided valuable knowledge and guidance on all aspects of the research. Dr. Madramootoo contributed to the conceptualization of all experiments and model development; assisted with the procurement of all materials, software codes, and instrumentation; and reviewed and edited all manuscripts, thesis chapters, and conference presentations.

List of publications and conference presentations related to the thesis:

A. Parts of this thesis have been published in or submitted to peer-reviewed journals:

1. **Gaj, N.** and Madramootoo, C.A., 2020. Effect of perforation geometry on pipe drainage in agricultural lands. *Journal of Irrigation and Drainage Engineering*, 146(7):1-15. DOI:10.1061/(ASCE)IR.1943-4774.0001482.
2. **Gaj, N.** and Madramootoo, C.A., 2021. Structural response of non-perforated and perforated corrugated high-density polyethylene pipes under variable loading. (*Under review: Biosystems Engineering*).
3. **Gaj, N.** and Madramootoo, C.A., 2021. Simulating upward soil-water flow from buried pipes with variable hydraulic characteristics. (*To be submitted*).
4. **Gaj, N.** and Madramootoo, C.A., 2021. Transient water table response and steady soil-water flux from perforated subsurface irrigation pipes. (*To be submitted*).

B. Parts of this thesis have been presented at scientific conferences:

1. **Gaj, N.** and Madramootoo, C.A., 2018. Finite element modelling of entrance resistance for perforated HDPE subsurface drainage pipes. Annual General Meeting and Technical Conference of the Canadian Society for Bioengineering (CSBE/SCGAB). Oral presentation. Guelph, Ontario. July 22-25.
2. **Gaj, N.** and Madramootoo, C.A., 2016. Optimizing the openings on buried HDPE pipes for drainage applications. 69th National Conference and Annual Meeting of the Canadian Water Resources Association (CWRA). Oral presentation. Montréal, Quebec. May 25-27.
3. **Gaj, N.** and Madramootoo, C.A., 2015. Optimizing perforations in buried high density polyethylene pipes for drainage applications. Annual General Meeting and Technical Conference of the Canadian Society for Bioengineering (CSBE/SCGAB). Oral presentation. Edmonton, Alberta. July 05-08.
4. **Gaj, N.** and Madramootoo, C.A., 2015. Optimizing perforations in buried high density polyethylene pipes for drainage applications. Annual International Meeting of the American Society of Agricultural and Biological Engineers (ASABE). Oral presentation. New Orleans, Louisiana. July 26-29.

Table of Contents

List of Figures

List of Tables

List of Abbreviations and Symbols

AASHTO	American Association of State Highways and Transportation Officials
ANOVA	Analysis of Variance
ASTM	American Society for Testing and Materials
FEA	Finite Element Analysis
FEM	Finite Element Method
GWL	Groundwater Level
HDPE	High-Density Polyethylene
MAE	Mean Absolute Error
NSE	Nash-Sutcliffe Efficiency
PBIAS	Percentage Bias
PDE	Partial Differential Equation
PVC	Polyvinyl Chloride
RMSE	Root Mean Square Error
USCS	United Soil Classification System
USDA	United States Department of Agriculture
2D	Two-Dimensional
3D	Three-Dimensional
A_p	Total perforation area per m of pipe
a_y	Longitudinal spacing of perforations
b	Depth of water table from surface
b_0	Initial depth of water table from surface at t= 0
D_d	Depth of drainage pipe from surface
D_{im}	Depth to the impermeable layer below pipe
d_e	Equivalent depth to the impermeable layer

d_{perf}	Diameter of circular perforation hole
E_p	Elastic modulus of pipe
E_s	Elastic modulus of soil
e	Void ratio
FC	Field capacity
F_y	Yield strength
f	Drainable porosity
H_a	Approach flow hydraulic head
H_d	Hydraulic head on the drain outlet
H_e	Entrance resistance head loss
H_x	Exit resistance head loss
H_w	Height of the water table relative to the drain
K_{sc}	Stress concentration factor
k_{sat}	Saturated hydraulic conductivity
L_{perf}	Length of rectangular perforation slot
L_T	Effective perforated length
N	Number of perforation lines
Q	Total discharge of a non-ideal drain
Q_0	Total discharge of an ideal drain
Q_{irr}	Irrigation soil-water flux
q	Drainage rate or design drainage coefficient
r	Radial distance from drainage pipe center
r_e	Effective drain radius
r_0	External drain radius
S	Lateral drain spacing

SF	Factor of safety
t	Independent time variable
w_{perf}	Width of rectangular perforation slot
w_r	Width of corrugation ridge
w_v	Width of corrugation valley
y_0	Pressure head in the control chamber
α_e	Entrance resistance
α_x	Exit resistance
ε_{pc}	Compressive strain in pipe
μ_p	Poisson ratio of pipe
μ_s	Poisson ratio of soil
σ	Normal or Cauchy stress
σ_e	Equivalent or von Mises stress
τ	Tangential or shear stress
ΔH	Difference in total hydraulic head
ΔV	Vertical deformation of pipe

Chapter 1

General Introduction

1.1 Rationale

Water management is central to food production in agriculture, especially in humid climates where excess soil-water must be removed through drainage during wet periods and supplemental irrigation must be supplied during dry periods of the growing season (Fyles and Madramootoo, 2016). Controlling the water table through drainage water management can lead to increased crop yields, improved trafficability for timely field operations (Skaggs, 2012), and reduced nutrient losses through drainage effluent (Drury et al., 2009; Heilman et al., 2012). Subsurface drainage systems on agricultural lands consist of a network of buried pipes that have gaps or openings to allow for water entry, and have been widely used across North America and Europe (Madramootoo et al., 2007; Stuyt and Dierickx, 2006). These systems can be designed to function as dual-purpose drainage and subsurface irrigation in water table management schemes (Yu et al., 2020). The system can be operated under three modes: drainage, controlled drainage, and subsurface irrigation (or subirrigation) with the use of weirs in a water control structure or control chamber (Skaggs, 1999). The level of the weir relative to the outlet level of the buried drainage pipes determines the mode of operation. In drainage mode, the weir level is set below the outlet, while in controlled drainage mode the weir level is raised to a predetermined elevation above the outlet (Skaggs, 2012). In subsurface irrigation mode, water is added to the control chamber via pumping in order to supply water through the buried perforated pipes and raise the water table in the unsaturated root zone to satisfy the evapotranspiration requirements of the crop (Fouss et al., 1999).

Currently, variable perforation characteristics such as shape, size, and configuration have not been fully incorporated into the analysis and design of corrugated pipes used in subsurface drainage and irrigation systems. While research has addressed key perforation-related

challenges from a hydraulic design perspective, very little work has been done to address similar challenges from a structural design perspective. Consequently, the question with regards to how many perforations should be used to perforate corrugated pipes in order to maximize flowrate, but not cause structural failure due to stress concentrations from overburden soil pressure when installed remains unanswered. Some pipe manufacturers advertise larger opening areas with wide rectangular slots, but it is not known how the slot size affects the stress concentration around the perforations and whether increasing the slot width can cause excessive deformation or lead to failure from local buckling in the pipe wall. Furthermore, the flowrate through circular holes in corrugated pipes has not been established for variable hole diameters and spacings on the pipe wall. This gap in knowledge has led to a growing interest in the use of fewer large circular holes to improve drainage performance. Questions on whether circular holes are better than rectangular slots from both hydraulic and structural design perspectives have been raised. Finally, the effect of variable perforation characteristics on subsurface irrigation has also not been thoroughly investigated.

Advances in computing power have led to the development of computational tools such as finite element analysis (FEA), which can be used to solve physics-based problems with complex domain geometries. A buried pipe with perforations placed in the annular corrugation valleys is one such example of a domain with a complex geometry. New computational tools are extremely valuable in revisiting old problems in drainage design, and can be used to overcome the limitations of replicating laborious field studies and laboratory experiments that incur significant time and costs (Ayars and Evans, 2015). Accordingly, this research utilizes FEA, in conjunction with a series of sand tank experiments for model calibration, to investigate the effects of variable perforation characteristics on the hydraulic and structural response of corrugated pipes used in subsurface water management systems.

The following sub-sections explain the relevant perforation-related challenges in detail as they relate to the analysis and design of corrugated drainage pipes.

1.1.1 Evolution of plastic drainage pipes

Plain wall pipe conduits made from plastics such as high-density polyethylene (HDPE) and polyvinylchloride (PVC) were introduced in the US and Europe after World War II (Stuyt et al., 2005). The plain wall plastic pipes were lighter, easier to transport, and cheaper to install, resulting in significant cost savings over traditional clay and concrete tiles used in subsurface drainage. However, the use of continuous plastic conduits presented the first perforation-related challenges as circular holes or rectangular slots, on the pipe wall, were used for water entry from the surrounding soil (Kirkham and Schwab, 1951). The question of how many perforations would cause structural failure for buried plastic pipes subjected to overburden soil pressure was raised (Dierickx, 1980). Instead of answering this question directly, researchers at that time suggested using perforation areas between 1 - 2% of the pipe surface area per unit length in order to provide enough openings for adequate drainage performance. This suggestion was based on the conventional opening area of gaps between traditional clay or concrete tiles (Schwab and Fouss, 1999). Research was then aimed at answering the questions of what size and spacing of perforations on the pipe wall were needed to maximize the flow rate towards the pipe (Schwab and Kirkham, 1951).

Plain wall plastic pipes were not widely used in agricultural drainage, however, as flexible corrugated plastic pipes introduced in the 1970s were superior in strength (due to the corrugation profile) and were more suited to trenchless installation using mechanical plows (Stuyt et al., 2005). Questions similar to those for plain wall pipes were raised for corrugated pipes with respect to the number and size of perforations in the corrugation valley that was required for maximum drainage performance. Analytical approaches, sand tank experiments, and electrical analog experiments were used to derive solutions for estimating either the flow

rate through perforations or the hydraulic entrance resistance to flow towards buried perforated corrugated pipes (Dierickx, 1980; Mohammad and Skaggs, 1983; Skaggs, 1978). However, the entrance resistance for corrugated pipes with circular holes was not investigated and remains to be established to date. Some corrugated pipe manufacturers have attempted to benefit from this knowledge gap by advertising their products with larger opening areas (Mohammad and Skaggs, 1984) and more recently, emphasizing the use of fewer and larger holes to improve drainage performance. This growing interest in circular holes has raised pertinent questions about their effect on flow rate and entrance resistance, and how they compare with rectangular slots for water table drawdown in subsurface drainage systems.

1.1.2 Stress and deformation of buried pipes

The structural design of buried pipes was originally based on the "Iowa Formula" that predicted the ring deflection of the pipe under soil loads (Spangler, 1941; Watkins and Spangler, 1958). Improvements were made to the structural analysis of buried pipes by considering the response of the soil-pipe system under frictional loading using elastic theory (Burns and Richards, 1964). Although imposed live loads can be incorporated into the analysis to determine the structural response of buried pipes, previous studies have only considered wheel loads from standard highway trucks for culvert design (Kang et al., 2014). The structural response of buried corrugated HDPE pipes from agri-machinery wheel loads, which have very different characteristics from highway trucks, need further investigation.

The stress concentration around circular holes has previously been evaluated using FEA (Brachman and Krushelnitzky, 2002). However, these stress concentrations are limited to plain wall pipes under deep burial (leachate drains in landfills) with no consideration to hydrostatic loads from the water table. Important questions concerning the structural response of the perforated corrugated pipe have therefore remained unanswered. For example, the

permissible slot width, slot length, or hole diameter without causing excessive deformation or creating areas of large stress concentrations in the pipe wall are currently unknown for buried corrugated pipes. In addition, the structural response of single-wall polyethylene corrugated pipes under load combinations from variable soil pressure (due to textural differences), hydrostatic pressure (due to water table height), and live-load stress transmission (due to wheel load from agri-machinery) has not been thoroughly studied. The question of whether it is better to perforate buried corrugated pipes with holes or slots from a structural design point of view also arises.

1.1.3 Subsurface irrigation with corrugated pipes

Water table management using subsurface irrigation has been practiced in the US since the 1960s (Skaggs, 1999). Existing drainage infrastructure can be retrofitted to operate under the subsurface irrigation mode by installing additional corrugated pipes, resulting in closer lateral spacings based on crop and site-specific conditions (Elmi et al., 2010). As with controlled drainage, the primary benefits of subsurface irrigation are potential increases in crop yield (Mejia et al., 2000; Nelson, 2017) and improvements in water quality (Madramootoo et al., 2001; Mejia and Madramootoo, 1998). However, there is also the added benefit of reduced energy requirements with subsurface irrigation compared to sprinkler irrigation systems (Massey et al., 1983). Current practices for computing the lateral spacing of perforated pipes operated in subsurface irrigation mode assume that the exit head losses near the buried pipes are identical to the entrance losses when the system is operated under drainage mode, but this has not been verified experimentally. Field measurements show that exit head losses near perforated corrugated pipes can be as large as 41 cm (75% of total) in fields with a sandy loam soil profile under corn cultivation (Bournival et al., 1987). On the other hand, laboratory measurements in sand tanks suggest that exit head losses may be less than 3.7 cm, attributing the larger field measurements to clogged envelopes around the buried pipes (Prasher et al.,

1989). Nevertheless, direct relationships between variable perforation characteristics and exit head losses of buried corrugated pipe under subsurface irrigation conditions have not been established from these studies.

When operated in subsurface irrigation mode, the water table between parallel buried pipes rises into the unsaturated zone via capillary fluxes to meet the crop water requirements driven by evapotranspiration (Skaggs, 1991). Field observations have shown that up to 60 hrs can elapse before any discernible water table rise is recorded at the midplane of parallel drains (Skaggs, 1973). This transient water table response to subsurface irrigation has been simulated using analytical and numerical models (Mostaghimi et al., 1985; Skaggs, 1973; Tang and Skaggs, 1980), but the effects of the pipe perforations were either neglected or assumed to be the same as when operated under drainage mode. Sand tank experiments were used to investigate the effects of perforated corrugated pipes on the water table rise into the unsaturated zone (Mohammad and Skaggs, 1984). However, these experiments were limited to 4.8-mm-diameter holes and only reported results in terms of the total perforation area. The effect of variable perforation characteristics such as shape, size, and configuration on water table rise into the unsaturated zone has not been thoroughly studied for corrugated pipes operated under subsurface irrigation conditions.

Layered soils due to natural formation processes and differences in soil texture can be found in agricultural fields. Although the effect of soil heterogeneity on the lateral spacing of subsurface drainage systems has been studied (Khan et al., 1989; Sharma et al., 1991), very little work has been done on subsurface irrigation systems in layered soils. Research has shown that drains are best installed at the interface of two-layer systems for subsurface irrigation (Tang and Skaggs, 1980). However, studies have not demonstrated how soil heterogeneity impacts the exit head loss near perforated pipes in subsurface irrigation systems.

1.2 Research Objectives

The overarching goal of this research is aimed at answering the previously discussed questions that relate to whether circular holes are better than rectangular slots as perforations for corrugated HDPE pipes, which are used for subsurface drainage and irrigation in water management systems on agricultural lands. In order to achieve this main objective, four specific objectives were developed and used to investigate the effects of perforation shape, size, and configuration on both the hydraulic and structural responses of corrugated HDPE pipes. The specific objectives of this research are to:

1. Investigate the effects of perforation geometry (holes vs. slots) on the hydraulic entrance resistance of corrugated pipes by developing a 3D finite-element-based numerical model of the radial flow region around buried pipes. The model was calibrated with datasets from sand tank experiments to simulate subsurface drainage and water table drawdown under variable perforation characteristics.
2. Investigate the structural response of buried corrugated pipes (both non-perforated and perforated) by developing a 3D finite-element-based structural mechanics numerical model of HDPE pipes with an annular corrugation profile. The structural model was used to simulate the wall stress, vertical deflection, and stress concentration under frictional boundary loads from variable soil textures, water table positions, and agri-machinery wheel loads.
3. Investigate the hypothesis that the hydraulic exit resistance of buried perforated pipes operated under the subsurface irrigation mode is larger than the exit resistance of pipes operated in drainage mode. The 3D flow-based numerical model developed for Objective 1 was modified and used to simulate upward soil-water flow from subsurface irrigation pipes with variable perforation characteristics.

4. Investigate the transient water table rise and steady soil-water fluxes from subsurface irrigation pipes with two combinations of perforation characteristics. The water table response and subsurface irrigation fluxes were simulated for buried perforated pipes with various soil textures, lateral drain spacings, and buried depths.

The first objective addresses the concern that circular holes on corrugated pipes are hydraulically better than rectangular slots in lowering water table levels on agricultural fields via subsurface drains. The second objective addresses the questions of what is the largest size and maximum number of perforations (holes and slots) that can be placed on the pipe wall without causing structural failure under combinations of short-term live loads from field traffic, long-term dead loads from soil pressure, and hydrostatic loads from the water table level above the buried pipe. The third objective builds from the first and second objectives, and extends the flow-based model developed for Objective 1 to answer the question of whether the hydraulic resistance of buried corrugated pipes when operated under the subsurface irrigation mode, where the flow direction is reversed, is identical to that when operated under the drainage mode. The fourth objective uses the exit resistance relationships developed in Objective 3 to address questions about the effects of variable perforation characteristics on the water table rise in the unsaturated zone and soil-water fluxes during subsurface irrigation. Objectives 3 and 4 addresses the impact of heterogeneity from layered soils on the exit resistance and soil-water fluxes from perforated pipes buried at the layer interface, respectively. These four specific objectives collectively demonstrate how variable perforation characteristics can be integrated into the analysis and design of corrugated HDPE pipes.

1.3 Thesis Outline

This thesis is written following the manuscript-based convention, and each of the core chapters fulfills a specific research objective as defined in section 1.2. Chapter 2 presents a

comprehensive review of the existing literature focusing on:1) the hydraulic response of buried pipes operated under drainage mode, 2) the structural response of polyethylene pipes, and 3) the hydraulic response of buried pipes operated under subsurface irrigation mode. The literature review is followed by four integrated core manuscripts. The format of the manuscripts has been modified to be consistent with the requirements of the Library and Archives Canada. All figures and tables are included within the body of the manuscripts and supplementary materials are listed as appendices.

The first manuscript (Chapter 3) addresses Objective 1 and investigates the effects of perforation characteristics on subsurface drainage with corrugated pipes based on numerical simulations using finite-element modelling. Predictive relationships for the entrance resistance and relative flow rate (or delivery ratio) of corrugated pipes with variable perforation characteristics are presented. Chapter 3 also includes the results of the sand tank experiments used for calibrating the porous media flow numerical model.

The second manuscript (Chapter 4) addresses Objective 2 and investigates the structural response of corrugated HDPE pipes under variable loading conditions, which are representative of agricultural fields. The effects of two idealized friction conditions at the soil-pipe interface are assessed for buried corrugated pipes with and without perforations using linear elastic theory. The results of the vertical stress transmission from three distinct wheel loads of typical agri-machinery are also presented in Chapter 4.

The third manuscript (Chapter 5) addresses Objective 3 and builds from the findings of the previous two manuscripts as it relates to suitable perforation characteristics for buried corrugated pipes. Chapter 5 investigates the hydraulic exit resistance of perforated pipes operated under subsurface irrigation mode. Predictive equations for estimating the exit resistance as a function of perforation size and configuration are presented.

The fourth manuscript (Chapter 6) addresses Objective 4 and investigates the effect of perforations on the water table rise into the unsaturated zone for several soil textures, lateral drain spacings, and buried depths. The soil-water fluxes from subsurface irrigation pipes with variable perforation characteristics are also presented in Chapter 6.

Chapter 7 summarizes the main research results from the four core manuscripts and provides overall conclusions for the research in its entirety. The contributions to knowledge generated from this research and several recommendations for future studies are also given in Chapter 7.

1.4 References

Ayars, J. E., & Evans, R. G. (2015). Subsurface Drainage—What's Next? *Irrigation and Drainage, 64*(3), 378-392. doi: 10.1002/ird.1893

Bournival, P., Prasher, S., Von Hoyningen Huene, B., & S. Broughton, R. (1987). Measurements of Head Losses in a Subirrigation System. *Transactions of the ASAE, 30*(1), 183-0186. doi: https://doi.org/10.13031/2013.30424

Brachman, R. W. I., & Krushelnitzky, R. P. (2002). Stress Concentrations Around Circular Holes in Perforated Drainage Pipes. *Geosynthetics International, 9*(2), 189-213.

Burns, J. Q., & Richards, R. M. (1964). *Attenuation of stress for buried cylinders.* Paper presented at the Proceedings of the Symposium on Soil Structure Interaction, Tuscon, Arizona.

Dierickx, W. (1980). *Electrolytic analogue study of the effect of openings and surrounds of various permeabilities on the performance of field drainage pipes.* Doctoral thesis, Wageningen, Merelbeke, Belgium.

Drury, C. F., Tan, C. S., Reynolds, W. D., Welacky, T. W., Oloya, T. O., & Gaynor, J. D. (2009). Managing tile drainage, subirrigation and notrogen fertilization to enhance

crop yields and reduce nitrate loss. *Journal of Environmental Quality, 38*(3), 1193-1204.

Elmi, A. A., Madramootoo, C., Handyside, P., & Dodds, G. (2010). Water requirements and subirrigation technology design criteria for cranberry production in Quebec, Canada. *Canadian Biosystems Engineering, 52*, 1.1-1.8.

Fouss, J. L., Evans, R. O., Thomas, D. L., & Belcher, H. W. (1999). Operation of Controlled-Drainage and Subirrigation Facilities for Water Table Management. In R. W. Skaggs & J. Van Schilfgaarde (Eds.), *Agricultural Drainage* (Vol. 38, pp. 743-763). Wisconsin, USA: Madison Pubilsers.

Fyles, H., & Madramootoo, C. A. (2016). Water Management. *Emerging Technologies for Promoting Food Security* (pp. 117-134). Oxford: Woodhead Publishing.

Heilman, P., Kanwar, R. S., Malone, R. W., Ma, L., Hatfield, J. L., & Boyle, K. (2012). The Nashua agronomic, water quality, and economic dataset. *Journal of Soil and Water Conservation, 67*(6), 502-512.

Kang, J. S., Stuart, S. J., & Davidson, J. S. (2014). Analytical study of minimum cover required for thermoplastic pipes used in highway construction. *Structure and Infrastructure Engineering, 10*(3), 316-327. doi: http://dx.doi.org/10.1080/15732479.2012.754478

Khan, G. J., Shukla, K. N., Chauhan, H. S., & Ram, S. (1989). Verification of Kirkham's Problem of Layered Soil Drainage. *Journal of Irrigation and Drainage Engineering, 115*(4), 521-529. doi: doi:10.1061/(ASCE)0733-9437(1989)115:4(521)

Kirkham, D., & Schwab, G. O. (1951). The Effect of Circular Perforations on Flow into Subsurface Drain Tubes: Part I: Theory. *Agricultural Engineering, 32*(4), 211-214.

Madramootoo, C. A., Helwig, T. G., & Dodds, G. T. (2001). Managing water Tables to improve drainage water quality in Quebec, Canada. *Transactions of the ASAE, 44*(6), 1511. doi: https://doi.org/10.13031/2013.7034

Madramootoo, C. A., Johnston, W. R., Ayars, J. E., Evans, R. O., & Fausey, N. R. (2007). Agricultural drainage management, quality and disposal issues in North America. *Irrigation and Drainage, 56*(S1), S35-S45. doi: 10.1002/ird.343

Massey, F. C., Skaggs, R. W., & Sneed, R. E. (1983). Energy and Water Requirements for Subirrigation vs. Sprinkler Irrigation. *Transactions of the ASAE*, 126-133.

Mejia, M. N., & Madramootoo, C. A. (1998). Improved Water Quality Through Water Table Management in Eastern Canada. *Journal of Irrigation & Drainage Engineering, 124*(2), 116-122.

Mejia, M. N., Madramootoo, C. A., & Broughton, R. S. (2000). Influence of water table management on corn and soybean yields. *Agricultural Water Management, 46*(1), 73-89. doi: https://doi.org/10.1016/S0378-3774(99)00109-2

Mohammad, F. S., & Skaggs, R. W. (1983). Drain Tube Opening Effects on Drain Inflow. *Journal of Irrigation and Drainage Engineering, 109*(4), 393-404. doi: doi:10.1061/(ASCE)0733-9437(1983)109:4(393)

Mohammad, F. S., & Skaggs, R. W. (1984). Effect of drain tube openings on drainage and subirrigation. *Transactions of the ASAE*, 1455-1462.

Mostaghimi, S., Lembke, W. D., & Boast, C. W. (1985). Controlled-Drainage/Subirrigation Simulation for a Claypan Soil. *Transactions of the ASAE, 28*(5), 1557-1563.

Nelson, K. A. (2017). Soybean Yield Variability of Drainage and Subirrigation Systems in a Claypan Soil. *Applied Engineering in Agriculture, 33*(6), 801-809. doi: https://doi.org/10.13031/aea.12276

Prasher, S. O., Campbell, S. N., & Barrington, S. F. (1989). Laboratory Measurements of Head Losses From a Subirrigation Lateral. *Transactions of the ASAE, 32*(5), 1614-1618. doi: https://doi.org/10.13031/2013.31199

Schwab, G. O., & Fouss, J. L. (1999). Drainage Materials. In R. W. Skaggs & J. van Schilfgaarde (Eds.), *Agricultural Drainage* (Vol. 38, pp. 911-926). Wisconsin, USA: Madison Publishers.

Schwab, G. O., & Kirkham, D. (1951). The Effect of Circular Perforations on Flow into Subsurface Drain Tubes: Part II: Experiments and Results. *Agricultural Engineering, 32*(5), 270-274.

Sharma, H. C., Chauhan, H. S., Kapoor, P. N., & Ram, S. (1991). Ditch Drainage in Layered Soils. *Journal of Irrigation and Drainage Engineering, 117*(2), 184-200. doi: doi:10.1061/(ASCE)0733-9437(1991)117:2(184)

Skaggs, R. W. (1973). Water Table Movement During Subirrigation. *Transactions of the ASAE, 16*(5), 988-0993. doi: https://doi.org/10.13031/2013.37678

Skaggs, R. W. (1978). Effect of Drain Tube Opening on Water-Table Drawdown. *Journal of Irrigation and Drainage Division, (ASCE), 104*(IR1), 13-21.

Skaggs, R. W. (1991). Modeling Water Table Response to Subirrigation and Drainage. *Transactions of the ASAE, 34*(1), 169-0175. doi: https://doi.org/10.13031/2013.31640

Skaggs, R. W. (1999). Water Table Management: Subirrigation and Control Drainage. In R. Skaggs & J. van Schilfgaarde (Eds.), *Agricultural Drainage* (Vol. 38, pp. 695-718). Wisconsin, USA: Madison Publishers.

Skaggs, R. W. (2012). Drainage Water Management. *Journal of Soil and Water Conservation, 67*(6), 167A-172A. doi: 10.2489/jswc.67.6.167A

Spangler, M. G. (1941). *The Structural Design of Flexible Pipe Culverts*. (Bulletin 153). Ames, Iowa: Iowa Engineering Experiment Station.

Stuyt, L. C. P. M., & Dierickx, W. (2006). Design and Performance of Materials for Subsurface Drainage Systems in Agriculture. *Agric. Water Manage., 86*(1-2), 50-59. doi: 10.1016/j.agwat.2006.06.004

Stuyt, L. C. P. M., Dierickx, W., & Beltran, J. M. (2005). *Materials for subsurface land drainage systems*. FAO Irrigation and Drainage Paper 60. Rome, Italy.

Tang, Y. K., & Skaggs, R. W. (1980). Drain Depth and Subirrigation in Layered Soils. *Journal of the Irrigation and Drainage Division, 106*(2), 113-121.

Watkins, R. K., & Spangler, M. G. (1958). *Some Characteristics of the Modulus of passive Resistance of Soil: A Study in Similitude.* Paper presented at the Proceedings of the 37th Annual Meeting of the Highway Research Board, Washington, DC.

Yu, F., Frankenberger, J. R., Ackerson, J., & Reinhart, B. (2020). Potential Suitability of Subirrigation for Field Crops in the US Midwest. *Transactions of the ASABE, 63*(5), 1559-1570.

Chapter 2

Literature Review

2.1 Introduction

The central focus of this research is to investigate variable perforation characteristics of buried corrugated polyethylene pipes, and to show how these characteristics can be incorporated as input parameters into the analysis and design of subsurface drainage and irrigation systems used for water management on agricultural lands. Generally, buried pipes used in these water management systems are designed to satisfy two main criteria: 1) hydraulic capacity and 2) structural adequacy. The hydraulic design of buried corrugated pipes entails the determination of the required size (diameter), lateral spacing, and burial depth (below the surface) to remove, convey, and discharge excess soil-water from the crop root zone during wet periods of the growing season. The structural design entails the determination of the required pipe stiffness to provide stability against collapse or excessive deformation under applied loading during field operations. For dual-purpose drainage and subsurface irrigation systems, the hydraulic design component is extended to include provisions for supplying irrigation water during dry periods of the growing season. Consequently, previous research on the analysis and design of buried perforated pipes can be suitably categorized under three main themes: hydraulic response under drainage, structural response under loads, and hydraulic response under subsurface irrigation.

The literature review section of the thesis is divided into three sub-sections, addressing the three main themes or design components of buried pipes in water management systems. The first sub-section explores the hydraulic response of buried corrugated pipes operated under the drainage mode, focusing on the theoretical and experimental approaches used to evaluate the entrance resistance, and highlighting key laboratory and field studies done to assess the

impact of perforations on water table drawdown. The second sub-section provides a review of the structural response of buried high-density polyethylene (HDPE) pipes under static and dynamic loads, including an assessment of stress concentrations around perforations and vertical deformation of corrugated pipes under field conditions. The third sub-section focuses on the reverse hydraulics (upward flow) of buried pipes operated under the subsurface irrigation mode, examining previous work done on simulating the water table rise into the unsaturated zone.

2.2 Hydraulic response under subsurface drainage mode

Significant advances to modern agricultural land drainage date back to the early twentieth century when Hooghoudt (1940) developed equations for computing the lateral spacing of parallel ditches and buried tile drains in homogeneous soils (Vlotman et al., 2020a). These steady-state equations were derived using potential flow theory, Dupuit-Forchheimer (DF) theory, or a combination of both (van der Ploeg et al., 1999). The DF theory assumes that streamlines run horizontal and parallel to an impermeable stratum that lies below the drains (McWhorter and Marinelli, 1999); this impervious layer is necessary for sustaining perched or shallow water tables on flat agricultural lands (Vlotman et al., 2020b). For water management systems with buried pipes, the streamlines converge towards the pipe in a radial pattern as the midplane water table is lowered in order to remove excess soil-water from the root zone (drainage mode). The convergence of streamlines around the drain necessitates a correction to most lateral drain spacing equations to reconcile the assumptions of DF theory. Generally, the depth to the impermeable layer below the drain level is replaced by the Hooghoudt equivalent depth in drain spacing computations as a correction for the convergence head losses near the buried pipes (van der Ploeg et al., 1999). The equivalent

depth can be computed using closed-form solutions given by Moody (1996) or van der Molen and Wesseling (1991).

It is important to note that the correction for the convergence head loss due to radial flow is based on the assumption that the pipe wall is completely porous (ideal drain). Traditional tile drains (clay or concrete) are installed with gaps or spaces between individual tiles to permit water entry, while more commonly used HDPE or polyvinylchloride (PVC) pipes have finite perforations on the pipe wall for the same purpose (Stuyt et al., 2005). As a result, there is an additional head loss in the drainage system as the converging radial flow enters the finite openings or perforations on the pipe wall (nonideal drain). This entrance head loss can be incorporated into the equivalent depth computations by replacing the radius of the nonideal drain (r_0) with the effective radius (r_e) of a smaller ideal drain as established by Childs and Youngs (1958). Exact values of r_e can be computed from r_0 and the entrance resistance (α_e), which is a dimensionless geometric constant that represents the characteristics of finite openings or perforations on the pipe wall (Dierickx, 1999). The effect of these openings or perforations on the hydraulic response of buried pipes has been extensively studied since the 1950s. Table 2.1 summarizes the methodologies and findings of select studies for various interrelated hydraulic response parameters such as flow rate, head loss, water table drawdown, entrance resistance, and effective radius. The methodologies are classified into three broad approaches: theoretical analyses, sand tank experiments, and electrical analog models.

2.2.1 Theoretical analyses

Analytical solutions for the flow rate through tile drains with narrow gaps account for a large fraction of the theoretical approaches listed in Table 2.1. Kirkham (1950) was one of the earliest researchers to derive theoretical equations for computing the flow rate entering gaps between traditional clay tiles using the method of images. The equation was then used to

show that increasing the gap width does not result in significant increases to the flow rate of 150-mm-diameter tiles. Notably, Schwab et al. (1969) recorded water table drawdown in fields with clay tiles installed, and reported that the measurements were in agreement with the theoretical solutions of Kirkham (1950). Sneyd and Hosking (1976) reduced Kirkham's tile gap flow problem into a Fredholm integral equation, then used numerical methods to find solutions. The numerical solutions were an improvement to the flow rate of Kirkham (1950), which was computed as the average of the upper and lower limits. Further improvements were made to the tile gap flow problem by Prasad et al. (1981), who derived a dual Fourier cosine series from mixed boundary conditions, and then solved the resulting integral equation analytically. However, Hazenberg and Panu (1991a) showed that the Prasad et al. (1981) solution is only valid for the special case axisymmetric flows, and therefore, they reworked the problem and provided the correct solution for the general case non-axisymmetric flows.

Solving the problem of flow towards tile drain gaps provided the theoretical framework for formulating solutions to other types of opening such as holes and slots on the surface of plain wall pipes. The method of images was used by Kirkham and Schwab (1951) to derive an analytical equation for computing the flow rate through circular perforations. The solution utilized Hankel functions (also known as Bessel functions of the second kind and zero-order) and assumed the perforations were spherical sinks embedded in the pipe wall, following Muskat (1942) who developed equations for hydrocarbon flow into perforated vertical well casings for the petroleum industry. However, the formulation of both Muskat (1942) and Kirkham and Schwab (1951) ignores the effect of the impermeable nature of the casing or pipe wall, resulting in an erroneous estimate of the flow rate (Dierickx and Van Der Molen, 1981). An entirely different approach was taken by Engelund (1953), where a cylindrical plain wall pipe was developed into a flat plate and conformal mapping was used to derive the

Table 2.1. Survey of studies that investigated the effects of openings or perforations on the hydraulic response of buried pipes

Author	Pipe wall	Opening type/shape	Method or Approach	Main findings/conclusions	Hydraulic response parameter
Kirkham (1950)	PW	Gaps	Analytical solution/method of images.	Increasing the gap width from 0.8 mm to 6.35 mm (8-fold increase) only increases the flow rate by 36% for 150 mm diameter tiles.	Q/Q_0
Kirkham and Schwab (1951)	PW	Circular holes	Analytical solution/method of images.	Derived an analytical equation to compute flow rate through perforations.	Q/Q_0
Schwab and Kirkkam (1951)	PW	Circular holes	Electrical analogue experiments.	Increases in the delivery ratio is rapid up to 10 holes per 0.3 m (1 ft) of the pipe; doubling the diameter of holes did not double the flow.	Q/Q_0
Engelund (1953)	PW	Gaps and circular holes	Analytical solution/conformal mapping and Laplace equation with Fourier series.	Very little accuracy is lost if the pipe wall is assumed to be flat instead of cylindrical. Equations to compute the entrance head loss are presented.	H_e
Childs and Youngs (1958)	PW	Gaps	Sand tank experiments	Increases in gap width do not affect the midplane water table level. The concept of the effective radius is introduced in order to account for the effect of openings on tile drains.	H_w
Schwab et al. (1969)	PW	Gaps	Field measurements of clay tile-drains with gaps.	Water table drawdown agrees with the theoretical solution of Kirkham (1950) when midplane level is at	WTD

				least 0.6 m above drain level.	
Dennis and Trafford (1975)	PW	Gaps	Sand tank experiments	Using a gravel surround or envelope reduces entrance resistance and allows for an increase in drain spacing. Partial envelopes on the top half of the drain are as effective as complete surrounds.	α_e
Sneyd and Hosking (1976)	PW	Gaps	Numerical solution/ Laplace equation solved with Fredholm integral equation	Improved estimate of the flow rate through tile gaps compared to the Kirkham (1950) flow rate, which was taken as the average of an upper and lower limit.	Q/Q_0
Bravo and Schwab (1977)	PW, CW	Gaps and rectangular slots	Electrical analogue experiments	The delivery ratio is 44% for a 114 mm diameter (4-inch) corrugated pipe with rectangular slots.	Q/Q_0
Skaggs (1978)	CW	Rectangular slots	Numerical solution/Boussinesq equation solved with the finite difference method for water table drawdown.	The effect of perforations on water table drawdown is dependent on the profile depth and drain spacing. Deeper profiles and narrower drains have a larger effect on drawdown for perforated pipes.	WTD
Skaggs and Tang (1979)	CW	Rectangular slots	Numerical solution/Richards equation solved with the finite difference method for water table drawdown.	Improvement to Skaggs (1978) by considering 2D saturated-unsaturated flow. The water table drawdown is not sensitive to incremental changes in pipe diameters. The effect of perforations depends on profile depth and drain spacing.	WTD
Nierwenhuis and Wesseling	PW	Rectangular slots and circular	Numerical solution/conformal mapping	Increasing the number of perforation rows is more effective than increasing the size of the opening. The thickness of envelopes greater than 7.5 mm do not	α_e

(1979)		holes	with the relaxation method.	reduce the entrance resistance, regardless of the conductivity of the material.	
Dierickx (1980)	PW, CW	Rectangular slots and circular holes	Electrical analogue experiments	Experiments show that the Engelund (1953) and Sneyd and Hosking (1976) solutions can be used to compute entrance resistance for plain wall pipes. Approximate solution presented for corrugated pipes with rectangular slots.	α_e
Prasad et al. (1981)	PW	Gaps	Analytical solution/ Dual Fourier cosine series via Laplace solved with Fredholm integral equation	Presents solution to flow in tile gaps for the general non-axisymmetric flows as an improvement to Sneyd and Hosking (1976). The delivery ratio increases rapidly as the spacing of the tile gaps decreases.	Q/Q_0
Dierickx and van der Molen (1981)	PW	Rectangular slots and circular holes	Electrical analogue experiments	Provides experimental evidence to show that Kirkham and Schwab (1951) solutions are in error because they did not consider the impermeable boundary of the pipe wall.	α_e
Mohammad and Skaggs (1983)	CW	Rectangular slots and circular holes	Sand tank experiments	The effective radius had the largest response as perforation area increased from 38 to 75 cm^2/m, resulting in r_e values increasing from 5 to 21 mm, respectively.	r_e
Hazenberg and Panu (1991a)	PW	Gaps	Analytical solution/Laplace equation solved with dual trigonometric series.	Corrected the work of Prasad et al. (1981) and provide a non-axisymmetric flow equation for tile drains with gaps.	Q

Hazenberg and Panu (1991b)	PW	Rectangular and square slots	Analytical solution/Laplace equation solved with dual trigonometric series.	A plain wall porous pipe is best approximated by long narrow rectangular slots, rather than many square holes or a continuous gap.	Q/Q_0
Panu and Filice (1992)	PW	Circular holes	Analytical solution/Laplace equation solved with dual trigonometric series.	Extended Hazenberg and Panu (1991b) work to consider circular perforations on plain wall pipe. Results show the delivery ratio is larger for circular holes compared to slots of the same area.	Q/Q_0
Kohler et al. (2001)	PW	Gaps	Field measurements of clay tile-drains with gaps.	Approach flow head loss was used to modify boundary conditions at clay tiles with 2 mm wide gaps to accurately simulate discharge.	H_a
Oyarce et al. (2016)	PW	Rectangular slots	Sand tank experiments	Perforation density has a small effect on entrance resistance compared to envelopes.	α_e

Note: PW = plain wall, CW = corrugated wall, Q/Q_0 = delivery ratio, Q = discharge through an nonideal pipe, Q_0 = discharge through an ideal or fully porous pipe, H_w = midplane water table level, H_e = entrance head loss, H_a = approach flow head loss, WTD = water table drawdown, r_e = effective radius, α_e = entrance resistance.

entrance head loss (H_e) for gaps and circular holes. Engelund (1953) argued that very little accuracy is lost by assuming the flow towards a flat perforated plate is mathematically similar to that of a perforated cylinder. One drawback from the head loss equations presented by Engelund (1953) is their narrow range of application to field conditions; gap spacings must be less than the pipe diameter, and the circumferential spacing of the holes must be at least two orders of magnitude greater than the diameter of circular holes for the solutions to be valid. Conformal mapping was also employed by Nierwenhuis and Wesseling (1979) to investigate the effect of envelopes (filter) on the entrance resistance of perforated plain wall pipes. However, only a 2D region of the pipe and filter system was mapped with the aid of the relaxation method to determine potentials at fixed grid points. Nevertheless, the relative effects of the filter system were demonstrated by Nierwenhuis and Wesseling (1979), showing that envelopes with thicknesses greater than 7.5 mm do not reduce the entrance resistance, regardless of the hydraulic conductivity of the filter material.

Recognizing that tile drains with gaps were being continuously replaced with perforated pipes, that the earlier solutions of Kirkham and Schwab (1951) were in error, and that the solutions of Engelund (1953) were limited in scope, Hazenberg and Panu (1991b) applied dual trigonometric series to derive an equation for computing the flow rate through rectangular and square slots. The square slots were conceptualized as an approximation to circular holes. The results from Hazenberg and Panu (1991b) showed that long narrow rectangular slots best represents a fully porous pipe wall compared to square holes or even continuous gaps in traditional tile drains. The solution to dual trigonometric series was further extended by Panu and Filice (1992) to consider the flow rate through exact circular holes in plain wall pipes. A comparison of the flow rates between the square hole approximated as a circular hole (Hazenberg and Panu, 1991b) and an actual circular hole showed that the latter will yield a larger flow rate (Panu and Filice, 1992). However, upon inspection of the

boundary condition at the perforation surface, these analytical solutions by Hazenberg and Panu (1991b) and Panu and Filice (1992) are only valid for cases when the pipe is empty, a situation that is highly impractical under field conditions and not representative of radial flow towards buried perforated pipes. Additionally, attempts to replicate the results presented by Panu and Filice (1992) have been unsuccessful, indicating that either the equations presented or the results may contain errors.

The effects of perforations on water table drawdown have also been explored using numerical approaches. Skaggs (1978) used the finite difference method to solve the Boussinesq equation and simulate water table drawdown for corrugated pipes perforated with rectangular slots. The simulations showed that deeper profiles, characterized by the depth to the impermeable layer, and narrower drain spacings magnify the effect of the perforations on water table drawdown. In fact, a 38% difference in 24-hr drawdown between an ideal drain and a conventionally perforated drain [based on Case 4 of Bravo and Schwab (1977)] was reported by Skaggs (1978) in soils with a 5.0 m deep profile. The numerical solution to the Boussinesq equation neglects lateral flow in the unsaturated zone above the water table. Consequently, Skaggs and Tang (1979) developed a 2D saturated-unsaturated finite-difference model to solve the more exact Richards equation, and simulate water table drawdown for buried perforated pipes. Various pipe diameters ranging from 50 to 150 mm were also investigated; the results indicated that water table drawdown is not sensitive to incremental changes in diameter. For example, drawdown between a nominal 75-mm and a 100-mm diameter corrugated pipe differed by 5.0 mm, which is negligible in field conditions. Furthermore, similar conclusions to Skaggs (1978) were drawn by Skaggs and Tang (1979) with respect to the effect of perforations on drawdown for deep soils and narrow spacings. Despite using the more theoretically accurate approach of the Richards equation, which

requires unsaturated soil-water properties, the less stringent Boussinesq approximation appears adequate for simulating water table drawdown between parallel drains.

2.2.2 Sand tank experiments

Despite their limitations (Stuyt et al., 2005), sand tank models best simulate flow through porous media because they satisfy Darcy's law (Dierickx, 1999). Early sand tank experiments using clay tile-drains with gap widths of 0.6 mm, 1.2 mm, and 2.4 mm were conducted by Childs and Youngs (1958), who concluded that increasing the gap width did not affect the midplane water table level (H_w). Importantly, Childs and Youngs (1958) introduced the concept of effective radius, which is the radius of a completely porous or ideal drain that is smaller than the actual or nonideal drain, in order to compensate for the gaps or perforations. Childs and Youngs (1958) recommended the use of pockets of highly permeable gravel, placed at the gap or butt joint of the segmented tile drains to increase the effective gap width. The gravel surround acts as a sink at the entry point, increasing the flow towards the tile drain. Dennis and Trafford (1975) pursued the recommendation of Childs and Youngs (1958) and used sand tank experiments to investigate three arrangements of gravel envelopes around tile drains (complete, top half, and bottom half surrounds). The experiments by Dennis and Trafford (1975) showed that both partial and complete gravel surrounds are effective in reducing the entrance resistance of tile drain gaps, and that surrounds on only the top half of the drains were as effective at increasing the lateral spacing as a complete gravel envelope around the drain.

Mohammad and Skaggs (1983) investigated the effects of perforation area using sand tank experiments with corrugated polyethylene pipes. In addition, the location of the perforation along the pipe circumference, and the impact of a 50-mm thick complete gravel envelope were examined. Radial flow theory was used to derive the effective radius of the perforated pipes from the laboratory experiments. Mohammad and Skaggs (1983) reported that the

effective radius response was largest between perforation areas of 38 to 75 cm^2/m, resulting in r_e values from 5 to 21 mm, respectively. The circumferential location of the perforations had little impact on the effective radius. On the other hand, the sand tank experiments showed that the gravel envelope increased r_e by a factor of seven compared to a standard perforated pipe. Although the sand tank experiments included rectangular slots, a valid comparison of the shape effect between slots and holes could not be made since only one pipe sample with slots was tested. The main shortcoming, however, was the experimental set-up of the sand tank by Mohammad and Skaggs (1983), which only allowed for measurement of the approach flow head loss that includes both entrance and convergence head losses (Stuyt et al., 2005).

It was previously explained (section 2.2) that convergence head losses are not originally accounted for in DF theory, but can be compensated by using Hooghoudt's effective depth. The effective radii values presented by Mohammad and Skaggs (1983), therefore, cannot be used in drain spacing equations as the convergence head loss will be accounted for twice in the computations. The primary objective of the effective radius is to compensate only entrance head losses as explained by Childs and Youngs (1958). In the same study, Mohammad and Skaggs (1983) attempted to isolate the effects of the entrance head loss due only to perforations on the pipe wall using a surface transfer coefficient, but this parameter has units of 1/time and it was not demonstrated how it could be used in practice for the analysis and design of subsurface drainage. The entrance resistance as defined by Dierickx (1980), is both dimensionless and soil independent, and can be easily used to compute the effective radius for nonideal drains. As pointed out by Stuyt et al. (2005), the entrance resistance can be accurately computed if the radial flow pattern towards nonideal drains can be correctly modelled, which entails strategic piezometric head measurements close to the perforated pipe. Sand tanks are limited in their ability to facilitate representative piezometric

reading in this manner, but electrical analog models (section 2.2.3) or numerical models are better suited for simulating radial flow towards nonideal drains.

More recently, Oyarce et al. (2016) used sand tanks to evaluate the entrance resistance from plain wall PVC pipes with rectangular slots and a synthetic (geotextile) envelope. The authors concluded that perforation density (measured by opening area) has a small effect on entrance resistance compared to envelopes. Despite conforming to the general findings of previous sand tank experiments, the validity of the results presented by Oyarce et al. (2016) is questionable for several important reasons. Firstly, the number of piezometers (only three) were too few and not strategically positioned to accurately measure the head loss necessary for computing the entrance resistance. Secondly, the hydraulic head on the pipe at the perforation surface was not measured during the experiments. Instead, the authors estimated the head using data from the three piezometers. The hydraulic head on the pipe is one of the most important boundary conditions needed to estimate the entry head loss and warrants proper measurements during laboratory experiments. Thirdly, the pipes tested in the experiments were placed on a slope relative to the horizontal plane. This slope introduces a hydraulic gradient along the length of the pipe, which is not compatible with 2D radial flow theory. Nonetheless, the findings presented by Oyarce et al. (2016) are limited to plain wall pipes with wide slots, while corrugated pipes with narrow slots and holes are commonly used for subsurface drainage in North America and Europe.

2.2.3 Electrical analog models

Electrical analog models have proven to be extremely valuable in establishing much of what is known about the entrance resistance of buried perforated pipes (Dierickx, 1999). These analog models are based on Ohm's law, which governs the flow of electrical currents through conductors. Ohm's law is conceptually and mathematically similar to Darcy's law, which governs the flow of liquids through porous media (Goudarzi et al., 2018; Hagras and Agamy,

2014; Zhang and Schaap, 2019). Early analog models that were used to investigate the entrance resistance of perforated pipes consisted of thin metallic sheets and conductive paper, but these were limited to 2D flow problems (Dierickx, 1999). Investigating the 3D flow pattern towards perforations require electrolytic models that use conductive liquids, which was the case for the analog experiments done by Schwab and Kirkham (1951). These experiments used metal balls to represent spherical sinks for simulating flow towards circular holes in plain wall pipes as a method of validating the previously derived theoretical solutions of Kirkham and Schwab (1951) for the same flow problem. The experiments showed that the flow rate increases rapidly as the perforation increases up to 10 holes per 0.3 m (1.0 ft) of pipe. Kirkham and Schwab (1951) also found that relationships between perforation size and flow rate are nonlinear as doubling the diameter of holes did not double the flow rate through the pipe.

Although the electrolytic analog simulation results of Schwab and Kirkham (1951) compared well with results from the analytical equations of Kirkham and Schwab (1951), the solutions are erroneous as shown by Dierickx and van der Molen (1981). The agreement reported by Schwab and Kirkham (1951) via the validation experiments arise from the fact that identical boundary conditions for the pipe wall were modelled in both the theoretical and electric analog approaches; the impermeable surface of the pipe wall was ignored. Dierickx and van der Molen (1981) showed that the correct boundary condition is the pipe wall modelled as a surface of streamlines. Furthermore, a correction factor of two to Kirkham and Schwab (1951) equations was shown to improve predictions of the entrance resistance for plain wall pipes with circular holes.

Most of the research on the effect of openings prior to the mid-1970s had been done on plain wall pipes with gaps or perforations. With the introduction of corrugated HDPE pipes in the late 1970s (Stuyt et al., 2005), research shifted towards investigating the effects of

perforations when placed in the corrugation valley of the buried plastic pipes. Consequently, Bravo and Schwab (1977) evaluated the effects of rectangular slots in corrugated pipes using electrical analog models. Plain wall pipes with gaps and slots were also modelled to aid in calibrating the hydraulic boundary condition of the outermost radial equipotential (source). Results from the analog experiments showed that the delivery ratio (Q/Q_0) is 44% for models representing a 114-mm-diameter (4-inch nominal) corrugated pipe with five rows of slots (Bravo and Schwab, 1977). This particular finding (case 4) was subsequently used by Skaggs (1978) and Skaggs and Tang (1979) in numerical models to simulate the midplane water table drawdown between parallel drains (section 2.2.1).

However, it should be noted that in their theoretical model, Bravo and Schwab (1977) approximated the boundary condition at the perforation surface as step functions in the circumferential and longitudinal directions. This approximation was done to facilitate analytical solutions of the Laplace equation by variable separation, but may have introduced errors into the resulting equations derived for the theoretical flow into gaps and slots on plain wall drains. Moreover, these theoretical models were developed for calibrating the outer boundary condition, given as a radius equal to 381 mm for case 4, which was then terminated after coming within 8% of the experimental results. The validity of Bravo and Schwab (1977) results, especially the widely used case 4 (Q/Q_0 = 44%), is highly questionable given these confounding assumptions for the boundary conditions.

The most comprehensive work done on investigating the entrance resistance of buried pipes with openings was carried out by Dierickx (1980) using electrolytic analog models. Following Ernst (1954) constituent formulation of the total head loss for water flowing towards buried pipes in a drainage system, Dierickx (1980) isolated and focused on the approach flow (Kohler et al., 2001) in the radial zone around the pipe, establishing the approach flow head loss as the sum of the convergence and entrance head losses. Dierickx

(1980) used his analog model to conclusively validate the theoretical equations of Engelund (1953) and Sneyd and Hosking (1976) for computing the entrance resistance of plain wall pipes with variable perforation characteristics. It was through these experiments that Dierickx and van der Molen (1981) were able to demonstrate that the solutions of Muskat (1940) and Kirkham and Schwab (1951), and by extension Schwab and Kirkham (1951) were incorrect. Data from the electrolytic analog experiments were also used to validate an approximate analytical solution for the entrance resistance of corrugated pipes with rectangular slots (Dierickx, 1980). However, Dierickx (1980) did not run any experiments for corrugated pipes with circular holes, and therefore, a thorough comparison of the shape effect between slots and holes has not been made to date.

2.2.4 Perforation specifications

At the turn of the millennium, the use of flexible single-wall corrugated pipes for subsurface drainage systems was ubiquitous on agricultural lands (Schwab and Fouss, 1999). Pipe manufacturers and regulatory agencies developed standards for corrugated pipes, which include specifications for the shape, size, and configuration (three main characteristics) of perforations on the pipe wall. Table 2.2 lists the perforation specifications for corrugated polyethylene pipes (nominal 100-mm-diameter) from several engineering standards and pipe manufacturers that are currently being used across North America, Europe, and other countries worldwide. There is a wide range of specifications in perforation size and total area (A_p) as shown in Table 2.2. Rectangular slots are much more common across manufacturers, although most of their datasheets indicate some degree of flexibility in altering any of the three perforation characteristics to meet the requirements of customers. The number of

Table 2.2. Perforation specification for corrugated pipes by engineering standards and manufacturers

Reference document	Shape	Size[a] (mm)	N	A_p (cm^2/m)	Remarks
Standards					
AASHTO M252 (AASHTO, 2009)	holes	4.75	2	20	Class 2 - for subsurface drainage only
	slots	3 × 25	2	20	
ASAE EP260.5 (ASAE, 2015)	slots	1.5	-	45-60	Based on Mohamed and Skaggs (1983)
ASTM F667 (ASTM, 2016)	-	-	-	21	user specified shape, size, N
Manufacturers[b]					
ADS (2008)	slots	3 × 22	3	21	Type B - rows spaced 120°
Armtec (2016)	slots	1.3 × 12	4	37	
JM Eagle (2012)	slots	2.88 × 25	3	136	Class 2 - rows spaced 120°
Lane (2015)	slots	3 × 25	4	21	spaced every second valley
Prinsco (2018)	slots	1.02 × 18.42	4	44	spaced every valley
Soleno (2020)	slots	1.8 × 19	2	32	Type 2

Note: AASHTO = American Association of State Highways and Transportation Officials, ASAE = American Society of Agricultural Engineers, ASTM = American Society for Testing and Materials, N = number of perforation lines, A_p = total area of perforation per m length.
[a]slot size is given as width × length.
[b]nominal manufacturers specifications for 100 mm diameter pipe; shape, size and N can be adjusted to client's requirement

perforation lines or rows (N) vary from two to four, and the slot width is less than 3.0 mm for the select types of perforated pipe listed (Table 2.2). For adequate hydraulic performance, Schwab and Fouss (1999) recommend the use of 88 rectangular slots that should be 1.6 mm wide and 25 mm long, or 125 circular holes with diameters of 6.0 mm per meter length of corrugated pipe (100-mm-diameter). These two combinations of perforation shape, size, and quantity yield a total perforation area of 35 cm^2/m.

In Table 2.2, the total perforation area ranges from 20 to 136 cm^2/m as a result of the variation in perforation size and distribution along the pipe wall in both the circumferential and longitudinal (axial) directions. Interestingly, 50% of the sources in Table 2.2 specifies a minimum perforation area of 20 cm^2/m for corrugated pipes. This lower bound for A_p is based on the opening area of gaps between traditional clay tile drains (Stuyt et al, 2005). However, Dierickx (1999) recommends a minimum area of 50 cm^2/m in order to obtain an acceptably low entrance resistance.

It is important to note that the range of area (45 - 60 cm^2/m) given by the ASAE EP260.5 (ASAE, 2015) standard corresponds to opening areas of 1.5 - 2.0% of the total surface area of the pipe wall. The standard claims that 1.5-mm wide slots, uniformly distributed along the pipe wall will result in an effective radius of 15 mm based on the work of Mohammad and Skaggs (1983). However, it was previously discussed that Mohammad and Skaggs (1983) inadvertently measured the approach flow resistance instead of the entrance resistance (section 2.2.2), and therefore the effective radius value is erroneous. Furthermore, the exact spatial distribution and length of the rectangular slots, specifications not included in ASAE EP260.5 (ASAE, 2015), ultimately determine the entrance resistance (and effective radius) of the pipe. Specifications such as the slot width and area of perforation are not sufficient for describing the entrance resistance of perforated pipes (Dierickx, 1999).

2.3 Structural response of polyethylene pipes

The structural analysis and design of buried pipes may be considered as a multi-step iterative process, where performance limits are used to assess the soil-pipe response to design loadings for case-specific field conditions. The design process is relatively generic, and has been thoroughly presented in the engineering literature with minor variations in methodology according to design functionality and end-use (Chambers and McGrath, 1981; Fouss, 1973; Moore, 2001; Moser, 2001; Watkins and Anderson, 2000). The design procedure outlined by Moore (2001) is the most comprehensive and has been widely used for assessing the structural adequacy of buried pipes (Brachman and Krushelnitzky, 2002, 2005; Krushelnitzky and Brachman, 2009).

2.3.1 Performance limits

Moser (2001) defined a performance limit for pipes as that point where once exceeded is deemed unacceptable for a specific design function. Traditionally, the structural design of buried pipes considers two broad categories of performance limits: structural integrity and serviceability (Chambers and McGrath, 1981). These performance limits have since been expanded to include material behaviour with time (long-term vs. short-term), and environmental effects such as UV degradation and reaction to solvents (Moore, 2001).

Watkins and Anderson (2000) argued that performance limits should be practical. The authors suggested using deformation criteria for establishing performance limits as these can be related to internal pipe stresses (due to external loading), which can be easily measured. It should be noted that performance limits do not necessarily constitute total failure but do reduce functionality (Watkins et al., 1975).

For HDPE pipes, the key performance limits according to Moore (2001) are: short-term yield, long-term cracking (material failure), ovaling and hoop compression (deflection), global and

local buckling, and UV and solvent degradation (durability). It should be noted that with the exception of the latter category, these performance limits are all influenced by the backfill soil in a conjugate soil-pipe system.

2.3.2 Design loads

Buried pipes must be able to withstand loads predominantly from earth pressures (geostatic stresses) due to backfilling and/or embedment. In addition to the geostatic stresses, an array of loading conditions arising from fluid transport, construction loads, and others (frost action, seismic activity, landslides) may need consideration in the design process (Moore, 2001). Vehicular wheel loads from construction and agricultural machinery can be superimposed by using Boussinesq's elastic solution to estimate the vertical stress at the crown of the buried pipe (Moser, 2001).

2.3.3 Soil-pipe interaction

The interface between the buried pipe and the surrounding soil (through arching action) plays an important role in predicting the response of the pipe structure to the subjected loads. Two idealized conditions (full slip and no-slip) at this interface have been investigated to establish the upper and lower limits of the interaction (Moore, 2001). The solutions of Hoeg (1968) were developed for cases where the ground is unstressed before pipe installation. Solutions also exist for prestressed ground conditions prior to installation, e.g. tunnelling (Einstein and Schwartz, 1979; Moore, 1988). The radial and shear stresses at the interface of the soil-pipe system can be found using equations given by Moore (2001). These equations can be used to compute resulting thrusts and bending moments at the crown and springline of the buried pipe. Subsequently, the maximum compressive and tensile circumferential wall stresses can be estimated from superposition of combined bending and normal stresses. These response stresses can then be checked against limiting stress values of the pipe material to ensure stability against failure (Moore, 2001).

2.3.4 Deflection

Deflection is usually more significant for flexible pipes as compared to rigid pipes and it depends on the stiffness of the soil surrounding the buried pipe. Early methods of estimating deflection were based on the section modulus of the pipe wall. The revised Iowa Formula as developed by Spangler (1941) was commonly used to compute pipe deflection despite several limitations in its assumption (Moser, 2001). Additionally, Moore (2001) gave the equations to compute vertical and horizontal deflections using elastic theory. Permissible deflection limits for flexible plastic pipes are normally set at 5% to 10% of the pipe diameter to satisfy pipe stiffness requirements at testing (ASTM, 1997). However, pipe failure can occur by some other performance limit being exceeded, and hence allowable deflection limits should be set for case-specific designs (Watkins and Anderson, 2000).

2.3.5 Effect of perforations on structural response

Numerous studies have been conducted to determine the parameters that affect the structural performance of buried pipes (Chambers and McGrath, 1981; Moore, 2001; Myers et al., 1967; Parker and Willardson, 1981; Watkins and Anderson, 2000; Watkins et al., 1975). However, very little work has been done to develop a criterion for perforating buried corrugated polyethylene pipes within the context of structural analysis and design. This gap led to a study that investigated the influence of circular perforations on the structural performance of plain wall buried pipes (Brachman and Krushelnitzky, 2002). The output was the first set of guidelines on perforating buried HDPE pipes from a structural design perspective. By extension, criteria were established for the perforation spacing circumferentially and longitudinally along the pipe wall. Usually, these were often determined by manufacturers' practice or end-user choice with the former being given by specifications (ASTM, 2016).

In relation to structural performance, it is noteworthy that the Bureau of Reclamation (2009) carried out investigations to determine whether perforations had an effect on the failure of toe drains. This was done after they discovered (via video inspection) that 50% of their toe drains were severely deformed or had collapsed altogether. Samples of HDPE and PVC pipes (150-mm to 600-mm diameter), perforated and non-perforated, and solid wall and corrugated, were tested by plate loading tests to derive pipe stiffness. Results showed that perforated pipes were not significantly weaker than non-perforated pipes, alluding to the fact that the corrugation ribs contribute more to load resistance as compared to the corrugation valleys where perforations are typically located. Results from other tests supported this assumption as perforations were shown to reduce pipe stiffness in solid wall pipes. However, plate loading tests do not capture the full response of soil-pipe interaction and they often overestimate pipe stiffness (Moore, 2001). In addition, Brachman et al. (2000) measured surface strains around an isolated perforation on a buried pipe and found it had a complex 3D response as strains were 2.7 times higher than that for non-perforated areas. These arguments present the case for using three-dimensional structural analysis to better predict the performance of buried pipes. Despite these limitations, however, the results from the plate loading tests were used to establish important recommendations on the selection of plastic pipes for toe drains by the Bureau of Reclamation.

Using three-dimensional elastic finite element analysis, Brachman and Krushelnitzky (2002) found that the parameters that affected stresses around the perforation were the pipe's thickness to diameter or dimension ratio (DR), the diameter of the perforation, and the spatial location (circumferential and axial) of the perforation. More specifically, stresses were shown to be maximum at the springlines, invert and crown of the buried pipes. Some of the main guidelines suggested were as follows: 1) the axial spacing of perforations were recommended to be greater than four times the diameter of the perforation, 2) the ideal positions for

perforations were at the quarter points (shoulders and haunches) as internal stresses were minimal in these areas, and 3) for perforations located at the quarter points, the maximum diameter of the perforation should be limited to 5% of the mean diameter of the pipe. Additionally, it was shown that a stress concentration factor (ratio of the stress at perforations to that at non-perforated sections) of 3.0 may be conservatively used for perforated pipes.

Interestingly, Brachman and Krushelnitzky (2002) suggested that it may be advantageous to use more than four holes at the quarter points. However, they cautioned positioning perforations too close to the crown, invert and springlines. This outlines a limitation of the study as it did not address the ideal number of perforations along the circumference of a plain wall buried pipe.

2.4 Hydraulic response under subsurface irrigation mode

Buried perforated corrugated pipes used in water management infrastructure can be operated as dual-purpose drainage and subsurface irrigation systems on agricultural lands. During subsurface irrigation mode, water is added to the system via control chambers to supply the crop's water requirement during dry periods of the growing season. The water movement in the unsaturated zone is facilitated by vertical capillary fluxes in to the root zone above the water table (Skaggs, 1981). However, significant lateral flows occur as the water leaves the buried pipe and the water table level at the midplane rises into the unsaturated zone (Skaggs, 1973). This reverse flow direction in subsurface irrigation mode is driven by the pressure difference between the water level in the control chambers and the water table level directly near the pipe. Head losses occur in subsurface irrigation systems as the water exits the pipe through openings (exit head loss), and as the soil-water diverges radially away from the pipe (divergence head loss) and into the unsaturated soil to raise the water table (Skaggs, 1991).

The design of subsurface irrigation systems is aimed at determining suitable lateral spacings and burial depths so that the system of parallel pipes can raise the water table to a predetermined level and supply the crop with water via upward flux. Ernst (1975) developed an equation to compute the lateral spacing of the pipes in a subsurface irrigation system under steady-state conditions. As with other drain spacing equations, DF theory was used by Ernst (1975) in the formulation of the equation, which is similar in form to the equation developed by Hooghoudt (1940) for buried pipes operated under the drainage mode. Consequently, the Hooghoudt equivalent depth can be used to correct for the divergence head loss as a result of the impermeable layer below the drain (Skaggs, 1981). Theoretically, the exit head loss can also be accounted for using the effective radius in a manner similar to the entrance head loss that occurs when the water flows towards the drain under drawdown (Skaggs, 1991). Most subirrigation systems are analyzed and designed under the assumption that the entrance head loss is the same as the exit head loss, and have therefore been designed using the entrance resistance (α_e) due to perforations when computing the effective radius. As such, very little work has been done to measure the exit head loss and develop functional predictive relationships between the head loss and variable perforation characteristics.

2.4.1 Exit head loss measurements

Head loss measurements in a subsurface irrigation system were recorded by Bournival et al. (1987) on fields under corn cultivation in southern Quebec. Piezometers were installed near the buried corrugated pipes to estimate the exit and divergence head losses. Head loss measurements of flow through the control chamber, main delivery lines (non-perforated), and pipe fittings (tee and elbow connectors) were also made by Bournival et al. (1987) during the study, but these were deemed marginal and accounted for less than 3.4 cm. On the other hand, the authors reported a total head loss of 55 cm, 75% of which was attributed to the exit

head loss due to perforations. Bournival et al. (1987) recommended raising the water level by 55 cm to compensate for the head losses and maintain the target water table level in the field.

However, Prasher et al. (1989) pointed out that the field measurements of Bournival et al. (1987) may have actually been divergent head losses only, as a result of clogged envelopes used around the corrugated pipes. The use of thin synthetic envelopes such as knitted polyesters can become clogged if they are not correctly designed for site-specific soil particle size distribution (Rollin et al., 1987). Therefore, laboratory measurements of head losses from subsurface irrigation laterals were made by Prasher et al. (1989) using a sand tank and a corrugated pipe with narrow rectangular slots. No significant exit head losses were reported from the lab measurements, which were found to range between 1.4 and 3.67 cm for flow rates between 4.2 and 17.1 litres/min, respectively. In contrast, divergence head losses as high as 47 cm within 25 cm of the pipe center were measured in the sand profile, leading Prasher et al. (1989) to conclude that it may been divergence losses that were measured in the field by Bournival et al. (1987). Nevertheless, a direct comparison between the field subsurface irrigation system of Bournival et al. (1987) and the sand tank facility of Prasher et al. (1989) shows that the perforations on the pipe systems have key differences that may affect the head loss readings. The buried corrugated pipes in the field had an opening area of 31.2 cm^2/m from 6.6-mm-long by 1.0-mm-wide rectangular slots (Bournival et al., 1987). The corrugated pipes used in the sand tank experiments by Prasher et al. (1989) had 12 lines of slots that were 9.0-mm-long by 0.17-mm wide, yielding an opening area of 11.7 cm^2/m. Based on the size of the slots, the total number of slots per meter length of pipe was 473 and 704 for the field site and laboratory sand tank pipes, respectively. The size, number, and distribution of slots were very different between the two cases. Specifically, the large number of perforation lines (12) used by Prasher et al. (1987) in the sand tank experiments are not representative of perforation specifications listed by manufacturers or engineering standards (Table 2.2) and

may be the reason why the exit head losses were comparatively small. Therefore, the conclusions drawn by Prasher et al. (1987) on exit losses cannot be generalized for all perforation characteristics on buried corrugated pipes used for subsurface irrigation.

2.4.2 Water table rise

The transient response of the water table rise into the unsaturated zone is also important to the analysis, design, and operation of subsurface irrigation systems. Skaggs (1973) reported field observations where at least 60 hrs elapsed before an initially draining midplane water table level started to rise in response to subsurface irrigation. As such, the finite difference method was used by Skaggs (1973) to simulate the water table rise into the unsaturated zone based on the Boussinesq equation. Comparisons were made between two analytical solutions of the Boussinesq equation and the numerical solutions. Field data and a Hele-Shaw model were used to validate the numerical solutions for both initially draining and horizontal water table profiles. The results showed that the analytical solution by variable separation technique can adequately be used to simulate the water table rise under subsurface irrigation conditions. However, the solutions presented by Skaggs (1973) only corrected the divergence head loss using Hooghoudt's effective depth. No consideration was given to the effects of perforations and exit losses of the buried pipes.

As with drainage, the Richards equation is the most theoretically correct for characterizing the movement of water in the unsaturated zone during subsurface irrigation (Nieber and Feddes, 1999). Tang and Skaggs (1980) used the finite difference method to solve the Richards equation in a two-layer system in order to assess the effect of drain depth on subsurface irrigation in layered soils. Results suggested that the buried pipes should be placed at the layer interface or in the upper section of the layer with the higher hydraulic conductivity. Increasing the burial depth is not advantageous to the water table rise in the

unsaturated zone (Tang and Skaggs, 1980). Once again, the effects of perforations were not incorporated into the analysis by Tang and Skaggs (1980).

Skaggs (1981) compared three design methods for determining the spacing and depth of subsurface irrigation systems: steady-state, transient state, and changing weather conditions. A case study using field data from a site in North Carolina was used to show how the water management model, DRAINMOD (Skaggs et al., 2012), can be used to design a dual-purpose subsurface drainage and irrigation system under changing weather conditions. The simulation results using 23 years of historical data indicated that a lateral spacing of 18 m would satisfy both drainage and subsurface irrigation requirements with pipe buried 1.0 m below the surface in a sandy loam soil. In contrast, a lateral spacing of 25 m would be required if the system was designed to only operate under the drainage mode (Skaggs, 1981). Similar studies of simulating the performance of subsurface irrigation systems under long-term changing weather conditions were done by Massey et al. (1983) and Mostaghimi et al. (1985) using DRAINMOD.

Massey et al. (1983) compared subsurface irrigation and sprinkler irrigation systems using 27 years of climatic data in eastern North Carolina and found that the former requires less energy than the latter. However, subsurface irrigation systems used 4 to 8 cm/yr more water than sprinkler irrigation systems (Massey et al., 1983). Mostaghimi et al. (1985) investigated the suitability of dual drainage and subsurface irrigation of corn in claypan soils in the American Mid-west. Simulations were run using 20 years of climate data, and showed that the optimum spacing for dual-purpose drainage and subsurface irrigation is 6 m based on a weir setting of 35 cm and a 5-yr recurrence interval (Mostaghimi et al., 1985). It is important to note that these studies conducted with DRAINMOD all assumed that the buried corrugated pipes had an effective radius of 5.1 mm, regardless of the actual perforation characteristics specific to each study. This value of the effective radius, which was the default setting in

DRAINMOD, is based on the work of Mohammad and Skaggs (1983), who measured the approach flow resistance under drainage conditions, and inadvertently double-counted the head loss due to the radial convergence (sections 2.2.2 and 2.2.4). Additionally, these studies assumed that the effective radius (and by extension the head loss due to perforations) is the same under drainage and subsurface irrigation modes.

The rise of the water table into the unsaturated zone under transient conditions was also simulated using sand tanks (Mohammad and Skaggs, 1984). The effect of seven different opening areas on drainage and subsurface irrigation was investigated by Mohammad and Skaggs (1984) using corrugated pipes with 4.8-mm-diameter holes. These sand tank experiments showed that the water table response increased with increasing perforation area up to 38.5 cm^2/m, but doubling the perforation area to 79 cm^2/m only resulted in a small increase in water table rise; use of a 5-cm thick gravel envelope also had a relatively small effect on the rate of water table rise under subsurface irrigation (Mohammad and Skaggs, 1984). However, the change in perforation area was facilitated mostly by changes in the longitudinal spacing of the holes along the length of the pipe. Mohammad and Skaggs (1984) did not document how this was done during the sand tank experiments. In addition, the number of perforation lines was fixed at six for all but two cases, and the perforation diameter was also held constant throughout the experiments. Therefore, the effect of variable perforation characteristics on the water table response under subsurface irrigation could not be established from the investigations of Mohammad and Skaggs (1984).

2.5 Conclusions and future directions

Complex mathematical formulations have been developed to describe the flow towards openings in buried pipes, but these are limited to a simple pipe geometry (plain wall) with gaps or perforations on the surface. Most of the analytical solutions were formulated with

erroneous hydraulic boundary conditions that do not reflect realistic drainage conditions in the field. Additionally, the resulting theoretical equations were often presented in the form of infinite series that have limited scope and very little practical value.

Sand tank studies were mainly used to investigate the impact of gravel and synthetic envelopes surrounding drainage pipes, but these were also primarily limited to tile drains or plain wall pipes. An exception to this was the study by Mohammad and Skaggs (1983), in which sand tank experiments with corrugated pipes were conducted to determine the effects of perforations. However, the approach flow resistance instead of the entrance resistance was inadvertently measured during the laboratory experiments. Electrical analog models offered more flexibility than sand tanks for evaluating the entrance resistance of perforated pipes. Dierickx (1980) carried out the most comprehensive 3D electrolytic experiments, and was able to provide both validation and correction for some of the earlier theoretical approaches on entrance resistance. Nonetheless, the entrance resistance of circular holes in corrugated pipes was not established. Wide variability in perforation specifications by regulatory agencies and pipe manufacturers indicate that there is a degree of flexibility in selecting perforation size, shape, and configuration for corrugated pipes used in subsurface drainage systems. As such, questions about the potential of circular holes in increasing flow rate and improving drainage performance has arisen among drainage practitioners and pipe manufacturers.

Little work has been done investigating the effects of perforations on buried corrugated polyethylene pipes. The use of elastic theory to model the structural response of buried pipes had been limited to plain wall pipes with circular holes. Specifically, the stress concentration from rectangular slots has not been thoroughly investigated. Studies have shown that the friction condition at the soil-pipe interface can influence the stress and deformation response

of the pipe, but this has not been studied for small diameter (<300 mm) corrugated pipes under variable loading conditions.

The pressure head on buried pipes and the upward diverging flow of water under subsurface irrigation conditions (reverse flow) is significantly different than the zero pressure head and downward converging flow under drainage conditions. Therefore, it may be incorrect to use the entrance resistance (drainage mode) due to perforations to account for the exit head losses near buried corrugated pipes operated under subsurface irrigation mode. Sand tank experiments by Prasher et al. (1989) have investigated the exit losses of perforated corrugated pipes under subsurface irrigation conditions, but their conclusions cannot be generalized for variable perforation characteristics. Mohammad and Skaggs (1984) simulated water table rise into the unsaturated zone using sand tanks. However, the effect of variable perforation characteristics of buried corrugated pipes on water table response under subsurface irrigation remains to be established.

The overall state of the current body of literature with respect to the hydraulic and structural response of buried perforated corrugated pipes shows that there are existing gaps in knowledge. This research is aimed at addressing these gaps by focusing on how variable perforation characteristics can be incorporated into the analysis and design of corrugated polyethylene pipes. Future research should focus on adding complexity to current numerical models to include 3D unsaturated flows for investigating the hydraulic response of buried pipes. In addition, future experiments aimed at capturing the strain response around perforations in buried corrugated pipes can be used to provide validation for finite-element based computational models.

2.6 References

ASAE. (2015). Design and Construction of Subsurface Drainage Sysytems on Agricultural Lands in Humid Areas *ASAE EP260.5*. St. Joseph, MI: ASABE.

ASTM. (1997). Standard Specification for Corrugated Polyethylene (PE) Pipe and Fittings. *ASTM F405*. West Conshohcken, PA.

ASTM. (2016). Standard Specification for 3 through 24 in. Corrugated Polyethylene Pipe and Fittings. *ASTM F667*. West Conshohocken, PA: ASTM International.

Bournival, P., Prasher, S., Von Hoyningen Huene, B., & S. Broughton, R. (1987). Measurements of Head Losses in a Subirrigation System. *Transactions of the ASAE, 30*(1), 183-0186. doi: https://doi.org/10.13031/2013.30424

Brachman, R. W. I., & Krushelnitzky, R. P. (2002). Stress Concentrations Around Circular Holes in Perforated Drainage Pipes. *Geosynthetics International, 9*(2), 189-213.

Brachman, R. W. I., & Krushelnitzky, R. P. (2005). Response of a landfill drainage pipe buried in a trench. *Canadian Geotechnical Journal, 42*(3), 752-762. doi: 10.1139/t05-005

Bravo, N. J., & Schwab, G. O. (1977). Effect of Openings on Inflow Into Corrugated Drains. *Transactions of the ASABE, 20*(1), 100-104. doi: 10.13031/2013.35500

Bureau of Reclamation. (2009). Physical Properties of Plastic Pipe Used in Reclamation Toe Drains, Report DSO-09-01. *Dam Safety Technology Program*. Denver, Co: U.S. Department of the Interior, Bureau of Reclamation, Technical Service Center.

Chambers, R. E., & McGrath, T. J. (1981). *Structural Design of Buried Plastic Pipe.* Paper presented at the International Conference on Underground Plastic Pipe. Schrock, B.J., (Ed), ASCE, New Orleans, La, 10-25.

Childs, E. C., & Youngs, E. G. (1958). The Nature of the Drain Channel as a Factor in the Design of a Land-Drainage System. *Journal of Soil Science, 9*(2), 316-331. doi: 10.1111/j.1365-2389.1958.tb01923.x

Dennis, C. W., & Trafford, B. D. (1975). The effect of permeable surrounds on the performance of clay field drainage pipes. *Journal of Hydrology, 24*(3–4), 239-249. doi: http://dx.doi.org/10.1016/0022-1694(75)90083-9

Dierickx, W. (1980). *Electrolytic analogue study of the effect of openings and surrounds of various permeabilities on the performance of field drainage pipes.* Doctoral thesis, Wageningen, Merelbeke, Belgium.

Dierickx, W. (1999). Non-Ideal Drains. In R. W. Skaggs & J. van Schilfgaarde (Eds.), Agricultural Drainage (Vol. 38, pp. 297-330). Wisconsin, USA: Madison Publishers.

Dierickx, W., & Van Der Molen, W. H. (1981). Effect of perforation shape and pattern on the performance of drain pipes. *Agricultural Water Management, 4*(4), 429-443. doi: http://dx.doi.org/10.1016/0378-3774(81)90031-7

Einstein, H. H., & Schwartz, C. W. (1979). Simplified analysis for tunnel supports. *Journal of Geotechnical Engineering, ASCE, 105*(4), 499-518.

Engelund, F. (1953). *On the laminar and turbulent flows of ground water through homogeneous sand*. København, Denmark: Transactions of the Danish Academy of Technical Sciences.

Ernst, L. F. (1954). Awareness of stationary groundwater currents which can be depicted in a vertical plane. (Vol. 3, pp. 55). Groningen, The Netherlands: Land and Soil Institute T.N.O.

Ernst, L. F. (1975). Formulae for groundwater flow in areas with subirrigation by means of open conduits with a raised water level (pp. 33). Wageningen, The Netherlands: Institute for Land and Water Management Research.

Fouss, J. L. (1973). *Structural Design Procedure for Corrugated Plastic Drainage Tubing*. USDA Tech. Bulletin No.1466.

Goudarzi, B., Mohammadmoradi, P., & Kantzas, A. (2018). Direct pore-level examination of hydraulic-electric analogy in unconsolidated porous media. *Journal of Petroleum Science and Engineering, 165*, 811-820. doi: https://doi.org/10.1016/j.petrol.2018.02.068

Hagras, M. A., & Agamy, A. F. (2014). The effect of downstream perforated blanket on the safety against piping in heading-up structures. *Ain Shams Engineering Journal, 5*(1), 41-47. doi: https://doi.org/10.1016/j.asej.2013.07.008

Hazenberg, G., & Panu, U. S. (1991a). Analysis of flow into draintile in three-dimensional flow field. *Journal of Hydrology, 122*(1–4), 321-333. doi: http://dx.doi.org/10.1016/0022-1694(91)90186-L

Hazenberg, G., & Panu, U. S. (1991b). Theoretical analysis of flow rate into perforated drain tubes. *Water Resources Research, 27*(7), 1411-1418. doi: 10.1029/91wr00779

Hoeg, K. (1968). Stresses against underground structural cylinders. *Journal of Soil Mechanics and Foundation Engineering, ASCE, 94*(4), 833-858.

Hooghoudt, S. B. (1940). General Consideration of the Problem of Field Drainage by Parallel Drains, Ditches, Watercourses, and Channels. Groningen, The Netherlands: Bodemkundig Instituut.

Kirkham, D. (1950). Potential Flow into Circumferential Openings in Drain Tubes. *Journal of Applied Physics, 21*(7), 655-660. doi: doi:http://dx.doi.org/10.1063/1.1699726

Kirkham, D., & Schwab, G. O. (1951). The Effect of Circular Perforations on Flow into Subsurface Drain Tubes: Part I: Theory. *Agricultural Engineering, 32*(4), 211-214.

Kohler, A., Abbaspour, K., Fritsch, M., & Schulin, R. (2001). Functional Relationship to Describe Drains with Entrance Resistance. *Journal of Irrigation and Drainage Engineering, 127*(6), 355-362. doi: doi:10.1061/(ASCE)0733-9437(2001)127:6(355)

Krushelnitzky, R. P., & Brachman, R. W. I. (2009). Measured deformations and calculated stresses of high-density polyethylene pipes under very deep burial. *Canadian Geotechnical Journal, 46*(6), 650-664. doi: 10.1139/t09-011

Massey, F. C., Skaggs, R. W., & Sneed, R. E. (1983). Energy and Water Requirements for Subirrigation vs. Sprinkler Irrigation. *Transactions of the ASAE*, 126-133.

McWhorter, D. B., & Marinelli, F. (1999). Theory of Soil-Water Flow. In R. W. Skaggs & J. van Schilfgaarde (Eds.), *Agricultural Drainage* (Vol. 38, pp. 111-143). Wisconsin, USA: Madison Publishers.

Mohammad, F. S., & Skaggs, R. W. (1983). Drain Tube Opening Effects on Drain Inflow. *Journal of Irrigation and Drainage Engineering, 109*(4), 393-404. doi: doi:10.1061/(ASCE)0733-9437(1983)109:4(393)

Mohammad, F. S., & Skaggs, R. W. (1984). Effect of drain tube openings on drainage and subirrigation. *Transactions of the ASAE*, 1455-1462.

Moody, W. T. (1966). Nonlinear Differential Equation of Drain Spacing. *Journal of the Irrigation and Drainage Division, 92*(2), 1-10.

Moore, I. D. (1988). Static response of deeply buried elliptical tubes. *Journal of Geotechnical Engineering, ASCE, 114*(6), 672-687.

Moore, I. D. (2001). Buried Pipes and Culverts. In R. K. Rowe (Ed.), *Geotechnical and Geoenvironmental Engineering Handbook* (pp. 541-567): Springer US.

Moser, A. P. (2001). *Buried Pipe Design* (2nd ed.). USA: McGraw-Hill.

Mostaghimi, S., Lembke, W. D., & Boast, C. W. (1985). Controlled-Drainage/Subirrigation Simulation for a Claypan Soil. *Transactions of the ASAE, 28*(5), 1557-1563.

Muskat, M. (1942). The effect of casing perforations on well productivity. *Petroleum Technology, 5*, 175-187.

Myers, V. I., Rektorik, R. J., & C. A. Wolfe Jr. (1967). Deflection Tests and Trench Conditions for Plastic Drain Pipe. *Transactions of the ASABE, 10*(4), 454-457. doi: 10.13031/2013.39698

Nieber, J. L., & Feddes, R. A. (1999). Solutions for Combined Saturated and Unsaturated Flow. In R. W. Skaggs & J. van Schilfgaarde (Eds.), *Agricultural Drainage* (Vol. 38, pp. 145-212). Wisconsin, USA: Madison Publishers.

Nieuwenhuis, G. J. A., & Wesseling, J. (1979). Effect of perforation and filter material on entrance resistance and effective diameter of plastic drain pipes. *Agricultural Water Management, 2*(1), 1-9. doi: http://dx.doi.org/10.1016/0378-3774(79)90009-X

Oyarce, P., Gurovich, L., & Duarte, V. (2016). Experimental Evaluation of Agricultural Drains. *Journal of Irrigation & Drainage Engineering, 143*(4). doi: 10.1061/(ASCE)IR.1943-4774.0001134

Panu, U. S., & Filice, A. (1992). Techniques of flow rates into draintubes with circular perforations. *Journal of Hydrology, 137*(1–4), 57-72. doi: http://dx.doi.org/10.1016/0022-1694(92)90048-Z

Parker, J. J., & Willardson, L. (1981). Trench bottom effects on flexible pipe strength. *Transactions of the ASAE, 24*(5), 1188-1190.

Prasad, S. N., Alonso, C. V., & DeCoursey, D. G. (1981). Analysis of three-dimensional flows into draintile. *Journal of Hydrology, 51*(1–4), 295-303. doi: http://dx.doi.org/10.1016/0022-1694(81)90137-2

Prasher, S. O., Campbell, S. N., & Barrington, S. F. (1989). Laboratory Measurements of Head Losses From a Subirrigation Lateral. *Transactions of the ASAE, 32*(5), 1614-1618. doi: https://doi.org/10.13031/2013.31199

Rollin, A. L., Broughton, R. S., & Bolduc, G. F. (1987). Thin synthetic envelope materials for subsurface drainage tubes. *Geotextiles and Geomembranes, 5*(2), 99-122. doi: http://dx.doi.org/10.1016/0266-1144(87)90050-1

Schwab, G. O., DeBoer, D. W., & Johnson, H. P. (1969). Effect of Openings on Design of Subsurface Drains. *Journal of Irrigation and Drainage Division, (ASCE), 95*(IR1), 199-209.

Schwab, G. O., & Fouss, J. L. (1999). Drainage Materials. In R. W. Skaggs & J. van Schilfgaarde (Eds.), *Agricultural Drainage* (Vol. 38, pp. 911-926). Wisconsin, USA: Madison Publishers.

Schwab, G. O., & Kirkham, D. (1951). The Effect of Circular Perforations on Flow into Subsurface Drain Tubes: Part II: Experiments and Results. *Agricultural Engineering, 32*(5), 270-274.

Skaggs, R. W. (1973). Water Table Movement During Subirrigation. *Transactions of the ASAE, 16*(5), 988-0993. doi: https://doi.org/10.13031/2013.37678

Skaggs, R. W. (1978). Effect of Drain Tube Opening on Water-Table Drawdown. *Journal of Irrigation and Drainage Division, (ASCE), 104*(IR1), 13-21.

Skaggs, R. W. (1981). Water Movement Factors Important to the Design and Operation of Subirrigation Systems. *Transactions of the ASAE, 24*(6), 1553-1561. doi: https://doi.org/10.13031/2013.34489

Skaggs, R. W. (1991). Modeling Water Table Response to Subirrigation and Drainage. *Transactions of the ASAE, 34*(1), 169-0175. doi: https://doi.org/10.13031/2013.31640

Skaggs, R. W., & Tang, Y. K. (1979). Effect of Drain Diameter, Opening and Envelopes on Water Table Drawdown. *Transactions of the ASAE, 22*(2), 326-333.

Skaggs, R. W., Youssef, M. A., & Chescheir, G. M. (2012). DRAINMOD: Model Use, Calibration and Validation. *Transactions of the ASABE, 55*(4), 1509-1522.

Sneyd, A. D., & Hosking, R. J. (1976). Seepage flow through homogeneous soil into a row of drain pipes. *Journal of Hydrology, 30*(1–2), 127-146. doi: http://dx.doi.org/10.1016/0022-1694(76)90094-9

Spangler, M. G. (1941). *The Structural Design of Flexible Pipe Culverts*. (Bulletin 153). Ames, Iowa: Iowa Engineering Experiment Station.

Stuyt, L. C. P. M., Dierickx, W., & Beltran, J. M. (2005). *Materials for subsurface land drainage systems*. FAO Irrigation and Drainage Paper 60. Rome, Italy.

Tang, Y. K., & Skaggs, R. W. (1980). Drain Depth and Subirrigation in Layered Soils. *Journal of the Irrigation and Drainage Division, 106*(2), 113-121.

van der Molen, W. H., & Wesseling, J. (1991). A solution in closed form and a series solution to replace the tables for the thickness of the equivalent layer in Hooghoudt's drain spacing formula. *Agricultural Water Management, 19*(1), 1-16. doi: https://doi.org/10.1016/0378-3774(91)90058-Q

van der Ploeg, R. R., Horton, R., & Kirkham, D. (1999). Steady Flow to Drains and Wells. In R. W. Skaggs & J. van Schilfgaarde (Eds.), *Agricultural Drainage* (Vol. 38, pp. 213-263). Wisconsin, USA: Madison Publishers.

Vlotman, W. F., Smedema, L. K., & Rycroft, D. W. (2020a). Design of pipe drainage systems. *Modern Land Drainage: Planning, Design and Management of Agricultural Drainage Systems* (2nd ed., pp. 195-221). The Netherlands: CRC Press/Balkema.

Vlotman, W. F., Smedema, L. K., & Rycroft, D. W. (2020b). Water in the soil. *Modern Land Drainage: Planning, Design and Management of Agricultural Drainage Systems* (2nd ed., pp. 83-94). The Netherlands: CRC Press/Balkema.

Watkins, R. K., & Anderson, L. R. (2000). *Structural Mechanics of Buried Pipes*. Florida, USA: CRC Press.

Watkins, R. K., Shupe, O. K., & Willardson, L. S. (1975). Structural performance of buried plastic tubing. *Transactions of the ASAE, 18*(6), 1082-1084.

Zhang, Y., & Schaap, M. G. (2019). Estimation of saturated hydraulic conductivity with pedotransfer functions: A review. *Journal of Hydrology, 575*, 1011-1030. doi: https://doi.org/10.1016/j.jhydrol.2019.05.058

Connecting text to Chapter 3

The literature review in Chapter 2 showed that there are existing knowledge gaps about the effects of perforation characteristics on the hydraulic and structural responses of buried corrugated pipes. As a result, current analysis and design of subsurface water management systems do not incorporate variable perforation characteristics such as shape, size, and configuration. Wide variability in perforation specifications by regulatory agencies and pipe manufacturers has led to questions on whether large circular holes are better than rectangular slots in improving drainage performance. Therefore, it was imperative to investigate the effects of perforation geometry on pipe drainage in agricultural lands. In this study (Chapter 3), the entrance resistance of corrugated pipes with circular holes was established for the first time, allowing for a direct comparison of perforation geometries on the water table drawdown between parallel subsurface drains. The interaction between perforation characteristics were also assessed using a central composite design with results from 51 simulations, which were generated from a numerical model that was calibrated with sand tank experiments.

Chapter 3 was published in the *Journal of Irrigation and Drainage Engineering* (Gaj and Madramootoo, 2020a: http://dx.doi.org/10.1061/(ASCE)IR.1943-4774.0001482). The format of the manuscript has been modified here to ensure consistency with the style of this thesis. A list of the references cited in the manuscript is available at the end of the chapter.

Authorship contribution statement:

The author of this thesis was responsible for conceptualization, methodology, model development, calibration, formal analysis, investigation, data curation, and writing the original draft followed by all revisions and editing. Dr. Madramootoo provided supervision, aided in conceptualization, funding acquisition, and reviewed and edited the manuscript.

Chapter 3

Effects of Perforation Geometry on Pipe Drainage in Agricultural Lands

3.1 Abstract

Corrugated high density polyethylene pipes, where groundwater enters through perforations on the pipe wall, are widely used in subsurface drainage systems on agricultural lands. There has been a growing interest in using circular holes in the valleys of corrugated pipes to improve the hydraulic performance of subsurface drains. However, the effects of these circular perforations on the entrance resistance (α_e), delivery ratio (Q/Q_0), drain spacing, and water table drawdown have not been adequately investigated for corrugated pipes. This study uses a numerical model, calibrated with datasets from sand tank experiments, to simulate the effects of perforation shape, size, and configuration on α_e and Q/Q_0. The results show that Q/Q_0 in corrugated pipes with circular holes is 20% lower than that for plain wall pipes with the same perforation configuration. Perforations shaped as rectangular slots have half the α_e of circular holes with the same surface area. It is concluded that the use of rectangular slots is hydraulically more advantageous than circular holes in the valleys of corrugated pipes.

Author keywords: corrugated pipes, drawdown, entrance resistance, perforation, subsurface drains

3.2 Introduction

Since their introduction in the late 1970s, corrugated high density polyethylene (HDPE) pipes have largely replaced traditional clay tiles and concrete pipes as the primary material for subsurface drains on agricultural lands (Stuyt et al., 2005). These drains are used to control the position of the groundwater table as part of a water management system for crop production. Corrugated HDPE pipes used in subsurface drainage systems offer several

advantages over clay and concrete pipes. These benefits include a lower weight per unit length, easier handling and installation via mechanized plowing (Schwab and Fouss, 1999), and a higher durability with a service life in excess of 100 years (PPI, 2003). Subsurface drainage on arable lands is estimated at about 8 million ha in Canada (Madramootoo et al., 2007), 15.1 million ha in the contiguous US (Sugg, 2007), and over 9.7 million ha in Northwestern Europe (Germany, the Netherlands, UK) (AHDB, 2018; ICID, 2016; Stuyt et al., 2005).

Generally, subsurface drainage pipes have a finite number of openings or perforations distributed on the pipe wall (non-ideal drains) that allows for the entry of water from the surrounding soil. Previous studies have investigated the effect of these perforations on either the total discharge (Q) or the delivery ratio (Q/Q_0) of non-ideal drains, where Q_0 is the total discharge from a pipe with a completely porous pipe wall (ideal drain). These studies used a mixture of electrical analog models, sand tank models, and mathematical approximations. The early electrical analog models of Kirkham and Schwab (1951) were shown to be in error as they neglected the effects of the pipe wall in their model formulation (Dierickx and Van Der Molen, 1981). Sand tank models, which best satisfy Darcy's Law (Dierickx, 1999), were used by Childs and Youngs (1958) and Dennis and Trafford (1975), but were limited to clay tiles with gaps to permit water entry. Mathematical solutions were developed by Sneyd and Hosking (1976), Prasad et al. (1981), Hazenberg and Panu (1991a, 1991b), and Panu and Filice (1992). However, these analytical approaches were limited to plain wall pipes with either gaps or rectangular slots, and the solutions were often given as infinite trigonometric series with limited scope for physical interpretations and very little practical value (Dierickx, 1999).

To address some of these concerns, a study using an electrolytic analog model was undertaken by Dierickx (1980) to estimate the entrance resistance (α_e) of non-ideal drains.

The α_e is a dimensionless geometric constant that represents the additional hydraulic head loss, as a result of the convergence of the flow lines (or streamlines) towards the perforations on the pipe wall (Stuyt and Dierickx, 2006). The experimental work by Dierickx (1980), however, largely focused on validating existing analytical solutions for perforations on plain wall pipes. Dierickx (1980) also investigated corrugated pipe with slots, but no analog experiments were performed to simulate corrugated pipes with circular holes as perforations. Recently, there has been a growing interest in using fewer large circular holes in the valleys of corrugated pipes to improve the hydraulic performance of subsurface drains. For corrugated pipes, existing literature on perforations does not adequately address questions about whether rectangular slots are better than circular holes, or how perforation design variables interact with each other, or which perforation design variable has the largest effect on the hydraulic performance. In addition, the effect of slots vs. holes on drain spacing and water table drawdown has not been adequately assessed. Skaggs (1978) investigated the effect of slots on water table drawdown, but the solutions were based on the inaccurate formulation of Q/Q_0 following Bravo and Schwab (1977).

This study uses a numerical model to simulate and evaluate the effects of perforation shape, size, and configuration on two hydraulic performance indices, α_e and Q/Q_0, for HDPE pipes. The numerical model is calibrated with datasets from sand tank experiments using plain wall and corrugated HDPE pipes. The results from the numerical simulations are used to develop non-linear, multivariate prediction equations, which can be used for computing α_e and Q/Q_0 given a perforation shape, size, and configuration. Additionally, the effects of perforation shape on drain spacing and water table drawdown for a typical agricultural field are also evaluated.

3.3 Materials and Methods

A sand tank facility was fabricated at the Water Innovation Lab of McGill University to conduct a series of experiments using three physical models of perforated pipes buried in a saturated porous medium. Stuyt et al. (2005) suggested that α_e, being a theoretical concept, can be accurately computed if the flow pattern towards non-ideal drains can be modelled. The direct computation of α_e using hydraulic head measurements is based on the theory of radial flow (Appendix 3A) towards a subsurface drain flowing full with a free flowing outlet. The results from the sand tank experiments were used to calibrate and validate a three-dimensional (3D) finite-element-model of the radial flow region surrounding the pipe. The calibrated numerical model was then used to perform numerical simulations with an array of perforation shape, size, and configuration to test their effects on α_e and Q/Q_0.

3.3.1 Physical Model

Fig. 3.S1 in the supplemental data shows the experimental set-up of the sand tank facility. The sand tank walls are constructed from 12.5-mm-thick acrylic plastic, and the tank is cuboidal in shape with a 60-cm square cross section base and 100-cm height. Rainfall is simulated through a series of six sprinklers fed from an overhead 250-L supply reservoir. A control valve and overflow pipe are used to regulate and maintain a steady-state flow rate into the system. Drainage discharge is measured with a 1.8-m long rectangular flume fitted with an 11° V-notch weir. The effluent is collected in a reservoir and pumped backed to the overhead supply reservoir. A discharge chamber with gates is used to adjust the hydraulic head on the outlet pipe for submerged flow conditions. The drainage pipe's center is located 30.6 cm from the base of the tank and centrally between the side walls.

Three drainage pipe models with different perforation designs and wall profiles were used in the sand tank experiments. A plain wall HDPE pipe with circular holes (Model PWH) for

perforations allowed for the benchmarking of the numerical model and to evaluate the effects of the wall profile on α_e and Q/Q_0. The second and third models were commercially available corrugated HDPE drainage pipes with circular holes (Model CWH) and rectangular slots (Model CWS) for perforations, respectively. The perforation design for each pipe model is summarized in Table 3.1. All models were perforated at the four quarter points (shoulders and haunches) of the pipe (Fig. 3.1), where the internal stresses are usually minimal (Brachman and Krushelnitzky, 2002). For the corrugated pipe models, the perforations were placed in the valleys of the corrugation, which is common industry practice.

Table 3.1. Drainage pipe models and perforation design used in the sand tank experiments

Pipe model	ID (cm)	Perforation shape	Perforation size (cm)	N	a_y (cm)	L_T (cm)	A_p (cm^2/m)
PWH	10.16	circular holes	0.48[a]	4	2.00	30.0	36.2
CWH	10.80	circular holes	0.48[a]	4	1.64	24.7	44.1
CWS	10.80	rectangular slots	0.2 x 2.0[b]	4	3.29	26.3	48.6

Note: PWH = plain wall with holes; CWH = corrugated wall with holes; CWS = corrugated wall with slots; ID = internal diameter of pipe; N = number of perforation lines; a_y = spacing between perforations; L_T = effective length of perforations; A_p = total area of perforation per m length.
[a]diameter of holes.
[b]length of slot.

The porous medium used in the experiments was classified as a poorly graded, medium sand (SP) following the Unified Soil Classification System (USCS) guidelines (Das, 2007) based on laboratory tests carried out on representative samples. The effective size (d_{10}), coefficient of uniformity (C_U), and specific gravity (G_s), needed for estimating the saturated hydraulic conductivity (k_{sat}) of the porous medium, are 0.34 mm, 2.1, and 2.662, respectively (Please see Fig. 3.S2 and Table 3.S1in the supplemental data for the further details). The specific surface (S_s) of the soil solids is 5.36 m^2/kg and was determined following Chapuis and Légaré

(1992). The porous medium was compacted lightly in layers of approximately 50 mm thick for each pipe model.

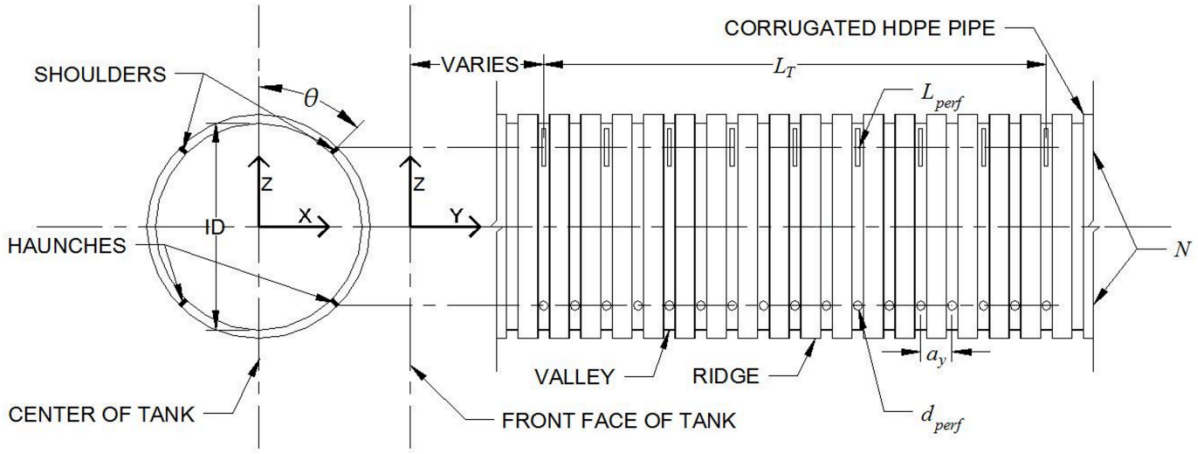

Fig. 3. 1. Definition sketch of the perforation design variables on the drainage pipe.

Note: Shoulders and haunches are the quarter points (θ = ±45°) on the circumference of the drainage pipe; N = number of perforation lines; a_y = spacing between perforations; L_T = effective length of perforations; L_{perf} = length of rectangular perforation slot; d_{perf} = diameter of circular perforation hole.

3.3.2 Sand Tank Experiments and Measurements

Steady-state experiments were carried out at four different gate levels in the discharge chamber, establishing the variable hydraulic head boundary condition on the drain outlet (H_d). The top of the first gate (10-cm in height) was approximately 39.5 cm above the datum, which is taken as the base of the tank as shown in Fig. 3.2. Successive gates (5-cm in height) were placed on top of the first gate for the other submerged flow conditions. The porous medium in the sand tank was saturated to the surface of the sand for 24 hours to obtain a constant hydraulic head boundary condition at the source (H_s). Three trials for each gate level were carried out as repetitions during all experimental runs. The tank was drained until a free surface developed at the outlet between each successive trial. Discharge and piezometric head readings were measured as the two main response state variables. The discharge was

computed from the head readings upstream of the calibrated v-notch weir (coefficient of discharge = 0.642). The weir head readings were measured with an SR-50 sonic sensor connected to a Campbell CR23X micro-logger (Campbell Scientific®, Logan, Utah) with

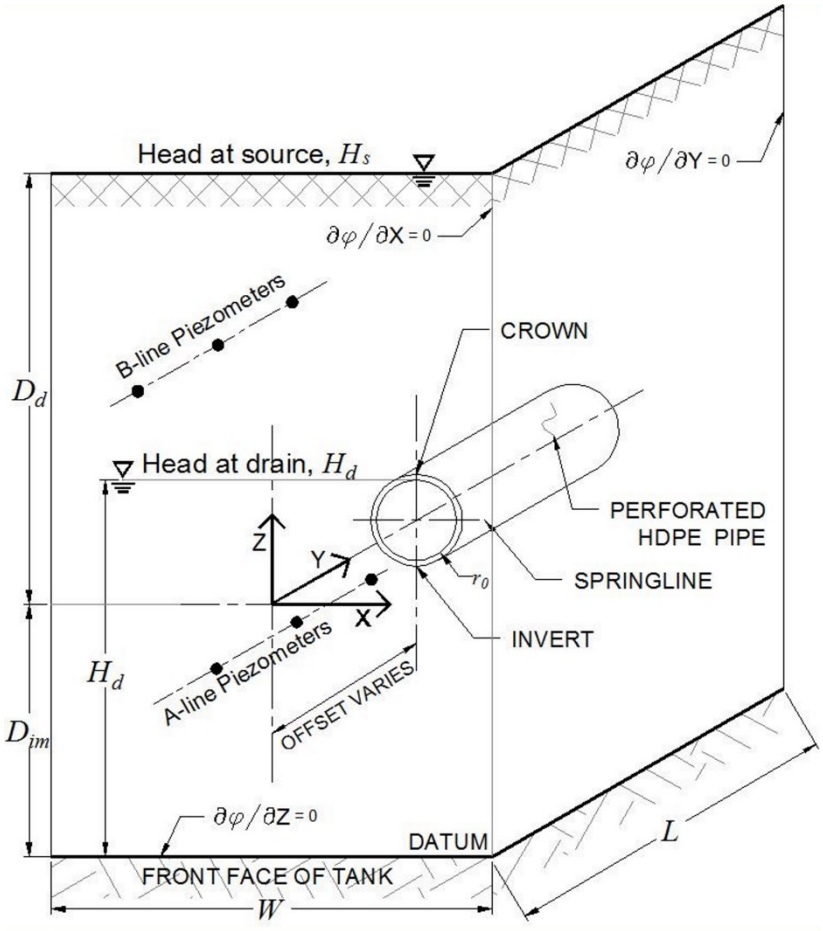

Fig. 3. 2. Definition sketch of the sand tank parameters and hydraulic boundary conditions.

Note: The A-line piezometers are located below the pipe springline (Z = 0), while the B-line piezometers are above; D_d = depth of drainage pipe from surface; D_{im} = depth to the impermeable layer below pipe; H_d = hydraulic head on the drain outlet; H_s = hydraulic head on the source; r_0 = external drain radius.

continuous real-time output. A constant weir head reading on the output display was assumed to be indicative of attaining steady-state flows during the experiments. Additionally, all measurements were recorded after a 30-min warm-up time had elapsed from the start of each experiment. Piezometric head readings were recorded using six piezometers, which were installed at two levels in the sand tank using 10 mm diameter hollow tubes. Three piezometer

ports at level A were installed 15 cm from the base and side walls. At level B, the ports were placed 55 cm from the base and 10 cm from the side wall (Fig. 3.2). The results from the sand tank experiments are given in Table 3.S2 as supplemental data.

3.3.3 Numerical Model

COMSOL Multiphysics version 5.3 (COMSOL Multiphysics, 2017a) was used to implement the numerical equivalence of the sand tank models. COMSOL's Subsurface Flow Module was used to replicate the complete geometry of the sand tank for the problem domain, to impose the constant hydraulic boundary conditions at the source and drain outlet, and to incorporate the porous medium matrix characteristics using the Darcy's law interface. COMSOL uses the finite-element-method (FEM) to solve for the dependent pressure variable, which arises from the partial differential equation (PDE) describing single-phase fluid flow through a porous media under a constant potential (COMSOL Multiphysics, 2017b). The distribution of the total hydraulic potential in the domain and the discharge fluxes through the perforations were computed as part of the post-processing stage of the numerical analysis, allowing for a direct comparison of the simulated values with the results of the sand tank experiments.

3.3.3.1 Governing Equations and Boundary Conditions

The governing equation for single-phase fluid flow in a saturated, homogeneous, and isotropic porous medium is given by the 3D Laplace PDE as:

$$\frac{\partial^2(\varphi)}{\partial X^2} + \frac{\partial^2(\varphi)}{\partial Y^2} + \frac{\partial^2(\varphi)}{\partial Z^2} = 0;\ \Omega \in (X, Y, Z) \tag{3.1}$$

where φ is the total hydraulic potential (or hydraulic head) referenced to Cartesian coordinates in the problem domain (Ω) as shown in Fig. 3.2. Eq. (3.1) is the combination of

Darcy's Law with the mass conservation principle assuming that the fluid and the porous medium matrix are incompressible and the flow is pressure driven. The total hydraulic head is taken as the sum of the pressure head and the elevation head above the datum. Eq. (3.1) is used to solve for the pressure head in COMSOL as part of the steady state boundary value problem with the following five boundary conditions:

$$\varphi_1(Z) = H_d; \in (X, Y) \tag{3.2}$$

$$\varphi_2(Z) = H_s = D_d + D_{im}; \in (X, Y) \tag{3.3}$$

$$\left(\frac{\partial \varphi}{\partial X}\right)_{X=X_1} = 0; \in (Z, Y) \tag{3.4}$$

$$\left(\frac{\partial \varphi}{\partial Y}\right)_{Y=Y_1} = 0; \in (X, Z) \tag{3.5}$$

$$\left(\frac{\partial \varphi}{\partial Z}\right)_{Z=D_{im}} = 0; \in (X, Y) \tag{3.6}$$

where D_d is the depth of the drainage pipe from the surface, and D_{im} is the depth to the impermeable layer below the pipe (Fig. 3.2). The boundary conditions described by Eqs. (3.2) and (3.3) are Dirichlet type (prescribed hydraulic head), while Eqs. (3.4), (3.5), and (3.6) are Neumann type (prescribed no-flow surface). Importantly, the boundary condition of the drainage pipe wall in the numerical model is also prescribed as a no-flow surface with the exception of the perforated areas. The Dirichlet boundary condition given by Eq. (3.2) is prescribed at the surface of the perforation between the porous medium and the pipe. This soil-pipe interface forms a plane boundary with the perforation surface (Dierickx, 1999). For the condition of the pipe with radius, r_0, flowing full with a free-flow outlet, H_d in Eq. (3.2)

is $D_{im} + r_0$. Symmetry along the ZY plane at the center of the model was implemented to reduce computational time and increase efficiency.

3.3.3.2 Discretization and Calibration

The discretization of the numerical model domain was done with the aid of COMSOL's physics-controlled mesh generator. A mesh refinement study was done to determine suitable mesh parameters at which the model output converges to a solution as the number of elements increases. Several built-in mesh settings ranging from "Coarse" to "Finer" (Table 3.S3) were used in the refinement study. The mesh refinement was terminated after adjustments to obtain a relative error of less than 1% between successive output response at convergence. The final mesh selected had the smallest elements (1.5 mm) at the perforations on the pipe wall (Fig. 3.S3).

After mesh refinement, the numerical model was calibrated using k_{sat} as the calibration parameter and Q as the response variable (Figs. 3.S4, 3.S5, and 3.S6). An initial estimate of k_{sat} was computed with two prediction equations, the Kozeny-Carman (KC) equation (Chapuis and Aubertin, 2003) and a pedo-transfer function (Mbonimpa et al., 2002). These two k_{sat} equations were selected based on the recommendations of Chapuis (2012) who evaluated several predictive functions for non-plastic soils.

Three performance statistics (Appendix 3.B) were used to compare the measured and simulated datasets for the calibration of the numerical model. Legates and McCabe (1999) recommend at least one absolute and one relative statistical indicator when assessing model performance. The root mean square error (RMSE) was chosen as an absolute indicator, while the Nash-Sutcliffe efficiency (NSE) (Nash and Sutcliffe, 1970) and the percentage bias (PBIAS) were chosen as two relative indicators (Table 3.S4). Further details of the mesh study and model calibration are given as supplemental data.

3.3.3.3 Benchmarking the numerical model

A closed-form analytical solution of radial planar flow was used as a benchmark for the numerical model and to check the influence of the tank's width (W) and depth on the radial flow convergence towards the pipe. The radial distance to the side wall was taken as half the tank width ($r = W/2$) as measured from the center of the drainage pipe. For a completely porous drainage pipe (ideal drain) buried in a saturated, homogenous, isotropic, and incompressible porous medium, the radial planar flow is given as (Selvadurai, 2000):

$$Q_{0a} = \frac{2\pi k_{sat} L_0 (\varphi_2 - \varphi_1)}{ln\left(r/r_0\right)} \tag{3.7}$$

where Q_{0a} is the analytical total discharge, L_0 is the length of the fully porous drainage pipe, φ_2 is the hydraulic potential at a radial distance (r), and φ_1 is the hydraulic potential on the surface of the drainage pipe with radius r_0. For a direct comparison with Eq. (3.7), Model PWH was modified to simulate a fully porous pipe wall (Model PWF). The adjustment was done by removing the perforations to create a simple geometry with a lower number of elements, reducing the computational time after discretization. Then, H_d was prescribed across the pipe wall to represent a fully porous surface. Benchmark simulation results with Model PWF were then compared against the solution of Eq. (3.7) for various values of r and D_{im}.

3.3.4 Numerical Simulations of Entrance Resistance and Delivery Ratio

After calibration, the three finite element models (one for each of the three pipe models) were used to simulate the effects of perforation shape, size, and configuration on α_e and Q/Q_0. Hydraulic heads in the approach flow zone (H_a) were measured using 72 point probes in the numerical model, and the computation of α_e was done using the H_a dataset in accordance with the radial flow theory (Appendix 3.A). Dierickx (1999) stated that for plain wall pipes the total number and diameter of perforations had the largest effect on α_e, while the pipe radius

was less important. Similarly, the total number of slots had a larger effect on α_e than the slot width (Dierickx, 1999). Based on these earlier findings, three main perforation design variables were selected as inputs for the numerical simulations in this research: the number of perforation lines along the pipe length (N), the longitudinal spacing between the perforations (a_y), and the perforation diameter (d_{perf}) or length (L_{perf}) for circular holes or rectangular slots, respectively (Fig. 3.1). In addition, only pipes with a nominal 100-mm diameter were used in the numerical simulations, since a design variable screening exercise (not presented) showed that α_e is not significantly different for drainage pipes with 75 mm and 150 mm diameters under the same perforation design.

A statistical-based approach in the form of a central composite design was used for the experimental design of the numerical simulations. The central composite design is a class of second-order designs used in fitting response surfaces (Myers et al., 2016). In this study, the central composite design was used to test for the effect of the perforation design variables and their interaction on the output variable (or response). The design was also used to develop non-linear, multivariate prediction equations using both α_e and Q/Q_0 as responses in the regression model:

$$y = \beta_0 + \sum_{i=1}^{k} \beta_i x_i + \sum_{i=1}^{k} \beta_{ii} x_i^2 + \sum_{i=1}^{k-1} \sum_{j=i+1}^{k} \beta_{ij} x_i x_j + \varepsilon \quad (3.8)$$

In Eq. (3.8), y is the response variable; x_i, x_j (i = 1, 2, 3; $j = i + 1$, 3) are the independent design variables with k design levels; $x_1 = N$; $x_2 = d_{perf}/L_{perf}$; $x_3 = a_y$; β_0 is the intercept (constant) term; β_i, β_{ii}, and β_{ij} are the linear, quadratic, and bilinear (interaction) least square regression coefficients, respectively; and ε is the model error (Myers et al., 2016). The design variables and their associated levels (k) used in the numerical simulations are summarized in Table 3.2. The values for the design levels were selected based on current perforation specifications from corrugated pipe manufacturers, and represent the physical limits of the

design variables (d_{perf}, L_{perf}, and a_y). The low levels are the minimum specified values, while the high levels are the maximum specified values for the design variables. The medium level is simply the average of the high and low levels. Only a maximum of 10 perforation lines is permitted for Model CWS, because the combination of N and L_{perf} is limited by the pipe circumference. Similarly, the maximum d_{perf} is limited to 0.56 cm by the width of the pipe's corrugation valley (0.61 cm). The minimum a_y of 1.645 cm represents a perforation in every valley, while a perforation in every second and third valley is represented by the medium and high level values, respectively. Therefore, the maximum number of perforations is obtained with combinations of high N and low a_y values. The statistical design of the numerical simulations and the analysis of variance (ANOVA) of the results were achieved using JMP Version 14 (SAS Institute Inc., 2018). The ANOVA was used to test for the significance (5% level) of the design variables and to assess the goodness of fit of the prediction equations.

Table 3.2. Design variables and design levels (k) used in the numerical simulations

Model	Design variable	Design level		
		Low	Medium	High
PWH and CWH	N	2	12	22
	d_{perf} (cm)	0.44	0.50	0.56
CWS	N	2	6	10
	L_{perf} (cm)	1.00	1.75	2.50
PWH, CWH, and CWS	a_y (cm)	1.645	3.290	4.935

Note: For the design variables low levels are the minimum specified values; high levels are the maximum specified values; medium levels are the average of the high and low levels; d_{perf} = diameter of hole; L_{perf} = length of slot.

3.4 Results and Discussion

3.4.1 Physical Model Experiments

The measured values of discharge (Q_m) ranged between 1.01 and 1.49 x10^{-4} m^3/s across all three pipe models used in the sand tank experiments (Table 3.S2). The observed piezometric head (H_{PZO}) varied between 60.2 to 69.5 cm and 70.3 to 79.6 cm for the A and B level

piezometers, respectively. Reliable H_{PZO} measurements for a fourth gate level with Model CWS were not obtainable from the experiments, because a constant head level on the sand surface could not be maintained. This effect may be due to the fact that Model CWS had the largest total perforation area (A_p) of the three models. Also, the k_{sat} was highest in the experiments with Model CWS due to the repacking of the sand tank. The repacking was done to facilitate a change in pipe models for the experiments.

In order to prevent a high exit gradient at the soil-pipe interface, which would result in local erosion around the perforations (Dierickx, 1983; Stuyt et al., 2005), the sand tank experiments were conducted under submerged conditions. The porous medium was first saturated from the outlet pipe to reduce the exit gradient before turning on the sprinklers. The submerged outlet conditions created a back pressure, equal to H_d, on the surface of the pipe wall. Hence, the trend of Q_m decreasing with increasing H_d in Table 3.S2 is expected, since the difference in total hydraulic head (ΔH) is also reducing. The effects of the increase in back pressure are also shown in the H_{PZO} datasets as both levels of piezometer readings increase with H_d for each model.

Models PWH and CWH had circular holes of the same size (d_{perf} = 0.48 cm) for perforations and a similar configuration on the pipe wall. However, a direct comparison between Q_m and H_{PZO} (Table 3.S2) for these two models would not be accurate, since the in-situ void ratio (e) changed after the sand was repacked. Similarly, it would be erroneous to use the datasets from the sand tank experiments to assess the effect of perforation shape, i.e. hole vs. slot, between the two corrugated models (CWH and CWS) due to repacking. These changes in e result in changes in k_{sat} and highlight a major limitation of using sand tank models to experiment on α_e (Dierickx, 1999). The use of a numerical model, therefore, effectively overcomes this drawback and allows for the examination of perforations on subsurface

drainage pipes in greater detail. As such, the datasets in Table 3.S2 were used to calibrate and verify the numerical models. The calibration results are presented as supplemental data.

3.4.2 Influence of Tank Width on Radial Flow

The pipe wall in Model PWH was modified to simulate a fully porous boundary (Model PWF), and simulations were carried out to check the influence of the sand tank's side wall and base on radial planar flow. Fig. 3.3 shows the results from these simulations for various values of r (W/2) and D_{im}, which were each increased in increments of 20 cm up to 340 cm and 110.6 cm, respectively. The analytical solution of radial planar flow towards a fully porous pipe [Eq. (3.7)] was used as a benchmark for the simulation results. The results in Fig. 3.3 show that the flow, for all combinations of r and D_{im}, generally converges to the analytical solution of Q_{0a} (6.56 x 10^{-4} m^3/s) as computed for H_d = 40.1 cm. The effect of the tank wall is more pronounced than that of the tank depth up to r = 140 cm. The

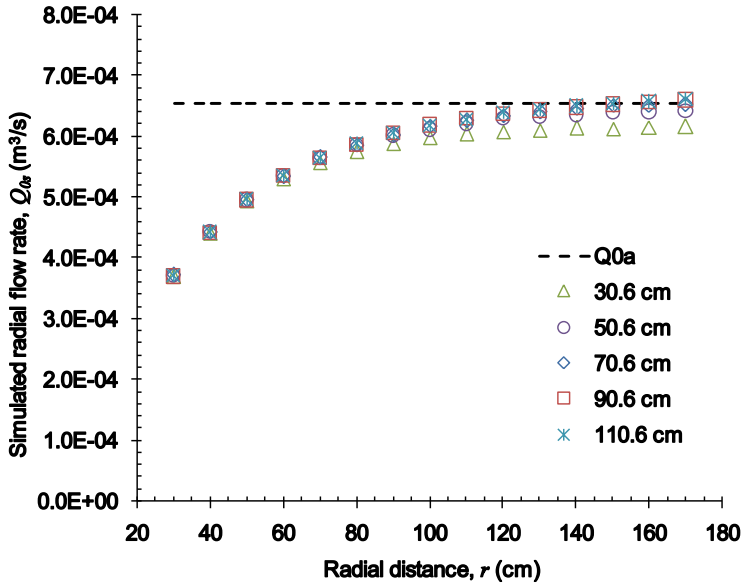

Fig. 3. 3. Variation of Q_{0s} with the tank width, W (r = W/2) and depth, D_{im} for Model PWF at H_d = 40.1 cm.

Note: Q_{0a} is the analytical discharge of an ideal drain under radial planar flow.

underestimation of the simulated flow rate (Q_{0s}) for r < 140 cm is due to the elongation of the converging streamlines caused by a constricted side wall. Therefore, to achieve full radial

planar flow towards the drainage pipe in the numerical simulations, r was adjusted to 150 cm from the drain center. The adjusted D_{im} was selected as 70.6 cm where the percent error between the Q_{0a} and Q_{0s} was less than 1%, which is generally acceptable in simulations (Cihan and Tyner, 2011).

As a final evaluation and benchmark of Model PWF, Q_{0s} was simulated with the adjusted tank dimensions (W/2 = 150 cm, D_{im} = 70.6 cm) and compared to Q_{0a} over a series of H_d values up to 55.1 cm as shown in Fig. 3.4. The simulated values all lie virtually on the equality (1:1) line, indicating an almost perfect fit. Therefore, these results confirm that adjusting half the tank width to 150 cm and depth to 70.6 cm in the numerical models will allow for the simulation of radial planar flow towards the drainage pipe.

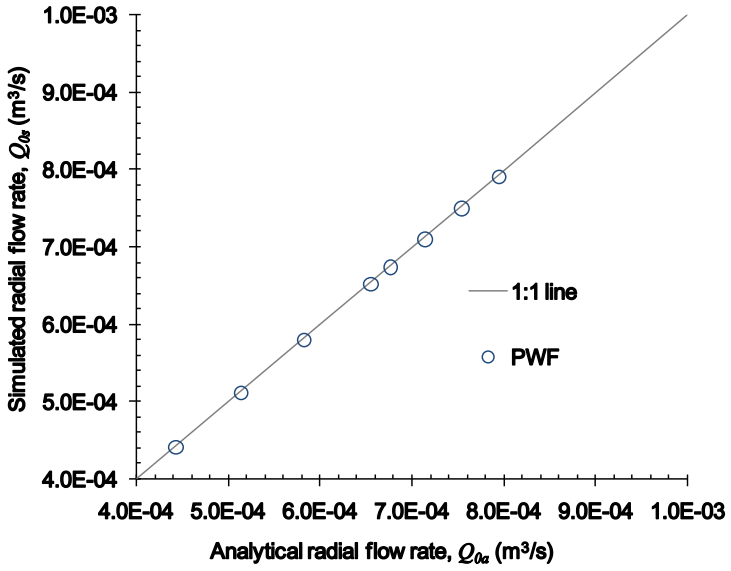

Fig. 3. 4. Comparison of Q_{0a} and Q_{0S} for model PWF with the adjusted tank dimensions and values of H_d up to 55.1 cm.

3.4.3 Entrance Resistance and Delivery Ratio

The statistical design using the central composite design yielded a total of 17 experimental runs per numerical model, comprising eight factorial points, six axial points, and three center points (please see Table 3.S5 in the supplemental data for the design matrix). Each point represents a specific combination of the three perforation design variables (N, d_{perf}/L_{perf}, and

a_y) at a given design level (Table 3.2). The combination of the design variables is limited by the circumference and corrugation profile of the pipe. The region of operability is therefore restricted in the analysis as extreme design points may take on unrealistic values. For example, the axial distance for three design variables is 1.682 for a rotatable central composite design (Myers et al., 2016). However, using this value for the axial distance produces negative N values at the axial points, which has no physical basis. Consequently, the axial distance for this study was selected as 1.0, which yields a face-centered cube with the axial points at the center of each cube face. The loss of rotatability is deemed trivial for this design since the region of interest is now cuboidal instead of spherical (Myers et al., 2016). A total of 51 experimental runs was simulated for the three numerical models to generate the datasets for computing the two responses: α_e and Q/Q_0. The computed responses are given as supplemental data (Table 3.S6).

Each set of responses was fitted to a second-order regression model with interaction using Eq. (3.8) with JMP Version 14 (SAS Institute Inc., 2018). An ANOVA was performed to statistically assess the resulting prediction models. The goodness of fit of the prediction models was assessed by the coefficient of determination (R^2) for which the lowest values of α_e and Q/Q_0 were 99.82 and 99.08 %, respectively. The ANOVA showed that the six prediction models were statistically significant ($p<0.0001$). The summary results of the model fit and ANOVA are given in the supplemental data (Tables 3.S7 and 3.S8). The full quadratic regression model, which contains all nine terms of Eq. (3.8) including the squared and interaction terms of the three design variables, was first evaluated for statistical significance. Terms that were not statistically significant ($p>0.05$) were removed and the regression model was refitted to Eq. (3.8) to produce the final refined model. The test for lack of fit also assesses how well the prediction model fits the response dataset. A low p-value ($p<0.05$) for lack of fit indicates a poor fit (Myers et al., 2009). All six refined prediction models (non-

significant terms removed) had p-values greater than 0.538 for the lack of fit test, indicating a good fit between the design variables and the response. Therefore, considering only the significant effect terms, the refined predictive models are:

$$PWH: \log_e \alpha_e = 0.419 - 0.214N - 1.325d_{perf} + 0.243a_y + 0.006N^2 - 0.005N \times a_y \quad (3.9)$$

$$PWH: Q/Q_0 = -0.067 + 0.044N + 0.502d_{perf} - 0.039a_y - 0.001N^2 \quad (3.10)$$

$$CWH: \log_e \alpha_e = 0.390 - 0.223N - 0.918d_{perf} + 0.268a_y + 0.006N^2 - 0.004N \times a_y \quad (3.11)$$

$$CWH: Q/Q_0 = 0.117 + 0.029N - 0.182d_{perf} - 0.090a_y + 0.030N \times d_{perf} - 0.002N \times a_y + 0.001N^2 + 0.010a_y^2 \quad (3.12)$$

$$CWS: \log_e \alpha_e = 0.328 - 0.433N - 0.295L_{perf} + 0.286a_y + 0.015N \times L_{perf} - 0.007N \times a_y - 0.024L_{perf} \times a_y + 0.022N^2 \quad (3.13)$$

$$CWS: Q/Q_0 = 0.080 + 0.060N + 0.038L_{perf} - 0.065a_y + 0.004N \times L_{perf} - 0.002N \times a_y - 0.003N^2 + 0.007a_y^2 \quad (3.14)$$

where d_{perf}, L_{perf} , and a_y are in cm. The response variable, α_e, as given by Eqs. (3.9), (3.11), and (3.13) was logarithmically transformed in accordance with the Box-Cox transformation for $\lambda = 0$ (Box and Cox, 1964), since α_e follows a log-normal distribution. Importantly, Eq. (3.11) allows for the computation of the entrance resistance for corrugated pipes with circular holes, which has not been previously reported.

3.4.3.1 Interaction Effects

The significant terms of the six prediction models were ranked using the LogWorth values, defined as $-\log_{10}$ (p-value), which is a scale adjustment to the model terms for very low p-values (SAS Institute Inc., 2018). Table 3.3 summarizes and ranks the LogWorth for the six prediction models. The ranking shows that the design variable *N,* which represents the number of perforation lines along the pipe, has the largest effect on α_e and Q/Q_0 for both plain and corrugated drainage pipes. In fact, the results in Table 3.3 show that the two design variables that control the geometric configuration of the perforations, N and a_y (perforation spacing along pipe length), have the largest influence on the two hydraulic performance indices (α_e and Q/Q_0). The ranked effects show that N and a_y are the most effective design variables to maximize Q/Q_0 and decrease α_e. The results in Table 3.3 also indicate that the perforation size parameters, d_{perf} and L_{perf}, generally do not have a large influence on α_e and Q/Q_0. The exception is L_{perf} in Model CWS, which indicates that the perforation slot length has a large effect on the discharge. These findings from the numerical and statistical modelling applied in this study support those of the electrical analogs for plain wall pipes with slots and holes as demonstrated by Dierickx (1980), who concluded that perforations with the smallest dimensions and greatest number are favorable for reducing α_e.

Table 3.3. Summary of design variables and all interaction effects ranked by LogWorth (higher values indicate greater effect)

Entrance Resistance, α_e			Delivery Ratio, Q/Q_0		
PWH	CWH	CWS	PWH	CWH	CWS
N (16.252)	N (16.857)	N (12.093)	N (12.390)	N (11.454)	N (9.355)
$N * N$ (12.086)	$N * N$ (12.620)	a_y (9.533)	a_y (6.500)	a_y (7.470)	a_y (6.617)
a_y (11.059)	a_y (12.248)	$N * N$ (8.040)	$N * N$ (6.159)	$N * N$ (5.578)	L_{perf} (5.952)
d_{perf} (5.034)	$N * a_y$ (4.494)	L_{perf} (7.770)	d_{perf} (3.290)	d_{perf} (4.573)	$N * N$ (3.806)
$N * a_y$ (4.704)	d_{perf} (3.938)	$N * L_{perf}$ (2.239)		$N * a_y$ (3.324)	$N * a_y$ (1.640)
		$N * a_y$ (2.102)		$N * d_{perf}$ (2.438)	$N * L_{perf}$ (1.495)
		$L_{perf} * a_y$ (1.359)		$a_y * a_y$ (2.159)	$a_y * a_y$ (1.487)

Note: N = number of perforation lines; a_y = spacing between perforations; d_{perf} = diameter of holes; L_{perf} = length of slots.

3.4.3.2 Effect of Pipe Wall Profile

Dierickx and Van Der Molen (1981) highlighted the importance of accounting for the pipe wall as an impermeable boundary when computing α_e. The exact shape of the corrugation, i.e. a sine wave or a block wave, has a negligible influence on the α_e in corrugated pipes (Stuyt et al., 2005). For perforations placed on the crown of the corrugations, the analytical solutions for plain wall pipe can be used to compute α_e (Dierickx, 1999). However, when perforations are placed in the valleys, the depth of the corrugation introduces an additional head loss. No previous work has investigated this effect on α_e and Q/Q_0 for corrugated pipes with circular holes as the perforation shape. To demonstrate the effect of the corrugations, Eqs. (3.9) to (3.12) were used to compute α_e and Q/Q_0 for Models PWH and CWH. The perforation diameter was set at 0.56 cm (d_{perf}) and the spacing was 1.645 cm (a_y), which represents a perforation in every corrugation valley for Model CWH. Computations were done for the full design range of N between 2 and 22 lines (Table 3.2). The entrance resistance results (Fig. 3.5a) show that α_e decreases with increasing A_p, which is the total perforation area common

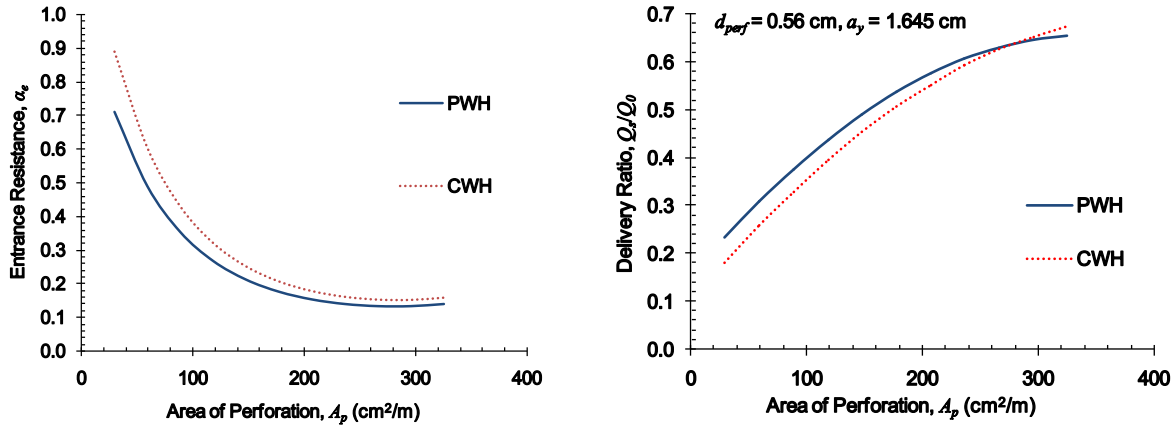

(a) (b)

Fig. 3. 5. The effects of wall profile on α_e (a) and Q/Q_0 (b) for pipes perforated with holes.

to both Models PWH and CWH. Fig. 3.5a shows that α_e for corrugated pipes with holes are higher than those for plain wall pipes. The difference in α_e between Models PWH and CWH varies from 0.019 to 0.17 with Model CWH giving values that are 18.2% greater on average.

This larger α_e results from the convergence of the streamlines in the corrugation valley before further contracting towards the circular perforation. For the special case with four lines of perforation ($N = 4$), A_p is approximately 60 cm^2/m and the difference in α_e is as large as 23%.

In contrast, Fig. 3.5b illustrates that the delivery ratio increases with A_p and is generally greater for Model PWH. However, Q/Q_0 becomes larger for Model CWH when the perforation area exceeds 296 cm^2/m, which corresponds to $N \geq 20$ lines in this example. This change in trend can be attributed to the difference in the effects of the N variable between the two prediction models. Model CWH has four effect terms with the N variable, while Model PWH only has two for the Q/Q_0 response (Table 3.3). Thus, as N increases, these effects become dominant and Q/Q_0 increases faster for Model CWH. It is also important to note that at such large perforation areas the effect of the pipe wall on α_e also diminishes (Fig. 3.5a). The delivery ratio for corrugated pipes with circular holes is about 20% lower than that for plain wall pipes having four lines of perforation with the same size and spacing (A_p = 60 cm^2/m).

3.4.3.3 Effect of Perforation Shape with Corrugated Pipes

The effect of the perforation shape on α_e and Q/Q_0 for corrugated pipes was investigated using Eqs. (3.11) to (3.14). In order to keep the perforation area constant between holes and slots, the slot length was computed to match the area of a single 0.56 cm diameter hole. For a 0.2 cm wide slot, an L_{perf} of 1.23 cm was computed. As before, a_y was set at 1.645 cm to represent a perforation in every corrugation valley. In this investigation of the shape effect, the upper range of N was limited to 10 lines (Table 3.2) as was used in the experimental design for Model CWS. Fig. 3.6a shows the decrease of α_e with A_p for both Models CWH and CWS. The difference in α_e varies from 0.06 to 0.2 between the two models. On average, α_e is two times greater (51%) for corrugated pipes with holes than those with slots of the same size. This difference may be explained by the orientation and distribution of the perforation

area on the pipe wall. The length of a slot is distributed along the circumference of the pipe wall, resulting in the streamlines that closely follows a radial planar flow convergence pattern (2D in the X-Z plane). In contrast, a circular hole of the same area contracts the streamlines in the XYZ dimensions, causing additional losses in hydraulic head at the entrance. For corrugated pipes with four lines of perforations (A_p = 60 cm^2/m), α_e is 57% higher if circular holes are used instead of slots with the same area.

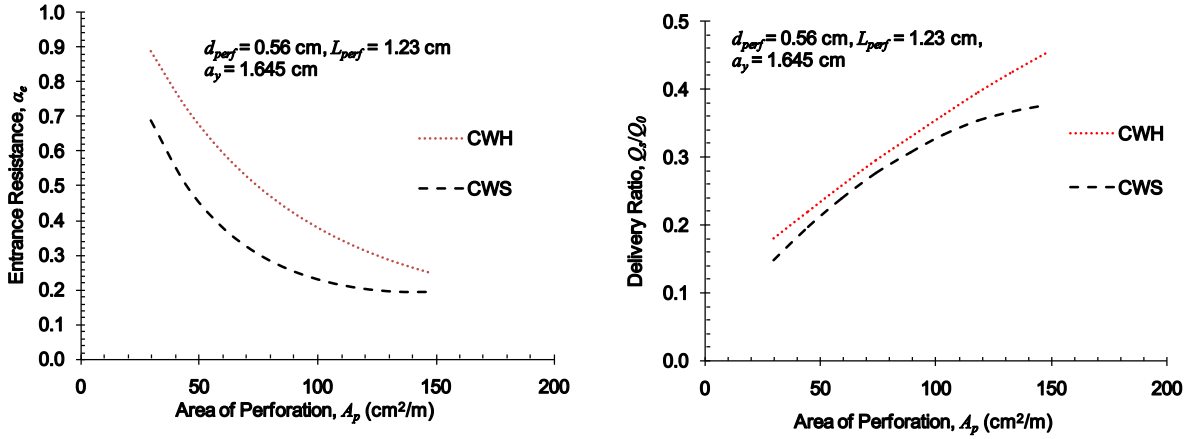

(a) (b)

Fig. 3. 6. The effects of perforation shape on α_e (a) and Q/Q_0 (b) for corrugated pipes.

Fig. 3.6b shows the increase in Q/Q_0 with A_p for Models CWH and CWS. The results show that corrugated pipes with holes yield a marginally higher (12% on average) discharge than those with slots. Notably, the difference in Q/Q_0 increases as the perforation area gets larger, which may also be explained by the effects of the variable N between the two prediction models. The N^2 effect term for Model CWH is ranked higher than that of Model CWS for the Q/Q_0 response (Table 3.3). Therefore, Q/Q_0 also increases faster for corrugated pipes with holes than those with slots as N increases. In comparison, Panu and Filice (1992) also concluded that circular holes produce a higher flow rate than rectangular slots of the same area. However, their research was limited to plain wall pipes, it considered only Q/Q_0, and they assumed a hydraulic potential of zero at the pipe radius, rendering their mathematical formula unsuitable for practical drainage applications. For corrugated pipes with four lines of

perforations (A_p = 60 cm^2/m), Q/Q_0 is only 8% higher if circular holes are used instead of slots with the same area. Hence, it would be more favourable to use corrugated pipes with slots to have a lower entrance resistance, rather than holes for a marginally larger discharge.

3.4.4 Application to Subsurface Drainage Design

The following example demonstrates the anticipated effect of perforations on drain spacing and water table drawdown for a typical agricultural field in Ormstown, Québec, Canada. The soil type in this region is a silt loam soil with a mean k_{sat} of 2.66 x 10^{-6} m/s and drainable porosity (f) of 0.027 m^3/m^3 (Rollin et al., 1987). For this analysis, a drainage system consisting of 100-mm-diameter corrugated HDPE pipes placed at an average depth of 1.5 m from the surface (D_d) and designed for a drainage coefficient (q) of 10 mm/d was assumed.

Hooghoudt's formula [Eq. (3.15)] was used to determine suitable values of drain spacing (S) for the field given a midpoint water table elevation (H_w) of 100 cm above the drain level; and is based on two-dimensional (2D) steady state flow using potential flow theory (Van der Ploeg et al., 1999):

$$q = \frac{8k_{sat}d_eH_w + 4k_{sat}H_w^2}{S^2} \tag{3.15}$$

where d_e is the equivalent depth to the impermeable layer below the drain. In the derivation of Eq. (3.15), it is assumed that the pipe is an ideal drain; and d_e is a function of D_{im}, r_0, and S (Moody, 1966). In order to account for perforations, Childs and Youngs (1958) introduced the concept of effective radius (r_e) where an ideal pipe with a smaller radius can be used as a substitute for r_0 in non-ideal drains. The α_e values for corrugated pipes with holes and slots of the same opening area (from the previous section) were used to compute r_e as:

$$r_e = (r_0)e^{-2\pi\alpha_e} \tag{3.16}$$

The corresponding d_e values were then computed from Eqs. (3.17) to (3.19) as given by Moody (1966):

$$d_e = \frac{D_{im}}{1+\frac{D_{im}}{S}\left[\frac{8}{\pi}\ln\left(\frac{D_{im}}{r_e}\right)-\zeta\right]}; 0 < \frac{D_{im}}{S} < 0.3 \tag{3.17}$$

$$\zeta = 3.55 - \frac{1.6D_{im}}{S} + 2\left(\frac{D_{im}}{S}\right)^2 \tag{3.18}$$

$$d_e = \frac{S\pi}{8\left[\ln\left(\frac{S}{r_e}\right)-1.15\right]}; \frac{D_{im}}{S} > 0.3 \tag{3.19}$$

The calculations show that corrugated pipes with slots generally yield a larger S than those with holes for an assumed D_{im} of 2.0 m below the drain level. For values of N between 2 to 10, S varies between 14.1 m to 16.3 m and 13.6 m to 16.0 m for corrugated pipes with slots and holes, respectively. Considering the special case of corrugated pipes with four lines of slots, S was computed as 15.3 m, which is 0.9 m greater than that for pipes with holes of the same size. For comparison, S is approximately 17.6 m for an ideal drainage pipe (α_e = 0), which shows that the entrance loss from perforations can account for at least 2.3 m difference (13.1%) in spacing between two parallel subsurface drains.

The water table drawdown for corrugated pipes with four lines of perforations was also computed to assess the effects of the perforation shape. The non-steady drawdown is based on the Van Schilfgaarde (1963) solution to the Boussinesq equation for the falling water table case given as (Huffman et al., 2013):

$$s = \left[\frac{9td_ek_{sat}}{f\ln\left(\frac{b_0(2d_e+b)}{b(2d_e+b_0)}\right)}\right]^{1/2} \tag{3.20}$$

where b_0 is the initial depth of the water table below the soil surface at $t = 0$. Fig. 3.7 shows the water table drawdown (b) at the midpoint between two parallel drains as computed using Eq. (3.20) for $S = 15.0$ m and $b_0 = 0.5$m.

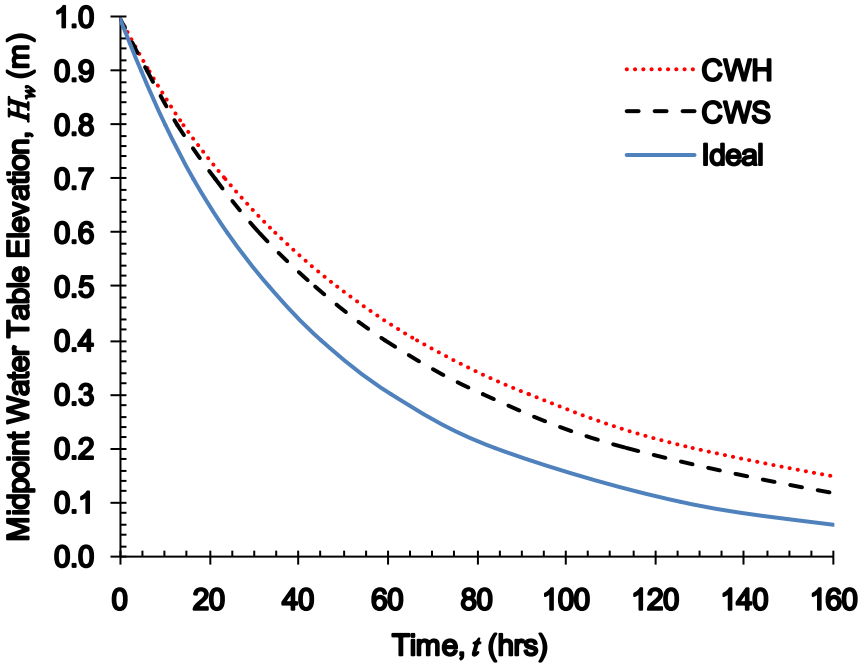

Fig. 3. 7. Water table elevation and drawdown at the midpoint between two parallel drains.

The results indicate that the drawdown rate is marginally faster for corrugated pipes with slots (CWS) when compared to those with holes (CWH) that have the same opening area. The difference between the drawdown was tested for statistical significance (5% level) based on the Welch's t-test (Moser and Stevens, 1992). The results (not presented) show that the difference between the drawdown for CWS and CWH is not statistically significant ($p = 0.785$), indicating that the perforation shape does not significantly affect the water table drawdown for $N = 4$ and $A_p = 60$ cm^2/m. In practice, however, it would be more efficient to increase L_{perf} to its maximum limit (2.5 cm) in order to take advantage of a larger opening area and facilitate a faster water table drawdown.

3.5 Summary and Conclusions

In this study, a numerical model, validated by results from sand tank experiments, was used to estimate α_e and Q/Q_0 of water flow through perforated subsurface drainage pipes. The radial flow region around plain wall and corrugated 100 mm diameter pipes was modelled using the COMSOL Multiphysics finite element code. Numerical simulations, based on a central composite design, were carried out with the following design variables: number of perforation lines ($2 \leq N \leq 22$), diameter of circular holes (0.44 cm $\leq d_{perf} \leq$ 0.56 cm), length of rectangular slots (1.00 cm $\leq L_{perf} \leq$ 2.50 cm), and longitudinal spacing between perforations (1.645 cm $\leq a_y \leq$ 4.935 cm). Finally, six non-linear multiple regression models were developed using the results from the numerical simulations, which can now be used to predict α_e and Q/Q_0 with the perforation design variables as input.

This study assessed the effect of the pipe wall profile on α_e for pipes with 0.56 cm diameter holes. The results showed that corrugated pipes with holes have a higher α_e than plain wall pipes with the same perforation configuration due to the convergence of streamlines in the corrugation valley. For the special case of N = 4 (A_p = 60 cm^2/m), α_e is 23% higher in corrugated pipes when compared to plain wall pipes. In contrast, Q/Q_0 is 20% lower for corrugated pipes with holes than that for plain wall pipes also having an A_p of 60 cm^2/m.

The effect of the perforation shape in corrugated pipes was also investigated for perforations having the same opening area and configuration. The results showed that α_e is 51% higher for corrugated pipes with holes, than those with slots of the same opening area. The difference in α_e results from the extra contraction of the streamlines around the circular holes in the XYZ dimensions, causing a higher loss in hydraulic head. However, Q/Q_0 is marginally greater for corrugated pipes perforated with holes under the same conditions. It is concluded that the use of rectangular slots is more hydraulically advantageous than circular holes in the valleys of

corrugated pipes. This study also assessed the anticipated effects of the perforation shape on drain spacing and water table drawdown for corrugated pipes. The results indicate that the drawdown at the midpoint between two parallel drains is not significantly different between holes and slots for $N = 4$ and $A_p = 60$ cm^2/m. Overall, with regards to the interest in using circular holes, the findings of this study demonstrate that rectangular slots are the better choice for improving the hydraulic performance of subsurface drains used in water management systems for crop production.

3.6 Acknowledgments

Funding for this research was provided by the Natural Science and Engineering Research Council of Canada (NSERC) and the James McGill Professor research award held by C. A. Madramootoo. The authors would like to thank the students in the Water Innovation Lab for assisting with the set-up of the sand tank facility and all laboratory testing. The authors are also grateful for the reviewers' comments during the review process.

3.7 References

AHDB (Agriculture and Horticulture Develpoment Board). (2018). *Field drainage guide: Principles, installations and maintenance*. Warwickshire, UK.

Box, G. E. P., and Cox, D. R. (1964). "An Analysis of Transformations." *J. R. Stat. Soc. B.*, 26(2), 211-252.

Brachman, R. W. I., and Krushelnitzky, R. P. (2002). "Stress Concentrations Around Circular Holes in Perforated Drainage Pipes." *Geosynth. Int.*, 9(2), 189-213.

Bravo, N. J., and Schwab, G. O. (1977). "Effect of Openings on Inflow Into Corrugated Drains." *Trans. ASABE*, 20(1), 100-104.

Chapuis, R. P. (2012). "Predicting the saturated hydraulic conductivity of soils: a review." *B. Eng. Geol. Environ.*, 71(3), 401-434.

Chapuis, R. P., and Aubertin, M. (2003). "On the use of the Kozeny-Carman equation to predict the hydraulic conductivity of soils." *Can.Geotech. J.*, 40(3), 616-628.

Chapuis, R. P., and Légaré, P. P. (1992). "A simple method for determining the surface area of the fine aggregates and fillers in bituminous mixtures." *In Effects of aggregates and mineral fillers on asphalt mixture performance*. American Society for Testing and Materials, ASTM STP Vol. 1147, pp. 177-186.

Childs, E. C., and Youngs, E. G. (1958). "The Nature of the Drain Channel as a Factor in the Design of a Land-Drainage System." *J. Soil. Sci.*, 9(2), 316-331.

Cihan, A., and Tyner, J. (2011). "2-D radial analytical solutions for solute transport in a dual-porosity medium." *Water Resour. Res.*, 47(4), W04507.

COMSOL Multiphysics. (2017a). *COMSOL Multiphysics v. 5.3a Reference Manual*. Stockholm, Sweden: COMSOL AB, www.comsol.com.

COMSOL Multiphysics. (2017b). *COMSOL Multipyhsics v. 5.3a: Subsurface Flow Module - User's Guide*. Stockholm, Sweden: COMSOL AB, www.comsol.com.

Das, B. M. (2007). *Fundamentals of Geotechnical Engineering*, 3rd ed., CL Engineering, United States.

Dennis, C. W., and Trafford, B. D. (1975). "The effect of permeable surrounds on the performance of clay field drainage pipes." *J. Hydrol.*, 24(3–4), 239-249.

Dierickx, W. (1980). *Electrolytic analog study of the effect of openings and surrounds of various permeabilities on the performance of field drainage pipes.* Doctoral thesis, Wageningen, Merelbeke, Belgium.

Dierickx, W. (1983). "Hydraulic Gradients Near Subsurface Drains and Soil Erosion." *Trans. ASAE*, 26(5).

Dierickx, W. (1999). *Non-Ideal Drains*. In R. Skaggs and J. van Schilfgaarde (Eds.), Agricultural Drainage, Vol. 38, pp. 297-330, Madison Publishers, Wisconsin, USA.

Dierickx, W., and Van Der Molen, W. H. (1981). "Effect of perforation shape and pattern on the performance of drain pipes." *Agric. Water Manage.*, 4(4), 429-443.

Hazenberg, G., and Panu, U. S. (1991a). "Analysis of flow into draintile in three-dimensional flow field." *J. Hydrol.,* 122(1–4), 321-333.

Hazenberg, G., and Panu, U. S. (1991b). "Theoretical analysis of flow rate into perforated drain tubes." *Water Resour. Res.*, 27(7), 1411-1418.

Huffman, R. L., Fangmeier, D. D., Elliot, W. J., and Workman, S. R. (2013). *Soil and Water Conservation Engineering*, 7th ed., ASABE: St Joseph, Michigan.

ICID (International Commission on Irrigation and Drainage). (2016). "Irrigation and Drainage in the World - A Global review: Germany." <http://icid.org/cp_country.php?CID=32#cp> (Apr. 04, 2019).

Kirkham, D., and Schwab, G. O. (1951). "The Effect of Circular Perforations on Flow into Subsurface Drain Tubes: Part I: Theory." *Agric. Eng.*, 32(4), 211-214.

Legates, D. R., and McCabe, G. J. (1999). "Evaluating the use of 'goodness-of-fit' measures in hydrologic and hydroclimatic model validation." *Water Resour. Res.*, 35(1), 233-241.

Madramootoo, C. A., Johnston, W. R., Ayars, J. E., Evans, R. O., and Fausey, N. R. (2007). "Agricultural drainage management, quality and disposal issues in North America." *Irrig. Drain.*, 56(S1), S35-S45.

Mbonimpa, M., Aubertin, M., Chapuis, R. P., and Bussière, B. (2002). "Practical pedotransfer functions for estimating the saturated hydraulic conductivity." *Geotech. Geol. Eng.*, 20(3), 235-259.

Moody, W. T. (1966). "Nonlinear Differential Equation of Drain Spacing." *J. Irrig. Drain. Div.*, 92(2), 1-10.

Moser, B. K., and Stevens, G. R. (1992). "Homogeneity of Variance in the Two Sample Means Test." *Am. Stat.*, 46(1), 19-21.

Myers, R. H., Montgomery, D. C., and Anderson-Cook, C. M. (2009). *Ch. 2: Building Empirical Models,* Response Surface Methodology: Process and Product Optimization Using Designed Experiments, 3rd ed., pp. 13-72, John Wiley and Sons, Inc, New Jersey.

Myers, R. H., Montgomery, D. C., and Anderson-Cook, C. M. (2016). *Ch. 8 - Design of Experiments for Fitting Response Surfaces - I*, Response Surface Methodology: Process and Product Optimization Using Designed Experiments, 4th ed., John Wiley and Sons Inc, New Jersey.

Nash, J. E., and Sutcliffe, J. V. (1970). "River flow forecasting through conceptual models part I - A discussion of principles." *J. Hydrol.*, 10(3), 282-290.

Panu, U. S., and Filice, A. (1992). "Techniques of flow rates into draintubes with circular perforations." *J. Hydrol.*, 137(1–4), 57-72.

PPI (Plastics Pipe Institute). (2003). *Design Service Life of Corrugated HDPE Pipe: TR-43/2003*. Washington, DC.

Prasad, S. N., Alonso, C. V., and DeCoursey, D. G. (1981). "Analysis of three-dimensional flows into draintile." *J. Hydrol.*, 51(1–4), 295-303.

Rollin, A. L., Broughton, R. S., and Bolduc, G. F. (1987). "Thin synthetic envelope materials for subsurface drainage tubes." *Geotext. Geomembranes*, 5(2), 99-122.

SAS Institute Inc. (2018). *JMP 14 Design of Experiments Guide*, Cary, NC.

Schwab, G. O., and Fouss, J. L. (1999). *Drainage Materials*. In R. W. Skaggs and J. van Schilfgaarde (Eds.), Agricultural Drainage, Vol. 38, pp. 911-926, Madison Publishers, Wisconsin, USA.

Selvadurai, A. P. S. (2000). *Partial Differential Equations in Mechanics: Volume1: Fundamentals, Laplace's Equation, Diffusion Equation, Wave Equation*, Springer-Verlag Berlin, Gerrmany.

Skaggs, R. W. (1978). "Effect of Drain Tube Opening on Water-Table Drawdown." *J. Irrig. Drain. Div.*, 104(IR1), 13-21.

Sneyd, A. D., and Hosking, R. J. (1976). "Seepage flow through homogeneous soil into a row of drain pipes." *J. Hydrol.*, 30(1–2), 127-146.

Stuyt, L. C. P. M., and Dierickx, W. (2006). "Design and Performance of Materials for Subsurface Drainage Systems in Agriculture." *Agric. Water Manage.,* 86(1-2), 50-59.

Stuyt, L. C. P. M., Dierickx, W., and Beltran, J. M. (2005). *Materials for subsurface land drainage systems*. FAO Irrigation and Drainage Paper 60. Rome, Italy.

Sugg, Z. (2007). *Assessing US Farm Drainage: Can GIS Lead to Better Estimates of Subsurface Drainage Extents?* World Resoures Institute (WRI),Washington DC.

Van der Ploeg, R. R., Horton, R., and Kirkham, D. (1999). *Steady Flow to Drains and Wells*. In R. Skaggs and J. van Schilfgaarde (Eds.), Agricultural Drainage, Vol. 38, pp. 213-263, Madison Publishers, Wisconsin, USA.

van Schilfgaarde, J. (1963). "Design of Tile Drainage for Falling Water Tables." *J. Irrig. Drain. Div.*, 89(2), 1-12.

Appendix 3.A: Computation of Entrance Resistance using Radial Flow Theory

Following the works of Dierickx (1980) and Stuyt et al. (2005), the theory of radial flow towards a subsurface drain was used to establish the relationship between piezometric head measurements and the entrance resistance of the drain. For ideal drains flowing full, the head loss for radial flow in a saturated, homogeneous, and isotropic soil is given as (Stuyt et al., 2005):

$$H_r = \frac{qS}{2\pi k_{sat}} \ln\left(\frac{r}{r_0}\right) \quad (3.A1)$$

where H_r is the difference in hydraulic head between a given point at a radial distance (r) and the surface of the drainage pipe (r_0), q is the drainage rate, S is the drain spacing, and k_{sat} is the saturated hydraulic conductivity of the soil. The radial resistance (α_r) is taken as the geometric component of Eq. (3.A1), and it represents a dimensionless and soil independent parameter:

$$\alpha_r = \frac{1}{2\pi} \ln\left(\frac{r}{r_0}\right) \quad (3.A2)$$

and thus,

$$H_r = \frac{qS}{k_{sat}} \alpha_r \quad (3.A3)$$

Similarly, for non-ideal drains with perforations, the head loss from the approach flow (H_a) can be written as:

$$H_a = \frac{qS}{k_{sat}} \alpha_a \quad (3.A4)$$

and the entrance head loss (H_e) closer to the pipe surface is:

$$H_e = \frac{qS}{k_{sat}} \alpha_e \quad (3.A5)$$

where α_a is the approach flow resistance, which includes the lumped radial and entrance resistance (α_e).

Fig. 3.A1 shows a plot of Eq. (3.A1), which yields a linear relationship between $\ln(r/r_0)$ and H_r. Imposing the approach flow head loss results in a curve that becomes parallel to H_r as $\ln(r/r_0)$ increases. Fig. 3.8 shows graphically that $H_e = H_a - H_r$, which is also the projected

intercept (c) of the linear section. The curved section of H_e will depend on the exact piezometer location closer to the pipe wall. Following Eq. (3.A5) and Fig. 3.8:

$$\alpha_e = \frac{c}{2\pi m} \tag{3.A6}$$

where c and m are determined from a least-square linear regression of the H_a vs. $\ln(r/r_0)$ datasets generated from the numerical simulations. The computed values of α_e from Eq. (3.A6) were standardized for a 1.0 m long pipe through multiplication by the effective perforated length (L_T).

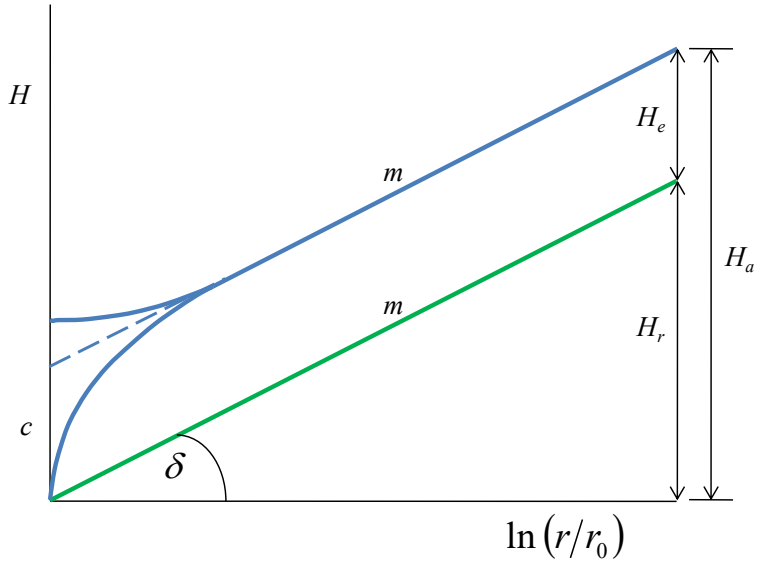

Fig. 3.A1. Radial (H_r) and approach (H_a) flow head loss as a function of $\ln(r/r_0)$.
Note: H_e is the entrance head loss, equivalent to the intercept (c) with slope $m = \tan \delta$).

The 72 probes were implemented in the radial flow zone surrounding the drainage pipe at eight radial distances (10, 11, 15, 19, 25, 33, 45, and 60 cm) in the XZ plane (Fig. 3.2) with intersecting lines at three angles (0°, 45°, and 135°) relative to the crown, and at three points along the pipe length in the ZY plane (y-direction). Two of the three points in the y-direction were placed directly in front of perforations closest to the mid-point of the pipe. The mean of the values from the three points was used to compute H_a following Dierickx (1980).

Appendix 3.B: Performance Statistics

The following equations were used for computing the performance statistics for the calibration and verification of the numerical model:

$$RMSE = \sqrt[2]{\frac{\sum_{i=1}^{n}(O_i - P_i)^2}{n}}$$

(3.B1)

$$NSE = 1.0 - \frac{\sum_{i=1}^{n}(O_i - P_i)^2}{\sum_{i=1}^{n}(O_i - \bar{O})^2} \quad (3.B2)$$

$$PBIAS = \frac{\sum_{i=1}^{n}(O_i - P_i)}{\sum_{i=1}^{n}(O_i)} \quad (3.B3)$$

where O_i is the ith measured value, P_i is the ith simulated value, $\bar{O}$ and is the mean of all O_i values in a given set.

Appendix 3.C: Supplemental Data

This appendix contains online supplementary material related to Chapter 3 that may be accessed via: http://dx.doi.org/10.1061/(ASCE)IR.1943-4774.0001482.

3.C.1 Introduction

This supporting information include texts, figures, and tables that were deemed as supplemental to the methods and results section of Chapter 3. The sections include a layout of the experimental set-up of the sand tank facility, the properties of the porous medium as determined from laboratory tests, the results from the sand tank experiments, the results from the mesh refinement study and calibration of the numerical models, and the results from the ANOVA for the six prediction models. All references cited are listed in section 3.6.

3.C.2 Experimental Set-up

The details of the sand tank facility are shown in Fig. 3.S1. Water enters the sand tank via the six rainfall simulators, which is fed by the supply reservoir. The control chamber regulates the hydraulic head on the outlet pipe using gates. The discharge over the gates flows into the rectangular flume which is fitted with an 11° V-notch weir to measure the flow rate.

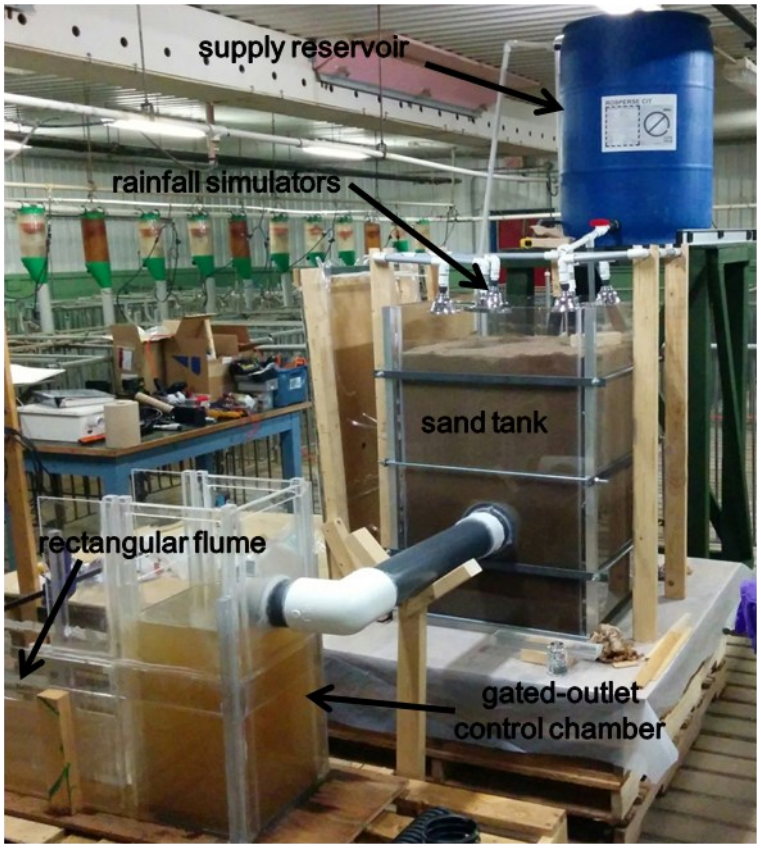

Fig. 3.S1. Layout of the facility used for the sand tank experiments.

3.C.3 Properties of the porous medium

A series of laboratory tests were carried out on representative samples of the porous medium in order to characterize the material and to determine key geotechnical parameters used in estimating the saturated hydraulic conductivity (k_{sat}). Table 3.S1 summarizes the mean values from the laboratory tests. The effective size (d_{10}) and the coefficient of uniformity ($C_U = d_{60}/d_{10}$) are determined from the particle size distribution (PSD) curves, which are shown in Fig. 3.S2. The PSD curves show that almost all of the material is retained on the No.200

sieve (75 μm), indicating the absence of a silt fraction. Sands with a low silt fraction are advantageous for drainage experiments since silt can migrate into the drainpipe and reduce the discharge capacity.

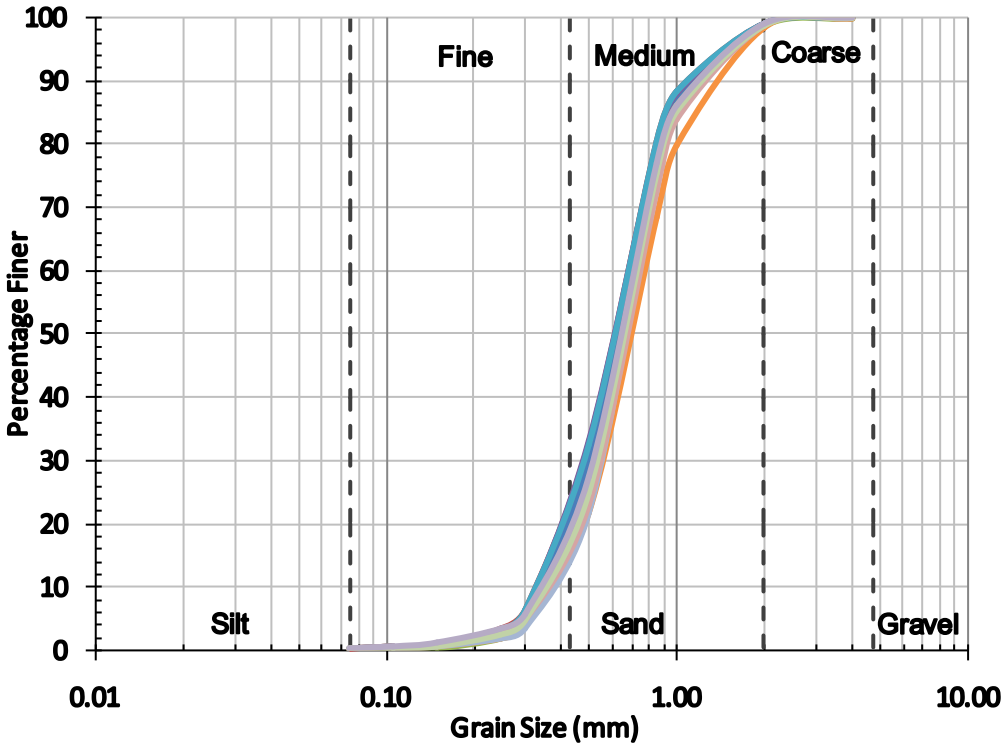

Fig. 3.S2. Particle size distribution (PSD) curves (n=12) for the porous medium.
Note: the grain size limits for the sand fractions (broken lines) are 4.75 - 2.00 mm (coarse), 2.00 - 0.425 mm (medium), and 0.425 - 0.075 mm (fine).

Table 3.S1. Characteristic geotechnical properties of the porous medium

Geotechnical parameter	Value
Effective size, d_{10} (mm)	0.34(0.03)
Coefficient of Uniformity, C_U	2.1(0.1)
Particle specific gravity, G_s	2.662 (0.02)
Maximum dry unit weight, $\gamma_{d\text{-}max}$ (kN/m^3)[a]	15.62 (0.06)
Optimum moisture content, OMC (%)[a]	7.7 (0.7)
Minimum dry unit weight, $\gamma_{d\text{-}min}$ (kN/m^3)	14.3 (0.05)
Specific surface, S_s (m^2/kg)[b]	5.36 (0.28)

Note: All values in parenthesis are the standard deviations.
[a]Standard Proctor.

[b]Chapuis and Légaré (1992).

3.C.4 Measured datasets from the sand tank experiments

The results from the sand tank experiments are summarized in Table 3.S2 for all values of H_d. The measured discharge (Q_m) was used as the response to calibrate the numerical model by adjusting k_{sat}. The observed piezometric head (H_{PZO}) was used as the response for the model validation.

Table 3.S2. Summary of the sand tank experimental results for the three pipe models

Pipe model	H_d (cm)	Q_m (m^3/s) x 10^{-4}	H_{PZO} (cm)					
			A1	A2	A3	B1	B2	B3
PWH	40.1	1.41	60.2	60.3	60.4	70.3	70.8	71.3
		(0.019)	(0.12)	(0.20)	(0.06)	(0.10)	(0.15)	(0.12)
	45.2	1.26	61.2	61.1	61.5	73.5	73.7	74.1
		(0.026)	(0.38)	(0.50)	(0.36)	(0.30)	(0.26)	(0.26)
	50.1	1.04	66.7	66.6	66.7	76.2	76.2	76.2
		(0.036)	(0.25)	(0.36)	(0.15)	(0.53)	(0.38)	(0.58)
	55.1	0.886	69.5	69.4	69.5	77.7	77.6	77.6
		(0.025)	(0.15)	(0.15)	(0.06)	(0.10)	(0.10)	(0.21)
CWH	40.1	1.36	62.5	62.5	62.6	75.2	75.0	75.0
		(0.085)	(0.15)	(0.10)	(0.36)	(0.20)	(0.23)	(0.25)
	45.2	1.31	65.1	65.1	65.1	76.9	76.7	76.9
		(0.031)	(0.15)	(0.25)	(0.15)	(0.21)	(0.15)	(0.10)
	50.1	1.07	67.0	67.1	67.1	77.7	77.7	77.8
		(0.028)	(0.15)	(0.15)	(0.21)	(0.25)	(0.40)	(0.26)
	55.1	1.01	68.8	69.0	69.0	79.6	79.5	79.4
		(0.027)	(0.64)	(0.59)	(0.72)	(0.49)	(0.38)	(0.38)
CWS	39.9	1.49	62.4	62.3	62.3	73.7	73.9	73.7
		(0.034)	(0.20)	(0.20)	(0.20)	(0.21)	(0.21)	(0.15)
	45.1	1.29	64.4	64.3	64.4	74.6	74.1	74.0
		(0.054)	(0.35)	(0.26)	(0.35)	(0.20)	(0.46)	(1.14)
	50.2	1.18	66.6	66.5	66.5	75.2	75.1	75.0
		(0.051)	(0.06)	(0.15)	(0.12)	(0.15)	(0.15)	(0.12)

Note: Values in parenthesis are the standard deviations (n =3); H_d = hydraulic head on the outlet; Q_m = measured discharge; H_{PZO} = mean observed piezometric head; A1, A2, and A3 are the A level piezometers; B1, B2, and B3 are the B level piezometers (see Fig. 3.2 in main text).

3.C.5 Mesh refinement study

The domain of the radial flow region surrounding the drainage pipe in the numerical model was discretized to determine an appropriate mesh size before calibration of the model. The mesh refinement study was implemented in COMSOL Multiphysics® version 5.3 (COMSOL Multiphysics 2017a) using the physics controlled mesh generator. COMSOL has several predefined or built-in mesh sizes that can be customized by the modeler. The common discretization practice is to begin with a coarse mesh size (large elements), then make adjustments to reduce the elements size until the output response (Q) is negligible. In this study, the mesh size was refined until the relative error (RE) between successive Q was below 1%. COMSOL has five adjustable parameters that control the mesh element size: the maximum element size, the minimum element size, the maximum element growth rate, the curvature factor, and the resolution of the narrow regions (COMSOL Multiphysics 2017a). The default values for these five parameters in COMSOL were unadjusted for the mesh sizes "Coarser" to "Finer1" (Table 3.S3). Systematic adjustments were made for the remaining mesh sizes until the target RE was met. The minimum element size was adjusted to 1.5 mm which is smaller than the smallest perforation dimension used in the experiments (the slot width is 2.0 mm for Model CWS). Additionally, the minimum element quality (MEQ) for each mesh size was assessed using COMSOL's mesh statistics tool. For geometries discretized in a 3D space, the minimum element quality should be greater than 0.1 as recommended by COMSOL. Fig. 3.S3 shows a typical mesh rendering for the domain of the numerical model (PWH) after discretization.

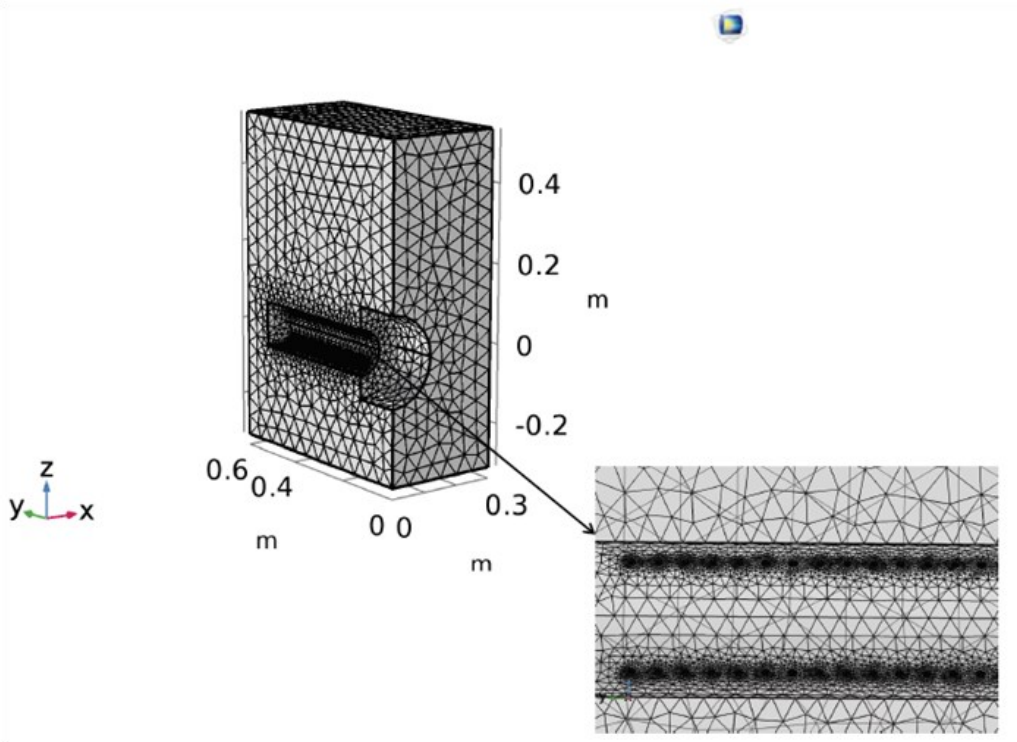

Fig. 3.S3. Mesh plot for the domain of Model PWH; (note: perforations shown in the enlarged section).

Table 3.S3. Mesh size and element quality for the three numerical models

Mesh Size	Model PWH			Model CWH			Model CWS		
	NoE	MEQ	RE(%)	NoE	MEQ	RE(%)	NoE	MEQ	RE(%)
Coarser	8111	0.191	-	7172	0.035	-	6393	0.068	-
Coarse	13893	0.234	6.78	8766	0.074	11.66	10562	0.085	1.62
Normal	24851	0.253	4.76	16406	0.073	9.81	18433	0.091	1.87
Fine	35181	0.276	7.95	31320	0.163	9.19	35075	0.177	1.68
Finer 1	101450	0.310	30.41	71680	0.196	1.05	71249	0.192	9.91
Finer 2	121214	0.320	21.60	82934	0.222	34.52	77170	0.213	6.26
Finer 3	142551	0.270	3.94	83592	0.192	6.17	83510	0.220	2.81
Finer 4	153513	0.274	6.61	102955	0.205	7.84	90238	0.189	4.30
Finer 5	176829	0.293	6.85	120158	0.201	0.37	94457	0.194	0.69
Finer 6	192637	0.293	1.00	-	-	-	-	-	-
Finer 7	201758	0.295	0.24	-	-	-	-	-	-

Note: PWH = plain wall with holes; CWH = corrugated wall with holes; CWS = corrugated wall with slots; NoE = number of 3D domain elements (including tetrahedral and pyramid), MEQ = minimum element quality (MEQ>0.1 for 3D domains), and RE = relative error in the response (Q) between successive mesh sizes.

3.C.6 Calibration of the numerical models

A combined parametric study was done in COMSOL using two parameters: an estimated range of k_{sat} values and the measured H_d values from the sand tank experiments. The estimated k_{sat} was first computed with two prediction equations. The Kozeny-Carman equation (Chapuis and Aubertin 2003):

$$\log[k_{sat}(m/s)] = A + \log\left[\frac{e^3}{G_S^2 S_S^2 (1+e)}\right] \quad (3.S1)$$

where A is constant that includes for the tortuosity and properties of the fluid (A=0.29 in this study), e is the void ratio of the medium, G_s is the specific gravity, and S_s is the specific surface area (m^2/kg). The second equation used to estimate k_{sat} was a pedo-transfer function by Mbonimpa et al. (2002) and is given as:

$$k_{sat}(cm/s) = 977.3 C_U^{1/3} d_{10}^2 \frac{e^5}{1+e} \quad (3.S2)$$

where C_U is the coefficient of uniformity, and d_{10} (cm) is the effective size. The in-situ void ratio measured from the sand tank experiments and the parameters from Table 3.S1 were used as input for Eqs. (3.S1) and (3.S2). The input range of k_{sat} for the parametric study was set at two standard deviations of the mean k_{sat} value between the two prediction equations. The calibrated k_{sat} value was determined by minimizing the mean absolute error (MAE) between the measured discharge (Q_m) from the physical sand tank experiments and the corresponding simulated discharge (Q_s) using the numerical model for all values of H_d. The MAE between Q_m and Q_s were plotted against k_{sat} as shown in Figs. 3.S4, 3.S5, and 3.S6 for

Models PWH, CWH, and CWS, respectively. The optimum k_{sat} was selected at the minimum MAE as the final calibrated value.

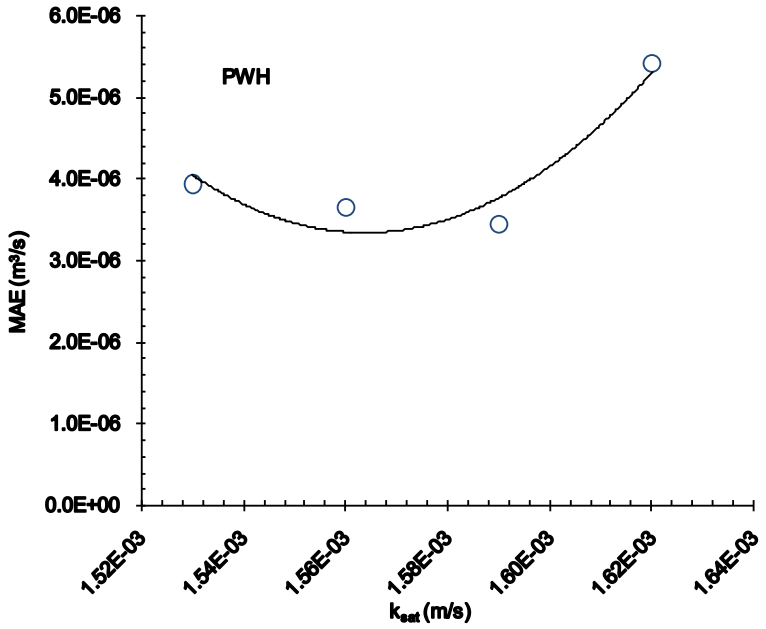

Fig. 3.S4. k_{sat} calibration curve for Model PWH.

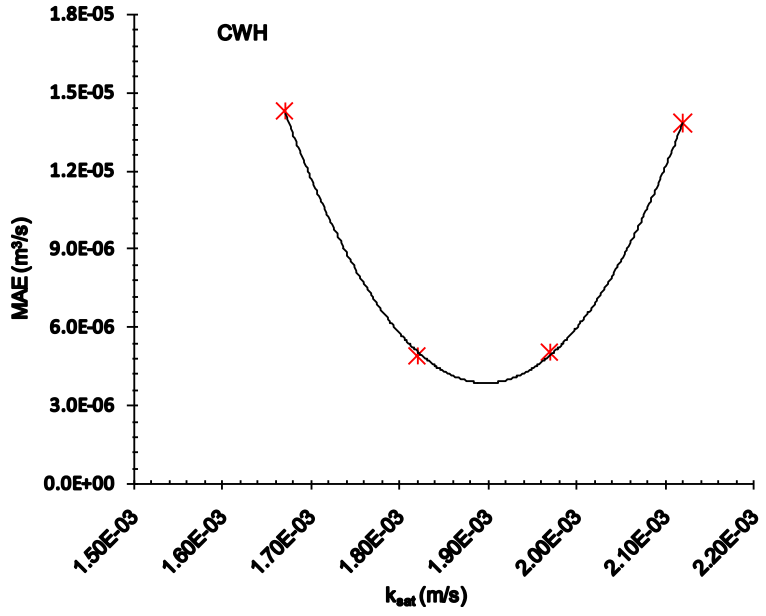

Fig. 3.S5. k_{sat} calibration curve for Model CWH.

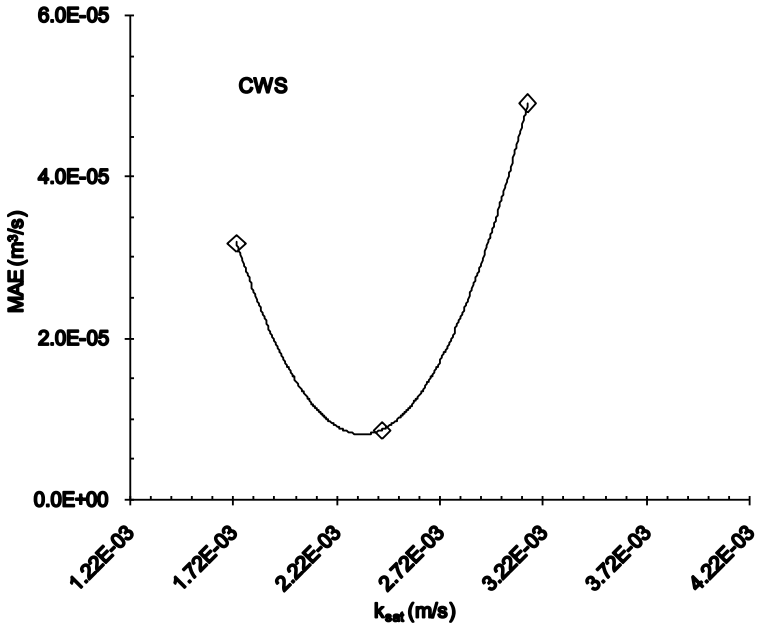

Fig. 3.S6. k_{sat} calibration curve for Model CWS.

Table 3.S4 shows the calibration performance statistics for the numerical models as assessed against the measured Q datasets. These calibrated k_{sat} values are well within one standard deviation of the predicted k_{sat} values for the porous medium used in the sand tank experiments. The calibrated k_{sat} values were then used to simulate Q and H_{PZ} with the numerical model for verification against the sand tank measurements. The goodness of fit between Q_m and Q_s is indicated by the favorable NSE values (NSE = 1.0 is best fit) for the three models in Table 3.S4. The negative PBIAS values indicate that the numerical model marginally (PBIAS = 0 is best fit) overestimates Q_s for all the three pipe models. The hydraulic head data recorded using the piezometers in the sand tank experiments were used as a second response variable to verify the numerical model after calibration. For the

comparison, six point probes were implemented in the numerical model to compute the simulated hydraulic head at the same location as their physical model counterparts. The assessment of this verification is also summarized in Table 3.S4, which shows NSE values greater than 0.64 for all models. The negative PBIAS values indicate an overestimation of H_{PZ} by the numerical models.

Table 3.S4. Model calibration and verification performance statistics

Pipe model	e	k_{sat} (m/s) x 10^{-3}	Calibration using Q			Verification using H_{PZ}		
			RMSE (m^3/s) x 10^{-6}	NSE	PBIAS (%)	RMSE (cm)	NSE	PBIAS (%)
PWH	0.761	1.57	4.28	0.95	-2.2	3.36	0.69	-4.4
CWH	0.801	1.90	4.77	0.90	-0.1	3.62	0.64	-4.3
CWS	0.850	2.35	4.27	0.89	-2.6	2.79	0.71	-3.9

Note: Q = discharge; H_{PZ} = piezometric head; e = in-situ void ratio of the sand; RMSE = root mean squared error [Eq. (3.B1)]; NSE = Nash-Sutcliffe efficiency [Eq. (3.B2)]; PBIAS = percentage bias [Eq. (3.B3)].

The maximum RMSE of 3.62 cm gives a scale of the discrepancy, which is most likely caused by experimental measurement errors in H_{PZ}. These errors may be attributed to the fact that the piezometers in the sand tank were made of 1.0 cm diameter tubes, while the piezometers in the numerical models have a smaller resolution of a discrete point or node. Secondly, the exact location of the piezometer tip in the sand tank was assumed to be at the same level as its base at the tank wall, but observation during repacking showed tip deflections of up to 1.5 cm due to the weight of the overburden sand. Thirdly, there may have been a small loss in head due to frictional resistance from the tube walls, underestimating the measured piezometric data. Nevertheless, the overall performance statistics indicate that the numerical models can be deemed as very good representations of the three pipe models.

3.C.7 Statistical design matrix and responses

The coded values for the design variables in Table 3.S5 result from the scale transformation of the design levels to a dimensionless quantity as part of the statistical analysis. In coded

units a low design level (minimum value) becomes -1, while a high design level (maximum value) becomes +1. The medium level (average value) becomes 0 after the transformation. The response from the numerical simulations are summarized in Table 3.S6.

Table 3.S5. Experimental Design Matrix for Face- Centered Cube (FCD)

Design Points	Runs	Coded Values		
		N	d_{perf}/L_{perf}	a_y
Factorial Points	1	-1	-1	-1
	2	-1	-1	1
	3	-1	1	-1
	4	-1	1	1
	5	1	-1	-1
	6	1	-1	1
	7	1	1	-1
	8	1	1	1
Axial Points	9	-1	0	0
	10	1	0	0
	11	0	-1	0
	12	0	1	0
	13	0	0	-1
	14	0	0	1
Center Runs	15	0	0	0
	16	0	0	0
	17	0	0	0

Note: the coded values are low (-1), medium (0), and high (1)

Table 3.S6. Response datasets from the numerical simulations of entrance resistance (α_e) and delivery ratio (Q/Q_0).

Runs	α_e			Q/Q_0		
	PWH	CWH	CWS	PWH	CWH	CWS
1	0.830	0.986	0.734	0.168	0.141	0.131
2	1.843	2.354	1.652	0.082	0.066	0.066
3	0.694	0.866	0.467	0.212	0.178	0.205
4	1.469	2.026	0.945	0.108	0.085	0.116
5	0.156	0.171	0.200	0.597	0.563	0.359
6	0.251	0.309	0.384	0.451	0.387	0.232
7	0.144	0.161	0.155	0.672	0.672	0.464
8	0.218	0.281	0.261	0.529	0.480	0.340
9	1.167	1.509	0.861	0.122	0.096	0.117
10	0.184	0.220	0.227	0.545	0.497	0.342
11	0.281	0.332	0.414	0.407	0.340	0.201
12	0.238	0.295	0.260	0.486	0.412	0.312
13	0.189	0.215	0.217	0.539	0.497	0.358
14	0.337	0.427	0.422	0.367	0.308	0.225
15	0.267	0.323	0.325	0.421	0.362	0.262
16	0.246	0.300	0.302	0.445	0.383	0.277

17	0.256	0.311	0.313	0.433	0.373	0.270

3.C.8 ANOVA and prediction model fit

Tables 3.S7 and 3.S8 summarizes the results from the ANOVA and lack of fit tests for the prediction models of α_e and Q/Q_0, respectively. The full quadratic model includes all regression effect terms including the squared and interaction terms. The refined model was derived after removing non-significant ($p>0.05$) effect terms. Lack of fit values below 0.05 indicate a poor fit (Myers et al. 2009).

Table 3.S7. Summary of model fit and ANOVA with response α_e

Model Parameter	Full Quadratic Model			Refined Model		
	PWH	CWH	CWS	PWH	CWH	CWS
R^2 (%)	99.951	99.958	99.924	99.889	99.915	99.816
Adjusted R^2 (%)	99.887	99.904	99.826	99.839	99.877	99.673
p-value for model	< 0.0001	< 0.0001	< 0.0001	< 0.0001	< 0.0001	< 0.0001
Lack of fit (p-value)	0.2394	0.2767	0.2746	0.5765	0.5387	0.8804

Note: R^2 is the coefficient of determination

Table 3.S8. Summary of model fit and ANOVA with response Q/Q_0.

Model Parameter	Full Quadratic Model			Refined Model		
	PWH	CWH	CWS	PWH	CWH	CWS
R^2 (%)	99.671	99.713	99.498	99.078	99.684	99.233
Adjusted R^2 (%)	99.248	99.344	98.852	98.770	99.439	98.637
p-value for model	< 0.0001	< 0.0001	< 0.0001	< 0.0001	< 0.0001	< 0.0001
Lack of fit (p-value)	1.9094	2.2417	2.7362	3.0371	1.7889	3.1342

Connecting text to Chapter 4

The previous chapter established the entrance resistance for corrugated pipes with holes and slots under drainage conditions. However, the literature review in Chapter 2 identified that the impact of perforations on the structural response of buried corrugated pipes has not been thoroughly investigated. Additionally, frictional loads that are representative of agricultural field conditions resulting from variable soil textures, water table positions, and agri-machinery wheel loads have not been considered in the structural analysis of buried corrugated pipes. Chapter 4 of this thesis used elastic theory and two idealized friction condition at the soil-pipe interface to simulate the wall stresses and vertical deflection of both non-perforated and perforated corrugated pipes under variable agricultural loading conditions. The stress concentrations around circular holes and rectangular slots were also evaluated.

Chapter 4 was re-submitted to *Biosystems Engineering* and is currently under a second round of review (Gaj and Madramootoo, 2021a). The format of the manuscript has been modified here to ensure consistency with the style of this thesis. A list of the references cited in the manuscript is available at the end of the chapter.

Authorship contribution statement:

The author of this thesis was responsible for conceptualization, methodology, model development, calibration, formal analysis, investigation, data curation, and writing the original draft followed by all revisions and editing. Dr. Madramootoo provided supervision, aided in conceptualization, funding acquisition, and reviewed and edited the manuscript.

Chapter 4

Structural Response of Non-perforated and Perforated Corrugated HDPE Pipes under Variable Loading

4.1 Abstract

The structural response of small diameter (<300 mm) corrugated high-density polyethylene (HDPE) drainage pipes installed on agricultural lands, has not been thoroughly examined. Additionally, characteristics of imposed wheel loads from agricultural field machinery are not adequately represented in conventional structural design practices for buried pipes. This study investigates the response of single-wall corrugated HDPE pipes (100 mm diameter) under loading from 12 agricultural soil textures, two water table positions, and three agri-machinery wheel loads using a finite-element-based numerical model. Effects from two friction conditions (smooth and bonded) at the soil-pipe interface were assessed. Simulations were also done to determine the impact of variable perforation characteristics (shape, size, and configuration) on the stress distribution and deformation of the corrugated pipes. The results show that bonded friction conditions generally induce larger stresses in the pipe wall than smooth friction conditions, but the differences are not statistically significant across all soil and load types. The critical load case occurs for a loaded grain wagon on silt loam soils. The results also indicate that perforations in the pipe wall induce high stress concentrations at the edges of rectangular slots and circular holes, increasing the risk for failure by ductile yielding. Specifically, corrugated HDPE pipes perforated with 0.56 cm diameter holes produce stresses that exceed the yield strength at buried depths shallower than 0.9 m. In conclusion, perforation characteristics should be considered when assessing the structural adequacy of corrugated HDPE pipes for land drainage.

Author keywords: subsurface drainage; structural response; agricultural soils; polyethylene; stress concentration; perforation

4.2 Introduction

Techniques for the structural analysis and design of buried pipes have become more complex and comprehensive since Marston (1930) proposed a theory to determine the soil loads on buried rigid pipes, and Spangler (1941) developed the "Iowa Formula" to predict the ring deflections in buried flexible pipes. Further advances to the theory were made by Watkins and Spangler (1958) when they modified the "Iowa Formula" by redefining the modulus of passive resistance from the soil supporting the buried pipes. However, a realistic and complex response of the soil-pipe system under external loading was best described in the solutions presented by Burns and Richards (1964) and Hoeg (1968). These solutions, based on elastic theory, account for the friction conditions at the soil-pipe interface, and have been widely used to design reinforced concrete, corrugated steel, and profiled plastic pipes for use in culvert and highway drainage. On agricultural lands, single-wall corrugated plastic pipes are used as drainage laterals, to remove excess soil-water from the root zone for crop production. Corrugated thermoplastic pipes are very cost-effective compared to other drainage materials (clay tiles, concrete) due to their lower weight per unit length, and their capacity for rapid field installation via mechanized plowing (Schwab & Fouss, 1999).

Several studies have investigated the response of large diameter (>300 mm) corrugated and plain wall plastic pipes that are used as culverts and storm drains, and are usually installed in trenches and then backfilled with compacted granular (or frictional) soils (Alzabeebee, 2019, 2020; Alzabeebee et al., 2018b; Arockiasamy et al., 2006; Chaallal et al., 2015a, 2015b; Dhar et al., 2004; Kang et al., 2009; Kraus et al., 2014; Moore & Hu, 1995; Watkins et al., 1987; Zhan & Rajani, 1997; Zhou et al., 2017). Conversely, the structural response of small

diameter (<300 mm) corrugated pipes buried in agricultural soils, e.g. sandy clays and silt loams (cohesive-frictional), has not been thoroughly examined. In addition, imposed live loads used in previous studies are typically characterized by wheel loads from standard highway trucks (Arockiasamy et al., 2006; Chaallal et al., 2015a; Kang et al., 2014; Katona, 1990, 2017; Robert et al., 2016; Sheldon et al., 2015; Watkins et al., 1987), which are much different from agri-machinery used on farmlands. Furthermore, the vertical stress transmission from the wheel loads is often estimated using simplistic assumptions for the tire contact area and stress propagation through the soil medium.

The contact area at the tire-soil interface is frequently assumed to be rectangular in shape with a uniform stress distribution (Alzabeebee, 2020; Alzabeebee et al., 2018a; Kang et al., 2014; Mai et al., 2014; Moore, 2001). On agricultural fields, experiments have shown that a super ellipse contact area with a non-uniform stress distribution is a better representation of the wheel loads at the tire-soil interface (Keller, 2005). Similarly, field experiments have shown that the vertical stress propagation can be accurately predicted with linear elasticity theory for wheel loads from harvesters and tractors on agricultural soils with water contents close to field capacity (Keller et al., 2014). Conventional techniques for the vertical stress propagation of wheel loads in buried pipe and culvert analysis are based on the simple prism model commonly known as the 2:1 method (Moore, 2001; Watkins et al., 1987) or the classical Boussinesq solution for concentrated loads (Alzabeebee et al., 2017; Moore, 2001). The 2:1 method approximates the contact stress distribution uniformly over the prism base area against the more realistic non-uniform stress distribution, resulting in an underestimation of the peak vertical stresses in the soil medium directly under the wheel load (Holtz, 1991). Alzabeebee et al. (2017) showed that the Boussinesq solution produces lower soil stresses on the top of the pipe compared to simulated stresses from finite element analysis (FEA). However, it is important to note that the comparison by Alzabeebee et al. (2017) may not be

entirely accurate, because tire loads were modelled as a uniform surface pressure of 900 kPa over a rectangular footprint, while the Boussinesq solution to traffic loads on highways cited in their study is based on an effective surface pressure of 1100 kPa acting on a circular footprint (Young et al., 1986). Keller et al. (2014) showed that the Boussinesq solution can produce soil stresses that are in agreement with simulated stresses from FEA, once the former is formulated as a series of smaller concentrated loads distributed over the tire contact area following Sohne (1953).

The two-dimensional (2-D) semi-analytical model, SoilFlex (Keller, Defossez, Weisskopf, Arvidsson, & Richard, 2006), addresses the above limitations for conventional live load stress transmission, allowing for a realistic representation of the tire contact area and accurate stress propagation from the wheel loads of agri-machinery through agricultural soils using the Sohne (1953) formulation of the Boussinesq equation. It should be noted that SoilFlex is principally three-dimensional (3D), but the model is described as 2-D because the output soil stresses are available in the 2-D planes that are perpendicular to the driving direction (under the transverse axis of tire) and/or in the driving direction (under the longitudinal axis of tire) (Keller et al., 2006). While SoilFlex is frequently used in compaction studies for agricultural soils (de Lima et al., 2017), the model has not been previously used to accurately simulate live load stress transmission as part of the structural design and analysis of buried corrugated plastic pipes.

Fouss (1973) developed a structural design procedure for corrugated high-density polyethylene (HDPE) pipes based on limiting the pipe deflection to 5% in order to keep wall stresses within the pipe's elastic region. The final step in Fouss's design procedure sets out provisions for perforating the pipe walls to allow for water entry. These provisions were used to recommend the dimensions for rectangular slots on a typical 100 mm diameter corrugated pipe, but they were based on a rule-of-thumb of prescribing a total opening area of one

percent of the pipe's outside wall surface area. Fouss (1973) did not investigate the effects of the slots on the wall stresses or pipe deflection, although two provisions were given to minimize the structural "weakening" of the pipe wall due to perforations. The first provision was to place the perforation in every second or third corrugation valley along the pipe's longitudinal axis, and the second was to limit the slot width to half of the corrugation valley's width. Neither of these conditions given by Fouss (1973) were supported by a thorough stress analysis of the effects of the perforations in corrugated HDPE pipes.

An important study on the stress distribution around perforations in buried drainage pipes was undertaken by Brachman and Krushelnitzky (2002), who investigated the stress concentrations around circular holes using 3D FEA. The results from their FEA study showed that the perforation size and spacing affected the stress concentration factor (K_{sc}) in the pipe wall, where K_{sc} was defined as the ratio of the stress at the perforation to the stress at the same location in a non-perforated pipe. Brachman and Krushelnitzky (2002), recommended guidelines for the hole size and spacing based on limiting the maximum K_{sc} value to 3.0. Nevertheless, these findings were derived for perforated plain wall pipes under deep burial, which are typically subjected to large overburden earth pressures (e.g. leachate collection systems in landfills or toe drains under earthen dams). Brachman and Krushelnitzky (2002) did not consider the effects of hydrostatic and imposed live loads, since they assumed water table levels were well below the pipe level and that the stresses from vehicular traffic were insignificant for deep burials. Additionally, the effect of the holes on the pipe deflection, usually expressed as a percent of the vertical deformation to the internal pipe diameter ($\Delta V/d_i$), was not assessed in their FEA study.

In this study, the structural response of single-wall corrugated HDPE pipes, typically used in trenchless subsurface drainage systems, is investigated under loading conditions that are applicable to large-scale crop production on agricultural lands. The main objective is to

develop a 3D finite-element-based numerical model of a representative 100 mm diameter corrugated pipe using COMSOL Multiphysics version 5.3 (COMSOL Multiphysics, 2017a) in order to simulate the wall stress and vertical deflection under applied loads. In addition, the effect of the interface friction condition on the stress distribution, and stress concentration around perforations are investigated. This research proposes a new way of incorporating perforation characteristics such as shape, dimension, and configuration into the structural analysis and design of buried corrugated HDPE pipes under variable loading in agricultural soils.

4.3 Structural Analysis of Flexible Buried Pipes

The analysis and design of flexible buried pipes is based on the elastic response of the soil-pipe system from surrounding boundary loads (Moore, 2001). The design criteria is governed by performance limits, which are broadly linked to the structural integrity and deflection of the pipe (Chambers & McGrath, 1981). For corrugated HDPE pipes, the key performance limits considered for design are: short-term yield, long-term cracking, global and local buckling, ovaling and hoop compression (deflection), and ultra-violet light and solvent degradation (Moore, 2001).

4.3.1 Soil-Pipe Interaction

The friction condition at the interface between the soil and pipe determines the structural response of the soil-pipe system. Elastic solutions for two idealized conditions, no friction (smooth) and full friction (bonded), are commonly used in the analysis of buried pipes. Moore (2001) adapted the solution of Hoeg (1968) and presented a unified approach for analysing buried circular pipes and culverts. The total stress distribution from the boundary loads on the external surface of the pipe wall at angle θ from the crown (Fig. 4.A1) is given as (Moore, 2001):

$$\sigma = \sigma_0 + \sigma_2 \cos 2\theta \tag{4.1}$$

$$\tau = \tau_2 \sin 2\theta \tag{4.2}$$

where σ is the normal stress, σ_0 is the uniform component of the normal stress, τ is the tangential shear stress, σ_2 and τ_2 are the non-uniform or harmonic component of normal and shear stresses, respectively. The stress components in Eqs. (4.1) and (4.2) are influenced by the arching effect, which describes the load transfer between a yielding soil mass and the stationary pipe structure (Tien, 1996). Arching factors, defined in terms of the mean (σ_m) and deviatoric (σ_d) stresses (Appendix 4.A), are used to compute the stress components as follows (Moore, 2001):

$$\sigma_0 = A_m \sigma_m \tag{3}$$

$$\sigma_2 = A_{d\sigma} \sigma_d \tag{4}$$

$$\tau_2 = A_{d\tau} \sigma_d \tag{5}$$

where A_m, $A_{d\sigma}$, $A_{d\tau}$ are the uniform normal, non-uniform normal, and non-uniform shear stress arching factors, respectively. The arching factors (Appendix 4.A) are a function of the soil and pipe stiffness, pipe geometry, and the interface friction condition (smooth or bonded) of the soil-pipe system.

4.3.2 Performance Limits

Performance limits specifications for corrugated HDPE pipes vary by design standards, codes of practice, and field applications. Most pipe manufacturers across North America follow design standards set by the American Society for Testing and Materials (ASTM) and American Association of State Highways and Transportation Officials (AASHTO). For subsurface drainage pipes used on agricultural lands, ASTM F667 (ASTM, 2016) specifies

minimum pipe stiffness values of 0.21 and 0.18 MPa to limit $\Delta V/d_i$ at 5 and 10%, respectively. In AASHTO M252 (AASHTO, 2009), the pipe deflection is limited to 5% for Type C pipes, which are single-wall corrugated pipes. Additionally, the widely used AASHTO Load and Resistance Factored Design (LRFD) bridge design specifications limits general pipe deflection to 5% (AASHTO, 2017).

4.3.3 Stress concentration

In buried pipes with perforations (holes and slots), the internal stress distribution in the pipe wall will be concentrated at the edge of the openings, creating localized areas of peak stresses known as stress concentration (Murakami, 2017). Failure in most structural elements originate at areas of high stress concentration, and therefore, a thorough evaluation of stress concentration is needed to ensure design stresses are kept within safe limits. Problems concerning the effects of circular holes in a plate subject to axial loads, have formed the foundation for investigating stress concentration in structural elements such as plates and shells. Design charts have also been generated for the stress concentration around a single hole in a plain wall cylinder. These solutions are very useful for benchmarking numerical models used in stress analysis studies, and are therefore utilized in this study in aid of mesh refinement and model verification.

4.4 Materials and Methods

4.4.1 Pipe Properties

The pipe's elastic modulus (E_p) and Poisson ratio (μ_p) are the main input parameters required to model the structural response to applied loads. Previous studies have used experimental data to support the assumption of linear elastic response for buried plastic pipes in numerical models (Brachman & Krushelnitzky, 2002, 2005; Bryden et al., 2014; Krushelnitzky & Brachman, 2009; Rajeev & Kodikara, 2011; Zhou et al., 2017). The yield strength (F_y) is

typically used to define the stress limit for material failure in the elastic zone. The Plastic Pipe Institute (PPI) provides E_p and F_y for polyethylene (PE) pipes based on the duration of loads, working temperature, and the type of PE resin (PPI, 2010). The mechanical properties for the linear elastic pipe model used in this study (Table 4.1) are based on design values specified by PPI for a typical 100 mm diameter single-wall corrugated HDPE pipe (PPI, 2010). The values in Table 4.1 (corrected to 20°C) satisfy the minimum requirements set out by ASTM F667 (ASTM, 2016) for PE resins with a 333410C cell classification according to ASTM D3350 (ASTM, 2014).

Table 4.1. Mechanical properties of corrugated HDPE pipe

Pipe Property	Short-term (initial)	Long-term (50 years)
Density, ρ_p (kg/m^3)	945	945
Elastic Modulus, E_p (MPa)	937.3	209.9
Poisson Ratio, μ_p	0.45	0.45
Yield Strength, F_y (MPa)	21.4	7.1

Note: Values satisfy requirements of PE cell class 333410C (ASTM D3350) adjusted to 20°C

The effect of temperature and PE resin type on μ_p is relatively negligible (Bilgin et al., 2007), and PPI recommends a design value of 0.45 for all load durations (PPI, 2010). In contrast, HDPE exhibits time-dependent viscoelastic behaviour due to material creep and stress relaxation (Bilgin, 2014). Strains are recoverable in a viscoelastic pipe model just as they are in a linear elastic model, but not instantaneously (Bilgin et al., 2007). As such, the stress response of buried HDPE pipes is affected by the duration of the applied loads, and the common practice is to use a time-dependent E_p in order to account for linear viscoelasticity (AASHTO, 2017; PPI, 2010; Zhou et al., 2017). For long-term loads such as hydrostatic and earth loads, the E_p value in Table 4.1 for the linear elastic pipe model was selected as the 50-yr secant modulus from stress relaxation tests (PPI, 2010). Similarly, the short-term or initial E_p in Table 4.1 was used for the pipe model when subjected to transient live loads in order to

simulate a linear elastic response (AASHTO, 2017; PPI, 2010). The design values of F_y in Table 4.1 were also based on the duration of the applied loads when used to assess the risk against material failure by ductile yielding.

4.4.2 Soil Properties

Mechanical soil properties are widely available for engineering soils classified under the Unified Soil Classification System (USCS). However, the US Department of Agriculture (USDA) textural classification system, which contains large datasets on the physical and hydraulic properties of agricultural soils, is more widely used in the design of subsurface drainage systems. A mapping scheme between the two systems developed by Garcia-Gaines and Frankenstein (2015) was used to adapt the USCS mechanical properties for USDA textural classes. There were overlaps between several of the USCS and USDA soils, resulting in six USCS soil classes mapped onto 12 USDA soil textures as shown in Table 4.2. The soil's elastic modulus (E_s), Poisson ratio (μ_s), and density (ρ_s) are the primary input parameters required for modelling the soil-pipe interaction and structural response of the buried pipe. While Fourie and Beer (1989) cautioned the assumption of linear elasticity for the soil response in soil-structure interaction problems, Moore and Hu (1995) stated that linear elasticity provides a very good soil model for many buried pipe problems. Katona (2017) showed that under small strains, linear elasticity produces results that are comparable

Table 4.2. Mechanical, physical, and hydraulic properties of soil textures with USCS and USDA classification

USDA	USCS	E_s[a]	μ_s[b]	n	CC	FC	wc_{FC}	$\rho_{s\text{-}dry}$	$\rho_{s\text{-}sat}$	$\rho_{s\text{-}FC}$	k_{sat}[c]
		MPa	-	$m^3\ m^{-3}$	%	$m^3\ m^{-3}$	$kg\ kg^{-1}$	$kg\ m^{-3}$	$kg\ m^{-3}$	$kg\ m^{-3}$	$m\ s^{-1} \times 10^{-6}$
Sand	SP	28.5 (27.8-63.3)	0.35 (±20%)	0.44	4	0.07	0.047	1484.0	1924.0	1554.0	50.53 (26.80-74.11)
Loamy Sand	SM	10.0 (8.8-16.3)	0.35 (±20%)	0.37	7	0.14	0.084	1669.5	2039.5	1809.5	11.50 (8.47-21.55)
Sandy Loam	SM	10.0 (8.8-16.3)	0.35 (±20%)	0.37	13	0.20	0.120	1669.5	2039.5	1869.5	3.56 (1.42-8.69)
Sandy Clay Loam	SC	79.1 (81.3-193.8)	0.25 (±28%)	0.37	26	0.29	0.174	1669.5	2039.5	1959.5	0.78 (0.28-3.03)
Sandy Clay	SC	79.1 (81.3-193.8)	0.25 (±28%)	0.39	36	0.30	0.186	1616.5	2006.5	1916.5	0.25 (0.08-0.69)
Loam	CL	27.4 (23.8-41.3)	0.45 (±16%)	0.39	22	0.28	0.164	1708.0	2098.0	1988.0	1.72 (0.77-4.58)
Silt Loam	ML	6.3 (6.5-15.5)	0.33 (±11%)	0.49	19	0.34	0.247	1377.0	1867.0	1717.0	4.00 (2.11-10.31)
Silt	ML	6.3 (6.5-15.5)	0.33 (±11%)	0.49	19	0.34	0.247	1377.0	1867.0	1717.0	4.00 (2.11-10.31)
Clay Loam	CL	27.4 (23.8-41.3)	0.45 (±16%)	0.40	40	0.34	0.202	1680.0	2080.0	2020.0	0.19 (0.06-1.06)
Silty Clay Loam	CL	27.4 (23.8-41.3)	0.45 (±16%)	0.43	32	0.36	0.226	1596.0	2026.0	1956.0	1.36 (0.64-3.89)
Clay	CH	11.2 (10.0-20.0)	0.45 (±16%)	0.40	50	0.36	0.214	1680.0	2080.0	2040.0	0.50 (0.08-1.92)
Silty Clay	CH	11.2 (10.0-20.0)	0.45 (±16%)	0.53	49	0.36	0.274	1316.0	1846.0	1676.0	0.50 (0.14-2.08)

Note: E_s = elastic modulus of soil, μ_s = Poisson ratio of soil, n = soil porosity; CC = clay content; FC = field capacity; wc_{FC} = water content at FC (gravimetric); $\rho_{s\text{-}dry}$ = soil dry density; $\rho_{s\text{-}sat}$ = soil density at saturation; $\rho_{s\text{-}FC}$ = soil density at field capacity.

[a]values are geometric mean; the values in parenthesis are the 25th and 75th percentile values.

[b]values are arithmetic mean; the values in parenthesis are the coefficient of variation.

[c]values are geometric mean; the values in parenthesis are the 25th and 75th percentile values.

to the elastic-perfectly plastic Mohr-Coulomb soil model in the finite-element analysis of buried culverts. Alzabeebee et al. (2018) also studied the effect of soil plasticity on the response of buried pipes under static and moving loads using finite-element analysis. Their results showed that the linear elastic and Mohr-Coulomb models simulated the same displacement at the pipe crown, which indicated that soil plasticity does not affect the accuracy the finite-element analysis of buried pipes. Furthermore, Keller et al. (2014) used linear elasticity to calibrate a numerical model and investigate stress transmission in agricultural soils with live loads from agri-machinery.

Under field conditions, variability in the soil parameters may exist due to compaction and soil moisture (Mouazen et al., 2002). The values in Table 4.2 are based on the results of laboratory tests on soil samples subjected to a wide range of field conditions. The geometric mean of E_s was used in this study due to large variability within soil classes as shown by the 25th and 75th percentile values (Table 4.2). On the other hand, the arithmetic mean was used for μ_s and ρ_s since their variability is less pronounced across the textural classes listed in Table 4.2.

The elastic constants (E_s and μ_s) in Table 4.2 were adapted from Bowles (1996), while the soil porosity (n), field capacity (FC), and clay content (CC) were adapted from Rawls et al. (1998). The soil density at full saturation ($\rho_{s\text{-}sat}$) and at field capacity ($\rho_{s\text{-}FC}$) were computed using conventional soil weight-volume phase relationships between n, water content (wc), and particle specific gravity (G_s) as given in Das (2016). It should be noted the degree of saturation at field capacity is 70% on average for the 12 USDA soil textures listed in Table 4.2. This high degree of saturation indicates that the soils at field capacity are closer to the saturated state than to a completely dry state, which is common for agricultural soils. Therefore, it is more practical and plausible to use the geometric mean of E_s as representative

for both saturated and field capacity conditions, since field samples are more likely to be collected in these states for laboratory testing of mechanical properties.

4.4.3 Design Loads

The design loads applied on the walls of the subsurface drainage pipe consisted of hydrostatic loads (HL) from the groundwater table, earth loads (EL) from the soil mass, and imposed live loads (LL) from agri-machinery traffic at the surface. Each load type was applied separately as a distinct loading case in the numerical simulations. The principle of superposition was used to combine the resulting output stresses and deformations in order to evaluate the overall pipe response under various load case combinations. The nomenclature and description of the load cases are summarized in Table 4.3.

Table 4.3. Nomenclature for the design load cases

Load Case Type	Code	Description
Hydrostatic load, HL	HL1	maximum water table level (soil surface)
	HL3	minimum water table level (center of drainage pipe)
Earth load, EL	EL1	fully saturated soil
	EL3	partially saturated soil (field capacity)
Live load, LL	LL1	vertical stress from grain wagon
	LL2	vertical stress from harvester
	LL3	vertical stress from tractor

Note: EL is dependent on matching HL condition

4.4.3.1 Hydrostatic loads

The hydrostatic pressure on the surface of the pipe depends on the height of the groundwater table relative to the drain center (H_w) and is given by:

$$\sigma_{vw} = \sigma_{hw} = \rho_w g H_w \tag{4.6}$$

where σ_{vw} and σ_{hw} are the vertical and horizontal hydrostatic pressures on the external surface of the pipe wall, ρ_w is the density of water (1000 kg/m^3) and g is the gravitational acceleration (9.81 m/s^2). For the loading analysis, two water table positions were considered (Fig. 4.1): maximum level (HL1) and minimum level (HL3). The HL1 condition occurs when the

groundwater level (GWL) is at the soil surface, and $H_w = D_d$, where D_d is the depth of the drainage pipe from the soil surface. The HL3 condition that occurs when the GWL is at the

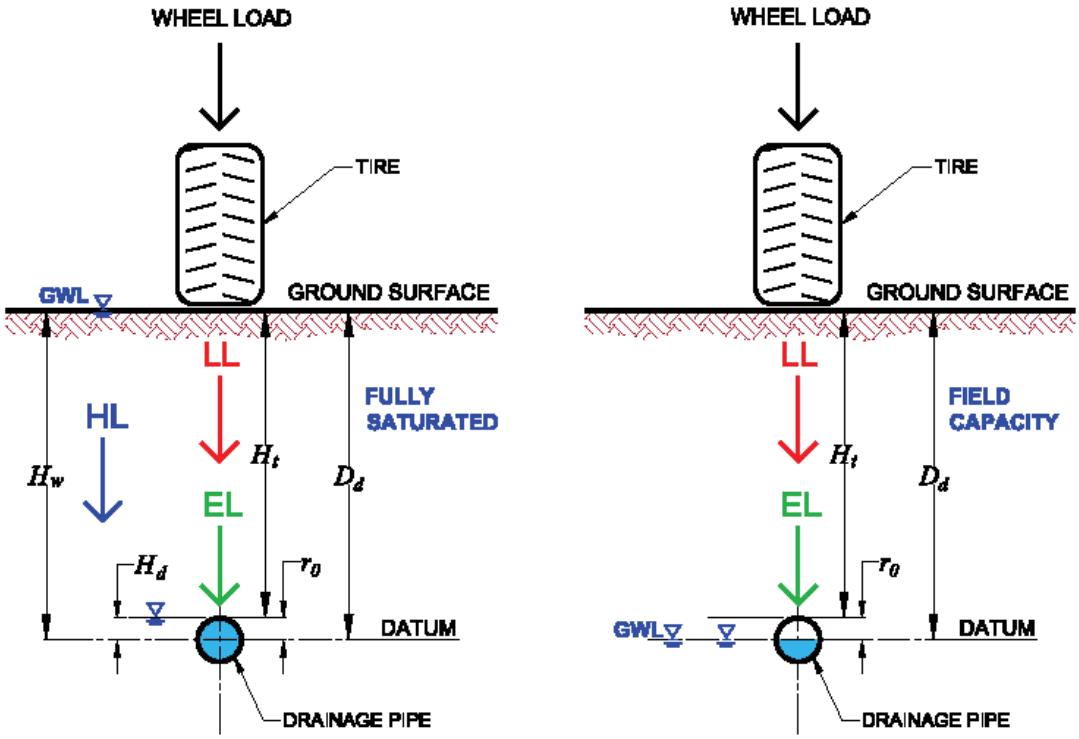

Fig. 4. 1. Design load cases and hydrostatic conditions.

Note: H_w and $H_d = 0$ for the minimum GWL.

center of the drainage pipe ($H_w = 0$). The corresponding hydrostatic pressure on the internal surface of the pipe wall (σ_i) was also computed as a design load with the hydraulic head on the drain outlet, H_d, replacing H_w in Eq. (4.6). The drainage pipe was assumed to be flowing full with a free-flow outlet for condition HL1 (Fig. 4.1), where H_d is equal to the external drain radius (r_0). For the HL3 condition, the pipe was assumed to be flowing half full with a free-flow outlet ($H_d = 0$).

4.4.3.2 Earth loads

For loading case EL, the static stress from the soil mass surrounding the buried pipe was computed using the following (Moore, 2001):

$$\sigma_{ve} = \rho_s g H_t \tag{4.7}$$

$$\sigma_{he} = K_0 \sigma_{ve} \tag{4.8}$$

$$K_0 = \frac{\mu_s}{(1-\mu_s)} \tag{4.9}$$

where σ_{ve} is the vertical earth stress, σ_{he} is the horizontal earth stress, K_0 is the at-rest lateral coefficient of earth pressure, and H_t is the height from the soil surface to the pipe crown (Fig. 4.1). The value of ρ_s in Eq. (4.7) is dependent on the two HL conditions previously described (section 4.4.3.1). For HL1, the soil is assumed to be fully saturated (EL1) and $\rho_s = \rho'_s = \rho_{s\text{-}sat} - \rho_w$, which represents the buoyant density of the soil solids. The soil mass was assumed to be at field capacity under HL3, representing a partially saturated condition (EL3), and therefore, $\rho_s = \rho_{s\text{-}FC}$ in Eq. (4.7).

4.4.3.3 Imposed live loads

The vertical stress from surface imposed loads (σ_{vi}) was computed for three types of vehicle commonly used on agricultural lands during farm operations: grain wagon, harvester, and tractor. The static wheel loads from these agri-machinery were computed for loading case LL. Previous studies have shown that static wheel loads produce the most adverse response for buried pipes when compared to dynamic wheel loads (Alzabeebee et al., 2018a; Sheldon et al., 2015; Yeau et al., 2009). The typical tire dimensions, inflation pressures, and axle load distributions are listed in Table 4.4. The grain wagon (Brent Avalanche Model 2096) and harvester (John Deere Model S790) were assumed to have storage capacities of 70.5 m^3 (2000 bushels) and 14.1 m^3 (400 bushels), respectively. It was also assumed that both grain wagon and harvester were loaded with grains and/or seeds having a maximum bulk density of 800 kg/m^3 following ANSI/ASAE D241.4 (ANSI/ASAE, 2017).

The axle load distribution for the grain wagon and harvester are based on the manufacturers' catalogues (Brent, 2016; John Deere, 2018). The tractor's (John Deere Model 8400R) axle

load was assumed to be distributed as 40%:60% front to rear axle following Keller et al. (2019). The maximum wheel load for each type of machinery in Table 4.4 was used to

Table 4.4. Tire, axle, and wheel load details used for imposed live loads

Machinery	Tire dimensions	Tire inflation pressure[a] (kPa)	Axle load distribution	Wheel load[b] (kN)
Grain Wagon	900/60 R38 steerable tandem	240	48% on each tandem 4% on tongue	168.1[c]
Harvester	900/60 R38 front	320	60% front axle	94.3[c]
	620/75 R26 rear		40% rear axle	62.8[c]
Tractor	380/85 R38 front	160	40% front axle	28.0
	480/80 R50 rear		60% rear axle	42.0

[a] nominal tire pressure as recommended by manufacturer, [b] wheel loads are for a single tire per axle, [c] based on the max. grain bulk density (800 kg/m^3).

estimate the stress transmission of σ_{vi} with increasing depth. The stress transmission was simulated with SoilFlex (Keller et al., 2006), which calculates the stress state in soils due to agricultural field traffic. SoilFlex uses the wheel load, tire pressure, and tire dimensions as input, and computes σ_{vi} using stress propagation equations developed by Boussinesq (1885), Frohlich (1934), and Sohne (1953) for homogeneous, isotropic, and elastic soil masses (Keller et al., 2006). The contact area at the tire-soil interface in SoilFlex was modelled as a super ellipse following Keller (2005) and Schjonning et al. (2008).

4.4.4 Model Implementation

Numerical models of a single-wall corrugated HDPE drainage pipe with and without perforations were developed using COMSOL Multiphysics® version 5.3 (COMSOL Multiphysics, 2017a). The structural response of the buried pipe was formulated as a boundary value problem for which the theory of elasticity under small strains is assumed to be valid. The solid mechanics interface in COMSOL's Structural Mechanics Module was used to create the pipe geometry, assign material properties, prescribe boundary loads, and

specify end fixity constraints on the surfaces of the pipe. The boundary load on the external pipe wall was computed using Eq. (4.1) for normal stresses (σ_r), and Eq. (4.2) for shear stress (τ_θ). Hoop symmetries in the XY and ZY planes (Fig. 4.2) were utilized in order to reduce computational time, resulting in only the first quadrant of the pipe being modelled. No displacement in the hoop direction (normal to the surface) was prescribed for these symmetries at the pipe's crown ($\theta = 0$) and springline ($\theta = \pi/2$). Similarly, axial symmetries in the ZX planes (at the center of the corrugation valleys) were implemented to reduce the model size, and a free displacement (no end restraints) boundary conditions was prescribed at each end. COMSOL uses the finite element method (FEM) to solve for the dependent displacement vector field, **u** (r, θ, a), which results from the deformation of a solid mass under loading (COMSOL Multiphysics, 2017b). The resulting stresses in the pipe wall and the vertical deflection at the crown were computed as outputs during post-processing. These model outputs were evaluated against the recommended design strength and performance limits for corrugated HDPE pipes.

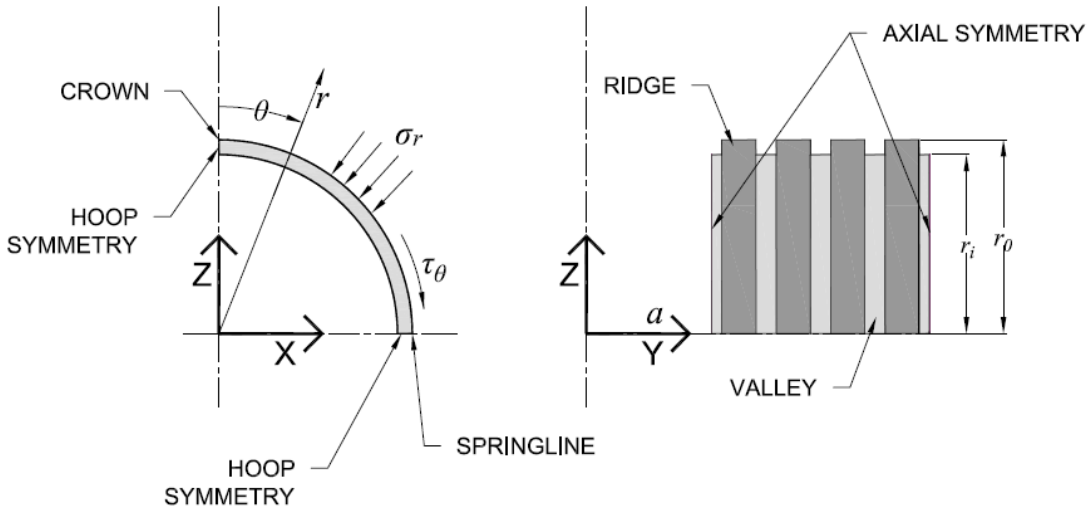

Fig. 4. 2. Definition sketch and boundary conditions on the pipe surfaces (1st quadrant).

4.4.5 Mesh Refinement and Verification

A mesh refinement study was done in order to establish appropriate mesh size parameters for the discretized pipe geometry. Analytical solutions for computing stresses and deformation in corrugated pipes with perforations have not been previously established. Therefore, Lame's solutions (Lamé, 1852) for stresses in a plain wall cylinder subjected to σ_0 (Vullo, 2014) were used as a benchmark for the numerical model (Fig. 4.S1). COMSOL's built-in physics-controlled mesh generator was used to create mesh sizes ranging from "Coarser" to "Finer". The default "Coarser" mesh size varies from 20.9 mm to 4.4 mm, while the default "Finer" mesh size varies from 6.05 mm to 0.44 mm. The convergence towards the analytical solution is shown in Fig. 4.S2. The "Finer 2" mesh size was refined to within 1% relative error of the analytical solution of the normalized hoop (σ_θ/σ_0) and radial (σ_r/σ_0) stresses (Figs. 4.S3 and 4.S4).

For further refinement of the mesh size around the perforations, Kirsch's solution (Kirsch, 1898) to the hole in plate problem (Fig. 4.S5) was used as a benchmark following Brachman and Krushelnitzky (2002). The meshing parameters for "Finer 2" were adjusted to within 1% relative error of the analytical solution for the plane stress distribution at the edge of the hole (Murakami, 2017), giving the refined mesh size "Finer 4" (Figs 4.S6 and 4.S7).

Finally, a verification exercise using the "Finer 4" mesh size was done by comparing the analytical solutions of the K_{sc} for a single hole in a thin plain wall cylinder (Wu & Mu, 2003). Two scenarios were used in the verification exercise: a) uniform pressure on the internal surface, and b) axial tension on the cylinder's edge in the longitudinal direction (Fig. 4.S8). The verification results show that the maximum stresses predicted by COMSOL with a "Finer 4" mesh size are within 5% of the analytical solutions. Therefore, the "Finer 4" mesh parameters were adopted for the perforated corrugated HDPE models for the numerical simulations. The 3D finite element mesh for "Finer 4" is presented in Fig. 4.3 for the

perforated pipe model. The discretized mesh shows 42775 tetrahedral elements, representing the pipe model used with circular perforations placed in every corrugation valley (Fig. 4.4). The array function in COMSOL was used to extend the single-pitch model in Fig. 4.3 up to three pitch lengths (4.935 cm) in order to investigate the effects of the axial spacing of perforations on the stress and deformation of the corrugated pipe. The dimensions of the finite-element pipe model are given in Fig. 4.4. Maximum and minimum element sizes for the refined mesh are 2 mm and 0.082 mm, respectively. The detailed methods and results for the mesh refinement and verification exercises are given as supplemental data.

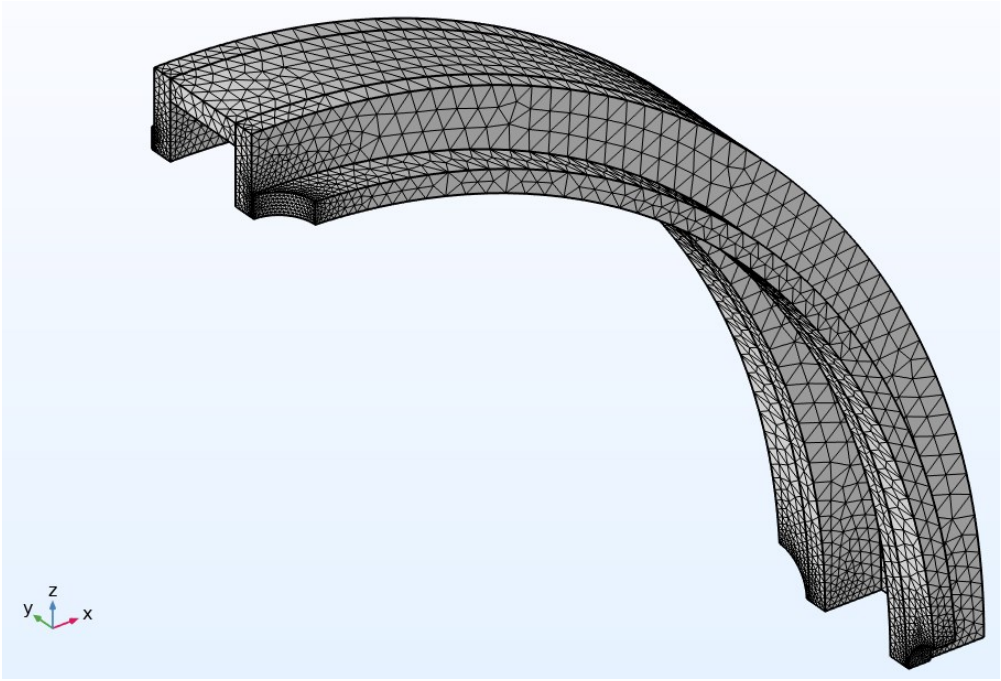

Fig. 4. 3. Three dimensional (3D) finite element mesh of the perforated pipe model.

4.4.6 Numerical Simulations and Design Variables

The numerical model of a non-perforated pipe was used in a series of parametric studies to investigate the structural response of corrugated HDPE pipes due to loading conditions described in section 4.4.3. In addition, two numerical models of perforated pipes were used to simulate the effects of perforation shape, size, and configuration on K_{sc} and $\Delta V/d_i$ for

corrugated HDPE pipes. Following Brachman and Krushelnitzky (2002), K_{sc} is defined in this study as

$$K_{sc} = \frac{(\sigma_e)_{perf}}{(\sigma_e)_{non-perf}} \tag{4.10}$$

where $(\sigma_e)_{perf}$ is the peak equivalent stress in the perforated pipe and $(\sigma_e)_{non\text{-}perf}$ is the peak equivalent stress in the non-perforated pipe at the same location. COMSOL computes σ_e using the von Mises formulation (Pilkey & Pilkey, 2008) with the principal stresses as

$$\sigma_e = \sqrt[2]{\frac{1}{2}\left[\left(\sigma_{p1} - \sigma_{p2}\right)^2 + \left(\sigma_{p2} - \sigma_{p3}\right)^2 + \left(\sigma_{p3} - \sigma_{p1}\right)^2\right]} \tag{4.11}$$

where σ_{p1} , σ_{p2} , and σ_{p3} are the first, second, and third principal stresses, respectively. The use of σ_e allows for a direct comparison against F_y for HDPE (Table 4.1) in order to assess the risk of failure by ductile yielding. The vertical deformation of the pipe at the crown, represented by $\Delta V/d_i$, was computed from COMSOL's simulation output values of the displacement field in the Z coordinate direction. The computed $\Delta V/d_i$ allows for a direct assessment of the corrugated HDPE pipe deflection against the 5% performance limit criterion.

The two shapes investigated with the perforated pipes models were circular holes (Model CWH) and rectangular slots (Model CWS). The primary perforation design variables considered (Fig. 4.4) were the number of perforation lines (N), the diameter of the holes (d_{perf}), length of the slots (L_{perf}), and the longitudinal spacing between perforations (a_y). Following standard industry practice (Stuyt et al., 2005), the perforations were positioned in the center of the valleys of the annular corrugation profile (Fig. 4.4) for both pipe models. The dimensions of the corrugation profile shown in Fig. 4.4 are representative of commercially available HDPE pipes used in agricultural land drainage. Small variations in

the dimension for the width of the ridge (w_r) and valley (w_v) of the corrugation generally exist between competing pipe manufacturers. However, these variations in the pitch ($w_r + w_v$) have very little effect on the pipe's geometric properties such as the cross sectional area (A_{pcs}) and the area moment of inertia (I_p), which controls the pipe stiffness (Krein, 1983). Furthermore, both A_{pcs} and I_p were deemed as non-sensitive parameters when computing the soil-pipe response to loading (analysis not presented).

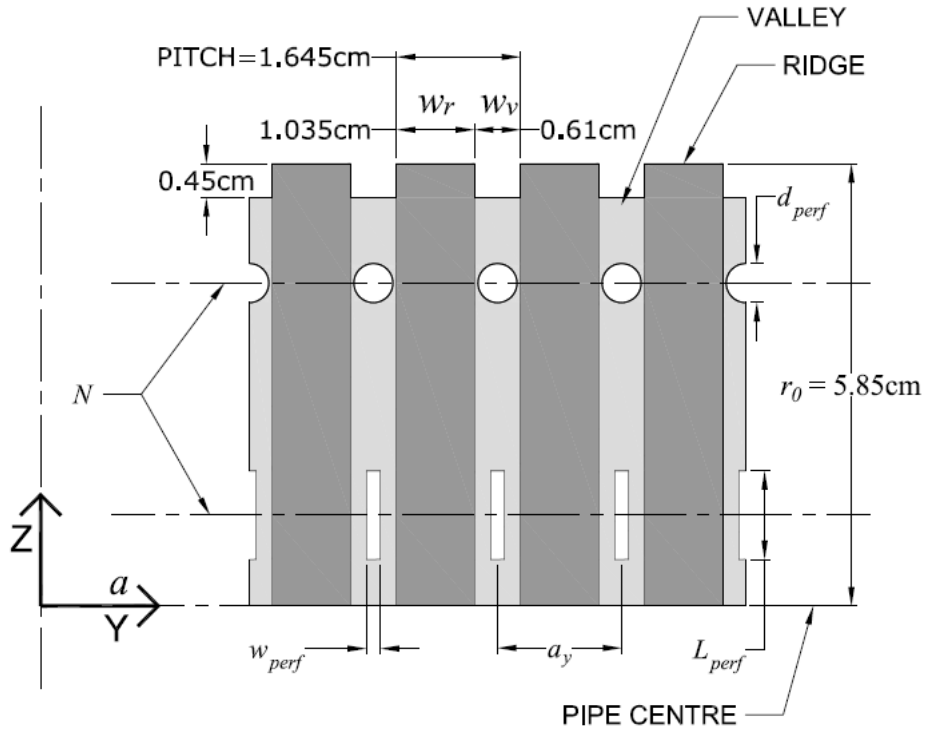

Fig. 4. 4. Perforation design variables and corrugation profile of drainage pipe.

Practical values for the perforation design variables were based on previous work by Gaj and Madramootoo (2020), who investigated the effects of perforations on the hydraulic performance of corrugated pipes. In this study, the range of values for N varies from 4 to 22 for Model CWH, and from 4 to 10 for Model CWS (the upper range is limited by the combination of L_{perf} and N around the pipe circumference). For Model CWH, the effect of d_{perf} was investigated over a range of 0.44 cm to 0.56 cm, given that the hole size is limited by w_v (0.61 cm). The effect of L_{perf} was examined between 1.0 cm to 2.5 cm using Model

CWS. The design variable a_y is controlled by the pitch of the corrugation, and is 1.645 cm, 3.290 cm, and 4.935 cm for perforations placed in every first, second, and third corrugation valley, respectively (Fig. 4.4).

The buried depth (or D_d) of the drainage pipe ultimately governs the boundary stress level on the outer surface of the pipe wall. Installation of drains by trenchless pipe laying machines becomes expensive and impractical at depths greater than 2.5 m (Madramootoo, 1999). Suitable design values for D_d are usually determined as part of the hydraulic design of the drainage pipe, and can vary between 0.9 m to 1.6 m across many soil and crop types on agricultural lands (Huffman et al., 2013). Furthermore, a minimum cover of 0.6 m for 100 mm diameter pipes is recommended by ASAE EP260.5 (ASAE, 2015) in order to avoid excessive deflection from agri-machinery traffic, and to prevent additional load on the pipe due to frost heave pressures in cold climates (Madramootoo, 1999). Therefore, D_d was also selected as an input design variable, with a range of 0.6 m to 1.6 m, for the numerical simulations in this study.

4.5 Results and Discussion

4.5.1 Vertical stress transmission from live loads

The vertical stress transmission of σ_{vi} using SoilFlex for the wheel loads from three types of agri-machinery is shown in Fig. 4.5. These stresses represent the peak σ_{vi}, located directly under the wheel in the direction of driving. Fig. 4.5 shows that σ_{vi} is largest for the loaded grain wagon (LL1) and smallest for the tractor (LL3). The stress decay pattern in Fig. 4.5 is similar for all three types of machine, and the difference in the stress magnitude becomes marginal as the depth increases. Importantly, the contact stress at the tire-soil interface was modelled in SoilFlex using representative tire inflation pressure and dimensions (Table 4.4). The resulting contact stresses (Figs. 4.S9-4.S11) are distributed non-uniformly over the tire-

soil interface, accurately capturing the stress distribution pattern under agri-machinery wheels as previously verified by field measurements using pressure transducers (Keller, 2005; Keller et al., 2014). These contact stresses were then used as the upper boundary condition when computing the vertical stress transmission through the soil medium in SoilFlex. At depths greater than 1.6 m, σ_{vi} is < 35 kPa for the three types of wheel load (Fig. 4.5), and therefore, applied boundary stresses from the combined earth and hydrostatic pressures (EL+HL) are

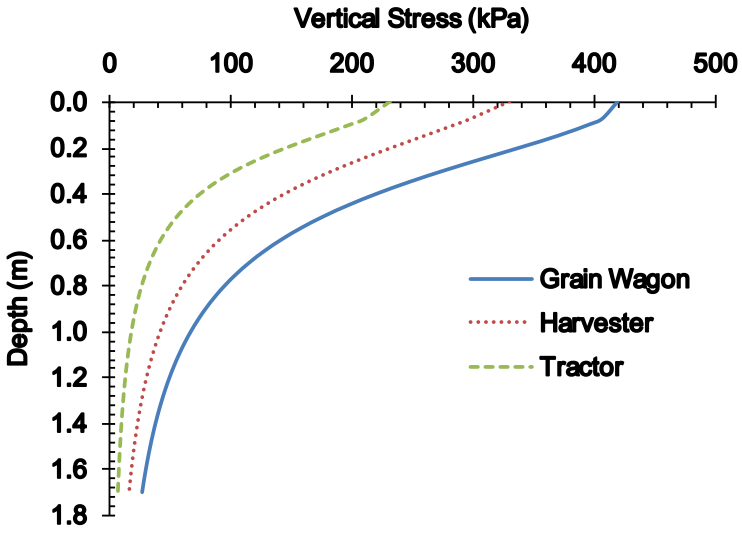

Fig. 4. 5. Stress transmission of σ_{vi} for the max. wheel loads of three agri-machinery.

likely to dominate the pipe response when D_d is > 1.6 m. In contrast, Fig. 4.5 shows that σ_{vi} is > 40 kPa for the wheel loads at a depth of 0.6 m. These larger applied boundary stresses from the wheel loads at such shallow depths may cause excessive pipe deformation, whereas those from the EL+HL cases at a similar depth can be deemed negligible in comparison. Hence, the LL design loading cases become central when assessing the structural response of corrugated HDPE pipes buried at depths between 0.6 - 1.6 m.

4.5.2 Response of non-perforated corrugated pipes

4.5.2.1 Effect of interface friction condition

The stresses in the pipe wall of a non-perforated corrugated HDPE pipe were simulated under loading from the previously described design load cases (Table 4.3) for the 12 USDA soil textures (Table 4.2), two water table conditions, and three agri-machinery wheel loads. The applied boundary stresses from these design load cases were computed for both the smooth and bonded interface friction conditions using arching factors (Appendix 4.A). The simulation results show that the pipe wall stresses (σ_e) are generally larger when the boundary stresses are modelled with the bonded friction condition at the soil-pipe interface. The maximum stress deviation ($\Delta\sigma_e$) occurs for corrugated pipes buried in a sandy clay loam (SC) soil, where σ_e (bonded) are 12.7% and 29.6% larger than σ_e (smooth) for the LL and EL cases, respectively (Table 4.S1). Moore (2001) reported a similar finding for plain wall HDPE pipes, and concluded that the bonded condition produces conservative pipe wall stresses. However, results from two particular loading conditions used in this study indicate an exception to this trend. For the LL cases with sandy loam (SM) and silt loam (ML) soils, σ_e (smooth) are 3.7% and 6.4% larger than σ_e (bonded), respectively.

The departure in trend for the SM and ML soils can be explained by the arching mechanism of the soil-pipe system, which is driven by the complex relationship between the soil and pipe elastic constants. Both SM and ML soils were simulated with relatively small values of E_s (Table 4.2) compared to the other soil types. These lower soil moduli yielded the largest arching factors for the smooth interface friction condition (Table 4.2). As a result, the applied boundary stresses for the smooth friction condition with the SM and ML soils are considerably larger than those for the other soil types under the LL cases.

For most of the remaining load case and soil type combinations in Table 4.S1, values of $\Delta\sigma_e$ are < 3%. It is worth noting that the even though the difference between σ_e (smooth) and σ_e (bonded) can be as large as 30% for the EL case with SC soils (EL-SC), the absolute magnitude of the wall stresses are very small (<1.0 MPa) for the EL cases with all soil types. In fact, the difference may be considered negligible for both the LL and EL cases. In order to confirm this assumption, the difference between σ_e (smooth) and σ_e (bonded) was tested for statistical significance (5% level) using the Welch's t-test (Moser & Stevens, 1992). The results (not presented) show that the difference in σ_e is not statistically significant when tested within each load case and soil type combination. These results indicate that although the friction condition at the soil-pipe interface has an effect on the simulated pipe wall stresses, the difference is insignificant for 100 mm diameter corrugated HDPE pipes buried between 0.6 to 1.6 m. Therefore, for simplicity, only the average values of σ_e (smooth) and σ_e (bonded) are presented elsewhere in this study.

4.5.2.2 Wall stresses

Figs. 4.6a and 4.6b show the variation of the maximum σ_e with D_d for two soil textures and the various LL and EL + HL cases, respectively. The ML and SC soil textures were presented because they represent the maximum and minimum stress response in the buried corrugated pipe, respectively. Fig. 4.6a indicates that the stresses in the pipe wall generally decrease non-linearly with increasing depth for the three LL cases, regardless of the soil type. More notably, σ_e for case LL1-ML is at least one order of magnitude larger than those for LL3-SC. This disparity in σ_e can be explained by the differences in soil stiffness between the ML and SC soils, and by the variation in the applied wheel loads. Case LL1-ML represents a loaded grain wagon's wheel load on a silt loam soil, which has the lower E_s (Table 4.2). In comparison, case LL3-SC represents the smaller wheel load of a tractor on a sandy clay loam soil, which has a larger E_s and is therefore stiffer than the ML soil. More importantly, the

resulting stresses from the LL cases are well below the short term F_y of HDPE pipes (21.4 MPa).

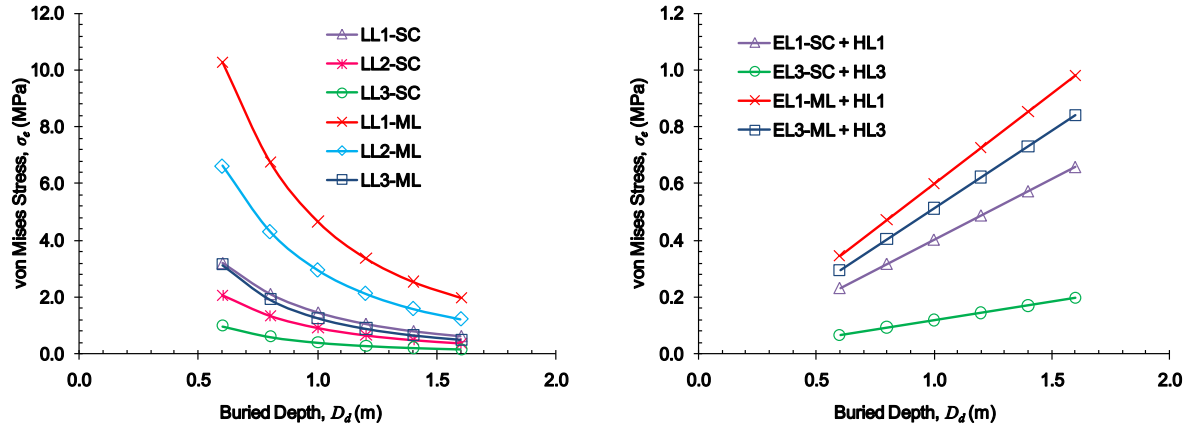

(a) (b)

Fig. 4. 6. Variation of the maximum σ_e with D_d in non-perforated pipes under load cases (a) LL and (b) EL + HL.

Fig. 4.6b shows that σ_e increases linearly with D_d for all of the combined EL + HL cases. Higher stresses in the pipe wall occur for the ML soil under both fully and partially saturated conditions. As previously discussed, the lower σ_e values for the SC soil can be explained by the larger soil stiffness in comparison to the ML soil. The long term F_y of HDPE pipes is 7.1 MPa, which is far greater that the maximum σ_e for the EL + HL cases. Therefore, failure of non-perforated corrugated HDPE drainage pipes by ductile yielding is highly unlikely under the field traffic, soil, and water table conditions investigated in this study. To facilitate the estimation of the maximum σ_e as a function of D_d for all load case and soil type combinations considered in this study, regression equations were fitted to the simulated σ_e values (Table 4.S2). The predicted-simulated relationship for the regression equations developed are shown in Figs. 4.S12-4.S13 (Appendix 4.C).

It is important to note that the stresses presented in Figs. 4.6 (a) and 4.6 (b) are the maximum σ_e, which occurs on the inner surface of the corrugation valley at the pipe's springline. Fig. 4.7 maps the local distribution of σ_e within the structural elements of a single-wall non-

perforated corrugated pipe profile for case LL1-ML at D_d = 0.6 m. The contour stress plot illustrates that the variation of σ_e for a corrugated pipe follows the general trend for stress distribution in a plain wall pipe, where stresses are maximum at the crown and springline. This trend can be explained by the harmonic nature of the applied radial boundary stress, $\sigma_2 \cos 2\theta$, which is maximum at the crown (θ = 0°) and the springline (θ = 90°). Moreover, the cross section geometry also influences the local variation of σ_e in corrugated pipes.

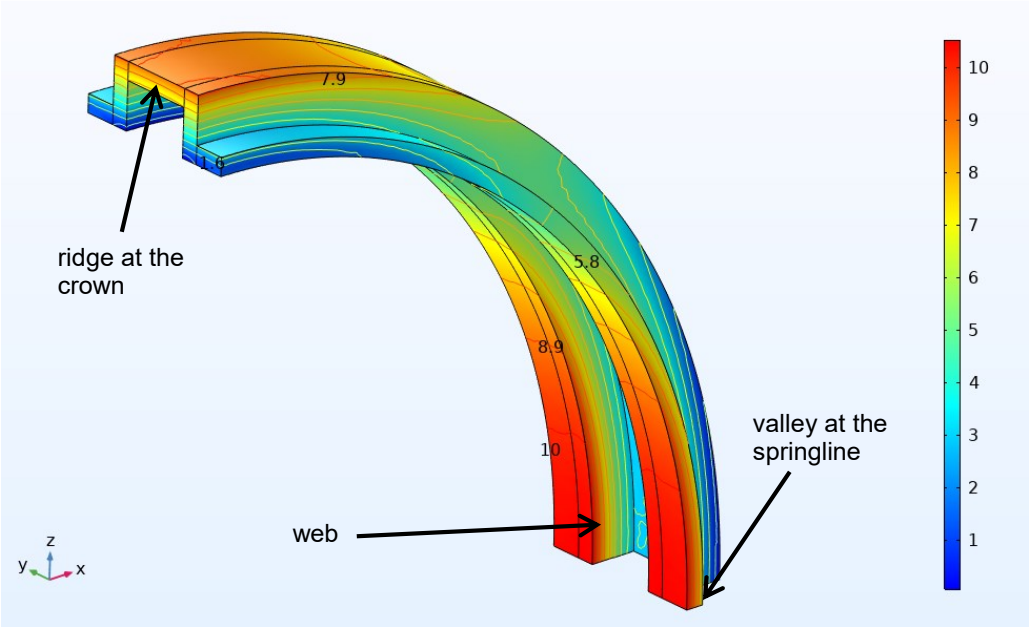

Fig. 4. 7. von Mises stress (σ_e) distribution in a non-perforated corrugated HDPE pipe (MPa) for load case LL1-ML at 0.6 m burial depth.

For example, σ_e in the corrugation valley transitions from minimum at the crown to maximum at the springline. The transition is reversed for the corrugation ridge, where a large σ_e occurs on the outer surface of the ridge at the pipe's crown. In comparison, there is very little variation in σ_e within the corrugation web, where the stresses are intermediate in magnitude. These local variation in σ_e can be explained by the mechanics of flexural stresses in the pipe section. Analogous to engineering beams, reaction thrusts and bending moments develop at the crown and springline of the pipe in response to the applied loads (Moore, 2001). The combined normal and bending stresses from the reactions will result in maximum

compressive hoop stresses in the top flange above the neutral axis (ridge) at the crown and in the bottom flange below the neutral axis (valley) at the springline (Appendix 4.B). This effect is appropriately reflected by σ_e in the corrugated pipe response (Fig. 4.7) given that the compressive hoop stress represents the major principal stress (σ_{p1}), which, is also considerably larger than the other principal stresses in buried pipes (Brachman & Krushelnitzky, 2002).

4.5.3 Response of corrugated pipes with circular holes

4.5.3.1 Wall stresses around holes

Model CWH was used to investigate the effect of d_{perf} on the stress distribution in the pipe wall for the specific case with four lines of perforation (N = 4) spaced in every corrugation valley (a_y = 1.645 cm). Figs. 4.8a and 4.8b present the maximum σ_e as a function of D_d for

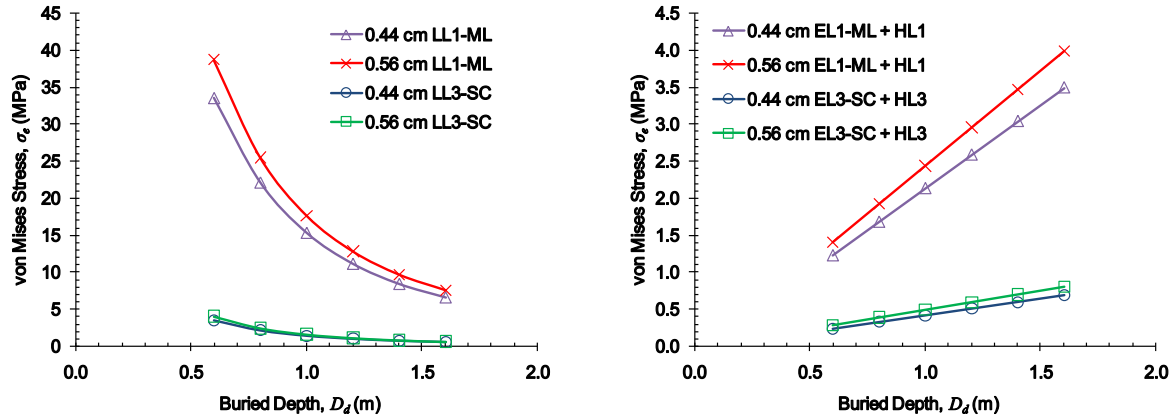

(a) (b)

Fig. 4. 8. Variation of the maximum σ_e with D_d for two perforation diameters under load cases (a) LL and (b) EL +HL.

two hole diameters under loading from the most extreme LL and EL + HL cases, respectively. These extreme load cases were selected because they induce the maximum and minimum stress response for a non-perforated corrugated HDPE pipe as previously shown (Figs. 4.6a and 4.6b).

Figs. 4.8a and 4.8b show that the variation of σ_e with D_d for a perforated pipe follows the same trends as those for a non-perforated pipe. However, the magnitudes of the wall stresses are considerably greater due to the stress concentration around the perforation. The stresses in the pipe wall for load case LL1-ML exceeds the short term F_y of HDPE pipes (21.4 MPa) at depths shallower than 0.9 m (Fig. 4.6a). This finding suggests that corrugated HDPE pipes with circular perforations should be buried at a depth of at least 0.9 m in silt loam soils (or soils with similar stiffness) in order to reduce the risk of failure against the imposed stresses from a loaded grain wagon. It should be noted that when stresses exceed F_y, a non-linear pipe model is more suitable for capturing the redistribution of stresses after ductile yielding. However, non-linear pipe models require additional input parameters that are not currently available for small diameter, single-wall corrugated HDPE pipes subjected to the agricultural loading conditions used in this study. The use of linear elasticity for modelling single-wall corrugated HDPE pipes serves as a reasonable first approximation to the problem of stress response in buried pipes (Moore & Hu, 1995). Further research conducted with strain gauge experiments are needed to generate the required input data necessary for characterizing the non-linear behaviour of single-wall corrugated HDPE pipes. On the other hand, Fig. 4.8b shows that there is virtually no risk of failure due to long-term ductile yielding under the soil and water table conditions considered (EL + HL), since the wall stresses in a perforated pipe are well below 7.1 MPa (Table 4.1).

The results in Figs. 4.8a-4.8b also demonstrate that σ_e is generally larger (≈15%) for a corrugated pipe with 0.56 cm diameter holes than that with 0.44 cm diameter holes for all load cases. The increase in σ_e with increasing d_{perf} can be explained by the concentration of the compressive hoop stresses in the corrugation valley of the pipe. This effect is comparable to the stress concentration around a hole in a plate with a finite width, subject to an axial load on the boundary (Murakami, 2017). As the diameter of the hole increases, the net cross

sectional area of the valley in the hoop direction decreases. This reduction in area forces the compressive hoop stress to concentrate around the edges of the hole closest to the corrugation web. Fig. 4.9 illustrates this effect for the perforated pipe subjected to load case LL1-ML at D_d = 0.6 m. The maximum σ_e occurs on the edge of the 0.56 cm diameter hole in the corrugation valley at the springline of the pipe.

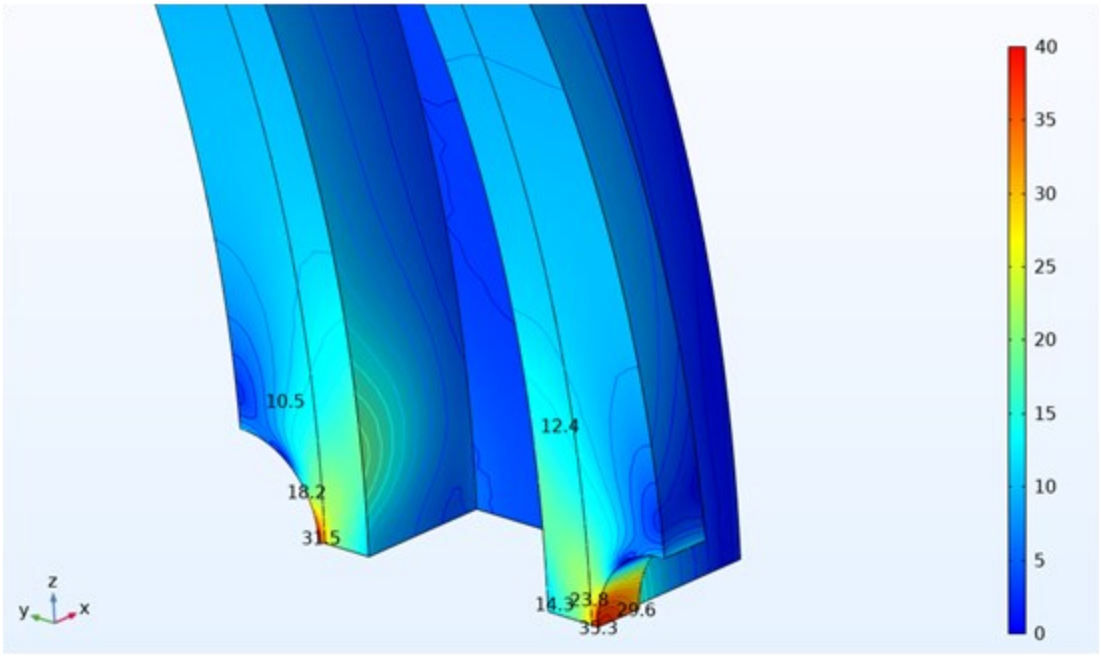

Fig. 4. 9. Peak von Mises stress (σ_e) at the edge of a circular hole located at the pipe springline (MPa). Perforations placed in every corrugation valley (a_y = 1.645 cm).

4.5.3.2 Stress concentration factor for holes

To further investigate the effect of d_{perf} in corrugated pipes, Eq. (4.10) was used to compute K_{sc} values for the perforated drainage pipe under all load cases considered. The results (not presented) show that D_d does not affect K_{sc}. A small variation (< 4%) in K_{sc} between the LL and EL + HL cases exists, but this can be deemed negligible. Consequently, the mean K_{sc} is presented in Fig. 4.10 as a function of d_{perf} normalized by the width of the corrugation valley, w_v. Fig. 4.10 shows that the stress concentration also increases with the perforation diameter. Brachman and Krushelnitzky (2002) reported similar increases in K_{sc} with d_{perf} for plain wall pipes under deep burials, indicating that the effect of d_{perf} is present in buried pipes regardless

of the wall geometry. However, the presence of the web next to the corrugation valley limits the increase in K_{sc}, which is shown to approach a limiting value of 4.3 as d_{perf}/w_v approaches unity.

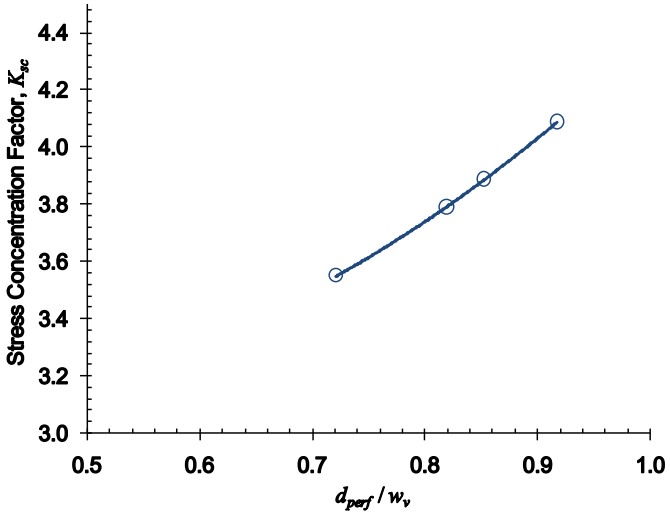

Fig. 4. 10. Stress concentration factors (K_{sc}) for circular holes in corrugated pipes. The perforation diameter (d_{perf}) is normalized by the width of the corrugation valley (w_v).

A quadratic regression equation was fitted (R^2 = 99.9%) to the data in Fig. 4.10 in order to establish a predictive relationship between K_{sc} and d_{perf}

$$(K_{sc})_{holes} = 2.78\left(\frac{d_{perf}}{w_v}\right)^2 - 1.83\left(\frac{d_{perf}}{w_v}\right) + 3.42 \quad (4.12)$$

where d_{perf} and w_v are in consistent units. It is important to note that this relationship is applicable to circular holes located at the springline of the pipe. If the holes are located at the pipe's quarter points (shoulders and haunches), then both the wall stresses and K_{sc} will be lower in magnitude. However, flexible corrugated pipes are installed by trenchless drain laying plows on agricultural lands, and the exact location of the perforation relative to the crown cannot be controlled. It is, therefore, both practical and realistic to account for perforations oriented at the springline, which represents the most critical position that will induce the maximum stresses in buried pipes.

4.5.3.3 Deformation due to holes

The effect of d_{perf} on the deformation of the corrugated pipe was also investigated using Model CWH. Figs. 4.11a and 4.11b show the percent vertical deflection ($\Delta V/d_i$) at the pipe's crown in response to the extreme load cases of LL and EL + HL, respectively. The general

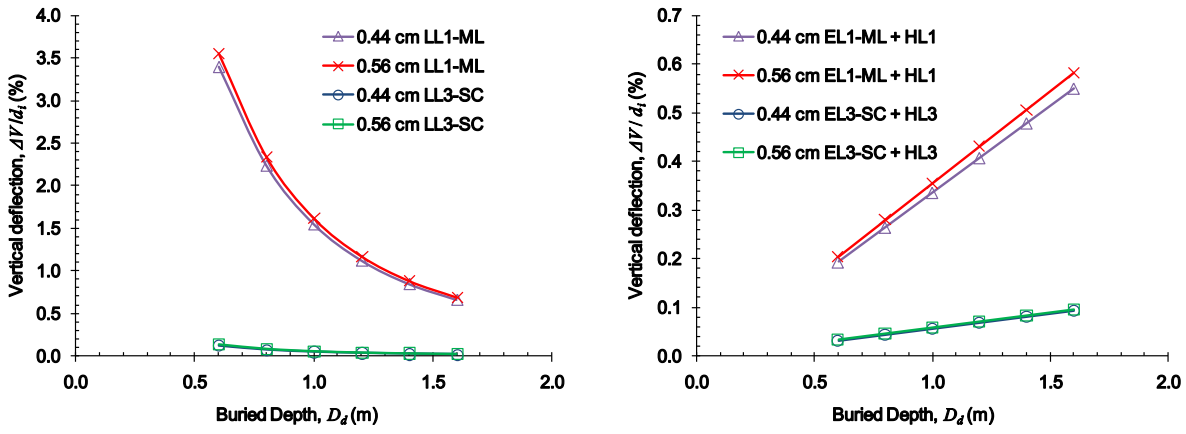

(a) (b)

Fig. 4. 11. Vertical deflection ($\Delta V/d_i$) for two perforation diameters under load cases (a) LL and (b) EL +HL.

trend for $\Delta V/d_i$ with increasing D_d is similar to that of σ_e; i.e. decreasing for case LL and increasing for case EL + HL. The $\Delta V/d_i$ for 0.56 cm holes are generally 5% greater than those for 0.44 cm holes under all load cases, and therefore, the effect of the perforation diameter on the deflection of corrugated HDPE pipes can be considered negligible.

Overall, the maximum $\Delta V/d_i$ is 3.5% and it occurs at a buried depth of 0.6 m for load case LL1-ML (Fig. 4.11a). Under the same load conditions, a non-perforated pipe will deflect at the crown by 3.2% of its diameter (not presented). This comparison shows that introducing four lines of circular holes in the corrugation valley can increase the pipe deflection by 10%. These results are comparable to parallel plate test results reported by Walker (1979), who showed that corrugated HDPE pipes with perforations had deflections that were 5% greater than those for non-perforated pipes. Nonetheless, the short-term deflection due to a loaded grain wagon is within the 5% recommended performance limit. Importantly, the pipe

deflections under long-term soil and water table conditions (EL + HL) does not exceed 0.6% of its diameter at the deepest burial depth (Fig. 4.11b).

4.5.4 Effect of axial spacing

The spacing between perforations in the longitudinal or axial direction (a_y) can influence the local stress distribution in the pipe wall. Accordingly, Model CWH was used to investigate the effect of a_y on the stress and deformation of corrugated HDPE pipes. The 0.56 cm diameter holes were modelled in the corrugation valley at the crown and springline for the special case of N = 4. The length of Model CWH in the Y-direction was varied in order to facilitate axial distances of 1.645, 3.29, and 4.935 cm between holes in every first, second and third corrugation valley, respectively. Fig. 4.12a shows the distribution of σ_e for the three axial distances under load case LL1-ML, which represents the largest of the applied boundary loads. The perforations spaced in every corrugation valley (a_y = 1.645 cm) induces stresses in the pipe wall that are approximately 10% larger than those with a wider spacing. Brachman and Krushelnitzky (2002) investigated the interaction between closely spaced holes in the axial direction for buried plain wall pipes. Their analysis showed that there was no interaction between holes that had a spacing greater than four times the perforation diameter. The results presented in Fig. 12a are in general agreement with Brachman and Krushelnitzky (2002), because the difference in σ_e is negligible for holes spaced more than two valleys away (a_y/d_{perf} > 4). Furthermore, the results also indicate that the presence of the web in a corrugated pipe inhibits direct interaction between perforations in the axial direction (Fig 4.13); and as such, holes may be placed at the closest possible spacing (in every valley) as determined by the pitch of the corrugated pipe.

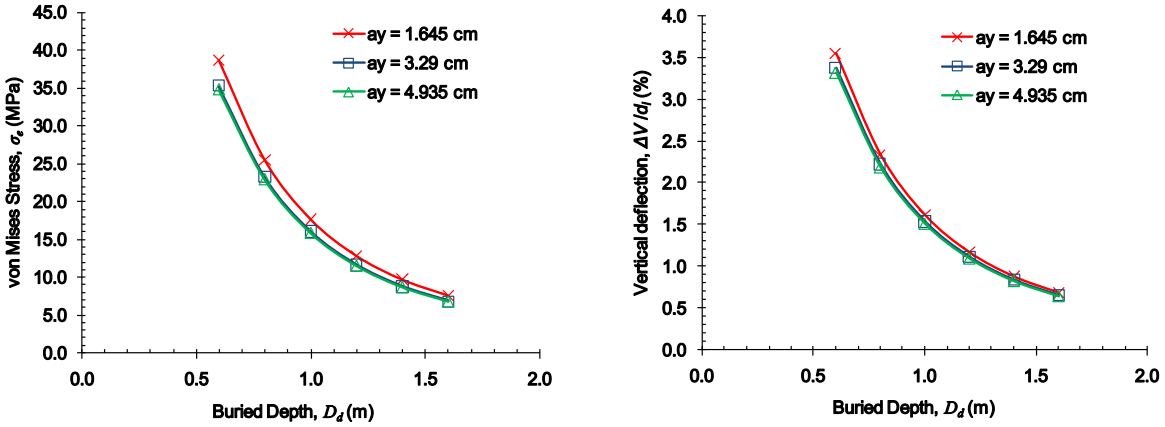

(a) (b)

Fig. 4. 12. Effect of axial spacing (a_y) on (a) σ_e and (b) $\Delta V/d_i$ for 0.56 cm diameter holes and load case LL1-ML.

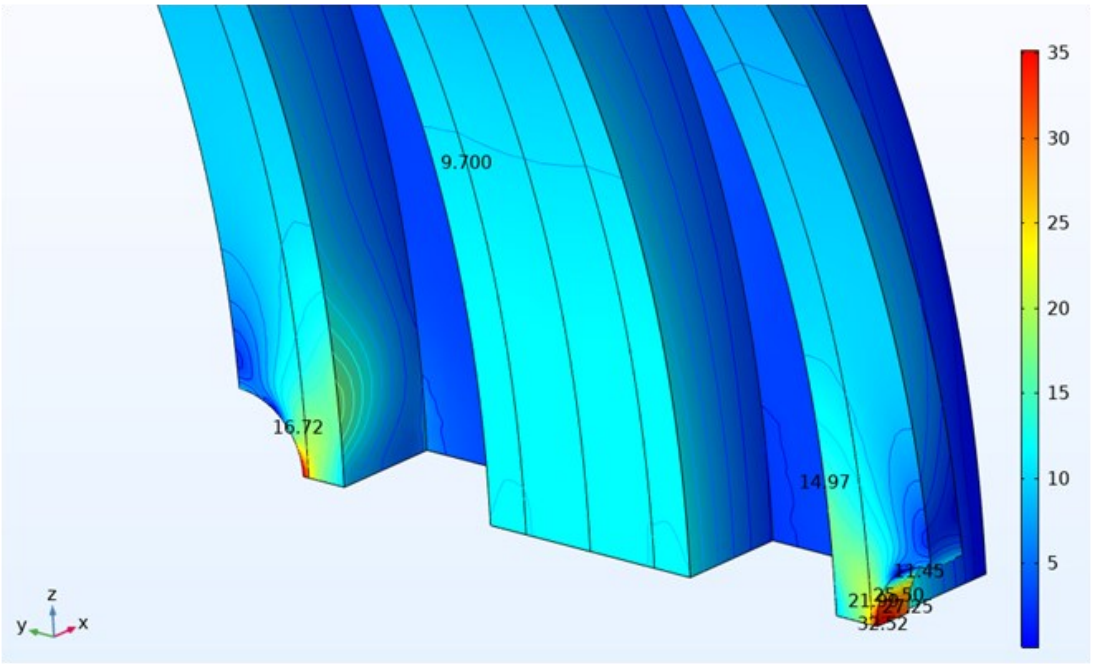

Fig. 4. 13. Effect of axial spacing on von Mises stress (σ_e) around perforations (MPa) placed in every second corrugation valley (a_y = 3.29 cm).

The deformation of the pipe under the same perforation pattern and loading conditions was also investigated. Fig. 4.12b illustrates that there is virtually no difference in $\Delta V/d_i$ between holes with varying axial distances. This result can be explained by the fact that the pipe stiffness, which controls deflection through E_p and I_p, is a property of the cross-section area that manifests itself in the circumferential direction. Therefore, deflection is not sensitive to

changes in the pipe geometry in the axial direction as a result of the perforations. These results suggest that it is therefore feasible to place a perforation in every valley for corrugated pipes.

4.5.5 Effect of Circumferential spacing

The circumferential or hoop spacing of circular perforations is dependent on the value of N for a given configuration. Any increase in N will reduce the spacing between two adjacent perforations in the hoop direction of the pipe. Model CWH was used to investigate the effect of N on the stress and deformation of the corrugated HDPE pipe. Three configurations of equally spaced perforations (N = 4, 12 and 22) in every corrugation valley (a_y = 1.645 cm) were selected for the analysis (Fig. 4.S14). The 0.56 cm diameter holes were oriented in a manner that placed one of the perforations at the pipe's springline. This pattern was chosen to simulate the maximum wall stresses, which occurs in the corrugation valley at the springline. Fig. 4.14a shows the results from the stress analysis under load case LL1-ML. Generally, an increase in N reduces σ_e around the perforations in the pipe wall. The reduction in σ_e is approximately 13% as N increases from 4 to 12, and 11% as N increases from 12 to 22. While

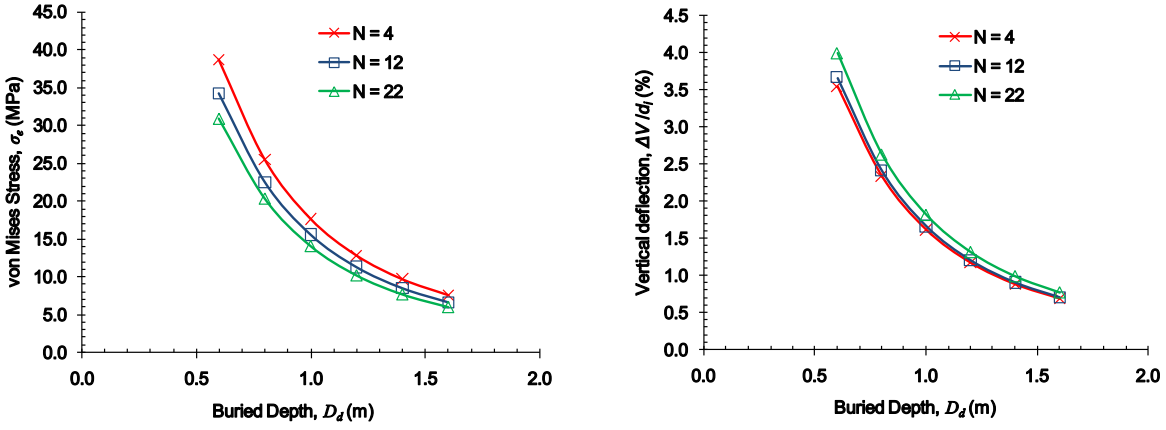

(a) (b)

Fig. 4. 14. Effect of N on (a) σ_e and (b) $\Delta V/d_i$ for 0.56 cm diameter holes and load case LL1-ML.

this effect appears to be counter-intuitive, a similar observation was reported for plain wall pipes by Brachman and Krushelnitzky (2002), who showed that the stress concentration

generally decreases with increases in N. The decrease in σ_e can be explained by the interaction of the stress field between two adjacent holes in a thin plate (Pilkey & Pilkey, 2008). When the boundary stress is applied parallel to the direction of the holes, the stress concentration decreases if the spacing between the hole is small (<10 × d_{perf}). For N = 12 and 22 in Model CWH, the circumferential spacing (arc length) between any two holes is 4.05 and 1.75 times d_{perf}, respectively. The small arc lengths between the holes in the hoop direction may therefore account for the decrease in σ_e relative to the wall stresses when N =4 (arc length >10 × d_{perf}).

In contrast, the vertical deflection of the pipe increases with an increasing N (Fig. 4.14b). The increase in $\Delta V/d_i$ is approximately 3% as N increases from 4 to 12, and 12% as N increases from 4 to 22. This increase in deformation can be explained by the loss in pipe stiffness due to the presence of a larger number of perforations in the hoop direction. As previously discussed (section 4.5.4), the pipe stiffness is a function of the cross-section in the hoop direction. Therefore, a large increase in N will reduce the overall I_p between the crown and springline, resulting in an increase of the pipe deflection. Although the values of $\Delta V/d_i$ in Fig. 4.14b are still below the 5% performance limit, the results suggest that increasing the number of holes in the hoop direction may increase the risk of failure by excessive deformation for corrugated HDPE pipes at shallow burial depths (D_d = 0.6 m).

4.5.6 Response of corrugated pipes with rectangular slots

4.5.6.1 Wall stresses around slots

The previously discussed trends of the stress distribution and deformation for Model CWH are generally applicable to Model CWS under the same loading conditions. Specifically, the effects of the axial and circumferential spacing of the perforations are expected to be common for both holes and slots. However, the dimensions of the rectangular slots (L_{perf} and

w_{perf}) may affect the local stress concentration in the pipe wall in a manner similar to d_{perf}. Thus, Model CWS was used to investigate the effects of L_{perf} and w_{perf} on the pipe response (σ_e and $\Delta V/d_i$) under load case LL1-ML. For consistency, four lines of perforations (N=4) placed at the springline in the every corrugation valley of the pipe wall (a_y=1.645 cm) was chosen for the perforation configuration during the simulations.

To assess the effects of L_{perf} between 1.0 and 2.5 cm, simulations were run with a fixed w_{perf} of 0.2 cm. The results (not presented) show that the wall stresses only increase by 5.3% over the range of L_{perf} investigated. A Welch's t-test indicated that the increase in σ_e is not statistically significant (p = 0.89) at a 5% significance level, and therefore, L_{perf} may be considered as an unimportant factor affecting the wall stresses in corrugated pipes. On the other hand, σ_e in the pipe wall was found to be greatly influenced by changes in w_{perf}. Using a fixed L_{perf} of 1.75 cm (mid-point of range), simulations were carried out with w_{perf} varying from 0.1 to 0.56 cm (same as maximum d_{perf}). The results show that σ_e increases by a factor of 2.7 over the range of the slot width examined (Fig. 4.15).

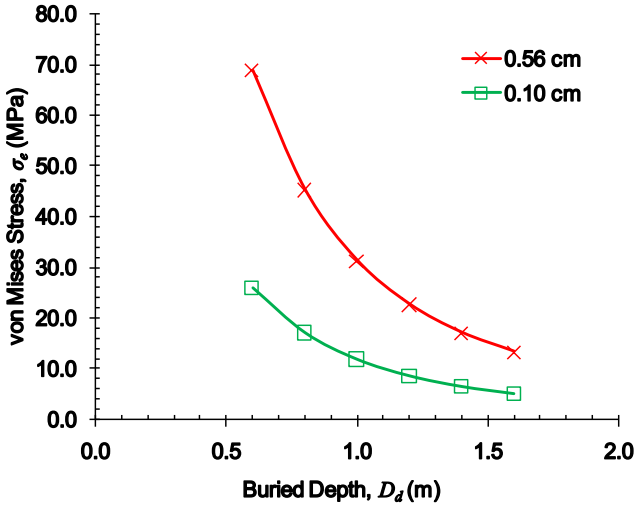

Fig. 4. 15. Effect of w_{perf} on σ_e in the pipe wall for rectangular slots under load case LL1-ML.

The large increase in σ_e with increasing w_{perf} can be explained by the concentration of the compressive hoop stress in the pipe wall. In fact, this effect is very similar to the response of

σ_e with increasing d_{perf} (section 4.5.3.1). The magnitude of σ_e, however, is far greater for w_{perf} than d_{perf} at their maximum value of 0.56 cm. This disparity can be attributed to the difference in shape between the circular holes and rectangular slots. Furthermore, the sharp edges at the corner of the slots can produce areas of infinitely high stresses (singularities) in numerical models. To mitigate this limitation, the mesh refinement parameters were further adjusted in Model CWS. An assessment of the mesh size was done using the notch in plate problem following Murakami (2017). The results from the refinement (Fig. 4.S15) show that the refined mesh size is sufficient for modelling the high stresses at the tip of the notch, and is therefore suitable for Model CWS (see supplemental data for further details).

4.5.6.2 Stress concentration factor for slots

Using Eq. (4.10), values of K_{sc} for corrugated pipes with rectangular slots were computed for all load cases. Fig. 4.16 shows that K_{sc} increases with an increasing w_{perf}. This effect is expected, because the net cross-sectional area in the corrugation valley decreases in the hoop direction as w_{perf} increases. As previously discussed for holes (section 4.5.3.2), the presence of the corrugation web establishes an upper limit of K_{sc}, which is 9.2 when w_{perf} /w_v approaches unity.

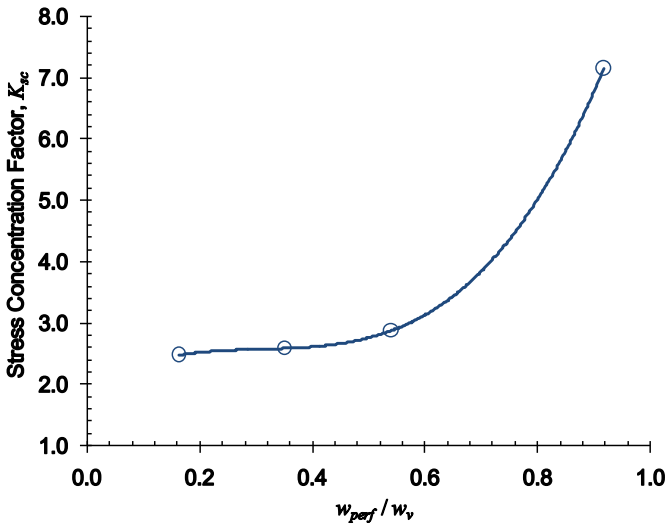

Fig. 4. 16. Stress concentration factors (K_{sc}) for rectangular slots in corrugated pipes. The perforation width (w_{perf}) is normalized by the width of the corrugation valley (w_v).

A cubic regression equation was fitted (R^2 = 99.9%) to the data in Fig. 4.16, establishing a predictive relationship between K_{sc} and w_{perf}

$$(K_{sc})_{slots} = 19.58\left(\frac{w_{perf}}{w_v}\right)^3 - 18.17\left(\frac{w_{perf}}{w_v}\right)^2 + 5.88\left(\frac{d_{perf}}{w_v}\right) + 1.92 \qquad (4.13)$$

where w_{perf} and w_v are in consistent units. Interestingly, the results in Fig. 4.16. suggests that limiting w_{perf} to half of w_v , as recommended by Fouss (1973), will result in K_{sc} values below 2.7. For comparison, holes will produce a K_{sc} of 3.2 when d_{perf} is half of w_v [Eq. (4.12)], indicating that slots may be more advantageous in limiting the stress concentration around perforations in a corrugated pipe. Furthermore, slot widths can be as large as 0.57 times the width of the corrugation valley, if the aim is to keep K_{sc} under 3.0. Eq. (4.13) is applicable to rectangular slots located at the springline of the pipe.

4.5.6.3 Deformation due to slots

The effects of L_{perf} and w_{perf} on the deformation of the pipe was investigated under the same conditions described in section 4.5.6.1. The results for L_{perf} (not presented) show that the vertical deflection increases by 6.5% for slot lengths between 1.0 and 2.5 cm. This increase is not statistically significant (p = 0.86) as determined by a Welch's t-test at a 5% significance level. The results for w_{perf} are presented in Fig. 4.17, which show that an increase in the slot width from 0.1 to 0.56 cm, causes the vertical deflection to increase by 26% under load case LL1-ML.

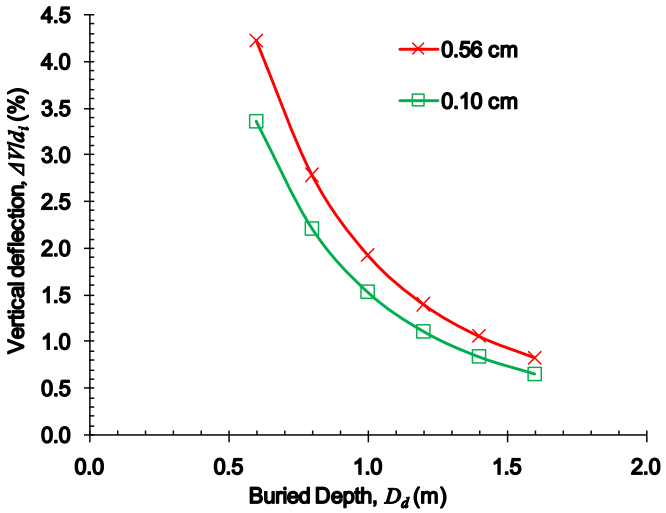

Fig. 4. 17. Vertical deflection ($\Delta V/d_i$) for two perforation widths under load case LL1-ML.

The maximum $\Delta V/d_i$ is 4.23% for corrugated pipes buried at a depth of 0.6 m and perforated with 0.56 cm wide slots. As previously established, a non-perforated pipe will deflect at the crown by 3.2% of its diameter, which illustrates that four lines of rectangular slots in the corrugation valley can increase the pipe deflection by 32%. This increase in deformation due to w_{perf} is three times larger than that for 0.56 cm diameter holes under the same loading conditions and perforation configuration. The difference can be explained by the length of the slot (1.75 cm), which is three time larger than d_{perf} in the hoop direction. The larger perforation area due the slot in the corrugation valley causes a larger reduction to I_p in the hoop direction of the pipe. As a result, a drainage pipe with the 0.56 cm wide and 1.75 cm long slots will have a lower stiffness and larger deflection than a pipe with 0.56 cm holes.

4.5.7 Design implications for corrugated pipes

The findings in this study have significant implications for the structural design of flexible corrugated HDPE pipes that are used as drainage laterals on agricultural lands. The structural response of buried corrugated pipes is largely affected by the texture of the surrounding soil and the characteristics of the applied boundary loads. The short-term wheel loads from agri-machinery will induce the maximum wall stresses for pipes buried in soils with a small

elastic modulus (<10 MPa) such as sandy loams and silt loams (Table 4.2). The combined earth and hydrostatic loads are long-term loads that induce wall stresses in non-perforated corrugated pipes (<1.0 MPa) that are well below the yield strength of HDPE (7.1 MPa).

Perforations placed in the corrugation valley, to allow for water entry, will influence the local stress distribution and deformation of buried HDPE pipes. Collectively, the results from this study have demonstrated that the perforation geometry and dimensions have the largest effect on the pipe response to the applied boundary loads. Wall stresses may exceed the F_y of corrugated pipes perforated with circular holes or wide slots, whenever the burial depth is shallower than 0.9 m in silt loam soils (or soils with a similar stiffness). It is therefore important that the selection of the perforation shape, size, and configuration be guided by the appropriate field conditions (soil type, water table, and field traffic) as part of the design of buried corrugated drainage pipes. Practitioners can estimate the magnitude of stress concentrations using Eqs. (4.12) and (4.13) for holes and slots, respectively. An assessment of the risk against failure by ductile yielding can be made by using a modified form of Eq. (4.10) in conjunction with an estimate of the wall stresses for non-perforated corrugated pipes using the regression coefficients in Table 4.S2 (Supplementary data).

For illustration, the following example is used to compare the anticipated effect of the perforation shape for a drainage pipe under fixed design conditions from a typical agricultural field in Soulanges County, Québec, Canada. The field has a clay loam soil with an average bulk density of 1500 kg/m^3 (Tait et al., 1995). The properties for the clay loam (CL) soil type in Table 4.2 are assumed to be representative of the field in Soulanges County. A subsurface drainage system is to be installed on the site comprising 30 laterals of 100 mm inside diameter corrugated HDPE pipes. The planned spacing and buried depth of the drainage pipes are 15 m and 0.8 m, respectively. It is also assumed that loaded grain wagons will traverse the field during harvesting when the water table level is at the drain center and the CL soil is at

field capacity (LL1-CL and EL3-CL+HL3). The perforation dimensions under consideration are: 0.56 cm diameter circular holes and 1.23 × 0.2 cm rectangular slots. These dimensions will both give a total perforation area of 60 cm^2/m when $N = 4$ and $a_y = 1.645$ cm.

From Eqs. (4.12) and (4.13), the computed K_{sc} values were 4.083 and 2.585 for the holes and slots, respectively. These results clearly indicate that the 0.56 cm diameter holes will induce a larger stress in the wall of the pipe due to higher stress concentrations. However, in order to assess the risk against ductile yield failure, the magnitude of the wall stresses must also be computed. The stresses in the perforated pipe for each load case can be estimated by

$$(\sigma_e)_{perf} = K_{sc}(\sigma_e)_{non-perf} \tag{4.10a}$$

Using the coefficients in Table 4.S2 for CL soils and Eqs. 4.S4 and 4.S5 (supplementary data), the values for $(\sigma_e)_{non\text{-}perf}$ when $D_d = 0.8$ m are 2.89 and 0.19 MPa for load cases LL1-CL and EL3-CL+HL3, respectively. The principle of superposition can be applied to give a total wall stress of 3.08 MPa for the non-perforated pipe. Thus, the wall stress in the perforated pipe with holes is expected to be 12.57 MPa using Eq. (4.10a). Under identical field conditions, the wall stress for the pipe with slots is expected to be 7.96 MPa, which is 58% less than that for holes. The risk against failure can be assessed by

$$SF_{yield} = \frac{F_y}{(\sigma_e)_{perf}} \tag{4.14}$$

where SF is the factor of safety against yield. Applying Eq. (4.14) shows that corrugated HDPE pipes perforated with slots can provide an SF of 2.68, which is above the common threshold of 2.0 for working stresses (Moore, 2001). In contrast, the pipe perforated with holes provide an SF of 1.7, presenting a higher risk for failure under working conditions. From a structural design perspective, rectangular slots with $w_{perf} \leq 0.5\ w_v$ are more advantageous, because they present a lower risk of failure under working conditions.

It should be noted that the deformation of the perforated corrugated pipes is expected to be within the 5% performance limit specification for buried pipes under the most extreme loading conditions investigated in this study. However, these results demonstrate that perforated pipes can fail by ductile yielding while deflections remain within the permissible limit, especially for shallower burial depths. Therefore, the influence of the perforation shape, size, and configuration warrants a thorough evaluation and incorporation into the structural design of corrugated HDPE pipes when used as drainage laterals on agricultural lands.

4.6 Conclusions

Numerical models were used to investigate the structural response of corrugated HDPE pipes under loading conditions typically experienced on agricultural lands. The boundary loads under two idealized friction conditions (smooth and bonded) at the soil-pipe interface were estimated for 12 soil textures, two water table positions (soil surface and the drainage pipe center), and three agri-machinery types (tractor, harvester, and grain wagon). Additionally, the impact of perforations (circular holes and rectangular slots) on σ_e and $\Delta V/d_i$ were examined for corrugated HDPE pipes. The main findings in this study show that:

- The vertical stress transmission of wheel loads is largest for the loaded grain wagon and smallest for the tractor, decreasing to values less than 35 kPa at depths below 1.6 m.
- The bonded friction condition generally induces a larger σ_e in the pipe wall than the smooth condition. The maximum difference occurs for pipes buried in a sandy clay loam (SC) soil. However, the differences in σ_e are statistically insignificant for 100 mm diameter corrugated HDPE pipes across all soil types and load cases investigated.
- The stress response for non-perforated pipes is greater under the LL cases compared to the EL+HL cases across all soil types.

- The critical load case occurs for a silt loam soil that has a loaded grain wagon on the surface, directly above the drainage pipe (case LL1-ML).
- Corrugated pipes with 0.56 cm diameter holes have a high risk of material failure by ductile yielding when the buried depths are shallower than 0.9 m with load case LL1-ML.
- The slot width has a larger effect on the wall stresses than the slot length for corrugated pipes. An increase in the slot length does not result in an increase in the wall stresses. However, values of w_{perf} greater than 0.5 w_v can result in high stress concentrations in the corrugation valley, increasing the risk for failure by ductile yielding.
- The axial and circumferential spacing of the perforations do not affect the stress distribution in the pipe wall. Perforations can be placed in every valley of the corrugation profile along the pipe length, because there is no interaction of stresses in the axial direction. The spacing in the circumferential direction is limited only by the physical dimensions of the perforation and not by the interaction of the stresses in the hoop direction.
- The vertical deflection of the pipe under all loading conditions are within the 5% performance limit specification used by practitioners for buried pipes. However, perforations in the pipe wall will induce high stress concentrations at the edges of the slots and holes, and therefore, the risk for failure by ductile yielding may take precedence over deflection.

The simulated stresses were used to establish relationships between the perforation dimensions and K_{sc}. These relationships allow for the incorporation of perforations in the structural design of buried corrugated pipes. The estimated K_{sc} can be used to compute the wall stresses and assess the risk of failure for drainage pipes with either holes or slots under

field conditions. As assessment was made between the two perforation shapes with the same opening area and configuration. The results demonstrated that rectangular slots have a lower risk of failure against ductile yielding compared to circular holes, provided that $w_{perf} \leq 0.5\ w_v$. Therefore, perforations should be incorporated into the structural design of single-wall corrugated HDPE pipes used in subsurface drainage systems under variable loading in agricultural soils.

4.7 Acknowledgements

Funding for this research was provided by the Natural Science and Engineering Research Council of Canada (NSERC) and the James McGill Professor research award held by C.A. Madramootoo. Special thanks to Prof. Thomas Keller of the Swedish University of Agricultural Sciences for generously providing the SoilFlex model and supporting documentation. The authors are also very grateful for the reviewers' comments during peer review.

4.8 References

AASHTO. (2009). Standard Specification for Corrugated Polyethylene Drainage Pipe. *AASHTO M252*. Washington, DC.

AASHTO. (2017). AASHTO LRFD Bridge Design Specifications *LRFD-8*. Washington, DC.

Alzabeebee, S. (2019). Response of buried uPVC pipes subjected to earthquake shake. *Innovative Infrastructure Solutions, 4*(52), 1-14. doi: https://doi.org/10.1007/s41062-019-0243-y

Alzabeebee, S. (2020). Influence of Backfill Soil Saturation on the Structural Response of Buried Pipes. *Transportation Infrastructure Geotechnology, 7*(2), 156-174. doi: 10.1007/s40515-019-00094-7

Alzabeebee, S., Chapman, D. N., & Faramarzi, A. (2018a). A comparative study of the response of buried pipes under static and moving loads. *Transportation Geotechnics, 15*, 39-46. doi: https://doi.org/10.1016/j.trgeo.2018.03.001

Alzabeebee, S., Chapman, D. N., & Faramarzi, A. (2018b). Innovative approach to determine the minimum wall thickness of flexible buried pipes. *Geomechanics and Engineering, 15*(2), 755-767. doi: https://doi.org/10.12989/gae.2018.15.2.755

Alzabeebee, S., Chapman, D. N., Jefferson, I., & Faramarzi, A. (2017). The response of buried pipes to UK standard traffic loading. *Geotechnical Engineering, 170*(1), 38-50. doi: http://dx.doi.org/10.1680/jgeen.15.00190

ANSI/ASAE. (2017). Density, Specific Gravity, and Mass-Moisture Relationships of Grains for Storage *ANSI/ASAE D241.4*. St. Joseph, MI: ASABE.

Arockiasamy, M., Chaallal, O., & Limpeteeprakarn, T. (2006). Full-Scale Field Tests on Flexible Pipes under Live Load Application. *Journal of Performance of Constructed Facilities, 20*(1), 21-27. doi: doi:10.1061/(ASCE)0887-3828(2006)20:1(21)

ASAE. (2015). Design and Construction of Subsurface Drainage Sysytems on Agricultural Lands in Humid Areas *ASAE EP260.5*. St. Joseph, MI: ASABE.

ASTM. (2014). Standard Specification for Polyethylene Plastics Pipe and Fittings Materials *ASTM D3350* (pp. 7). West Conshohocken, PA: ASTM International.

ASTM. (2016). Standard Specification for 3 through 24 in. Corrugated Polyethylene Pipe and Fittings. *ASTM F667*. West Conshohocken, PA: ASTM International.

Bilgin, Ö. (2014). Modeling Viscoelastic Behavior of Polyethylene Pipe Stresses. *J. Mater. Civ. Eng., 26*(4), 676-683. doi: 10.1061/(asce)mt.1943-5533.0000863

Bilgin, Ö., Stewart, H. E., & O'Rourke, T. D. (2007). Thermal and Mechanical Properties of Polyethylene Pipes. *J. Mater. Civ. Eng., 19*(12), 1043-1052.

Boussinesq, J. (1885). *Application des Potentiels à l'étude de l'équilibre et du Mouvement des Solides Élastiques*. Paris: Gauthier-Villars.

Brachman, R. W. I., & Krushelnitzky, R. P. (2002). Stress Concentrations Around Circular Holes in Perforated Drainage Pipes. *Geosynthetics International, 9*(2), 189-213.

Brachman, R. W. I., & Krushelnitzky, R. P. (2005). Response of a landfill drainage pipe buried in a trench. *Canadian Geotechnical Journal, 42*(3), 752-762. doi: 10.1139/t05-005

Brent. (2016). Brent Avalanche 96-Series Dual-Auger Grain Carts Retrieved Sept. 15, 2019, 2019, from https://media.unverferth.com/brent/grain-handling/brent-avalanche-double-auger-grain-cart.pdf

Bryden, P., El Naggar, H., & Valsangkar, A. (2014). Soil-Structure Interaction of Very Flexible Pipes: Centrifuge and Numerical Investigations. *International Journal of Geomechanics, 15*(4), 1-10.

Burns, J. Q., & Richards, R. M. (1964). *Attenuation of stress for buried cylinders.* Paper presented at the Proceedings of the Symposium on Soil Structure Interaction, Tuscon, Arizona.

Chaallal, O., Arockiasamy, M., & Godat, A. (2015a). Field Test Performance of Buried Flexible Pipes under Live Truck Loads. *Journal of Performance of Constructed Facilities, 29*(5), 04014124. doi: doi:10.1061/(ASCE)CF.1943-5509.0000624

Chaallal, O., Arockiasamy, M., & Godat, A. (2015b). Numerical Finite-Element Investigation of the Parameters Influencing the Behavior of Flexible Pipes for Culverts and Storm Sewers under Truck Load. *Journal of Pipeline Systems Engineering and Practice, 6*(2), 04014015. doi: doi:10.1061/(ASCE)PS.1949-1204.0000186

Chambers, R. E., & McGrath, T. J. (1981). *Structural Design of Buried Plastic Pipe.* Paper presented at the International Conference on Underground Plastic Pipe. Schrock, B.J., (Ed), ASCE, New Orleans, La, 10-25.

COMSOL Multiphysics. (2017a). COMSOL Multiphysics v. 5.3a Reference Manual. Stockholm, Sweden: COMSOL AB, www.comsol.com.

COMSOL Multiphysics. (2017b). COMSOL Multiphysics v. 5.3a: Structural Mechanics Module - User's Guide. Stockholm, Sweden: COMSOL AB www.comsol.com.

Das, B. M. (2016). Ch. 2: Geotechnical Properties of Soil *Principles of Foundation Engineering* (8th ed., pp. 11-16). Boston, MA: Cengage Learning.

de Lima, R. P., da Silva, A. P., Giarola, N. F. B., da Silva, A. R., & Rolim, M. M. (2017). Changes in soil compaction indicators in response to agricultural field traffic. *Biosystems Engineering, 162*, 1-10. doi: https://doi.org/10.1016/j.biosystemseng.2017.07.002

Dhar, A. S., Moore, I. D., & McGrath, T. J. (2004). Two-Dimensional Analyses of Thermoplastic Culvert Deformations and Strains. *Journal of Geotechnical and Geoenvironmental Engineering, 130*(2), 199-208. doi: doi:10.1061/(ASCE)1090-0241(2004)130:2(199)

Fourie, A. B., & Beer, G. (1989). An Illustration of the Importance of Soil Non-Linearity in Soil-Structure Interaction Problems. *Computers and Geotechnics, 8*, 219-241.

Fouss, J. L. (1973). *Structural Design Procedure for Corrugated Plastic Drainage Tubing*. USDA Tech. Bulletin No.1466.

Frohlich, O. K. (1934). *Druckverteilung im Baugrunde*. Wien: Springer Verlag.

Gaj, N., & Madramootoo, C. A. (2020). Effects of Perforation Geometry on Pipe Drainage in Agricultural Lands. *Journal of Irrigation & Drainage Engineering, 146*(7), 12. doi: 10.1061/(ASCE)IR.1943-4774.0001482.

Garcia-Gaines, R. A., & Frankenstein, S. (2015). USCS and the USDA Soil Classification System: Development of a Mapping Scheme (pp. 46). Hanover, NH: US Army Engineer Research and Develpoment Center (ERDC).

Hoeg, K. (1968). Stresses against underground structural cylinders. *Journal of Soil Mechanics and Foundation Engineering, ASCE, 94*(4), 833-858.

Holtz, R. D. (1991). Ch5. Stress distribution and settlement of shallow foundations. In H. Fang (Ed.), *Foundation Engineering Handbook* (2nd ed.). New York: Springer Science+Business Media.

Huffman, R. L., Fangmeier, D. D., Elliot, W. J., & Workman, S. R. (2013). Water Table Management. *In Soil and Water Conservation Engineering* (7th ed., pp. 321-349). St. Joseph, Michigan: Amercan Society of Agricultural and Biological Engineers (ASABE). doi:10.13031/swce.2013.14.

Imhoff, S., Da Silva, A. P., & Fallow, D. (2004). Susceptibility to Compaction, Load Support Capacity, and Soil Compressibility of Hapludox. *Soil Sci. Soc. Am. J., 68*, 17-24.

John Deere. (2018). Grain Harvesting: Combines and front end equipment Retrieved Sept. 30, 2019, from https://www.lectura-specs.com/en/model/agricultural-machinery/combine-harvesters-john-deere/s790-11687880

Kang, J. S., Han, T. H., Kang, Y. J., & Yoo, C. H. (2009). Short-term and long-term behaviors of buried corrugated high-density polyethylene pipes. *Composites: Part B, 40*, 404-412.

Kang, J. S., Stuart, S. J., & Davidson, J. S. (2014). Analytical study of minimum cover required for thermoplastic pipes used in highway construction. *Structure and Infrastructure Engineering, 10*(3), 316-327. doi: http://dx.doi.org/10.1080/15732479.2012.754478

Katona, M. G. (1990). Minimum Cover Heights for Corrugated Plastic Pipe Under Vehicle Loading. *Transportation Research Record*(1288), 127-135.

Katona, M. G. (2017). Influence of Soil Models on Structural Performance of Buried Culverts. *International Journal of Geomechanics, 17*(1), 1-14. doi: doi:10.1061/(ASCE)GM.1943-5622.0000684

Keller, T. (2005). A Model for the Prediction of the Contact Area and the Distribution of Vertical Stress below Agricultural Tires from Readily Available Tire Parameters. *Biosystems Engineering, 92*(1), 85-96.

Keller, T., Berli, M., Ruiz, S., Lamandé, M., Arvidsson, J., Schjonning, P., & Selvadurai, A. P. S. (2014). Transmission of vertical soil stress under agricultural tyres: Comparing measurements with simulations. *Soil & Tillage Research, 140*(106-117).

Keller, T., Defossez, P., Weisskopf, P., Arvidsson, J., & Richard, G. (2006). SoilFlex: A model for prediction of soil stresses and soil compaction due to agricultural field traffic including a synthesis of analytical approaches. *Soil & Tillage Research, 93*, 391-411.

Keller, T., Sandin, M., Colombi, T., Horn, R., & Or, D. (2019). Historical increase in agricultural machinery weights enhanced soil stress levels and adversely affected soil functioning. *Soil & Tillage Research, 194*, 1-12.

Kirsch, G. (1898). Die Theorie der Elastizitat und die Bedurfnisse der Festigkeitslehre. *Journal of the Association of German Engineers, 42*, 797-807.

Kraus, E., Oh, J., & Fernando, E. G. (2014). Impact of Repeat Overweight Truck Traffic on Buried Utility Facilities. *Journal of Performance of Constructed Facilities, 28*(4), 04014004. doi: doi:10.1061/(ASCE)CF.1943-5509.0000454

Krein, H. L. (1983). Parameter Design Model for Corrugated Tubing. *Polymer Engineering and Science, 23*(5), 285-292.

Krushelnitzky, R. P., & Brachman, R. W. I. (2009). Measured deformations and calculated stresses of high-density polyethylene pipes under very deep burial. *Canadian Geotechnical Journal, 46*(6), 650-664. doi: 10.1139/t09-011

Lamé, G. (1852). *Leçons sur la théorie mathématique de l'élasticité des corps solides*. Paris: Bachelier.

Madramootoo, C. A. (1999). Planning and Design of Drainage Systems. In R. W. Skaggs & J. van Schilfgaarde (Eds.), *Agricultural Drainage* (Vol. 38, pp. 871-892). Wisconsin, USA: Madison Publishers.

Mai, V. T., Moore, I. D., & Hoult, N. A. (2014). Performance of two-dimensional analysis: Deteriorated metal culverts under surface live load. *Tunnelling and Underground Space Technology, 42*, 152-160. doi: https://doi.org/10.1016/j.tust.2014.02.015

Marston, A. (1930). *The Theory of External Loads on Closed Conduits in the Light of the Latest Experiments*. (Bulletin 96). Ames, Iowa: Iowa Engineering Experiment Station.

Moore, I. D. (2001). Buried Pipes and Culverts. In R. K. Rowe (Ed.), *Geotechnical and Geoenvironmental Engineering Handbook* (pp. 541-567): Springer US.

Moore, I. D., & Hu, F. (1995). Response of Profiled High-Density Polyethylene Pipe in Hoop Compression. *Transportation Research Record*(1514), 29-36.

Moser, B. K., & Stevens, G. R. (1992). Homogeneity of Variance in the Two Sample Means Test. *The American Statistician, 46*(1), 19-21. doi: 10.2307/2684403

Mouazen, A. M., Ramon, H., & Baerdemaeker, J. D. (2002). Effects of Bulk Density and Moisture Content on Selected Mechanical Properties of Sandy Loam Soil. *Biosystems Engineering, 83*(2), 217-224. doi: https://doi.org/10.1006/bioe.2002.0103

Murakami, Y. (2017). *Theory of Elasticity and Stress Concentration*. West Sussex, UK: John Wiley and Sons, Ltd.

Pilkey, W. D., & Pilkey, D. F. (2008). *Peterson's Stress Concentration Factors* (3rd ed.). New Jersey: John Wiley and Sons, Inc.

PPI. (2010). Handbook of Polyethylene Pipe *2nd Edition*. Irving, Texas: Plastic Pipe Institute (PPI).

Rajeev, P., & Kodikara, J. (2011). Numerical analysis of an experimental pipe buried in swelling soil. *Computers and Geotechnics, 38*, 897-904. doi: 10.1016/j.compgeo.2011.06.005

Rawls, W. J., Gimenez, D., & Grossman, R. (1998). Use of Soil Texture, Bulk Density, and Slope of the Water Retention Curve to Predict Saturated Hydraulic Conductivity. *Transactions of the ASAE, 41*(4), 983-988.

Rees, D. W. A. (2006). Ch2: Strain Analysis *Basic Engineering Plasticity: An Introduction with Engineering and Manufacturing Applications* (pp. 40). Oxford, UK: Butterworth-Heinemann.

Robert, D. J., Rajeev, P., Kodikara, J., & Rajani, B. (2016). Equation to predict maximum pipe stress incorporating internal and external loadings on buried pipes. *Canadian Geotechnical Journal, 53*(8), 1315-1331. doi: 10.1139/cgj-2015-0500

Schjønning, P., Lamandé, M., Tøgersen, F. A., Arvidsson, J., & Keller, T. (2008). Modelling effects of tyre inflation pressure on the stress distribution near the soil–tyre interface. *Biosystems Engineering, 99*(1), 119-133. doi: https://doi.org/10.1016/j.biosystemseng.2007.08.005

Schwab, G. O., & Fouss, J. L. (1999). Drainage Materials. In R. W. Skaggs & J. van Schilfgaarde (Eds.), *Agricultural Drainage* (Vol. 38, pp. 911-926). Wisconsin, USA: Madison Publishers.

Sohne, W. (1953). Druckverteilung im Boden und Bodenverformung unter Schlepperreifen. *Grundlagen der Landtechnik 5*, 49-63.

Spangler, M. G. (1941). *The Structural Design of Flexible Pipe Culverts*. (Bulletin 153). Ames, Iowa: Iowa Engineering Experiment Station.

Stuyt, L. C. P. M., Dierickx, W., & Beltran, J. M. (2005). *Materials for subsurface land drainage systems*. FAO Irrigation and Drainage Paper 60. Rome, Italy.

Tait, R., Madramootoo, C. A., & Enright, P. (1995). An instrumented, field-scale research facility for drainage and water quality studies. *Computers and Electronics in Agriculture, 12*, 131-145.

Tien, H. (1996). *A Literature Study of the Arching Effect.* MSc. Thesis, MIT, Boston, MA.

Vullo, V. (2014). *Circular Cylinders and Pressure Vessels: Stress Analysis and Design*. Switzerland: Springer International.

Walker, P. N. (1979). Pipe Stiffness of Permanently Deflected Corrugated Plastic Drain Tubing. *Transactions of the ASAE, 22*(6), 1313-1316. doi: 10.13031/2013.35205

Watkins, R. K., Dwiggins, J. M., & Altermatt, W. E. (1987). Structural Design of Buried Corrugated Polyethylene Pipes. *Transportation Research Record*(1129), 12-20.

Watkins, R. K., & Spangler, M. G. (1958). *Some Characteristics of the Modulus of passive Resistance of Soil: A Study in Similitude.* Paper presented at the Proceedings of the 37th Annual Meeting of the Highway Research Board, Washington, DC.

Wu, H., & Mu, B. (2003). On stress concentration for isotropic/orthotropic plates and cylinders with a circular hole. *Composies: Part B, 34*, 127-134.

Yeau, K. Y., Sezen, H., & Fox, P. J. (2009). Load Performance of In Situ Corrugated Steel Highway Culverts. *Journal of Performance of Constructed Facilities, 23*(1), 32-39. doi: doi:10.1061/(ASCE)0887-3828(2009)23:1(32)

Young, O. C., Brennan, G., & O'Reilly, M. P. (1986). Simplified tables of external loads on buried pipelines (pp. 53). London, UK: Transport and Road Research Laboratory (TRRL).

Zhan, C., & Rajani, B. (1997). Load Transfer Analyses of Buried Pipe in Different Backfills. *Journal of Transportation Engineering, 123*(6), 447-453. doi: doi:10.1061/(ASCE)0733-947X(1997)123:6(447)

Zhou, M., Du, Y., Wang, F., Arulrajah, A., & Horpibulsuk, S. (2017). Earth pressures on the trenched HDPE pipes in fine-grained soils during construction phase: Full-scale field trial and finite element modeling. *Transportation Geotechnics*, *12*, 56-69.

Appendix 4.A: Structural Analysis Equations

The applied boundary loads on the external face of the pipe wall are as shown in Fig. 4.A1 for the 1st quadrant of the pipe's cross section. The sign convention for the radial and tangential stresses in COMSOL are also shown.

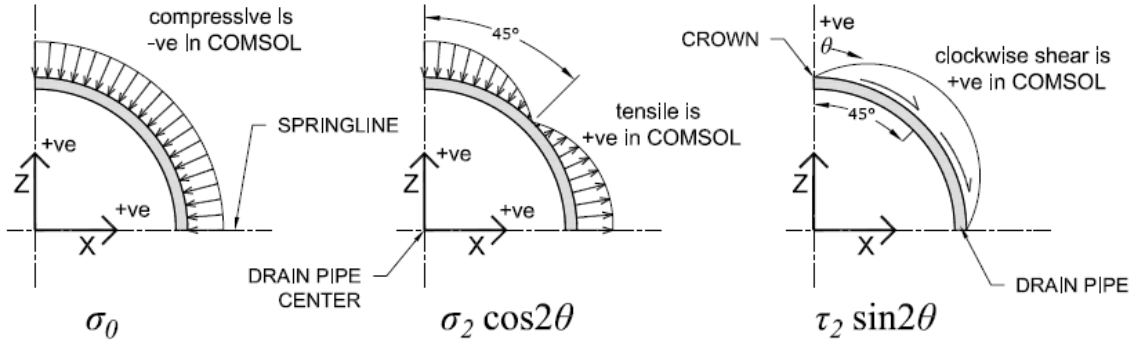

Fig. 4.A1. Distribution of the uniform (σ_0) and harmonic (σ_2, τ_2) components of the applied boundary stresses on the pipe wall.

The following equations were used in the computation of the boundary stresses at the soil-pipe interface (Moore, 2001):

$$\sigma_m = \frac{(\sigma_v + \sigma_h)}{2} \tag{4.A1}$$

$$\sigma_d = \frac{(\sigma_v - \sigma_h)}{2} \tag{4.A2}$$

$$A_m = \frac{2(1-\mu_s)}{1+C(1-2\mu_s)} \tag{4.A3}$$

$$A_{d\sigma} = \frac{4(1-\mu_s)[4+3C(1-2\mu_s)-2F]}{\Delta} \quad \text{for a bonded interface} \tag{4.A4}$$

$$A_{d\sigma} = \frac{12(1-\mu_s)}{2F+5-6\mu_s} \quad \text{for a smooth interface} \tag{4.A5}$$

$$A_{d\tau} = \frac{16(1-\mu_s)(F+1)}{\Delta} \quad \text{for a bonded interface} \tag{4.A6}$$

$$A_{d\tau} = 0 \quad \text{for a smooth interface} \tag{4.A7}$$

$$\Delta = C(1-2\mu_s)(5-6\mu_s+2F) + 2F(3-2\mu_s) + 4(3-4\mu_s) \tag{4.A8}$$

$$C = \frac{E_s d_m}{[2(1+\mu_s)(1-2\mu_s)E_p A_{pcs}]} \quad \text{compressibility ratio} \tag{4.A9}$$

$$F = \frac{E_s d_m^3}{[48(1+\mu_s)E_p I_p]} \quad \text{flexibility ratio} \tag{4.A10}$$

where d_m is the mean pipe diameter, E_s is the soil's elastic modulus, μ_s is the soil's Poisson ratio, E_p is the pipe's elastic modulus, A_{pcs} is the pipe's cross section area per unit length, and I_p is the area moment of inertia per unit length.

For corrugated pipes with an annular profile, I_p was computed as (Fouss, 1973)

$$I_p = \frac{1}{12(w_r+w_v)}\begin{bmatrix} 2(thk)(r_0-r_i)^3 + w_v(thk)^3 \\ +w_r(thk)^3 \\ +3(thk)(r_0-r_i)^2(w_v+w_r) \end{bmatrix} \tag{4.A11}$$

where *thk* is the pipe thickness (1.7 mm), and all other parameters are as shown in Fig. 4.3. The computed A_{pcs} and I_p was 2.63 x 10^{-3} m^2/m and 1.126 x 10^{-8} m^4/m, respectively.

Appendix 4.B: Flexural Stresses, Strains, and Buckling

The combined normal and bending stresses resulting from the reaction thrusts and bending moments at the crown and springline of the pipe were computed as (Moore, 2001)

$$\sigma_c = \frac{T}{A_{pcs}} + \frac{|M|y_c}{I_p} \tag{4.B1}$$

$$\sigma_t = \frac{T}{A_{pcs}} - \frac{|M|y_c}{I_p} \tag{4.B2}$$

where σ_c and σ_t are the hoop compressive and tensile stresses, T and M are the reaction thrusts and bending moments, respectively; and y_c is the distance from the neutral axis to the most extreme fibres in the pipe cross section (Fig. 4.B1).

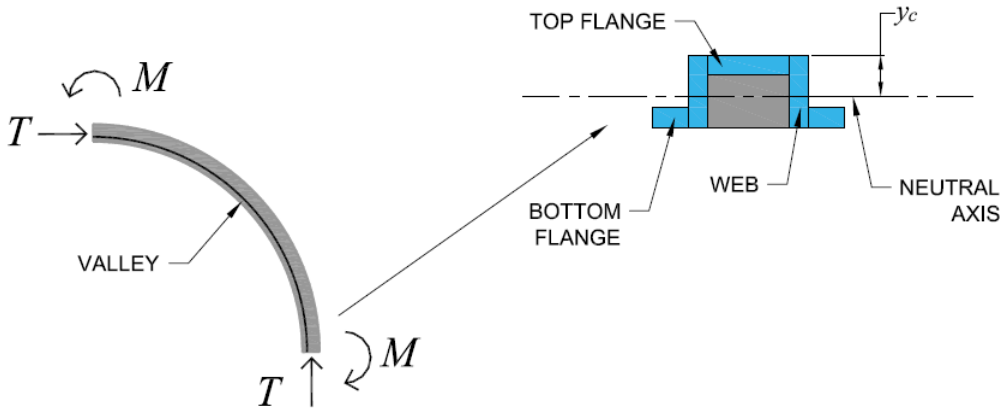

Fig. 4.B1. Reaction thrusts and moment at the crown and springline. Note the corrugation section showing flanges and web relative to neutral axis (exploded view).

The flexural stresses were computed for the most critical load case (LL1-ML), in order to check the adequacy of the pipe's cross section. The results show that σ_c is 7.58 MPa and σ_t is 5.1 MPa for the corrugated HDPE pipe at D_d = 0.6 m (most critical loads). The allowable compressive stress for HDPE is given as 6.9 MPa by PPI (2010). Therefore, the pipe section will most likely be inadequate in sustaining the stresses from a loaded grain wagon or equivalent on a silt loam soil at depths ≤ 0.6 m. Increasing the burial depth will reduce the compressive stresses in the pipe wall below the acceptable level.

The maximum strain was computed to check the validity of assuming a linear elastic response under small strains for corrugated HDPE pipes. The reactions from load case LL1-ML at D_d = 0.6 m was used to compute the combined compressive strain (ε_{pc}) in the corrugated HDPE pipe wall as (Moore, 2001)

$$\varepsilon_{pc} = \frac{T}{A_{pcs}E_p} + \frac{|M|y_c}{I_p E_p} \tag{4.B3}$$

The results show that the maximum ε_{pc} is 0.81%, which is less than the 1% limit typically used for small strains in the theory of elasticity (Rees, 2006). Therefore, the assumption of a linear elastic response is valid for corrugated HDPE pipes subjected to the most critical loading condition in this study.

The global buckling of the pipe section was also checked for stability against the critical thrust (T_b), given by Moore (2001) as

$$T_b = 1.2\, p_f \left(E_p I_p\right)^{1/3} \left[\frac{E_s}{(1-2\mu_s)}\right]^{2/3} R_h \tag{4.B3}$$

where p_f is a performance factor (0.55 for granular soils) and R_h is an embedment factor based on the width of the trench. For pipe installed via mechanical plowing, R_h was taken as 1.0 based on D_d = 0.6 m. The computation gives T_b = 150 kN per m length of the pipe wall, which is far greater than the maximum thrust at the springline of the pipe (16.6 kN per m) under load case LL1-ML. Thus, failure by buckling is highly unlikely for the 100 mm diameter corrugated HDPE pipes commonly used in subsurface drainage systems on agricultural lands.

Appendix 4.C: Supplemental Data

This appendix contains material related to Chapter 4 that was submitted as supplementary data to *Biosystems Engineering* for review.

4.C.1 Introduction

This supporting information include texts, figures, and tables that were deemed as supplemental to the methods and results section of Chapter 4. The sections include the results from the mesh refinement study and verification of the numerical models, the tire contact pressure plots from SoilFlex, the computed arching factors, and the regression equations for corrugated pipe stresses. All references cited are listed in section 4.8.

4.C.2 Mesh refinement results

4.C.2.1 Plain wall cylinder

A plain wall cylinder (Fig. 4.S1) with open ends was used for benchmarking the numerical model in COMSOL's Structural Mechanics module (COMSOL Multiphysics, 2017b). The cylinder has a wall thickness of 0.645 cm, an external radius (r_0) of 5.725 cm, and a length of 11.0 cm. These dimensions are based on a sample of plain wall HDPE pipe used in sand tank experiments by the authors (Gaj and Madramootoo, 2020). The boundary conditions on the surfaces of the cylinder are defined in section 4.4.4 of the main text. However, no non-uniform radial normal (σ_2) or tangential shear (τ_2) boundary loads were applied on the wall surface for benchmarking. Instead an external uniform radial normal (σ_0) boundary stress of 8.58 kPa was applied on the outer surface of the pipe wall, allowing for a direct comparison of the internal stress distribution from analytical solutions.

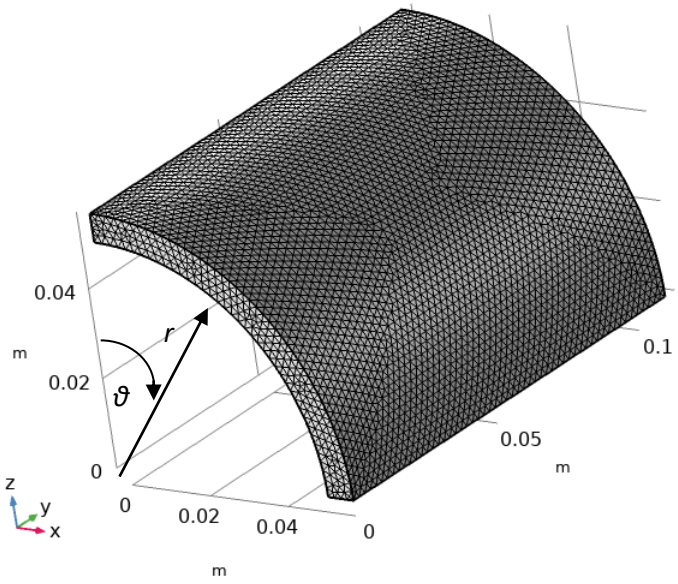

Fig. 4.S1. Plain wall cylinder model with "Finer2" mesh size.

For an open-ended cylinder subjected to uniform radial pressure on the surfaces, the internal stresses can be computed from Lamé's equations (Lamé, 1852) as given by Vullo (2014):

$$\sigma_\theta = \frac{\sigma_i r_i^2 - \sigma_0 r_0^2}{r_0^2 - r_i^2} + \frac{(\sigma_i - \sigma_0) r_i^2 r_0^2}{r^2 (r_0^2 - r_i^2)} \quad (4.S1)$$

$$\sigma_r = \frac{\sigma_i r_i^2 - \sigma_0 r_0^2}{r_0^2 - r_i^2} - \frac{(\sigma_i - \sigma_0) r_i^2 r_0^2}{r^2 (r_0^2 - r_i^2)} \quad (4.S2)$$

where σ_θ is the circumferential or hoop stress in θ the direction, σ_r is the radial stress across the pipe thickness, r_i is the internal pipe radius, and σ_i is the radial pressure applied on the inside surface of the pipe, which was set as zero for this benchmarking exercise.

The default mesh parameters for the "Coarser" mesh setting was used in COMSOL's mesh generator to create the reference mesh size for the plain wall cylinder model. Adjustments to five mesh control parameters were made in successive iterations in order to converge to the analytical solution of Eq. (4.S1). These five parameters are the: maximum element size, minimum element size, maximum element growth rate, curvature factor, and resolution of the narrow regions (COMSOL Multiphysics, 2017a). Fig. 4.S2 shows the results of the mesh convergence towards the analytical solution for the normalized hoop stress (σ_θ / σ_0) across the full thickness of the pipe.

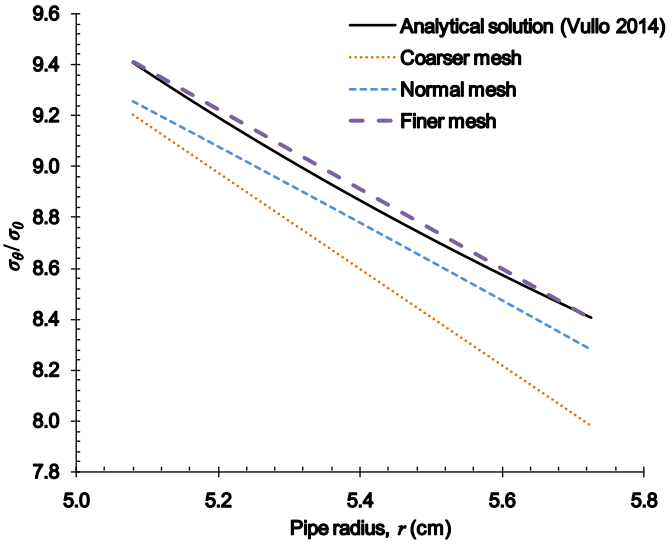

Fig. 4.S2. Normalized hoop stress (σ_θ / σ_0) distribution across the pipe wall for various mesh size.

The results show that the "Finer" mesh overestimated the analytical solution. Thus, refinements were made to the five mesh control parameters until the relative error (RE) was within 1% of the analytical solution. Simulation results with the refined mesh (Finer 2) are shown in Figs. 4.S3 and 4.S4 for comparison with the analytical solutions for σ_θ/σ_0 and σ_r/σ_0, respectively.

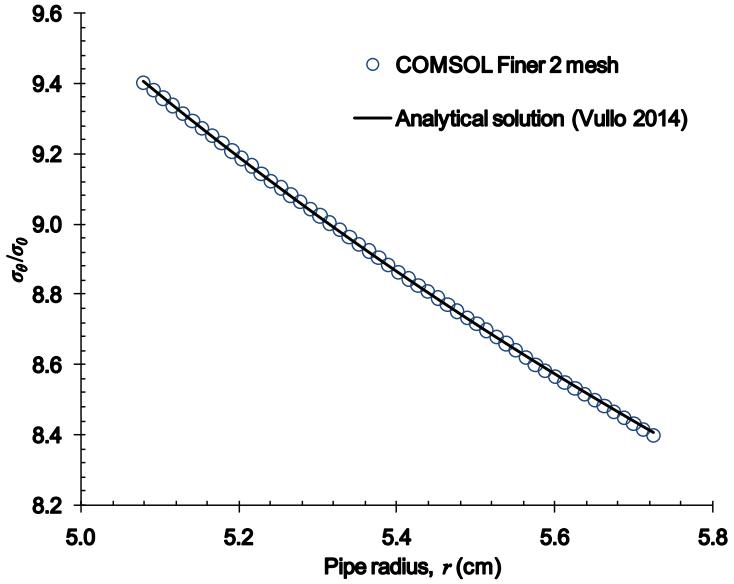

Fig. 4.S3. Comparison of σ_θ/σ_0 after mesh refinement.

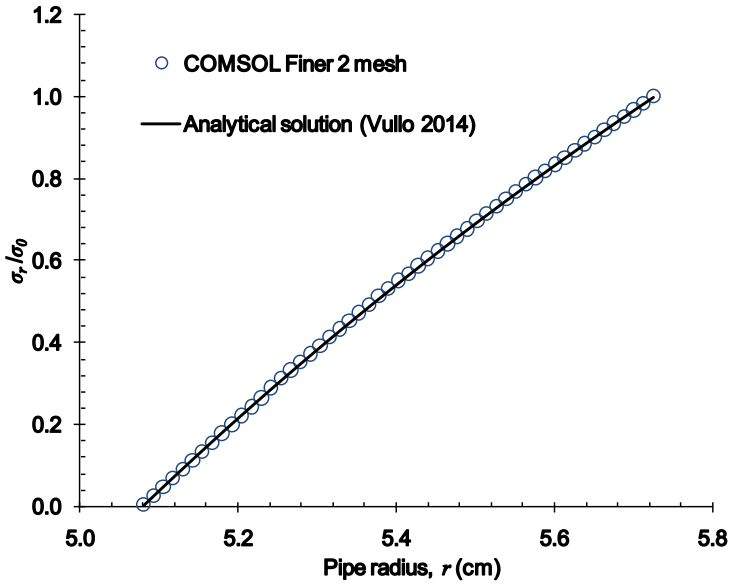

Fig. 4.S4. Comparison of σ_r/σ_0 after mesh refinement.

4.C.2.2 Plate with hole

The presence of perforations in the pipe wall requires smaller mesh elements within the vicinity of the holes. Consequently, a thin square plate with sides of 11.0 cm and a thickness of 0.645 cm was modelled in COMSOL (Fig. 4.S5) to use as a benchmark for mesh refinement (Brachman and Krushelnitzky, 2002). A 0.44 cm diameter hole was placed at the center of the plate, which was subjected to a uni-axial compressive boundary stress in the y-direction (σ_y). For simplicity, only one-quarter of the domain geometry was modelled, and no stresses were applied in the x-direction(σ_x = 0). Roller type constraints (no displacements) were applied in the z-direction (out of plane), and symmetry boundary conditions (no displacement) were prescribed along the central axes of the plate.

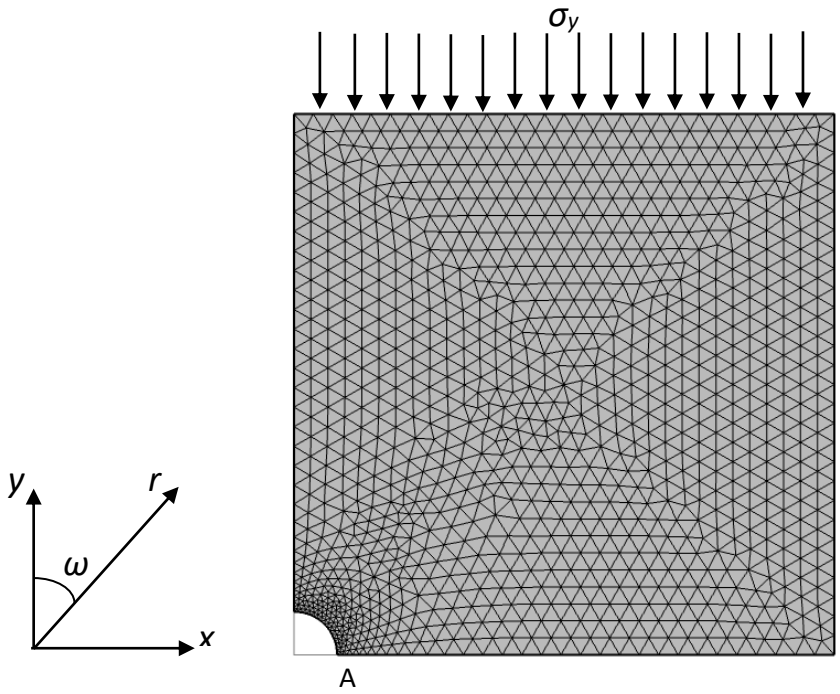

Fig. 4.S5. Thin plate with single hole model for mesh refinement around perforation.

The stress distribution along the edge of the hole can be found analytically by Kirsch's solution (Kirsch, 1898) for a hole in an infinite plate subjected to remote boundary stresses. This boundary value problem solves for the Airy's stress function, and utilizes the Saint

Venant's principle, allowing for a uniform stress field away from the hole. The resulting stress distribution function in polar coordinates (r, ω) is given by Murakami (2017) as

$$\sigma_\omega = \frac{\sigma_y}{2}\left(1 + \frac{r_{perf}^2}{r^2}\right) - \frac{\sigma_y}{2}\left(1 + \frac{3\, r_{perf}^4}{r^4}\right)\cos 2\omega \qquad (4.S3)$$

where is σ_ω is the rotational stress distribution, and r_{perf} is the radius of the hole in the plate. The origin of the polar coordinate system is located at the center of the hole (Fig. 4.S5) and ω is positive in the clockwise direction. The stress results from the mesh refinement for $\omega = 90°$ is shown in Fig. 4.S6. The stress concentration factor (K_{sc}) here is defined as the ratio of σ_ω/σ_y, and it reaches a maximum value of 3.0 at the edge of the hole perpendicular to the direction of the applied boundary stress (Point A).

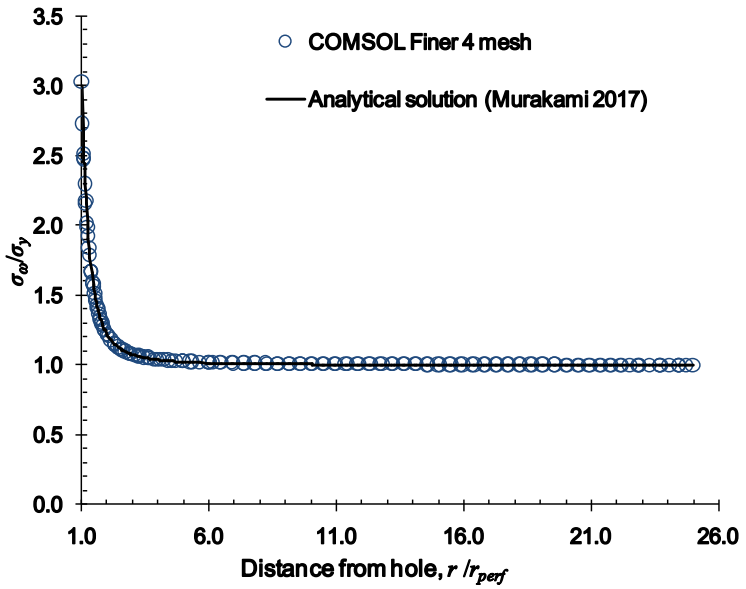

Fig. 4.S6. Comparison of the stress concentration (σ_ω/σ_y) at the edge of a hole in a thin plate.

The refined mesh size (Finer 4) was selected based on the lowest RMSE (6.37 Pa) between the COMSOL output and the analytical solution using Eq. (4.S3). The stress distribution in the plate is shown in Fig. 4.S7, which shows the stress concentrated along the edge perpendicular to the direction of the compressive load.

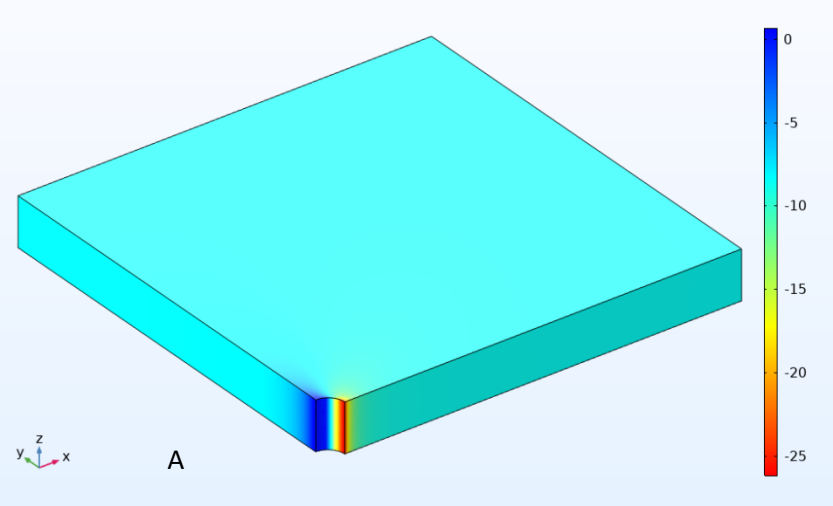

Fig. 4.S7. Stress distribution in the thin plate with a hole subjected to compressive stress (kPa).

4.C.2.3 Plain Wall Cylinder with hole

As a verification of the "Finer 4" mesh size, a plain, thin wall cylinder with a single hole in the center was modelled (Fig. 4.S8). The cylinder has a wall thickness of 0.05 cm, an external radius (r_0) of 7.5 cm, and a length of 12.0 cm. The diameter of the hole was 0.6 cm, and the cylinder was subjected to a uniform pressure on the internal surface (8.58 kPa) and an axial tension (2.02 N) on the edge in the y-direction.

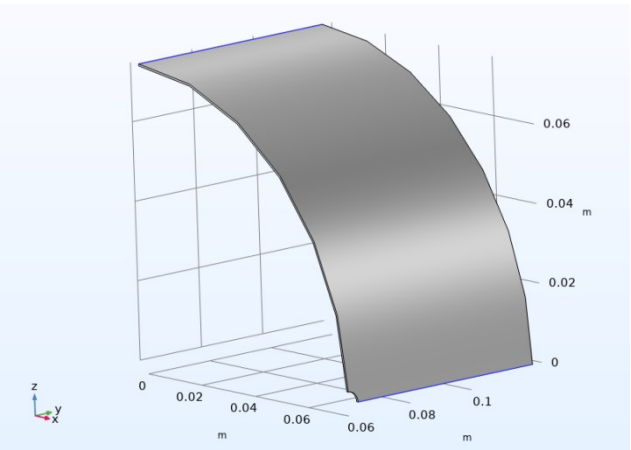

Fig. 4.S8. Plain thin wall cylinder model with a single hole at the center.

The analytical solution for a cylinder with a single hole under the identical loading conditions modelled is given by Wu and Mu (2003). The resulting stress concentration factors are 3.292 and 3.816 for the internal pressure and axial load, respectively. The RE values between the simulated and analytical stress concentration factors are less than 5.0%, indicating that the final refined mesh size is adequate for the numerical simulations.

4.C.3 Live load tire contact stress

The contact stress at the tire-soil interface was generated from SoilFlex (Keller et al., 2006). The area of contact between the tire and soil was modelled as a super ellipse (Keller, 2005; Schjønning et al., 2008) for the three types of machinery (grain wagon, harvester, and tractor), and are shown as the base of the stress plots in Figs. 4.S9, 4.S10, and 4.S11, respectively. The driving direction of the wheel is in the y-direction as shown.

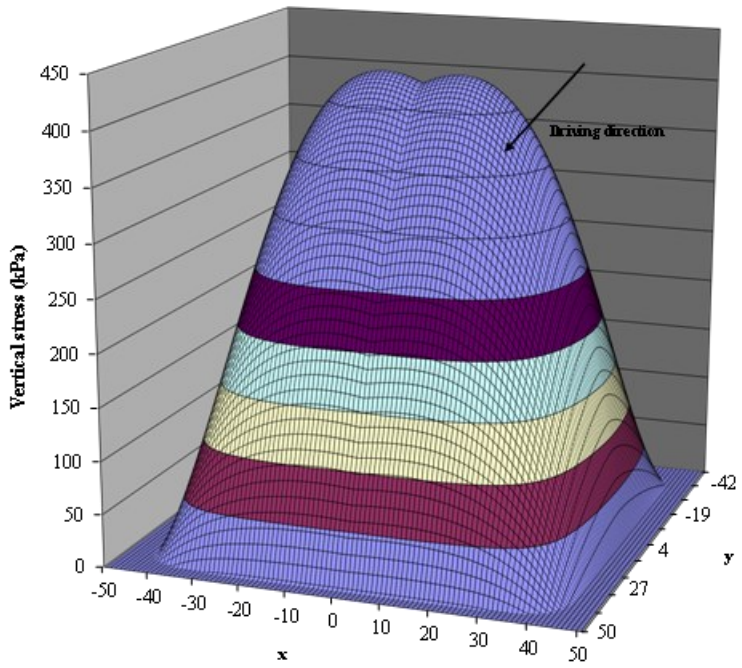

Fig. 4.S9. Contact stress for a single wheel load from a loaded grain wagon (168.1 kN).

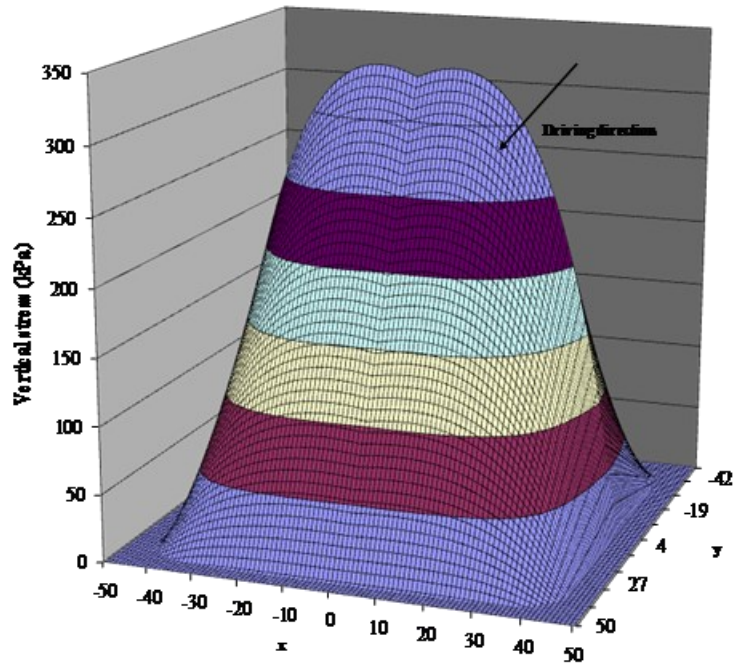

Fig. 4.S10. Contact stress for a single wheel load from a loaded harvester (94.3kN).

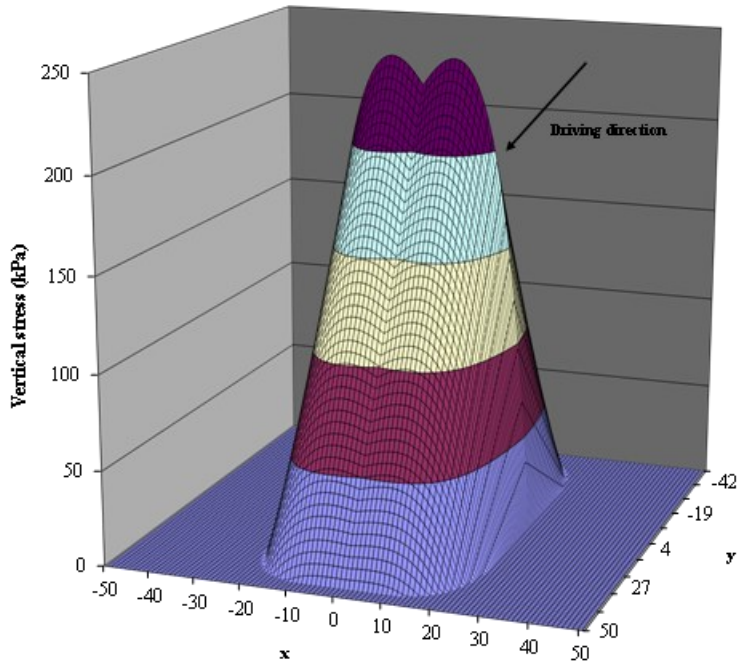

Fig. 4.S11. Contact stress for a single wheel load from a tractor (42kN).

4.C.4 Arching factors for soil-pipe interaction

The arching factors for the smooth and bonded interface friction conditions were computed for the design load cases and soil textures used in this study. The computations indicated that there was no difference in the arching factors among the three LL, and between the EL1 and EL3 load cases within the same soil texture. Similarly, the computed arching factors were identical for soil textures with the same USCS classification. Hence, only the arching factors for the six USCS soil types are presented in Table 4.S1.

Table 4.S1. Arching factors and stress deviation ($\Delta\sigma_e$) for soil type and load cases

Soil Type[a]	A_m		$A_{d\sigma}$				$A_{d\tau}$		$\Delta\sigma_e$ (%)[b]	
			Smooth		Bonded		Bonded			
	LL	EL	LL	EL	LL	EL	LL	EL	LL	EL
SP	0.88	0.41	0.06	0.01	-0.87	-0.57	1.86	1.17	0.26	11.2
SM	1.11	0.74	0.18	0.04	-0.88	-0.81	2.07	1.69	-3.7	2.4
SC	0.61	0.2	0.03	0.01	-0.74	-0.33	1.52	0.67	12.7	29.6
ML	1.21	0.9	0.27	0.07	-0.83	-0.88	2.12	1.88	-6.36	-0.13
CL	0.77	0.38	0.06	0.01	-0.81	-0.53	1.73	1.09	0.84	1.64
CH	0.94	0.62	0.14	0.03	-0.82	-0.73	1.92	1.52	0.12	1.2

Note: Arching factor $A_{d\tau}$ (smooth) = 0 for all soil types and load cases (See Appendix 4.A).
[a]Unified Soil Classification (USCS).
[b]Stress deviation between the smooth and bonded interface friction condition, expressed as a percentage of σ_e (bonded).

4.C.5 Regression equations for corrugated pipe stresses

The simulation results were used to generate regression equations for predicting wall stresses in non-perforated corrugated HDPE pipes as a function of D_d. For the LL cases, power functions were found to give the best fit between σ_e and D_d, while for the EL + HL cases linear functions gave the best fit. The regression equation were

$$\sigma_e = c_1 D_d^{m_1} \tag{4.S4}$$

$$\sigma_e = m_2 D_d + c_2 \tag{4.S5}$$

where σ_e is the von Mises pipe wall stress in MPa, D_d is the burial depth in m, c_1, c_2, m_1 and m_2 are the regression coefficients (Table 4.S2). The goodness of fit for each function is

indicated by the coefficient of determination (R^2) in Table 4.S2. Note that due to the overlap, these coefficients are valid for the USDA soil textures within the same USCS soil type.

Table 4.S2. Regression coefficients for non-perforated corrugated pipe stress

Soil Type	Load Case	Regression coefficients				R^2 (%)
		m_1	c_1	m_2	c_2	
SP	LL1	-1.67537	2.23676	-	-	99.766
	LL2	-1.71821	1.41611	-	-	99.753
	LL3	-1.87359	0.61198	-	-	99.905
	EL1+HL1	-	-	0.48379	-0.02638	100.000
	EL3+HL3	-	-	0.21125	-0.01236	100.000
SM	LL1	-1.67537	3.51367	-	-	99.766
	LL2	-1.71821	2.22453	-	-	99.753
	LL3	-1.87359	0.96135	-	-	99.905
	EL1+HL1	-	-	0.61819	-0.03424	100.000
	EL3+HL3	-	-	0.46762	-0.02736	100.000
SC	LL1	-1.67537	1.41743	-	-	99.766
	LL2	-1.71821	0.89739	-	-	99.753
	LL3	-1.87359	0.38781	-	-	99.905
	EL1+HL1	-	-	0.42570	-0.02298	100.000
	EL3+HL3	-	-	0.12727	-0.00745	100.000
ML	LL1	-1.67537	4.52834	-	-	99.766
	LL2	-1.71821	2.86693	-	-	99.753
	LL3	-1.87359	1.23897	-	-	99.905
	EL1+HL1	-	-	0.63370	-0.03514	100.000
	EL3+HL3	-	-	0.54565	-0.03192	100.000
CL	LL1	-1.67537	1.99042	-	-	99.766
	LL2	-1.71821	1.26015	-	-	99.753
	LL3	-1.87359	0.54459	-	-	99.905
	EL1+HL1	-	-	0.49722	-0.02716	100.000
	EL3+HL3	-	-	0.26006	-0.01522	100.000
CH	LL1	-1.67537	2.62685	-	-	99.766
	LL2	-1.71822	1.66308	-	-	99.753
	LL3	-1.87359	0.71871	-	-	99.905
	EL1+HL1	-	-	0.53995	-0.02966	100.000
	EL3+HL3	-	-	0.36009	-0.02106	100.000

The predicted-simulated relationships for the SP regression models developed in Table 4.S2 are shown in Figs. 4.S12 and 4.S13 for the LL and EL+HL cases, respectively. A graphical representation of the goodness-of-fit between the predicted and simulated data is also demonstrated by the closeness of the plotted points to the equality (1:1) line. The predicted stresses all lie virtually on the 1:1 line in both Figs 4.S12 and 4.S13, indicating an excellent

fit to the measured stresses. Note that similar plots (not presented) were obtained for the remaining soil types in Table 4.S2; only the magnitude of stresses on the axes are different.

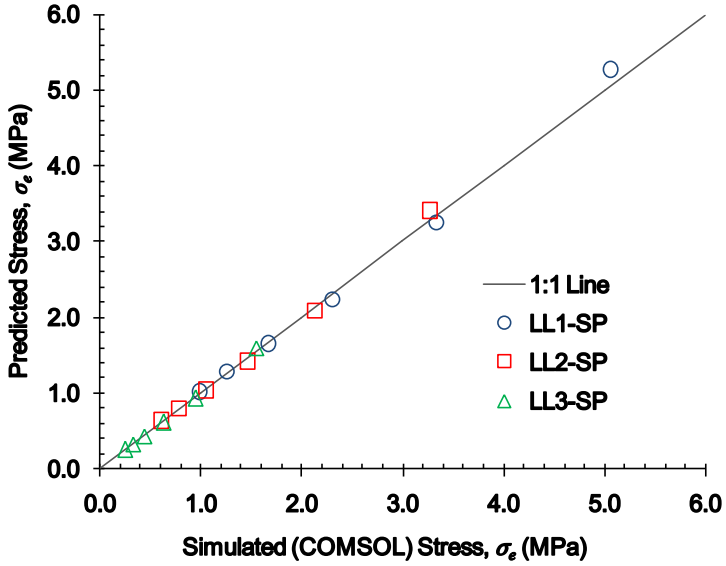

Fig. 4.S12. Comparison of the predicted and simulated stresses for non-perforated pipes under the LL cases with SP soil.

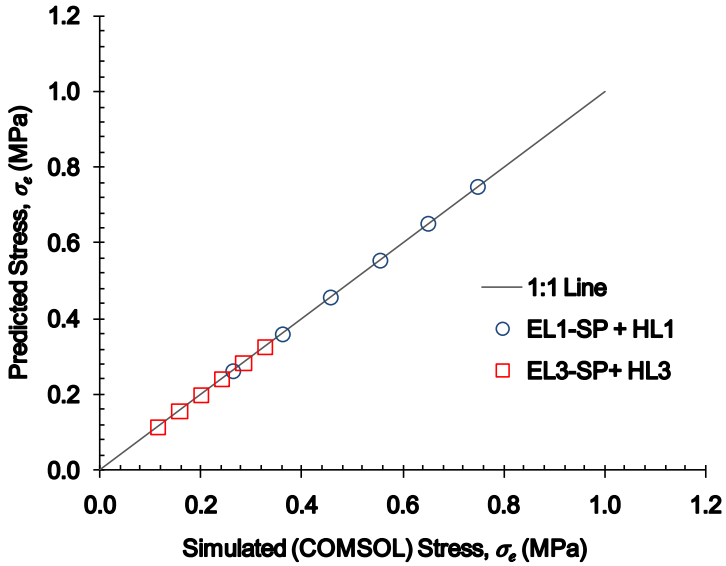

Fig. 4.S13. Comparison of the predicted and simulated stresses for non-perforated pipes under the EL+HL cases with SP soil.

4.C.6 Configuration around circumference

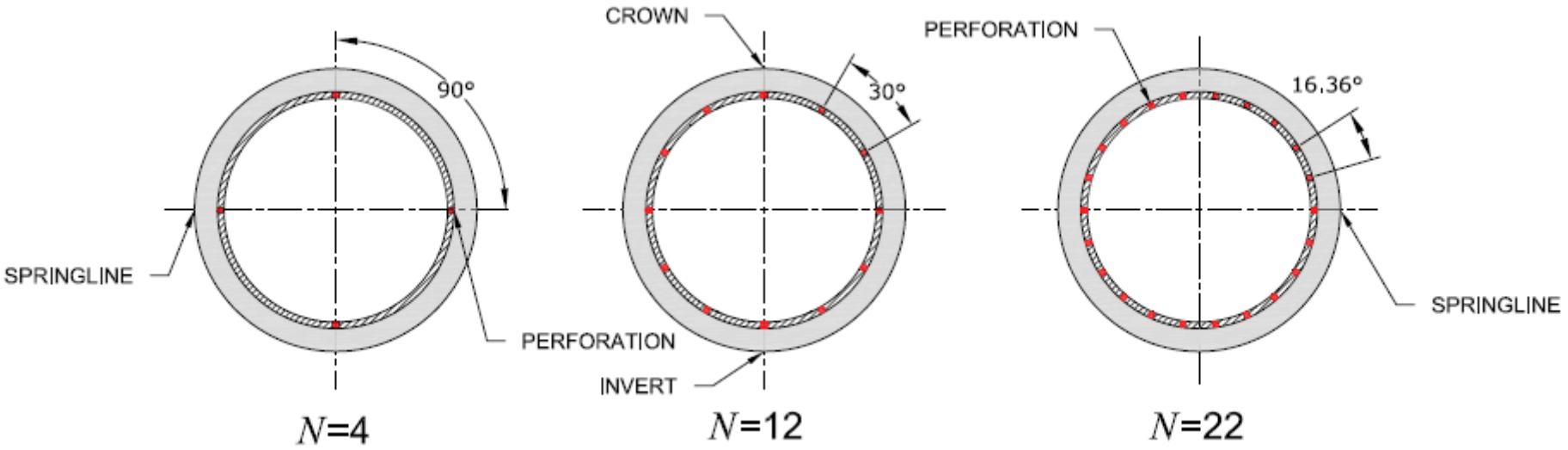

Fig 4.S14. Configuration of the perforation lines (*N*) based on the circumferential spacing between two perforations. Note that perforations are located at the springline for each configuration.

4.C.7 Additional refinement results for Model CWS

The mesh size for "Finer 4" was further refined for Model CWS in order to mitigate the effects of stress singularities at the sharp edge of the perforation. The notch in plate problem was used as a benchmark for comparison following Murakami (2017). The stress distribution results from COMSOL after refinement is shown in Fig. 4.S15. The general agreement with the analytical solution was found to be acceptable for numerical simulations (R^2 = 99.2%).

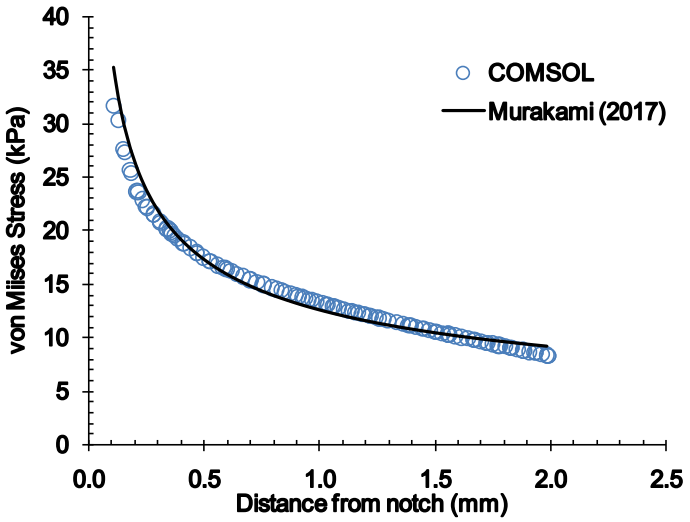

Fig 4.S15. Comparison of the stress distribution for the notch in plate problem.

Connecting text to Chapter 5

Chapters 3 and 4 demonstrated the advantage of rectangular slots over circular holes from both a hydraulic and structural design perspective for perforated corrugated pipes, respectively. However, the hydraulic response under drainage conditions, as represented by the entrance resistance, might not be the same for corrugated pipes under subsurface irrigation conditions. As explained in the literature review (Chapter 2), the effects of variable perforation characteristics on exit head losses has not been adequately studied. Chapter 5 of this thesis compared the hydraulic resistance due to perforations in buried corrugated pipes when operated under the drainage and subsurface irrigation modes. It was hypothesized that the exit resistance under subsurface irrigation mode is larger than the entrance resistance under water drawdown due to the reversed hydraulics of upward soil-water movement. The impact of heterogeneity from layered soils on the exit resistance was also investigated.

Chapter 5 is being prepared for submission to *Advances in Water Resources* (Gaj and Madramootoo, 2021b). The format of the manuscript has been modified here to ensure consistency with the style of this thesis. A list of the references cited in the manuscript is available at the end of the chapter.

Authorship contribution statement:

The author of this thesis was responsible for conceptualization, methodology, model development, formal analysis, investigation, data curation, and writing the original draft followed by all revisions and editing. Dr. Madramootoo provided supervision, aided in conceptualization, funding acquisition, and reviewed and edited the manuscript.

Chapter 5

Simulating Upward Soil-Water Flow from Buried Pipes with Variable Hydraulic Characteristics

5.1 Abstract

Differences in the boundary condition near buried corrugated pipes used for combined drainage and irrigation show that the hydraulic resistance due to perforations are not identical under both drainage and subsurface irrigation modes. No studies to date have sufficiently examined how perforation characteristics such as size and configuration affect the exit head loss of buried corrugated pipes used for subsurface irrigation. This research proposes a new dimensionless parameter called the exit resistance that accounts for variable perforations, and can be used in the computation of exit head loss, due to capillary rise under subsurface irrigation. Datasets obtained from 189 numerical simulations were used to investigate how the size and configuration of rectangular slots affect the exit resistance. The results show that the number and configuration of slots on the pipe wall has the largest impact on the exit resistance. Slots placed in every corrugation valley provide the least resistance compared to those spaced in every second or third valley. Exit resistance was also found to vary with the pressure head on the subsurface irrigation pipes. The impact of heterogeneity from layered soils on the exit resistance of buried perforated pipes was also investigated. The results indicated that the exit resistance is not influenced by soil heterogeneity. In general, the results from this study implies that it is better to perforate buried corrugated pipes with slots in every corrugation valley to reduce exit head losses and maximize upward soil-water fluxes in subsurface irrigation systems.

Author keywords: exit resistance; perforation; corrugated pipes; head loss; subsurface irrigation; layered soils

5.2 Introduction

Dual-purpose drainage and subsurface irrigation systems on agricultural lands are used to both remove excess soil-water during the wet periods, and to provide irrigation water during dry periods of the growing season (Yu et al., 2020). Buried perforated corrugated polyethylene pipes, with a typical diameter between 75 and 100 mm, are commonly used as the primary material in these dual-purpose water management systems. The subsurface irrigation system, also known as subirrigation, can supply water to the crop root zone via capillary rise or upward flux. This upward movement of water in the unsaturated soil zone above the water table has both agronomic and water quality benefits. Previous studies demonstrated increases in corn and soybean yields (Galganov, 1991; Mejia et al., 2000; Nelson, 2017). Improved water quality through the reduction of nutrient losses has been shown by several researchers (Drury et al., 1996; Madramootoo et al., 2001; Mejia and Madramootoo, 1998). Efficiently designed and operated subsurface irrigation systems are therefore essential as future crop production expands to meet an increasing global food demand compounded by a changing climate.

The main objective in the design of a subsurface irrigation system is to determine the spacing and depth of the drains to supply water for optimum crop production (Skaggs, 1981). The steady-state equation developed by Ernst (1975) is commonly used to determine the required lateral drain spacing for subsurface irrigation systems. Corrections to Ernst's equation are typically made in order to account for the head losses that occur near the drains in the system (Skaggs, 1999). These losses occur due to the depth of the impermeable layer below the drains (Skaggs, 1981), and as a result of the finite perforations on the drainage pipe (Skaggs, 1991). Current design practices utilize the hydraulic entrance resistance to compensate for the head loss from perforations on subsurface irrigation/supply pipes (Skaggs, 1991, 1999). However, this parameter was derived for buried pipes operating under the drainage mode

where streamlines converge towards the perforation. The hydrodynamics of the water management system is reversed when operated under the subsurface irrigation mode. Applied irrigation water from a control chamber must first exit the buried supply pipes through the perforations, and then flow into the surrounding soil medium to raise the water table to a desired target level. In subsurface irrigation mode, the streamlines diverge away from the perforations on the supply pipe. The pressure head on the buried pipe is also larger when operated under the subsurface irrigation mode due to the increased water levels in the control chamber. These differences in boundary conditions raise the pertinent question of whether the hydraulic resistance and head loss of the system due to perforations are identical under both drainage and subsurface irrigation modes.

Determining the magnitude of head losses in a subsurface irrigation system is important for water management because it affects the amount of water that needs to be supplied to the field via the control chambers (Bournival et al. 1987). Total head losses as high as 55 cm were first measured by Bournival et al. (1987) in a field study with subsurface irrigation systems on a sandy loam soil in southern Quebec. Approximately 75% of the total head loss was attributed to exit head losses due to perforations (Bournival et al., 1987). On the other hand, laboratory measurements reported by Prasher et al. (1989) showed that exit losses may be significantly smaller (less than 3.7 cm), suggesting that the results reported by Bournival et al. (1987) may have actually been divergent head losses from clogged envelopes around the buried pipes.. However, this small exit head loss may be explained by the perforation pattern used on the test pipe by Prasher et al. (1989), which had 12 rows of narrow slots (0.17 mm x 9.81 mm) placed in every corrugation valley. Previous work has shown that a large number of perforation rows will significantly reduce the entry resistance and head loss of buried corrugated pipes under drainage mode (Gaj and Madramootoo, 2020). Thus, from a hydraulic perspective, the test pipe used by Prasher et al. (1989) was densely perforated,

resulting in comparatively small exit head loss measurements. Drainage pipes are typically perforated with less than six rows of perforations distributed equally along the pipe circumference and spaced in every second or third corrugation valley (ADS, 2008; Armtec, 2012; JM Eagle, 2012). Therefore, exit head losses may be appreciably larger for cases where the supply pipes are perforated with fewer slots. No studies to date have sufficiently examined how the size and configuration of perforations affect the exit head loss of buried corrugated pipes operated in the subsurface irrigation mode.

Subsurface irrigation systems can be installed on agricultural fields that have multiple soil layers due to natural formation processes. Soil texture usually varies between layers, resulting in heterogeneous hydraulic conductivities. The effect of soil heterogeneity on lateral spacing has been widely documented for two-layer systems under drainage mode (Khan et al., 1989; Sharma et al., 1991), but few studies have been done for subsurface irrigation systems in layered soils. Tang and Skaggs (1980) investigated the effect of drain depth in a two-layer subsurface irrigation system, and concluded that drains are best placed at the layer interface. However, their numerical study only considered cases where the upper layer had a lower conductivity relative to the layer below the drains. Subsurface irrigation systems have been installed in fields with a 0.5 m thick conductive sandy layer overlying a less conductive clay layer at the drain level (Galganov, 1991). Furthermore, head loss effects from perforations were not included in the simulations by Tang and Skaggs (1980). In this context another valid question arises. Does soil heterogeneity influence the exit resistance of perforated pipes in subsurface irrigation systems?

This research is aimed at investigating the exit head loss in corrugated pipes with hydraulic boundary conditions that are representative of subsurface irrigation water management systems used on agricultural lands. A new dimensionless parameter called the exit resistance,

is proposed to be used in the analysis and design of buried perforated pipes operated under the subsurface irrigation mode. The exit resistance accounts for variable perforation characteristics (size and configuration), and it can be used in computations of the exit head loss and subsequently, to determine the lateral drain spacing for subsurface irrigation systems. It is hypothesized that the exit resistance of buried perforated pipes operated under the subsurface irrigation mode is larger than the entrance resistance, its counterpart for water table drawdown when operated under the drainage mode, due to the reverse hydraulics of upward water movement. Specifically, the objectives of this study are (1) to compute the exit resistance of buried corrugated pipes in a subsurface irrigation system in order to test the hypothesis stated above, (2) to establish relationships between the exit resistance and variable perforation size and configuration using a 3D finite-element-based numerical model, and (3) to investigate the impact of heterogeneity from layered soils on the exit resistance of buried perforated pipes. The results from this study can be used to integrate perforation characteristics into the analysis and design of 100 mm diameter corrugated pipes for water management of agricultural lands.

5.3 Methodology

5.3.1 Upward soil-water movement during subsurface irrigation

In a subsurface irrigation system, the water table rises into the unsaturated zone via capillary forces to a predetermined target level, which is set relative to the buried drainage pipe (Fig. 5.1). The water table level at midpoint between two parallel drainage pipes typically experiences a sag from the target level because of the head losses in the system. Several theories have been developed to predict the water movement in the system based on assumptions of how the water flows laterally and vertically through the soil medium. Subsurface irrigation systems are typically designed to operate under steady-state or transient

conditions (Skaggs, 1999). For a steady-state operation, the water level in the control chambers is maintained at the constant target level of 50 - 75 cm below the soil surface (Crézé and Madramootoo, 2019; Singh et al., 2014; Stämpfli and Madramootoo, 2006). The resulting pressure head above the buried pipe provides the necessary energy to generate the soil-water fluxes through the porous medium. Skaggs (1981) stated that most of the water movement occurs laterally in the saturated zone under steady-state conditions, raising the midpoint water table to the target elevation.

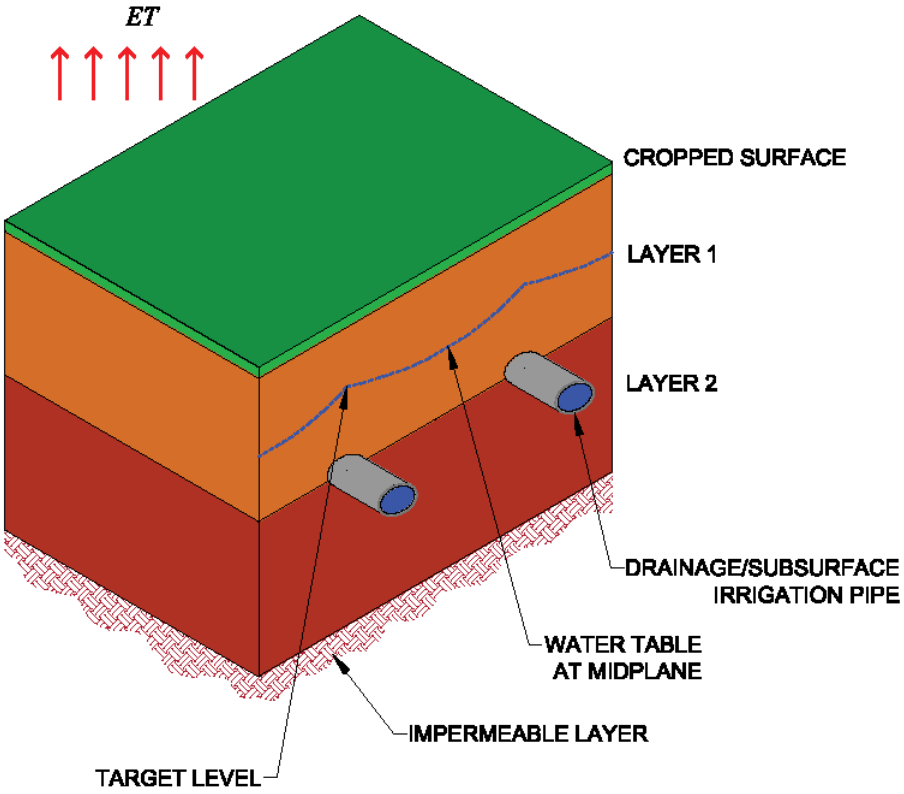

Fig. 5. 1. Three dimensional (3D) schematic diagram showing a typical subsurface irrigation system.
Note: ET is the evapotranspiration flux leaving the cropped surface.

Soil moisture then moves vertically as capillary or upward flux into the unsaturated root zone to meet the crop evapotranspiration (ET) demands (Skaggs, 1999). In steady-state conditions, the upward flux is deemed equivalent to ET and the deficit soil moisture in the unsaturated zone above the water table is continuously replenished by the upward soil-water flux.

Furthermore, this upward flux into the root zone is implicitly considered when selecting a design target level for a specific crop type and soil texture (Abbasi et al., 2020; Elmi et al., 2010; Madramootoo et al., 2001). In some soil textures, a small capillary fringe may develop above the water table, but all lateral movement in this layer is usually negligible because of the rapid decrease in hydraulic conductivity with water content (Skaggs, 1999).

In many subsurface drainage theories, flow below the water table usually employs the Dupuit-Forchheimer assumptions: (i) streamlines are horizontal, and (ii) the hydraulic gradient is equal to the tangent of the water table slope (McWhorter and Marinelli, 1999). However, the streamlines near buried pipes under subsurface irrigation mode are curvilinear due to head losses from the radial divergence of flow (Fig. 5.2). The total head loss in the radial flow region (ΔH), comprises the exit head loss due to the finite perforations on the pipe wall, and the divergent head loss due to the actual depth of the impermeable layer (D_{im}) below the drainage pipe.

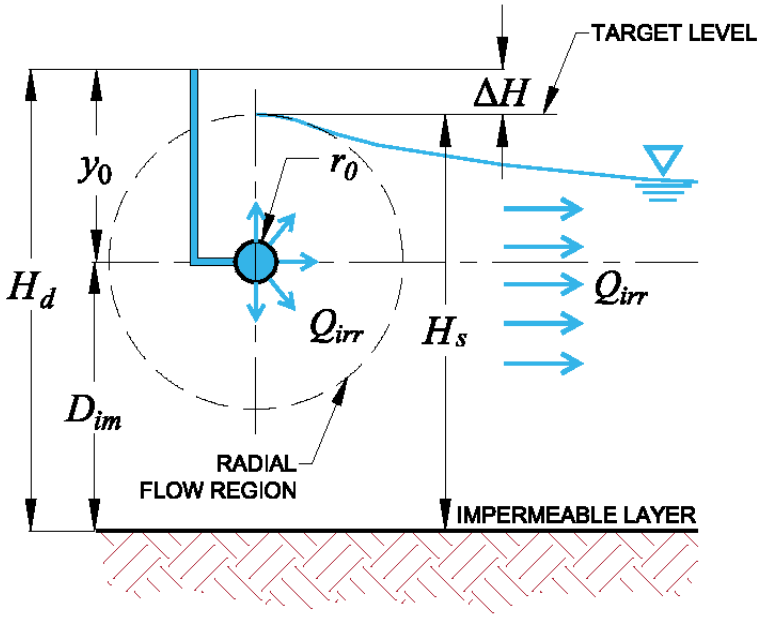

Fig. 5. 2. Flow region near a buried pipe in a subsurface irrigation system (2D view).

The exit head loss of buried pipes under subsurface irrigation mode, is analogous to the entrance head loss of buried pipes under drainage mode, and therefore, can be determined

from the mechanics of flow in the radial zone based on continuity (conservation of mass) and Darcy's law. Under radial flow theory (Stuyt et al., 2005), the continuity condition specifies that the irrigation soil-water flux (Q_{irr}) leaving the buried pipe through the perforations (Fig. 5.2) is equal to the upward *ET* flux leaving the cropped surface (Fig. 5.1) to maintain steady-state conditions.

In order to account for the distortion of streamlines as the irrigation soil-water flux exits the pipe perforations, a new geometric parameter called the exit resistance (α_x) is proposed in this study. The exit resistance is comparable to the entrance resistance (α_e) of buried perforated pipes operated under drainage mode. Similar to α_e, the exit resistance was also conceptualized as a dimensionless and soil independent parameter. Consequently, hydraulic head data from numerical simulations of radial flow near buried perforated pipes can be used to compute α_x following Gaj and Madramootoo (2020).

5.3.2 Numerical simulations of exit resistance

The exit resistance for various perforation size and configuration was computed from hydraulic head datasets obtained through simulations with a 3D finite-element-based numerical model. The discretized model (Fig. 5.3) is representative of the radial flow zone surrounding a nominal 100 mm diameter corrugated drainage pipe. The numerical model was implemented in COMSOL Multiphysics version 5.3 (COMSOL Multiphysics, 2017a) using the Subsurface Flow Module (COMSOL Multiphysics, 2017b). Only half of the radial flow region as shown in Fig. 5.3 was modelled due to symmetry along the pipe's longitudinal axis (Y-axis). The dimensions of the 3D model are 150-cm width (X-axis), 60-cm length (Y-axis), and 124-cm depth (Z-axis). A full description of the model's governing and boundary equations, discretization, and calibration is given by Gaj and Madramootoo (2020). A total of 235676 tetrahedral elements of varying sizes between 5 cm (maximum) and 0.15 cm (minimum) were used to generate the discretized mesh shown in Figs. 5.3 and 5.4 (exploded

view). The hydraulic head datasets are generated from the numerical model using 72 probes that are strategically placed in the radial and axial directions in the porous medium surrounding the buried pipe (Gaj and Madramootoo, 2020).

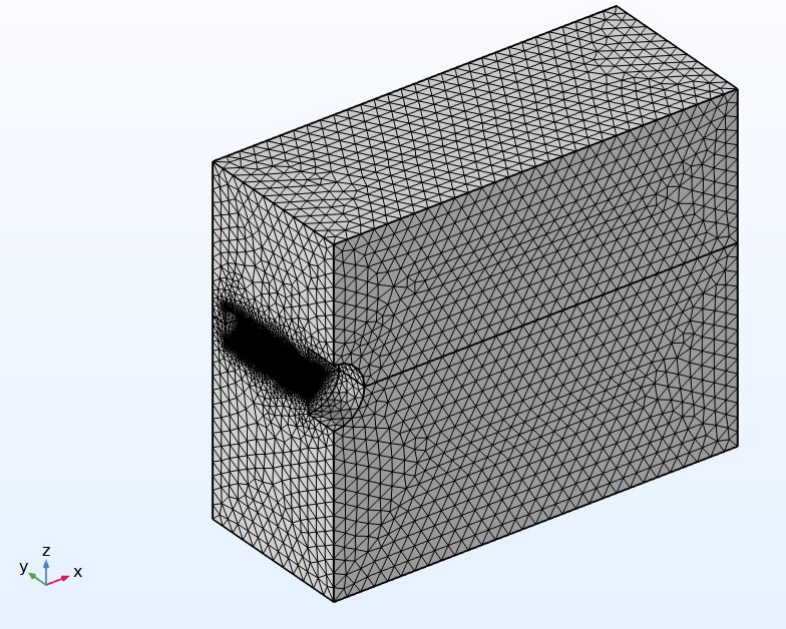

Fig. 5. 3. Three-dimensional (3D) finite-element model of the radial flow region near buried pipes.

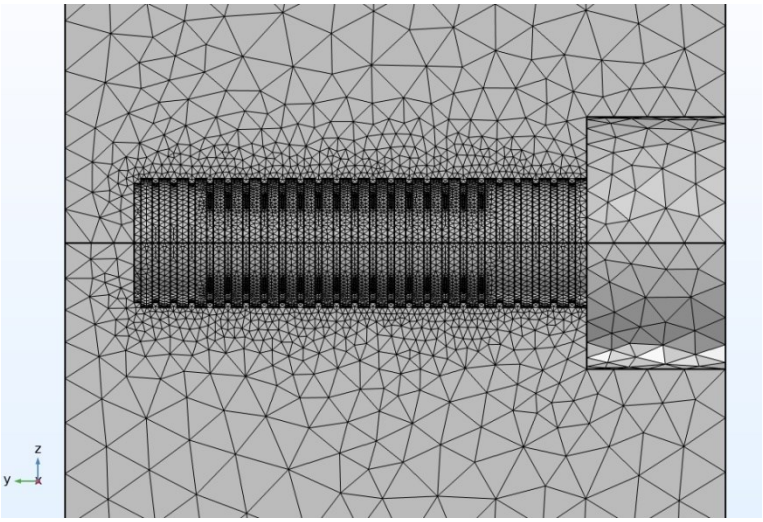

Fig. 5. 4. Exploded view of the finer mesh size used for the corrugated pipe and perforations.

The 3D numerical model (Fig. 5.3) was previously used for computing α_e of buried perforated corrugated pipes under drainage mode. The flow direction in the radial zone during subsurface irrigation is reversed, i.e. flow exiting the buried supply pipe and moving radially upward into the soil medium. Therefore, the Dirichlet boundary condition at the perforation surface on the buried pipe (φ_1) can no longer be described as flowing full with a free-flow outlet (Gaj and Madramootoo, 2020). The buried supply pipe will flow full under a pressure head (y_0), and thus, the hydraulic head at the perforation surface is

$$\varphi_1(Z) = H_d = y_0 + D_{im};\ \in (X, Y) \tag{5.1}$$

Eq. (5.1) was prescribed to the 3D numerical model for the simulations carried out in subsurface irrigation mode. Practical values of y_0 were chosen such that H_d is always greater than H_s (Fig. 5.2), which ensures that the hydraulic gradient will produce soil-water fluxes that exit the pipe via the perforations. It should be noted that the modification to the boundary condition at the perforation surface does not warrant a re-calibration of the model, because the boundary value problem formulated for radial flow under drainage is valid for radial flow under subsurface irrigation (Skaggs, 1991). Consequently, a comparison of the delivery ratios of the perforated pipes under subsurface drainage and irrigation modes was made to verify this assumption. The delivery ratio is defined as the ratio of discharge through a perforated or non-ideal pipe to the discharge through a fully porous or ideal pipe (Gaj and Madramootoo, 2020).

The design variables considered in the numerical simulations for α_e (Table 5.1) were the number of perforation lines (N), the length of the rectangular slot (L_{perf}), the longitudinal spacing (a_y), and the difference in head between H_d and H_s (ΔH). It has been previously demonstrated that rectangular slots are hydraulically more advantageous than circular holes when used as perforations for buried corrugated pipe to facilitate water table drawdown under

drainage (Gaj and Madramootoo, 2020). Thus, only the perforated pipe model with rectangular slots (Model CWS) was considered in the subsurface irrigation simulations.

Table 5.1. Design variables used in the numerical simulations of α_x.

Design Variable	Values used in simulations
Number of lines, N	4, 6, and 10
Length of slots, L_{perf} (cm)	1.00, 1.75, and 2.50
Longitudinal spacing, a_y (cm)	1.645, 3.290, and 4.935
Difference in head, ΔH (cm)	10, 20, 40, 48, 60, 80, and 100

The perforations were placed in the center of the corrugation valley, which is common practice for buried corrugated drainage pipes (Stuyt et al., 2005). The pitch of the pipe is 1.645 cm for the annular corrugation profile used in Model CWS (Fig. 5.4). Hence, the values of a_y in Table 5.1 represents perforations placed in every first, second, and third corrugation valley, respectively. The values of N and L_{perf} are also representative of perforation characteristics commonly used on commercially available corrugated high density polyethylene pipes (Gaj and Madramootoo, 2020). The range of values for ΔH in Table 5.1 was selected based on pressure head values used in field studies with subsurface irrigation systems (Bournival et al., 1987; Cordeiro and Sri Ranjan, 2012; Elmi et al., 2010; Smith et al., 1985). These studies covered a wide range of buried depths, soil types, and crop types across North America. Moreover, a head difference of 48 cm was included in the simulations in order to compare α_x with α_e and test the main hypothesis under equivalent hydraulic conditions. This subset of simulations for hypothesis testing resulted in 27 (3×3×3) combinations of N, L_{perf}, and a_y.

5.3.3 Layered soils in subsurface irrigation

Radial flow in a two-layer system was simulated with Model CWS to investigate the impacts of soil heterogeneity on the exit resistance. The porous medium domain (Fig. 5.3) was separated into two blocks in order to represent two distinct soil layers. The separation was

done so that the center of the buried corrugated pipe was positioned at the interface of the two soil layers following Tang and Skaggs (1980). The mesh size and number of elements in Model CWS were unaffected, because no changes were made to physical dimensions of the model domain or pipe geometry. Heterogeneity in the layered system was represented by the hydraulic conductivity (k_{sat}) assigned to each layer according to soil texture. A subset of four soil textures (Table 5.2) were adapted for the numerical simulations from Rawls et al. (1998), which contains a database of soil physical and hydraulic properties categorized according to the US Department of Agriculture (USDA) textural classification system. The corresponding Unified Soil Classification System (USCS) symbol for each texture following Garcia-Gaines and Frankenstein (2015) is also listed in Table 5.2.

Table 5.2. Physical and hydraulic properties of four USDA soils.

USDA	USCS	n[a]	$\rho_{s\text{-}sat}$[a]	k_{sat}[b]
		m^3/m^3	kg/m^3	m/s x 10^{-6}
Loamy Sand	SM	0.37	2039.5	11.50 (8.47-21.55)
Sandy Clay	SC	0.39	2006.5	0.25 (0.08-0.69)
Silt Loam	ML	0.49	1867.0	4.00 (2.11-10.31)
Clay	CH	0.40	2080.0	0.50 (0.08-1.92)

Note: n = soil porosity; $\rho_{s\text{-}sat}$ = soil density at saturation; k_{sat} = saturated hydraulic conductivity.

[a]values are the arithmetic mean adapted from Rawls et al. (1998)

[b]values are the geometric mean adapted from Rawls et al. (1998); the values in parenthesis are the 25th and 75th percentile values.

Four arrangements (Table 5.3) of the two-layer subsurface irrigation system were simulated using the soil textures listed in Table 5.2. In each arrangement, the soil with the larger conductivity was prescribed to the upper layer (Layer 1). The soil properties within each layer was assumed to be uniform and isotropic. Table 5.3 also summarizes the conductivity ratio (CR_{ks}) of the two-layer system, which was computed as k_{sat} (Layer 1)/k_{sat} (Layer 2).

Heterogeneous soils can be incorporated into subsurface drainage/irrigation design through the use of an average conductivity value in lateral drain spacing equations (Madramootoo,

1999). In layered soils, the average hydraulic conductivity can be computed as either the harmonic or arithmetic mean if the flow direction is perpendicular or parallel to the layers, respectively (Amoozegar and Wilson, 1999). Considering that most of the water movement in a subsurface irrigation system occurs laterally under steady-state conditions (Skaggs, 1981), the arithmetic mean would be more appropriate for estimating the average hydraulic conductivity (k_{sat-a}) as (Amoozegar and Wilson, 1999)

$$k_{sat-a} = \frac{(L_{z1}k_{sat-1}+L_{z2}k_{sat-2}+\cdots+L_{zn}k_{sat-n})}{\sum L_z} \quad (5.2)$$

where L_z is the thickness of the soil layer. A conductivity value computed with Eq. (5.2) is also known as the weighted average, and it accounts for the differences in the thickness of each layer in heterogeneous soils. The average hydraulic conductivity was computed for the four arrangements of two-layer systems (Table 5.3) using Eq. (5.2), and then used in simulations to represent an equivalent homogeneous one-layer system. These simulations allowed for a direct comparison of the exit resistance of buried pipes in a heterogeneous two-layer systems with the resistance from its equivalent homogeneous one-layer counterpart.

Table 5.3. Arrangement of two-layer subsurface irrigation systems for simulations

Layer arrangement	Conductivity Ratio, CR_{ks}
ML/CH	8
ML/SC	16
SM/CH	23
SM/SC	46

Note: Layer 1 has the larger hydraulic conductivity.

5.4 Results and Discussion

5.4.1 Comparison of entrance and exit resistances

In order to test the main hypothesis of this study, the hydraulic resistances of perforated corrugated pipes used in subsurface drainage and irrigation systems were evaluated to allow for an explicit comparison under an equivalent hydraulic head difference (ΔH = 48 cm). A total of 27 simulations, representing combinations of N, L_{perf}, and a_y, (section 5.3.2, Table 5.1) were carried out with Model CWS to generate the required hydraulic head data for computing α_x (subsurface irrigation mode). On the other hand, α_e (drainage mode) was computed from a predictive equation developed by Gaj and Madramootoo (2020) for the matching 27 combinations of the perforation characteristics. The results are shown in Fig. 5.5, which plots α_e and α_x relative to the equality (1:1) line. The hydraulic resistance values shown in Fig. 5.5 all lie above the 1:1 line, indicating that α_x is generally greater than α_e. As a result, the exit head loss due to perforations in a drainage pipe under subsurface irrigation mode will be larger than the entrance head loss of the pipe under drainage mode.

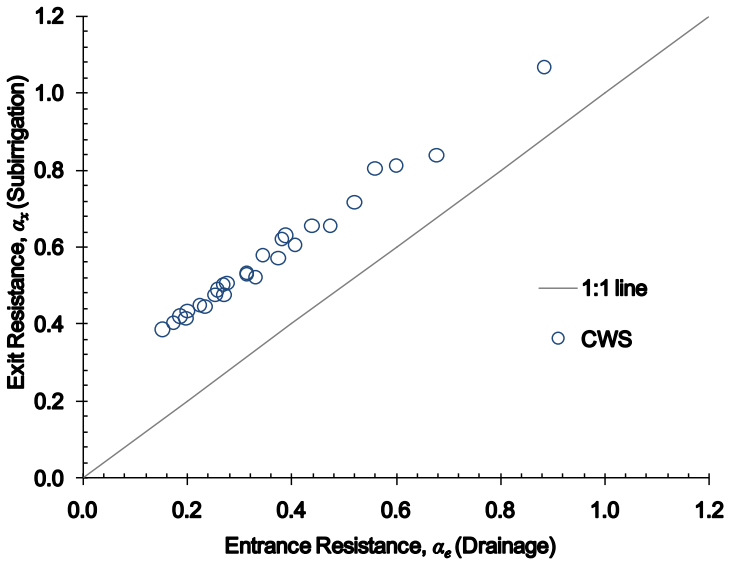

Fig. 5. 5. Comparison of hydraulic resistances under drainage and subsurface irrigation.

This disparity in head loss from the perforations can be explained by the reversal of flow through the porous medium. Under subsurface irrigation mode, the hydraulic head is highest at the soil-pipe interface, then it experiences a precipitous drop immediately outside the pipe surface before it gradually decreases in the radial direction and the streamlines diverge upwards and radially away from the perforations. This dissipation of the hydraulic head is illustrated in Fig. 5.6, which shows its distribution in the radial flow region around the buried pipe under subsurface irrigation mode. The buried pipe in Fig. 5.6 is perforated with four lines of rectangular slots (L_{perf} = 1.0 cm) placed in every corrugation valley (a_y = 1.645 cm).

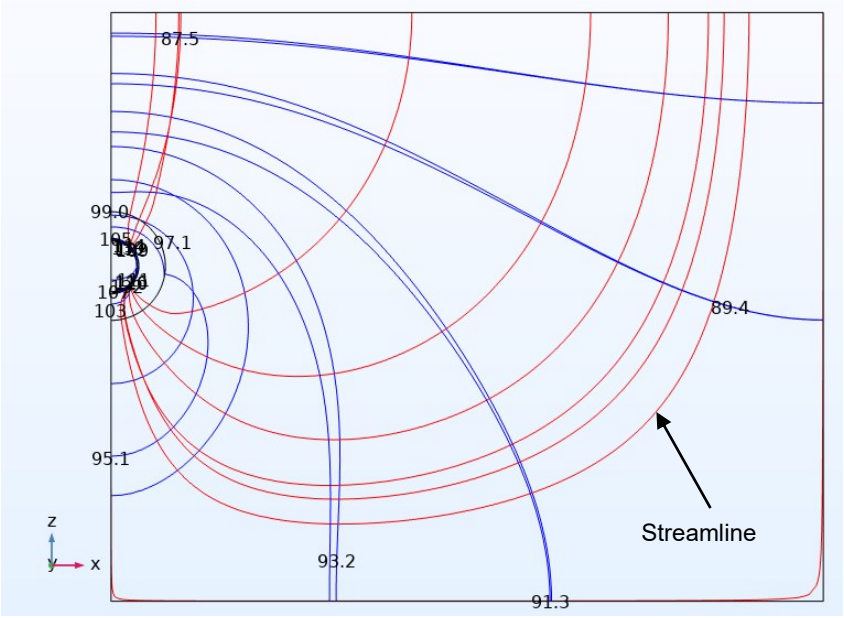

Fig. 5. 6. Hydraulic head (cm) dissipation in the flow region under subsurface irrigation mode.

Note the streamlines (red) indicate the flow diverging from the pipe perforations.

In this particular perforation scenario, the exit head loss accounts for approximately 57% of ΔH within a 5.0 cm radius from the pipe surface. The remaining 43% of ΔH is dissipated over the next 50 cm of the flow region, representing the divergent head loss in the subirrigation system. These results demonstrate that exit losses can potentially account for the largest fraction of the total head loss within the radial flow zone. In contrast, the hydraulic

head under drainage mode will drop steadily across the radial flow region, losing a larger fraction of energy before the flow converges towards the perforations on the pipe wall. Thus, the change in the pipe's boundary condition at the perforation surface due to the increased hydraulic head (H_d) is ultimately responsible for the larger exit resistance to flow of buried pipes when operated in the subsurface irrigation mode.

5.4.1.1 Hypothesis testing and generalized relationship

Further comparison of the hydraulic resistances shows that α_x is 1.7 times larger than α_e when taken as an average across all 27 combinations (section 5.3.2) of perforation design variables. This difference between α_x and α_e, however, is not best described as a constant that can be applied to all perforation characteristics. There is some degree of variability that is suitably illustrated (Fig. 5.7) by the non-linear increase of α_x/α_e expressed as a function of the total perforation area (A_p). The results in Fig. 5.7 show that the ratio of α_x to α_e can be as great as 2.5 when a buried corrugated pipe has a large perforation area (A_p = 300 cm^2/m). The results

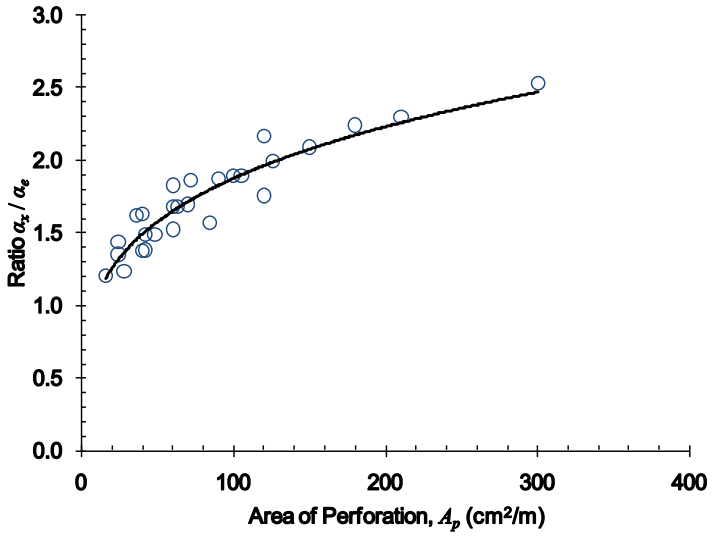

Fig. 5. 7. Ratio of α_x/α_e as a function of the total perforation area (A_p).

also indicate that α_x is approximately 20% larger than α_e for buried pipes with a small perforation area (A_p = 16 cm^2/m). Consequently, these differences in resistance values were tested for statistical significance (5% level) using the Welch's t-test (Moser and Stevens,

1992). The t-test results (not presented) show that the differences between α_x and α_e are statistically significant ($p < 0.05$) across all 27 perforation combinations, confirming the hypothesis of this study that α_x is significantly larger than α_e. Therefore, these findings strongly supports the use of the exit resistance to account for perforations in the analysis and design of subsurface irrigation systems.

Moreover, the following power law function was fitted ($R^2 = 87.2\%$) to the data in Fig. 5.7 in order to provide a predictive relationship between α_x/α_e and A_p

$$\frac{\alpha_x}{\alpha_e} = 0.593 A_p{}^{0.25} \tag{5.3}$$

where A_p is in cm^2/m. Eq. (5.3) can be used to estimate α_x in situations where an existing drainage system with buried corrugated pipes is to be retrofitted to operate under subsurface irrigation mode (Elmi et al., 2010; Galganov, 1991). Values of A_p for existing buried corrugated pipes are sometime reported by researchers (Bournival et al., 1987), but details on the exact dimensions and/or configuration of the perforations are often not properly documented. Therefore, Eq. (5.3) may prove to be very useful provided a relationship between α_e and A_p is also available. Dierickx (1999) presented several curves of α_e as a function of A_p, but only one of the curves is valid for corrugated drainage pipes. Furthermore, only 0.5 cm long slots were used to generate the curve presented by Dierickx (1999), restricting its use in practical situations. A better representative relationship between α_e and A_p for corrugated drainage pipes is presented in Fig. 5.S1 (supplemental data), which considers a wider array of perforation characteristics such as size and configuration.

5.4.1.2 Validity of radial model under subsurface irrigation

It is important to note that the flow rate through a fixed perforation size and configuration remained constant under both subsurface irrigation and drainage modes since ΔH was

identical in these simulations. This is fittingly demonstrated in Fig. 5.8, which plots the delivery ratios (Q_{irr}/Q_0 or Q_s/Q_0) for variable perforated pipes operated under each mode relative to the equality (1:1) line. The denominator, Q_0, is the flow rate through an ideal of fully porous pipe following Gaj and Madramootoo (2020). Values of Q_{irr}/Q_0 for the perforated corrugated pipes under subsurface irrigation mode were computed from the simulation results during post-processing. The corresponding Q_s/Q_0 for a buried corrugated pipe under drainage mode with the matching perforation combinations was computed from a predictive equation developed by Gaj and Madramootoo (2020). The results in Fig. 5.8 corroborate the validity of Model CWS for simulating radial flow under subsurface irrigation, confirming that no re-calibration of the model was necessary.

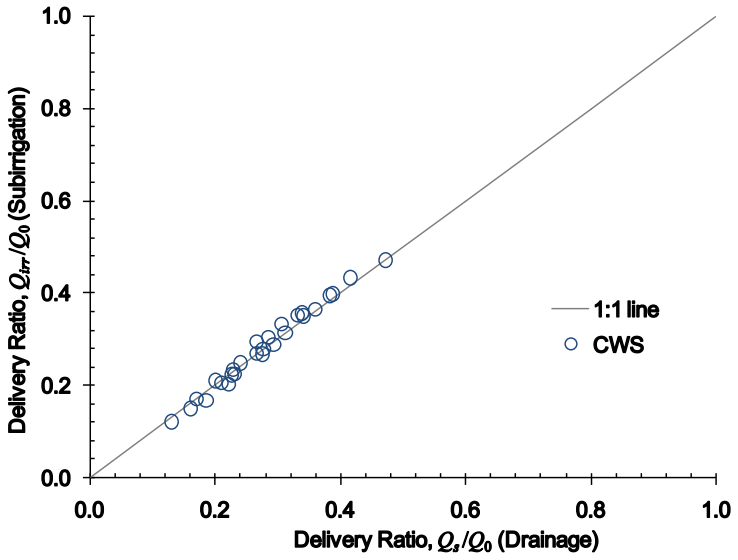

Fig. 5. 8. Comparison of delivery ratios under drainage and subsurface irrigation modes.

5.4.2 Exit resistance and perforation characteristics

5.4.2.1 Variable slot length

A series of parametric simulations (189 in total) using Model CWS and varying L_{perf} , N, and a_y, were carried out in order to establish explicit relationships with α_x for buried corrugated pipes under subsurface irrigation mode. As shown in section 5.4.1, H_d has a direct impact on

the exit losses as water flows out of the pipe perforations. Therefore, ΔH was also varied in these simulations in order to reflect typical field conditions for subsurface irrigation systems on agricultural lands. Fig. 5.9 shows that α_x generally decreases as ΔH increases for all values of L_{perf} (N and a_y were fixed at 4 and 1.645 cm, respectively). This trend is indicative of the fact that the highest resistance to flow through the perforations occurs when the hydraulic gradient is lowest at the soil-pipe interface (perforation surface). A low hydraulic gradient arises when there is a small difference between H_d and the water table level immediately outside the buried supply pipe (H_s). As ΔH increases, the hydraulic gradient increases and more energy is available to overcome the resistance to flow, resulting in lower values of α_x for the perforated pipe.

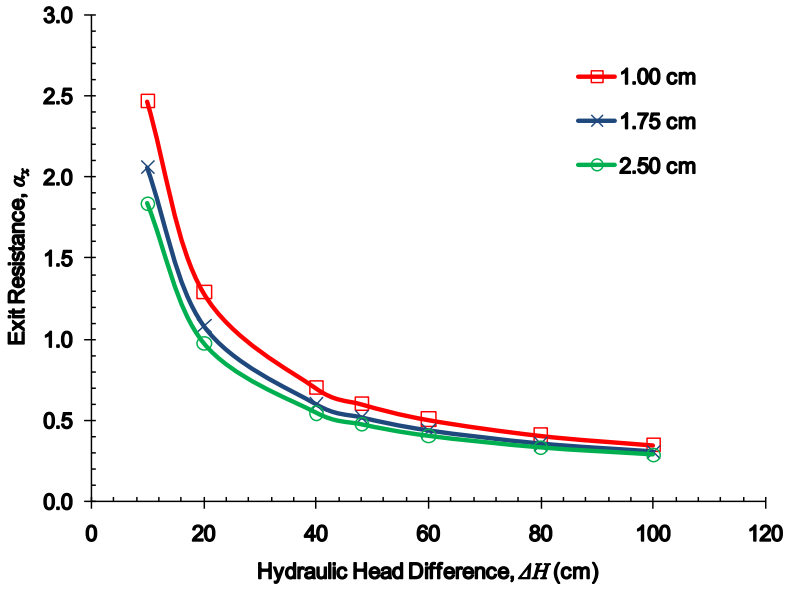

Fig. 5. 9. Variation of α_x with ΔH for select values of L_{perf}.

Fig. 5.9 also shows that there are differences in the resistance of the perforated pipe under subsurface irrigation due to L_{perf}. This difference in α_x is largest (34%) between L_{perf} values of 1.0 and 2.5 cm when ΔH is less than 10 cm. However, as ΔH increases, the difference due to L_{perf} becomes negligible. These results indicate that the length of a rectangular slot has a relatively minor impact on the exit losses of corrugated subsurface irrigation pipes.

Nevertheless, it may be beneficial to use values of L_{perf} greater than 1.75 cm in order to maximize the flow rate leaving the perforated pipes.

5.4.2.2 Variable perforation lines

Varying N during the simulations for Model CWS produced similar results to those obtained for variable L_{perf}. Fig. 5.10 shows that α_x decreases as N increases across all values of ΔH for a corrugated pipe with L_{perf} and a_y fixed at 1.0 cm and 1.645 cm, respectively. However, at the lower end of ΔH, the difference in α_x can be as large as 50% between 4 and 10 lines of perforations. These results indicate that N has a larger effect on α_x than L_{perf}, which is comparable to the findings for α_e of corrugated drainage pipes (Gaj and Madramootoo, 2020). The current industry practice of using four lines of perforations on buried drainage pipes (ADS, 2008; Armtec, 2012; JM Eagle, 2012) may result in larger exit losses for subsurface irrigation systems. As such, utilizing as many lines of rectangular slots as practical may be an efficient way of reducing the hydraulic resistance and minimizing the exit head loss of perforated pipes under subsurface irrigation mode. In fact, this finding is supported by the sand tank results of Prasher et al. (1989), which showed that there were no significant exit losses for corrugated pipes with N = 12. It is important to note that there is a constraint on increasing N with respect to the structural response of buried corrugated pipes under agricultural loading conditions. Previous work has shown that at shallow burial depths (less than 0.6 m), increases in N can cause increases in pipe deformation of up to 4% of the pipe's diameter at the crown (Gaj and Madramootoo, 2021). This increase in deformation is due to a reduction in pipe stiffness in the hoop direction. If the buried depth of corrugated supply pipes are greater than 0.6 m, N = 10 can be used as an upper limit for perforation lines without causing excessive deformation (not more than 5%) from agricultural field traffic loading (Gaj and Madramootoo, 2021).

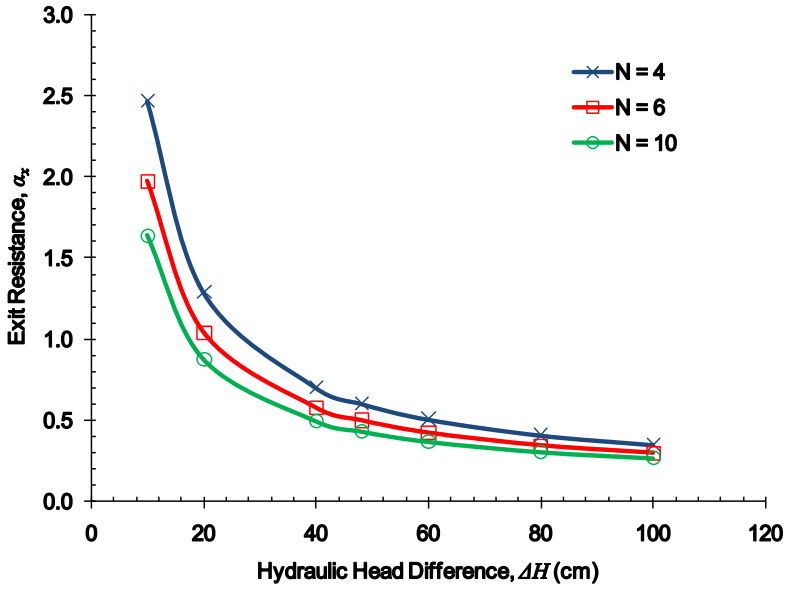

Fig. 5. 10. Variation of α_x with ΔH for select values of N.

5.4.2.3 Variable longitudinal spacing

The third and final perforation design variable that represents the longitudinal spacing, a_y, was then varied during the simulations with Model CWS (N = 4 and L_{perf} = 1.0 cm). The results are shown in Fig. 5.11, which indicates that α_x increases as the slots are spaced further apart. For example, slots spaced in every third corrugation valley (a_y = 4.935 cm) result in an

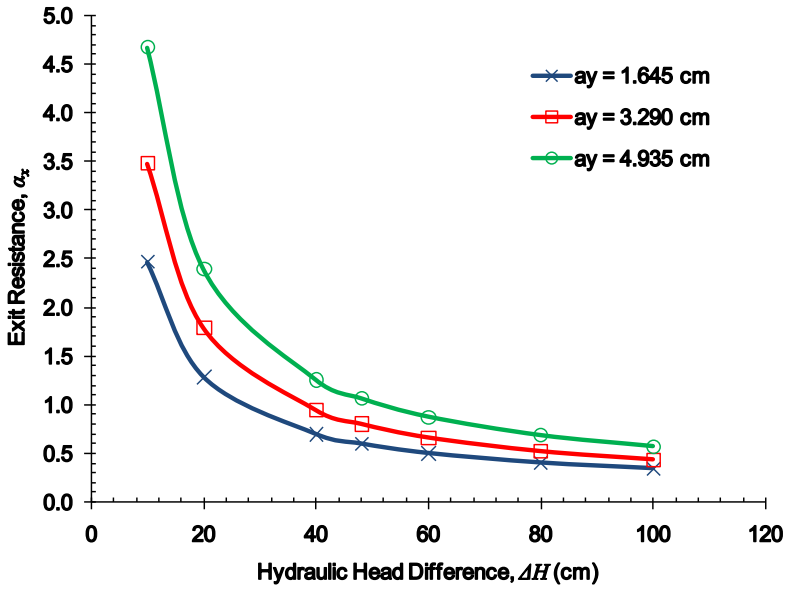

Fig. 5. 11. Effect of a_y on α_x as a function of ΔH.

increase in α_x by more than 60% compared to slots in every valley (a_y = 1.645 cm). Such increases in α_x can be explained by the distortion of the streamlines in the longitudinal direction (Y) as the flow exits the perforations (Fig. 5.12a and 5.12b). As a_y increases, the streamlines travel a larger distance between slots before they leave through the perforations, losing more energy and resulting in a more pronounced departure from 2D radial planar flow (Fig. 5.12b). In contrast, the streamlines exiting perforations that are closely spaced display a higher degree of radial planar flow as indicated in Fig. 5.12a. This trend exists across all values of ΔH for buried corrugated pipes, indicating that closer spaced perforations are beneficial in reducing the exit head loss in subsurface irrigation systems. As before, this finding mirrors that of α_e for buried corrugated drainage pipes, where a_y was ranked as second only to N for perforation variables that have the largest impact on hydraulic resistance (Gaj and Madramootoo, 2020).

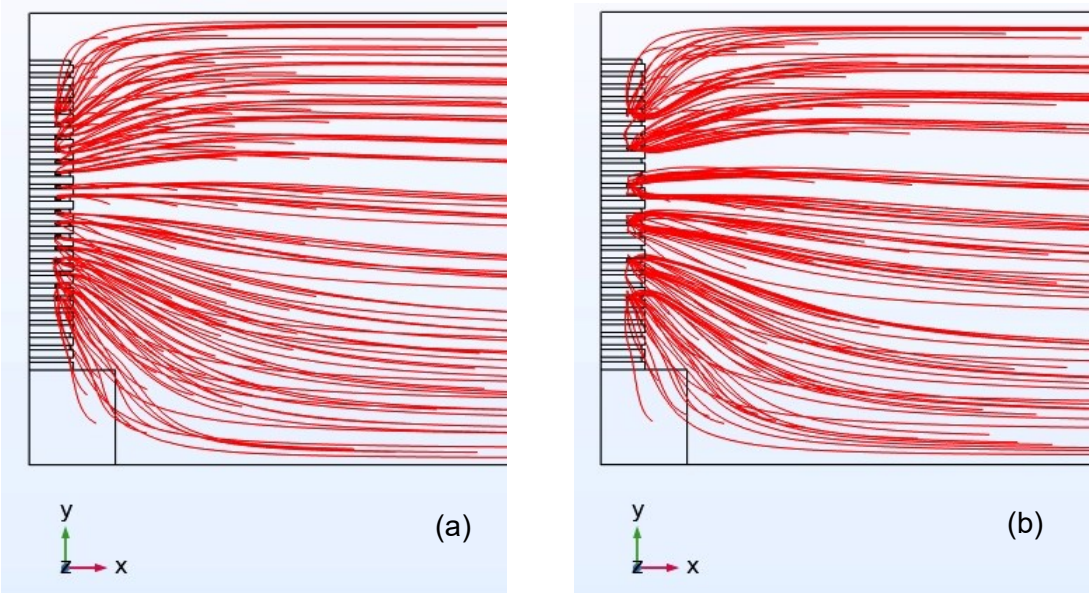

Fig. 5. 12. Plan view of corrugated pipe showing the distortion of streamlines due to longitudinal spacing of slots when (a) a_y =1.645 cm and (b) a_y =4.935 cm.

Altogether, these results show that the configuration of rectangular slots on the pipe wall (N and a_y) plays an important role in estimating α_x, and ultimately, the exit head loss of perforated corrugated pipes used in subsurface irrigation systems. From a hydraulic point of

view, it is advantageous to use slots in every corrugation valley in order to reduce α_x. From a structural point of view, there are no major disadvantages associated with placing slots in every valley. Previous work has shown that stress concentrations around perforations are not affected by a_y in corrugated pipes (Gaj and Madramootoo, 2021). As manufacturers continue to produce and market corrugated polyethylene pipes, rectangular slots placed in every corrugation valley should be promoted as the best perforations configuration to reduce hydraulic head losses (both entrance and exit) and maximize soil-water fluxes. In the case for subsurface irrigation systems, reducing exit head losses can assist with setting automated water table controls and conserving scare water resources. The non-linear regression equation (Eq. 5.S2) and its associated coefficients given in Tables 5.S1-5.S3 can be used to compute α_x as a function of ΔH and for select values of N, L_{perf}, and a_y. These regression coefficients were generated from the simulated hydraulic head datasets. The goodness of fit was evaluated by the coefficient of determination (R^2), which was greater than 99.3% for all 27 fitted equations.

5.4.3 Effect of layered soils on exit resistance

The effect of layered soils on α_x was investigated using Model CWS, which was adjusted to simulate radial flow through a corrugated pipe positioned at the interface of two soil layers. The resulting α_x due to varying perforation characteristics and ΔH combinations are shown in Fig. 5.13 for the heterogeneous arrangement of a loamy sand layer overlying a sandy clay layer (SM/SC). For comparison, simulations were also run with a single homogeneous layer having a weighted conductivity value ($k_{sat\text{-}a}$, Eq. 5.2) equivalent to that of the two-layer SM/SC system (CR_{ks} = 46). The exit resistance values plotted in Fig. 5.13 all lie on the equality line (1:1), indicating that there is no difference in α_x between the heterogeneous and homogeneous subsurface irrigation systems.

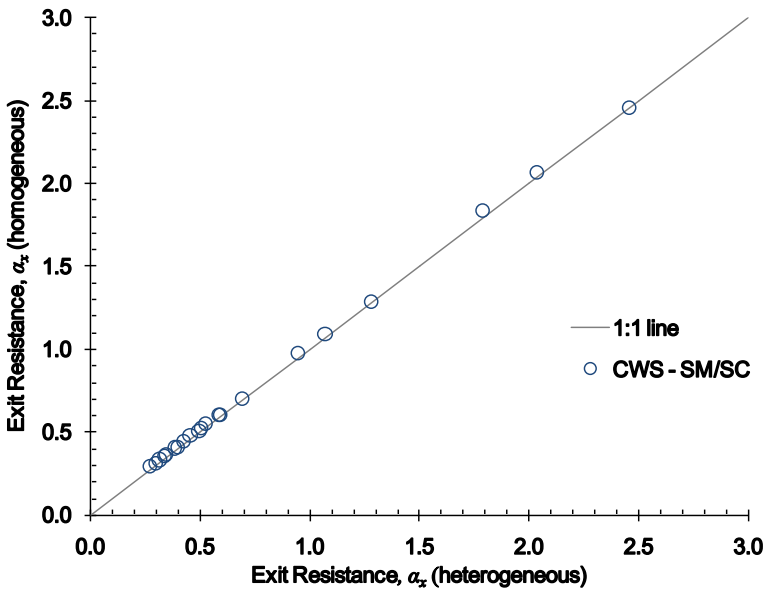

Fig. 5. 13. Comparison of α_x in a subsurface irrigation system with two layers (heterogeneous) against its equivalent one-layer system (homogeneous).

Note: the two-layer system comprises a loamy sand layer overlying a sandy clay layer (SM/SC) with CR_{ks} = 46.

The simulated pathway of the streamlines shown in Figs. 5.14a and 5.14b further supports the finding that α_x is not affected by heterogeneous soil layers. The streamlines within close proximity to the corrugated pipe are virtually identical for both the heterogeneous (Fig. 5.14a) and homogeneous (Fig. 5.14b) cases. It is only when the streamlines diverge radially upward and away from the perforations that those in the less hydraulically conductive SC layer are sharply refracted after entering the more conductive SM layer (Fig. 5.14a). This sharp refraction is certainly due to the large difference in k_{sat} between the two layers as this arrangement resulted in the highest conductivity ratio (CR_{ks} = 46), representing an extreme case of heterogeneity.

On the other hand, the ML/CH arrangement (Fig. 5.15) represents an intermediate case of heterogeneity with a CR_{ks} value of 8. The relatively lower conductivity ratio explains why the streamlines in Fig. 5.15 are refracted to a lesser degree than those in Fig. 5.14a. To further explore the streamline refraction across the layer interface of heterogeneous soils, simulations

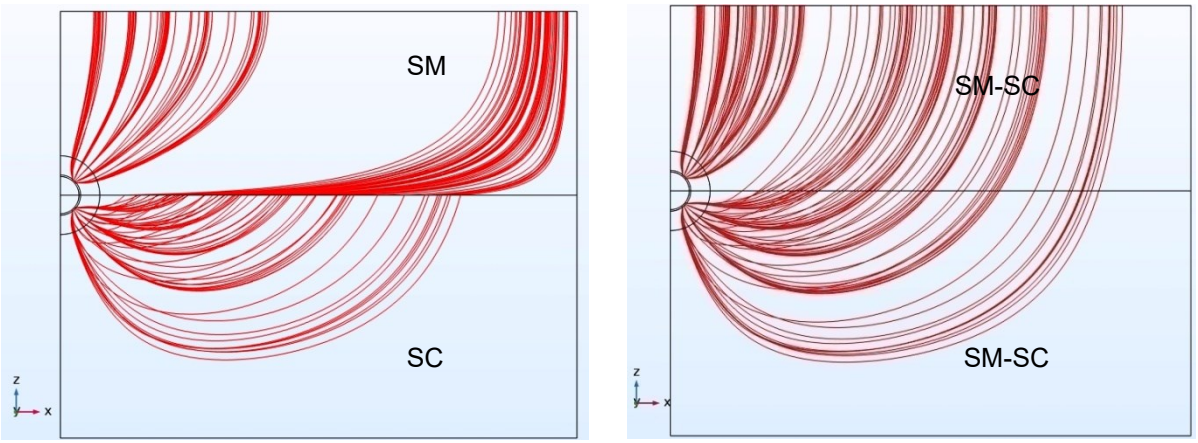

(a) (b)

Fig. 5. 14. Streamlines diverging from a perforated corrugated pipe in a (a) two-layer heterogeneous (SM/SC) and (b) equivalent one-layer homogenous (SM-SC) subsurface irrigation system.

were run using an additional two-layer arrangement to those listed in Table 5.3. The additional arrangement simulated a clay layer overlying a sandy clay layer (CH/SC) as shown in Fig. 5.16. The streamlines in Fig. 5.16 are mildly refracted because this arrangement represents a two-layer system with a CR_{ks} of 2. In fact, the refraction shown in Fig.5.16 is almost comparable to that for a homogeneous soil system (CR_{ks} = 1) as shown in Fig. 5.14b. These findings indicate that the degree of streamline refraction between two soil layers varies directly with the conductivity ratio, increasing as CR_{ks} increases.

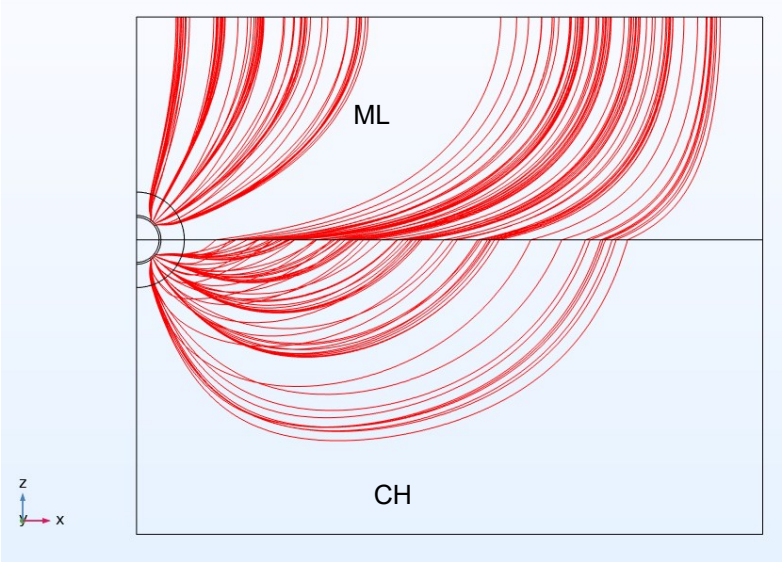

Fig. 5. 15. Streamline refraction in a silt loam over clay (ML/CH) two-layer system (CR_{ks} = 8).

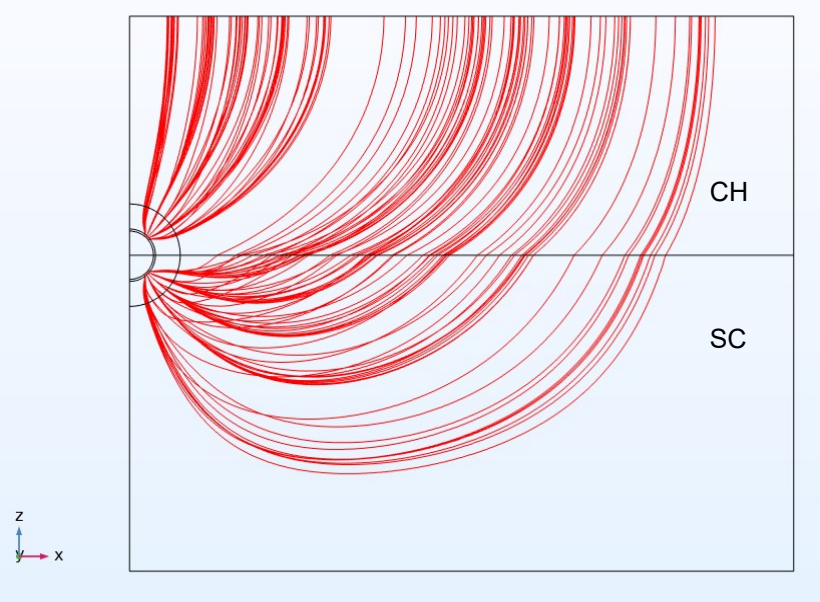

Fig. 5. 16. Streamline refraction in a clay over sandy clay (CH/SC) two-layer system (CR_{ks} = 2).

It is important to note that the streamline refractions in Figs. 5.14-5.16 occur well outside the vicinity of the pipe wall and they are not impacted by the pipe perforations. For the homogeneous case (CR_{ks} = 1), k_{sat} is constant throughout the flow region and there is no refraction of the streamlines (Fig. 5.14b). Moreover, the same trend of diverging streamlines near the pipe perforations was observed from simulations using the two remaining two-layer arrangements in Table 5.3 (ML/SC and SM/CH). The computed exit resistance values remained the same regardless of the soil textures above and below the buried perforated pipe (Figs. 5.S2-5.S4). These results provide conclusive evidence to support the conceptualization of α_x as a dimensionless parameter that is independent of k_{sat}, and only representative of the size and geometric configuration of perforations on the pipe wall. Therefore, α_x is not influenced by soil texture in either homogeneous soils or heterogeneous two-layered systems that may be encountered on agricultural lands.

5.5 Conclusions

A new dimensionless parameter, α_x, representing the hydraulic exit resistance of corrugated pipes due to perforations, is proposed in this study for incorporation into the analysis and design of buried pipes used in subsurface irrigation systems. Datasets obtained from 189 numerical simulations were used to investigate how the size and configuration of rectangular slots affect the exit resistance as the difference in hydraulic head between water levels in a control chamber and the surrounding soil increases from 10 to 100 cm. The exit resistance of perforated corrugated pipes operated under the subsurface irrigation mode in layered soils was also investigated. The major findings from this research indicate that:

- α_x is generally larger than its counterpart under drainage mode (α_e). The differences between the two resistances are statistically significant ($p < 0.05$).
- the configuration of rectangular slots on the pipe wall, as determined by N and a_y, has the largest impact on α_x. Pipes with slots in every corrugation valley (a_y = 1.645 cm) will provide the least resistance compared to those with larger longitudinal spacings.
- α_x decreases as ΔH increases, because more energy is available to overcome the resistance to flow during subsurface irrigation.
- the degree of streamline refraction between two heterogeneous soil layers varies directly with the conductivity ratio, increasing as CR_{ks} increases.
- α_x is not influenced by soil texture in either homogeneous soils or heterogeneous two-layered systems that are typically encountered on agricultural lands.

Altogether, the findings presented in this study extend the analysis and design of subsurface irrigation systems to include the exit resistance due to perforations in corrugated pipes. Exit head losses can now be computed for various perforation sizes and configurations, and as a function of the hydraulic head on buried subsurface irrigation pipes. These losses can be used

to make more informed decisions about the target water level in control chambers, in order to achieve more uniform rates of capillary rise in the unsaturated soil-water zone, to meet the ET demands of the crop. This can be of importance as water managers aim to automate the water table controls for conserving scarce water resources.

5.6 Acknowledgements

This research was funded by the Natural Science and Engineering Research Council of Canada (NSERC) and the James McGill Professor research award held by C.A. Madramootoo.

5.7 References

Abbasi, N. A., Madramootoo, C. A., Zhang, T., & Tan, C. S. (2020). Nitrous oxide emssions as affected by fertilizer and water table management unser corn-soybean rotation. *Geoderma, 375*, 114473. doi: https://doi.org/10.1016/j.geoderma.2020.114473

ADS. (2008). Single Wall HDPE Perforation Patterns *Technical Note*: Retrieved 30/08/2014, from Advanced Drainage System, <http://ads-pipecanada.ca/pdf/ca_en/A1.02-Single_Wall_Perf_Patterns.pdf>.

Amoozegar, A., & Wilson, G. N. (1999). Methods for Measuring Hydraulic Conductivity and Drainable Porosity. In R. W. Skaggs & J. van Schilfgaarde (Eds.), *Agricultural Drainage* (Vol. 38, pp. 1149-1205). Wisconsin, USA: Madison Publishers.

Armtec. (2012). HDPE Drainage Tubing (Big O) Product Guide *Drainage Solutions and Water Treatment*: Retrieved 15/01/2015, from <https://www.armtec.com/wp-content/uploads/HDPE-Drainage-Tubing-Big-O-Product-Guide.pdf>.

Bournival, P., Prasher, S., Von Hoyningen Huene, B., & S. Broughton, R. (1987). Measurements of Head Losses in a Subirrigation System. *Transactions of the ASAE, 30*(1), 183-0186. doi: https://doi.org/10.13031/2013.30424

Childs, E. C., & Youngs, E. G. (1958). The Nature of the Drain Channel as a Factor in the Design of a Land-Drainage System. *Journal of Soil Science, 9*(2), 316-331. doi: 10.1111/j.1365-2389.1958.tb01923.x

COMSOL Multiphysics. (2017a). COMSOL Multiphysics v. 5.3a Reference Manual. Stockholm, Sweden: COMSOL AB, www.comsol.com.

COMSOL Multiphysics. (2017b). COMSOL Multiphysics v. 5.3a: Subsurface Flow Module - User's Guide. Stockholm, Sweden: COMSOL AB. www.comsol.com.

Cordeiro, M. R., & Sri Ranjan, R. (2012). Corn Yield Response to Drainage and Subirrigation in the Canadian Prairies. *Transactions of the ASABE, 55*(5), 1771-1780.

Crézé, C. M., & Madramootoo, C. A. (2019). Water table management and fertilizer application impacts on CO2, N2O and CH4 fluxes in a corn agro-ecosystem. *Scientific Reports, 9*(2692). doi: https://doi.org/10.1038/s41598-019-39046-z

Dierickx, W. (1999). Non-Ideal Drains. In R. W. Skaggs & J. van Schilfgaarde (Eds.), Agricultural Drainage (Vol. 38, pp. 297-330). Wisconsin, USA: Madison Publishers.

Drury, C. F., Tan, C. S., Gaynor, J. D., Oloya, T. O., & Welacky, T. W. (1996). Influence of Controlled Drainage-Subirrigation on Surface and Tile Drainage Nitrate Loss. *Journal of Environmental Quality, 25*(2), 317-324. doi: https://doi.org/10.2134/jeq1996.00472425002500020016x

Elmi, A. A., Madramootoo, C., Handyside, P., & Dodds, G. (2010). Water requirements and subirrigation technology design criteria for cranberry production in Quebec, Canada. *Canadian Biosystems Engineering, 52*, 1.1-1.8.

Ernst, L. F. (1975). Formulae for groundwater flow in areas with subirrigation by means of open conduits with a raised water level (pp. 33). Wageningen, The Netherlands: Institute for Land and Water Management Research.

Gaj, N., & Madramootoo, C. A. (2020). Effects of Perforation Geometry on Pipe Drainage in Agricultural Lands. *Journal of Irrigation & Drainage Engineering, 146*(7), 12. doi: 10.1061/(ASCE)IR.1943-4774.0001482.

Gaj, N., & Madramootoo, C. A. (2021). Structural response of non-perforated and perforated corrugated HDPE pipes under variable loading. *Manuscript under review*.

Galganov, Y. T. (1991). *Subsurface Irrigation of Soybean.* PhD Doctoral Thesis, McGill University, Montreal.

Garcia-Gaines, R. A., & Frankenstein, S. (2015). USCS and the USDA Soil Classification System: Development of a Mapping Scheme (pp. 46). Hanover, NH: US Army Engineer Research and Develpoment Center (ERDC).

JM Eagle. (2012). Standard perforation pattern for Eagle Corr PE *Technical Bulletin*: Retrieved 29/12/2014, from <http://jmeagle.com/pdfs/Technical%20Bulletins/TB16.pdf>.

Khan, G. J., Shukla, K. N., Chauhan, H. S., & Ram, S. (1989). Verification of Kirkham's Problem of Layered Soil Drainage. *Journal of Irrigation and Drainage Engineering, 115*(4), 521-529. doi: doi:10.1061/(ASCE)0733-9437(1989)115:4(521)

Madramootoo, C. A. (1999). Planning and Design of Drainage Systems. In R. W. Skaggs & J. van Schilfgaarde (Eds.), *Agricultural Drainage* (Vol. 38, pp. 871-892). Wisconsin, USA: Madison Publishers.

Madramootoo, C. A., Helwig, T. G., & Dodds, G. T. (2001). Managing water Tables to improve drainage water quality in Quebec, Canada. *Transactions of the ASAE, 44*(6), 1511. doi: https://doi.org/10.13031/2013.7034

McWhorter, D. B., & Marinelli, F. (1999). Theory of Soil-Water Flow. In R. W. Skaggs & J. van Schilfgaarde (Eds.), *Agricultural Drainage* (Vol. 38, pp. 111-143). Wisconsin, USA: Madison Publishers.

Mejia, M. N., & Madramootoo, C. A. (1998). Improved Water Quality Through Water Table Management in Eastern Canada. *Journal of Irrigation & Drainage Engineering, 124*(2), 116-122.

Mejia, M. N., Madramootoo, C. A., & Broughton, R. S. (2000). Influence of water table management on corn and soybean yields. *Agricultural Water Management, 46*(1), 73-89. doi: https://doi.org/10.1016/S0378-3774(99)00109-2

Moser, B. K., & Stevens, G. R. (1992). Homogeneity of Variance in the Two Sample Means Test. *The American Statistician, 46*(1), 19-21. doi: 10.2307/2684403

Nelson, K. A. (2017). Soybean Yield Variability of Drainage and Subirrigation Systems in a Claypan Soil. *Applied Engineering in Agriculture, 33*(6), 801-809. doi: https://doi.org/10.13031/aea.12276

Rawls, W. J., Gimenez, D., & Grossman, R. (1998). Use of Soil Texture, Bulk Density, and Slope of the Water Retention Curve to Predict Saturated Hydraulic Conductivity. *Transactions of the ASAE, 41*(4), 983-988.

Sharma, H. C., Chauhan, H. S., Kapoor, P. N., & Ram, S. (1991). Ditch Drainage in Layered Soils. *Journal of Irrigation and Drainage Engineering, 117*(2), 184-200. doi: doi:10.1061/(ASCE)0733-9437(1991)117:2(184)

Singh, A. K., Madramootoo, C. A., & Smith, D. L. (2014). Impact of different water management scenarios on corn water use efficiency. *Transactions of the ASABE, 57*(5), 1319-1328. doi: doi: 10.13031/trans.57.10005

Skaggs, R. W. (1981). Water Movement Factors Important to the Design and Operation of Subirrigation Systems. *Transactions of the ASAE, 24*(6), 1553-1561. doi: https://doi.org/10.13031/2013.34489

Skaggs, R. W. (1991). Modeling Water Table Response to Subirrigation and Drainage. *Transactions of the ASAE, 34*(1), 169-0175. doi: https://doi.org/10.13031/2013.31640

Skaggs, R. W. (1999). Water Table Management: Subirrigation and Control Drainage. In R. Skaggs & J. van Schilfgaarde (Eds.), *Agricultural Drainage* (Vol. 38, pp. 695-718). Wisconsin, USA: Madison Publishers.

Smith, M. C., Skaggs, R. W., & Parsons, J. E. (1985). Subirrigation System Control for Water use Efficiency. *Transactions of the ASAE, 28*(2), 489-0496. doi: https://doi.org/10.13031/2013.32284

Stämpfli, N., & Madramootoo, C. A. (2006). Dissolved Phosphorus Losses in Tile Drainage under Subirrigation. *Water Quality Research Journal, 41*(1), 63-71.

Stuyt, L. C. P. M., Dierickx, W., & Beltran, J. M. (2005). *Materials for subsurface land drainage systems*. FAO Irrigation and Drainage Paper 60. Rome, Italy.

Tang, Y. K., & Skaggs, R. W. (1977). Experimental evaluation of theoretical solutions for subsurface drainage and irrigation. *Water Resources Research, 13*(6), 957-965. doi: 10.1029/WR013i006p00957

Tang, Y. K., & Skaggs, R. W. (1980). Drain Depth and Subirrigation in Layered Soils. *Journal of the Irrigation and Drainage Division, 106*(2), 113-121.

Yu, F., Frankenberger, J. R., Ackerson, J., & Reinhart, B. (2020). Potential Suitability of Subirrigation for Field Crops in the US Midwest. *Transactions of the ASABE, 63*(5), 1559-1570.

Appendix 5.A: Supplemental Data

This appendix contains material related to Chapter 5 that was prepared as supplementary data for submission to *Advances in Water Resources* for review.

5.A.1 Introduction

This supporting information include texts, figures, and tables that were deemed as supplemental to the methods and results section of Chapter 5. The sections in this supplementary information include the entrance resistance relationships for retrofitting

existing drainage systems to operate in the subsurface irrigation mode; regression models for exit resistances due to variable perforation characteristics; and the computed hydraulic resistances of buried pipes under subsurface irrigation in layered soils. All references cited are listed in section 5.7.

5.A.2 Entrance resistance relationship

A general relationship between α_e and A_p was developed using 45 combinations of N, L_{perf}, and a_y as the main perforation design variables for rectangular slots distributed on the buried pipe wall. The values of α_e were computed using a predictive equation developed by Gaj and Madramootoo (2020) for a nominal 100 mm diameter corrugated drainage pipe. The results are shown in Fig. 5.S1. for values of A_p between 8 and 300 cm^2/m. The trend in Fig. 5.S1. shows that α_e decreases rapidly as A_p increases up to a value of about 100 cm^2/m. Further increases in A_p only result in a marginal decrease in α_e.

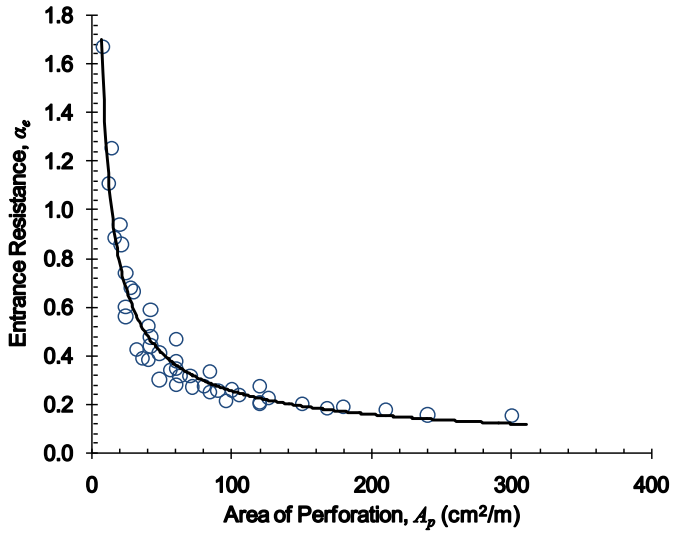

Fig. 5.S1. Entrance resistance of corrugated pipes with slots as a function of A_p.

A power law function was fitted (R^2 = 93%) to the data in Fig. 5.S1., giving

$$\alpha_e = 5.937 A_p^{-0.68} \quad (5.S1)$$

where A_p is in cm^2/m. The relationship between α_e and A_p presented by Eq. (5.S1). is valid for corrugated pipes perforated with rectangular slots in the corrugation valley. The equation may be used to determine α_e in situations when A_p is available, but the exact dimensions and/or configuration of the slots are not provided. Additionally, Eq. (5.S1). can be used in conjunction with Eq. (5.3) (section 5.4.1) to estimate α_x for buried perforated pipes operated in the subsurface irrigation mode.

5.A.3 Fitted regression models for exit resistances

The simulated hydraulic head datasets were used to develop prediction equations for α_x of buried corrugated pipes perforated with rectangular slots. Power law functions were found to give the best fit between α_x and ΔH (in cm) for select combinations of N, L_{perf}, and a_y. The regression equation fitted was

$$\alpha_x = c_3 \Delta H^{m_3} \tag{5.S2}$$

where c_3 and m_3 are the regression coefficients given in Tables 5.S1-5.S3. The goodness of fit for each of the fitted equations is given by the coefficient of determination (R^2) in Tables 5.S1-5.S3. Interpolation without significant loss of accuracy is permissible for values of N and L_{perf} that are within the design limits specified in Tables 5.S1-5.S3.

Table 5.S1. Regression coefficients for the exit resistance of corrugated pipes (a_y = 1.645 cm)

L_{perf} (cm)	N	Regression coefficients		R^2 (%)
		m_3	c_3	
1.00	4	-0.851	16.848	99.8
	6	-0.821	12.485	99.6
	10	-0.790	9.600	99.5
1.75	4	-0.827	13.251	99.7
	6	-0.799	10.240	99.6
	10	-0.772	8.308	99.4
2.50	4	-0.809	11.302	99.6
	6	-0.784	9.078	99.5
	10	-0.758	7.605	99.3

Table 5.S2. Regression coefficients for the exit resistance of corrugated pipes (a_y = 3.290 cm)

L_{perf} (cm)	N	Regression coefficients		R^2 (%)
		m_3	c_3	
1.00	4	-0.897	26.668	99.9
	6	-0.867	18.542	99.8
	10	-0.832	13.096	99.7
1.75	4	-0.872	19.643	99.8
	6	-0.841	14.161	99.7
	10	-0.809	10.545	99.6
2.50	4	-0.852	15.954	99.8
	6	-0.823	11.922	99.7
	10	-0.795	9.346	99.5

Table 5.S3. Regression coefficients for the exit resistance of corrugated pipes (a_y = 4.935 cm)

L_{perf} (cm)	N	Regression coefficients		R^2 (%)
		m_3	c_3	
1.00	4	-0.915	37.517	99.9
	6	-0.888	25.551	99.9
	10	-0.853	17.374	99.8
1.75	4	-0.892	27.056	99.9
	6	-0.862	18.945	99.8
	10	-0.828	13.553	99.7
2.50	4	-0.873	21.576	99.8
	6	-0.843	15.614	99.7
	10	-0.812	11.762	99.6

5.A.4 Subsurface irrigation in layered soils

Four arrangements of two-layer subsurface irrigation systems were simulated in order to evaluate α_x values using Model CWS. The results are shown in Figs. 5.S2, 5.S3, and 5.S4 for a silt loam layer overlying a clay layer (ML/CH), a silt loam layer overlying a sandy clay layer (ML/SC), and a loamy sand layer overlying a clay layer (SM/CH), respectively. The fourth arrangement (SM/SC) is presented in the main text (section 5.4.3).

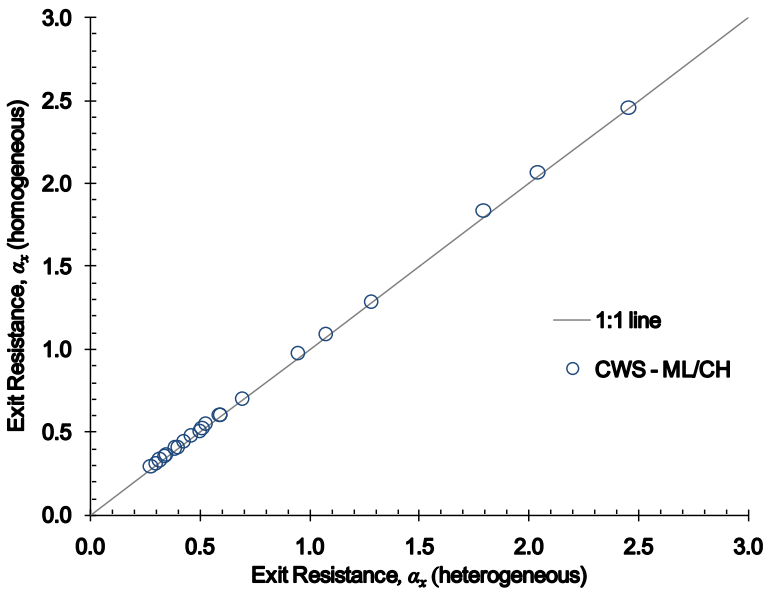

Fig. 5.S2. Comparison of α_x in a ML/CH two-layer subsurface irrigation system.

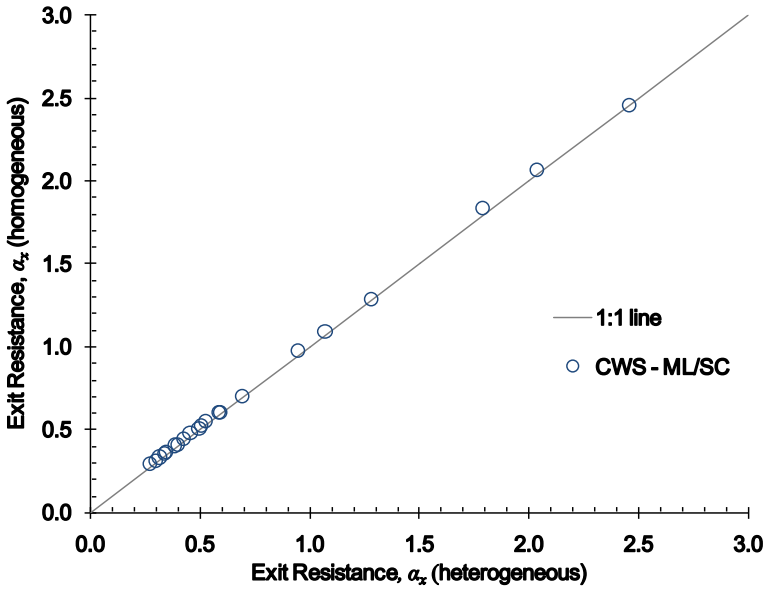

Fig. 5.S3. Comparison of α_x in a ML/SC two-layer subsurface irrigation system.

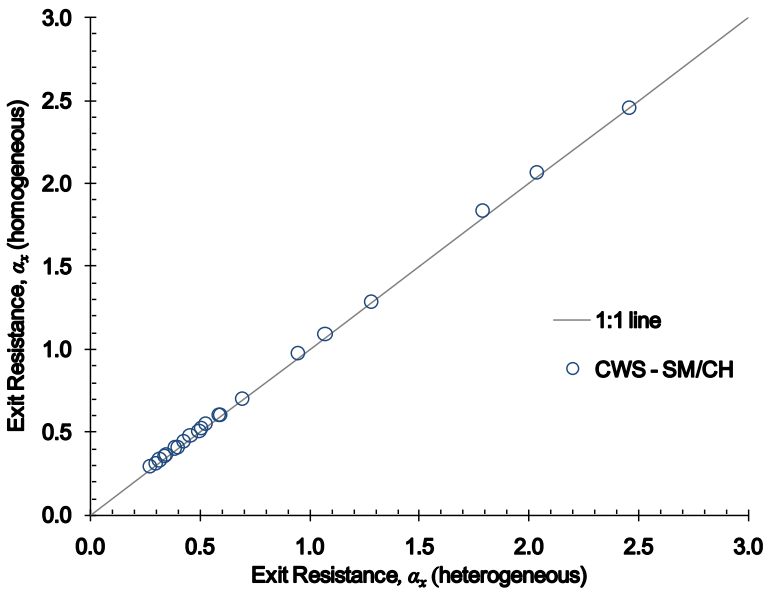

Fig. 5.S4. Comparison of α_x in a SM/CH two-layer subsurface irrigation system.

The results in Figs. 5.S2-5.S4 show that the α_x values are the same across all of the two-layer arrangements considered in this study. Therefore, it can be concluded that differences in k_{sat} due to soil texture do not have an impact on the exit resistance of buried perforated pipes.

Connecting text to Chapter 6

Chapter 5 demonstrated that the hydraulic resistance for buried perforated pipes operated under subsurface irrigation mode is different than when operated under drainage mode due to pressure head boundary condition at the soil-pipe interface. Therefore, the hydraulic response of subsurface irrigation systems under transient and steady-state conditions needs further investigation. It was explained in the literature review (Chapter 2) that the effects of variable perforation characteristics on the transient water table rise into the unsaturated zone has not been adequately studied. Chapter 6 of this thesis used the hydraulic exit resistance relationships developed in Chapter 5 as an input to simulate the transient water table response and steady soil-water fluxes from buried pipes with two combinations of perforation characteristics. Design parameters from variable soil textures, lateral drain spacing, and buried pipe depths were used in the simulations to study the effects of increasing the number and length of rectangular slots on the hydraulic response under subsurface irrigation mode. The impact of heterogeneity from layered soils on the soil-water fluxes was also investigated. Chapter 6 is being prepared for submission to *Transactions of the ASABE* (Gaj and Madramootoo, 2021c). The format of the manuscript has been modified here to ensure consistency with the style of this thesis. A list of the references cited in the manuscript is available at the end of the chapter.

Authorship contribution statement:

The author of this thesis was responsible for conceptualization, methodology, model development, formal analysis, investigation, data curation, and writing the original draft followed by all revisions and editing. Dr. Madramootoo provided supervision, aided in conceptualization, funding acquisition, and reviewed and edited the manuscript.

Chapter 6

Transient Water Table Response and Steady Soil-Water Flux from Perforated Subsurface Irrigation Pipes

6.1 Abstract

It is important to consider the water table rise into the unsaturated zone when designing subsurface irrigation systems that consist of buried perforated corrugated pipes. Corrections to drain spacing equations for head losses due to perforations are based on the entrance resistance, which is derived for buried pipes operating under the drainage mode. However, the boundary condition at the soil-pipe interface when operated under subsurface irrigation mode requires the use of the exit resistance to accurately account for perforations on the pipe wall. Simulations of a subsurface irrigation system with four soil textures, three lateral drain spacings, and three buried depths were carried out to demonstrate the effects of variable perforation characteristics on the transient water table rise into the unsaturated zone. Soil-water fluxes were also computed for the system when operated under steady-state conditions. Simulated water table rise exceeded or approached a pre-determined target water level of 1.65 m above the buried pipes in coarse-textured soils (loamy sands and silt loams) with lateral drain spacings as large as 10 m. Increasing the number and length of rectangular slots on the pipe wall (densely perforated) can reduce the water table response time to reach the target level by 15 hours in a silt loam soil and 25 hrs in a clay soil. The optimum drain spacing needed to sustain a soil-water flux of 6mm/day (common to Eastern Canada and mid-west US) can be increased from 15.1 to 16.2 m in loamy sands by using densely perforated pipes. In contrast, increasing perforations on buried pipes in clays and sandy clays will result in drain spacing increases of less than 0.2 m, because these fine-textured soils have a lower hydraulic conductivity. This study has demonstrated that variable perforation characteristics

can be included in the analysis and design of subsurface drainage systems for improving water management.

Author keywords: sub-irrigation; water table response; exit resistance; head loss; unsaturated zone

6.2 Introduction

Water table management on agricultural lands is typically implemented with buried perforated corrugated pipes that can be operated as a dual-purpose drainage and subsurface irrigation system. The system is managed in drainage mode during field operations for planting and harvesting, and could be used, where appropriate, in subsurface irrigation mode during the growing season to provide water to the crop root zone via capillarity (Gunn et al., 2016). There is an increasing potential for implementing subsurface irrigation for field crops across North America, especially in Eastern Canada and the US Midwest where conditions such as a flat topography, permeable soils, and a restrictive or impermeable soil layer exist (Marmanilo et al., 2021; Yu et al., 2020). Subsurface irrigation systems can be designed and operated under transient or steady-state conditions (Skaggs, 1999).

Water table rise into the unsaturated zone under transient conditions is an important consideration when designing subsurface irrigation systems. Field observations have shown that more than 60 hrs can elapse before any noticeable water table rise is recorded at the middle of parallel drains (Skaggs, 1973). This delay in response time depends on the lateral spacing and initial water table level (Skaggs, 1999). As with drainage, the spacing is governed by the hydraulic conductivity of the soil, which varies with soil texture and porosity. Managing water levels in order to attain the target elevation within acceptable timeframes, is key to the operation of subsurface irrigation systems (Evans and Skaggs, 1996). In addition, irrigation water requirements can be reduced by fine-tuning the control

points for starting and stopping subsurface irrigation (Smith et al., 1985). Transient-state equations developed by Skaggs (1973) can be used to compute the water table rise into the unsaturated zone for an initially horizontal water table profile at the buried pipe level. Corrections for the head losses near the supply pipe due to perforations have been made when simulating the transient water table response (Skaggs, 1991). However, these simulations used the effective radius computed from entrance resistance values (drainage mode) as a proxy to account for different perforation areas on the pipe wall. No explicit account, except for one case, of the actual perforation size and configuration were included in the simulations by Skaggs (1991). Recently, Gaj and Madramootoo (2021) investigated the validity of using the entrance resistance for 100 mm diameter corrugated pipes operated under the subsurface irrigation mode. They found that the boundary condition at the soil-pipe interface under the reversed flow direction caused a larger head loss and proposed the exit resistance (subirrigation mode) to correctly account for the pipe perforations. This implies that the steady-state solutions to compute lateral drain spacings or soil-water fluxes from pipes operating in subsurface irrigation mode (Huffman et al., 2013), also incorrectly employ the entrance resistance when accounting for perforations on the pipe wall. In addition, using the effective radius as a perforation proxy in steady-state drain spacing equations does not allow for the incorporation of perforations with different sizes and configurations into the system design. These shortcomings highlight the need to assess the impact of variable perforation characteristics on the water table rise in the unsaturated zone and steady soil-water fluxes during subsurface irrigation.

There is potential for maximizing fluxes or reducing exit head losses through the effective use of perforation dimensions and spacing in the design of corrugated pipes for subsurface irrigation. Gaj and Madramootoo (2021) developed prediction functions to relate the exit resistance with the length of rectangular slots, number of perforation lines, and longitudinal

spacing of perforations between the pipe corrugations. These non-linear prediction equations were established for varying hydraulic head differences, which allows for a direct consideration of the pressure head effect on the supply pipe due to the water level in the control chamber.

Heterogeneity in a layered soil system can be characterized by the varying hydraulic conductivities of each layer, and is typically included into drain spacing equations by using a weighted average conductivity (Madramootoo, 1999). The effect of buried pipe depths for subsurface irrigation systems with two heterogeneous soil layers was studied by Tang and Skaggs (1980). However, perforations on the pipe wall to allow for water exiting the pipe were not considered in their analysis. Gaj and Madramootoo (2021) showed that soil heterogeneity does not impact the exit resistance of buried perforated pipes in a subsurface irrigation system. Nonetheless, the influence of soil heterogeneity on soil-water fluxes from perforated pipes operated in subsurface irrigation mode has not been thoroughly investigated.

The water table response and soil-water flux from buried perforated pipes used in subsurface irrigation systems is investigated in this study. The objectives are to (1) simulate the transient water table rise in the unsaturated zone with various soil textures, lateral drain spacings, and buried depths; and (2) determine the soil-water fluxes and exit head losses under steady-state conditions. Two combinations of perforations characteristics were considered in order to assess their impact on the response of subsurface irrigation systems. In addition, the effect of heterogeneity from layered soils on the soil-water fluxes from buried perforated pipes was investigated. This research demonstrates how variable perforation characteristics on buried perforated pipes can be included in the analysis and design of agricultural water management systems.

6.3 Methodology

6.3.1 Design of subsurface irrigation systems

6.3.1.1 Transient state

Water table levels under field conditions constantly fluctuate in response to rainfall (q) or evapotranspiration (ET) in dual-purpose subsurface drainage and irrigation systems (Fig. 6.1). The transient design of such systems must account for the water table response under a range of initial and boundary conditions (Skaggs, 1999). The most exact theoretical approach for

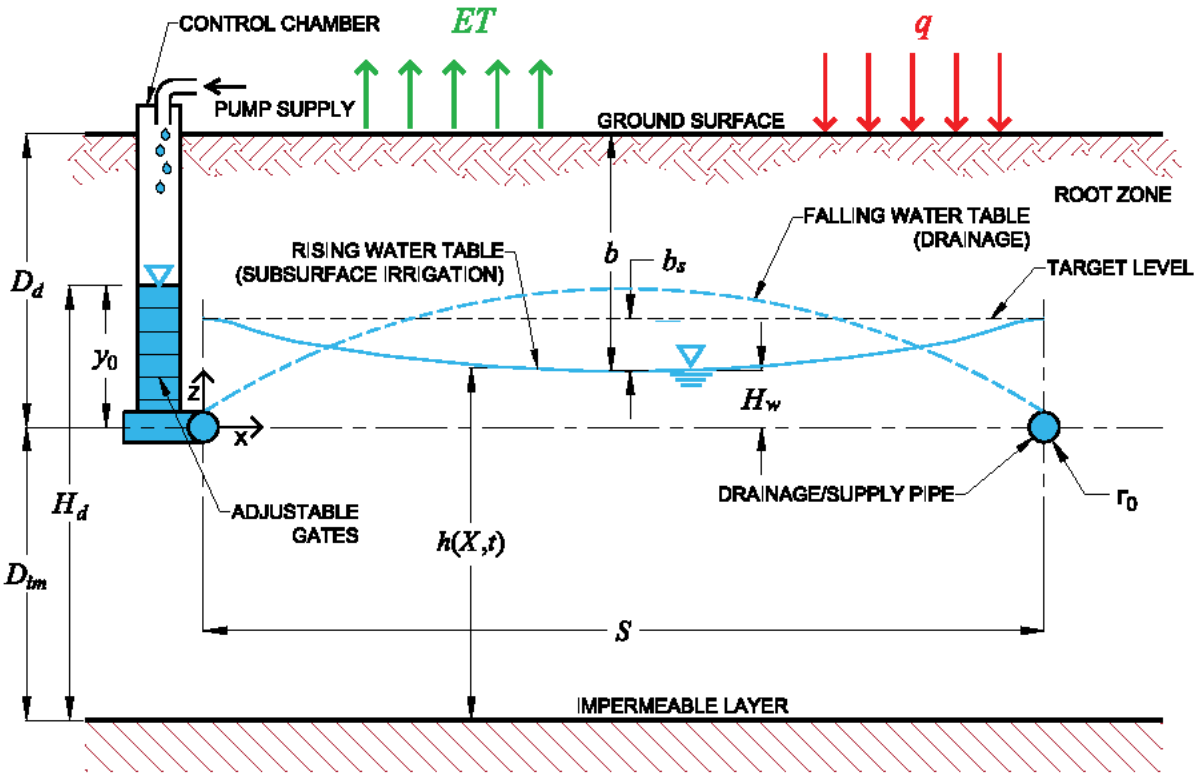

Fig. 6. 1. Definition sketch showing the water table movement under drainage and subsurface irrigation.
Note: Adjustable gates in control chamber used to set the target level.

characterizing the water movement in the unsaturated zone requires solving the Richards equation (Nieber and Feddes, 1999). However, this approach requires field-effective values of unsaturated soil-water properties that are not readily available or difficult to measure for routine analysis and design of subsurface parallel drain systems (Skaggs and Tang, 1976).

In fact, experiments conducted by Tang and Skaggs (1977) have shown that simpler approximate methods that require readily available soil-water datasets give results that are in very close agreement with solutions to the Richards equation. The Boussinesq equation is the most commonly used approximate approach for characterizing water table movement in the unsaturated zone (Skaggs, 1999). The nonlinear partial differential Boussinesq equations utilizes the Dupuit-Forchheimer assumptions and requires only the saturated hydraulic conductivity (k_{sat}) and drainable porosity (f) of the soil medium as input (Skaggs and Tang, 1976). Analytical solutions to the Boussinesq equation for the water table rise in the unsaturated zone were first presented by Skaggs (1973) in non-dimensional form as

$$H = 1 - \frac{4(1-D)}{\pi} \sum_{\omega=1,3,5\ldots}^{\infty} \left[\frac{1}{\omega} - \frac{8R}{\omega^3\pi^2}\right] e^{-\omega^2\pi^2\bar{H}\psi} \sin \omega\pi\xi \tag{6.1}$$

$$H = \frac{h}{H_d} \tag{6.2}$$

$$D = \frac{D_{im}}{H_d} \tag{6.3}$$

$$R = \frac{H_w}{H_d - D_{im}} \tag{6.4}$$

$$\psi = \frac{k_{sat}\, H_d}{f S^2}\, t \tag{6.5}$$

$$\bar{H} = \frac{1}{2H_d}(D_{im} + H_w + H_d) \tag{6.6}$$

$$\xi = \frac{X}{S} \tag{6.7}$$

where H, D, R, ψ, $\bar{H}$, and ξ are the non-dimensional parameters as defined in Eqs. (6.2-6.7). The height of the water table is h (X, t) and the hydraulic head on the buried supply pipe due to the water level in the control chamber is H_d as measured from the impermeable layer or

datum (Fig. 6.1). The pressure head on the supply pipe is y_0. The spatial coordinate in the horizontal direction between drains is X, and t is the time variable for the initial and boundary value problem. The lateral drain spacing of the supply pipes is S and the depth of the impermeable below the pipe center is D_{im}. The water table height at the mid-point between the supply pipes is H_w, which is taken relative to pipe center. For an initially flat water table level at the top of the supply pipe, $H_w = r_0$ at $t = 0$, where r_0 is the external radius of the pipe (Fig. 6.2).

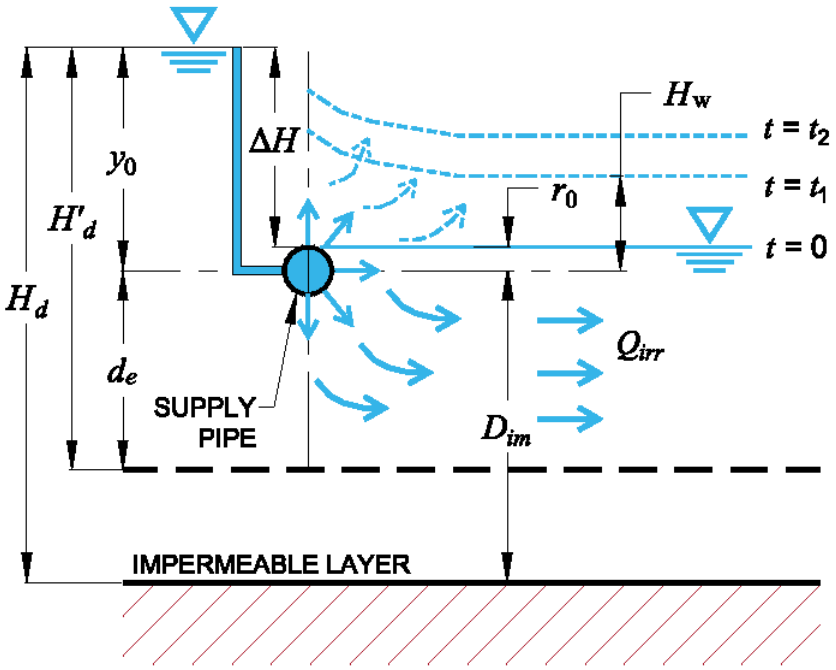

Fig. 6. 2. Rise of initial water table ($t = 0$) under pressure head (y_0) in the control chamber.

In order to account for the exit and divergent head losses (Gaj and Madramootoo, 2021), the parameters h, H_d, and D_{im} needs adjustments through Hooghoudt's equivalent depth (d_e), which is commonly used to reduce D_{im}. (Skaggs, 1981). These adjustments are best described in the theoretical formulation of the steady-state drain spacing equation as discussed in section 6.3.1.2. The series in Eq. (6.1) converges after the first two terms with an error of less than 5% (Skaggs, 1973). However, summations of the first five terms were used in this study

for increased accuracy. The transient-state solution for water table rise is based on linearizing the Boussinesq equation and solving by the separation of variables technique (Skaggs, 1999). Eq. (6.1) can be used to simulate the water table rise into the unsaturated zone for an initially flat water table or for an initially draining profile with a water table elevation of H_w at the midpoint (Skaggs, 1973).

6.3.1.2 Steady state

Ernst (1975) developed a steady-state equation to compute the required lateral drain spacing of supply pipes in subsurface irrigation systems. Similar to many other drain spacing equations, Ernst (1975) employed the Dupuit-Forchheimer assumptions for flow below the water table. The first of these assumes that all streamlines flowing towards or away from the supply pipe are horizontal, and the second assumes that the hydraulic gradient is equal to the tangent of the water table slope (McWhorter and Marinelli, 1999). Streamlines are curvilinear near the buried supply pipe due to divergent head losses from the radial soil-water fluxes (Fig. 6.2). A correction to the actual depth to the impermeable layer (D_{im}) is applied using d_e as compensation for the divergent head losses (Skaggs, 1981).

A second correction is necessary in order to account for additional head losses due to the finite perforations in the pipe wall (Skaggs, 1991). For buried corrugated pipes operated in subsurface irrigation mode, the exit resistance (α_x) is used to account for the distortion of streamlines as the soil-water flux exits the perforations (Gaj and Madramootoo, 2021). The exit head loss due to α_x can then be incorporated into lateral drain spacing equations using the effective radius (r_e) concept introduced by Childs and Youngs (1958)

$$r_e = (r_0)e^{-2\pi\alpha_x} \tag{6.8}$$

Integrating these two corrections for the divergent and exit head losses with the steady-state drain spacing equation by Ernst (1975) gives

$$S = \left[\frac{4k_{sat}b_s\left(2H'_d + \frac{H'_d}{H_d}b_s\right)}{Q_{irr}}\right]^{1/2} \tag{6.9}$$

where b_s is the allowable sag in the water table at the midpoint (Fig. 6.1), H'_d is the adjusted H_d based on d_e, and Q_{irr} is the irrigation soil-water flux leaving the buried pipes through the perforations (Fig. 6.2). For continuity, Q_{irr} is equal to ET under steady-state conditions. Values of d_e can be computed using the equations developed by (Moody, 1966) with S, D_{im}, and r_e as inputs. The solution of Eq. (6.9) is iterative when S unknown. For subsurface irrigation systems, a suitable value for b_s is 0.15 m or less (Huffman et al., 2013). The exit head loss (H_x) due to perforations on buried supply pipes in a subsurface irrigation system can then be computed from radial flow theory (Stuyt et al., 2005) as

$$H_x = \frac{Q_{irr}S}{k_{sat}}\alpha_x \tag{6.10}$$

Equation (6.10) can also be used to estimate the additional amount of water needed in the control chamber to supply subsurface irrigation to agricultural fields.

6.3.2 Simulating water table rise in the unsaturated zone

The water table rise into the unsaturated zone for four soil textures (Table 6.1) was simulated using Eq. (6.1) in order to investigate the impact of α_x on buried parallel-spaced supply pipes operated in subsurface irrigation mode. The hydraulic conductivity and drainable porosity are the two main soil properties required as input for Eq. (6.1). The conductivity values given in Table 6.1 were adapted from Rawls et al. (1998) for the four soil types categorized according to the US Department of Agriculture (USDA) textural classification system and the Unified Soil Classification System (USCS) following Garcia-Gaines and Frankenstein (2015). The drainable porosity reported in Table 6.1 was taken as the difference in volumetric water

content between saturation and field capacity (Amoozegar and Wilson, 1999). These two water content values were also adapted from Rawls et al. (1998) for the four soil textures.

Table 6.1. Hydraulic properties of four USDA soils.

USDA	USCS	k_{sat}[a]	f[b]
		m/s x 10^{-6}	m^3/m^3
Loamy Sand	SM	11.50 (8.47-21.55)	0.23
Sandy Clay	SC	0.25 (0.08-0.69)	0.09
Silt Loam	ML	4.00 (2.11-10.31)	0.15
Clay	CH	0.50 (0.08-1.92)	0.04

Note: k_{sat} = saturated hydraulic conductivity; f = drainable porosity
[a]values are the geometric mean adapted from Rawls et al. (1998); the values in parenthesis are the 25th and 75th percentile values.
[b]values were computed using data from Rawls et al. (1998).

The subsurface irrigation system used for the transient water table simulations consists of nominal 100 mm diameter corrugated supply pipes, which are buried at variable depths (D_d) below the ground surface. The impermeable layer was taken as the datum (Fig. 6.1) and assumed to lie 2.2 m below the ground surface. Simulations were run to determine the time taken (response time) to raise the midpoint water table in the unsaturated zone to a target elevation of 1.65 m above the datum. The response under three buried depths (Table 6.2) and

Table 6.2. Design variables used in water table rise simulations.

D_d (m)	ΔH (cm)	α_{x1}[a]	α_{x2}[a]
1.20	60	0.8856	0.3364
0.90	30	1.6698	0.6308
0.75	15	3.1485	1.0863

Note: D_d = buried depth; ΔH = total head difference; α_{x1} = sparsely perforated pipe; α_{x2} = densely perforated pipe
[a]values computed from non-linear regression equations (Gaj and Madramootoo, 2021).

three lateral drain spacings (5, 10, and 15 m) were simulated as part of the analysis for transient water table rise into the unsaturated zone. It was also assumed that the initial water table (t = 0) was horizontal and level with the top of the buried supply pipe. Therefore, the

resulting total head difference (ΔH) was taken as the difference between the target water level and the initial water table level, which varies with D_d (Table 6.2).

Two combinations of perforation size and configuration were selected for the water table response computations in order to demonstrate the anticipated effects of variable perforation characteristics during subsurface irrigation. The first combination, α_{x1} (Fig. 6.3), represents a sparsely perforated pipe that has four lines of perforation (N = 4) placed in every third corrugation valley (a_y = 4.935 cm). Each of the rectangular slots for α_{x1} had a length (L_{perf}) of 1.0 cm. For the second combination, N was increased to 6, L_{perf} was increased to 2.5 cm, and a_y was decreased to 1.645 cm (slots placed in every corrugation valley) in order to represent a densely perforated pipe (α_{x2}). The perforation width was fixed at 0.2 cm because this

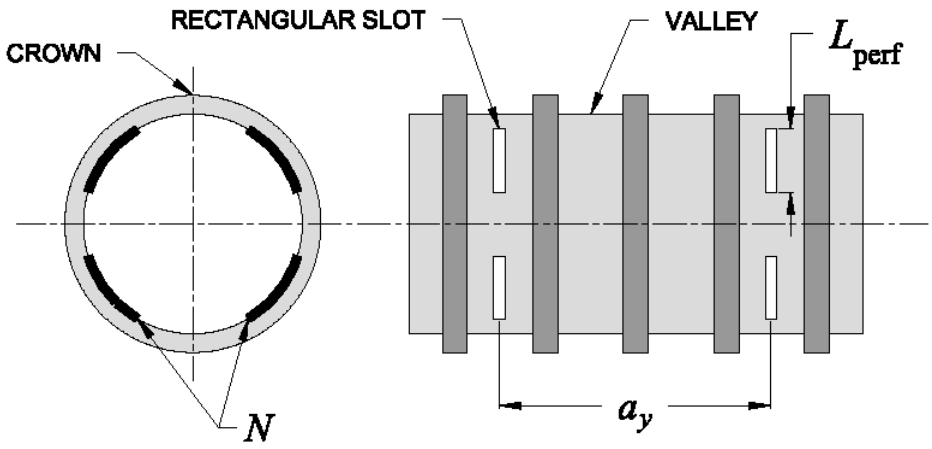

Fig. 6. 3. Corrugated supply pipe showing perforation design variables: number of perforation lines (N), length of rectangular slot (L_{perf}), and axial spacing (a_y).

parameter does not affect the pipe's hydraulic resistance (Gaj and Madramootoo, 2020). The exit resistance (α_x) for these two combinations of perforation characteristics were computed from non-linear regression equations of α_x as a function of ΔH and the specified values of N, L_{perf}, and a_y as given by Gaj and Madramootoo (2021). The computed α_x values are summarized in Table 6.2, which shows that α_{x2} (densely perforated pipe) has a lower hydraulic resistance for supply pipes in subsurface irrigation systems.

6.3.3 Soil-water fluxes

Steady-state soil-water fluxes (Q_{irr}) from the buried perforated supply pipe were computed with the transposed form of the Ernst equation (Eq. [6.9]). The four soil textures, three drain spacings, three buried depths, and two perforation combinations from the transient water table rise analyses (section 6.3.2) were also considered in the Q_{irr} computations. An allowable sag of 15 cm from the water table target level at the midpoint was used in Eq. (6.9) following Huffman et al. (2013). These computations were carried out in order to investigate the effects of S and D_d on Q_{irr}, while incorporating the impact of varying pipe perforations via α_x.

6.3.4 Fluxes in layered soils with numerical simulations

Numerical simulations with a three dimensional (3D) finite-element-based model developed by Gaj and Madramootoo (2021) was used for computing Q_{irr} from perforated pipes in a two-layer subsurface irrigation system. The 3D numerical model was developed and implemented as a steady-state boundary value problem in COMSOL Multiphysics version 5.3 (COMSOL Multiphysics, 2017a). Radial upward soil-water flow in the region around the buried perforated pipe was simulated with the Subsurface Flow Module in COMSOL, which solves for the unknown pressure head variable using the Darcy Law interface (COMSOL Multiphysics, 2017b). The model (Fig. 6.4) is 124 cm deep (Z-axis), 150 cm wide (X-axis), and 60 cm thick (Y-axis) with a nominal 100-mm diameter corrugated pipe buried 53.4 cm from the ground surface. Symmetry was applied along the vertical Z-Y plane to reduce computational time. The model has been calibrated with discharge data and verified against piezometric data obtained from sand tank experiments (Gaj and Madramootoo, 2020).

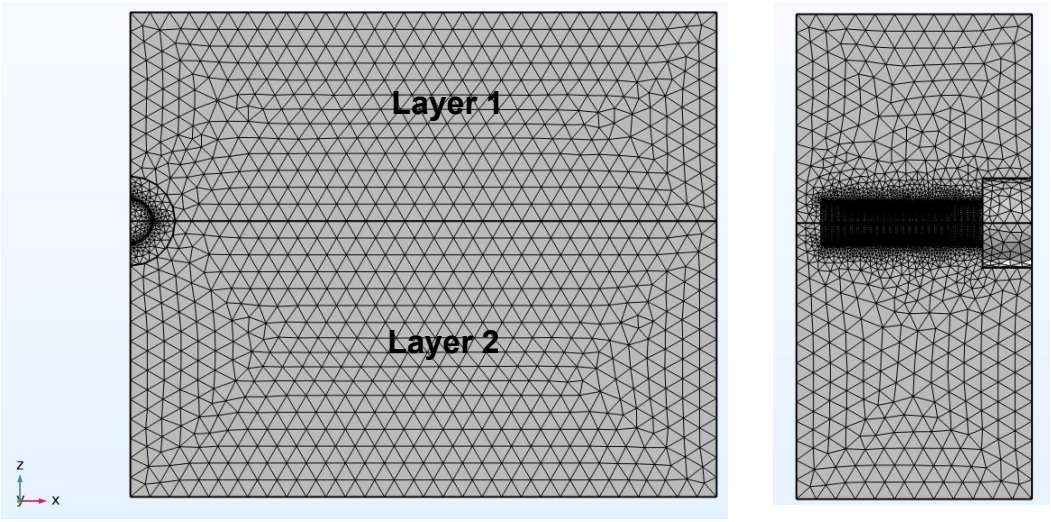

Fig. 6. 4. Orthographic projections of the three-dimensional (3D) finite-element model around a perforated pipe in a two-layer subsurface irrigation system. Front (left) and side (right) views.

Variable mesh sizes were used for the finite-element model in order to accurately compute the soil-water fluxes leaving the perforations on the pipe wall, resulting in a higher mesh concentration around the pipe as shown in the side view (right) of Fig. 6.4. The minimum and maximum element sizes were 0.15 and 5 cm, respectively. These mesh parameters produced 235676 tetrahedral elements after discretization. The governing equations, initial and boundary conditions, mesh analysis, calibration and verification of the numerical model is fully documented elsewhere (Gaj and Madramootoo, 2020; Gaj and Madramootoo, 2021).

Several combinations of two-layer systems (Table 6.3) were considered for the numerical simulations using the four soil textures given in Table 6.1. For simplicity, the hydraulic conductivity within each soil layer was modelled as a uniform and isotropic matrix, and therefore, heterogeneity in the two-layer system was characterized by differences in k_{sat} values. The conductivity ratio (CR_{ks}) was computed as the ratio of the k_{sat} values for the upper (Layer 1) to lower (Layer 2) soil layers, and was used as an indicator to describe differences in the soil-water flux response for the two-layer systems (Table 6.3).

Table 6.3. Combinations of two-layer systems for simulating soil-water fluxes (Q_{irr})

Two-layer description	Symbol	Conductivity Ratio, CR_{ks}	k_{sat-a} $\times 10^{-6}$ m/s
Sandy clay overlying Clay	SC/CH	0.5	0.392
Clay overlying Sandy Clay	CH/SC	2	0.357
Silt Loam overlying Clay	ML/CH	8	2.007
Silt Loam overlying Sandy Clay	ML/SC	16	1.864
Loamy Sand overlying Clay	SM/CH	23	5.237
Loamy Sand overlying Sandy Clay	SM/SC	46	5.094

Note: k_{sat-a} was computed with Eq. (6.11).

An equivalent one-layer homogeneous soil system with a buried perforated supply pipe was also used in the simulations following Gaj and Madramootoo (2021). The soil-water fluxes from the equivalent one-layer system, Q_{irr} (homogeneous), were then directly compared to the fluxes from the two-layer system, Q_{irr} (heterogeneous), in order to assess the former's suitability for use in design drain spacing equations such as Eqs. (6.1) and (6.9). The arithmetic mean of the hydraulic conductivities of the two heterogeneous soil layers was used to compute the average conductivity of its equivalent homogeneous soil layer (k_{sat-a}) as (Amoozegar and Wilson, 1999)

$$k_{sat-a} = \frac{(L_{z1}k_{sat-1}+L_{z2}k_{sat-2})}{L_{z1}+L_{z2}} \tag{6.11}$$

where L_z is the thickness of the soil layer. The subscripts 1 and 2 denote the parameter values for Layer 1 and Layer 2 in the two-layer system (Fig. 6.4), respectively. Equation (6.11) was used to compute the weighted average conductivity for the six combinations of two-layer systems (Table 6.3).

6.4 Results and Discussion

6.4.1 Transient water table rise

6.4.1.1 Response in variable soil texture

The predicted water table rise into the unsaturated zone at the midpoint of a subsurface irrigation system is shown in Figs. 6.5-6.8 for various soil textures, buried depth (D_d), drain spacing (S), and perforation characteristics. In general, the largest variability in the water table response occurs across the four soil textures investigated. For parallel-spaced buried supply pipes with a lateral drain spacing of 15.0 m, the water table did not reach the target elevation (1.65 m) after 200 hrs for all combinations of buried depths in the four soil textures (Figs. 6.5-6.8 [c, f, and i]). In contrast, the water table rise was fastest for supply pipes spaced at 5.0 m in the loamy sand (SM) and silt loam (ML) soils across all three buried depth (Figs. 6.5 and 6.7, respectively). There was virtually no water table response in sandy clay (SC) soils when S was greater than 10.0 m (Fig. 6.6). A similar trend was observed for the response in clay (CH) soils (Fig. 6.8). In fact, the simulated water table response under transient conditions suggest that lateral drain spacings in both SC and CH soils should be less than 5 m if the target elevation is to be attained within an acceptable duration of time. For most agricultural soils, this acceptable duration is typically between 48 to 72 hours as the soil-water moves laterally in the saturated zone, then vertically as upward flux into the unsaturated zone above the water table in subsurface irrigation systems (Evans and Skaggs, 1996).

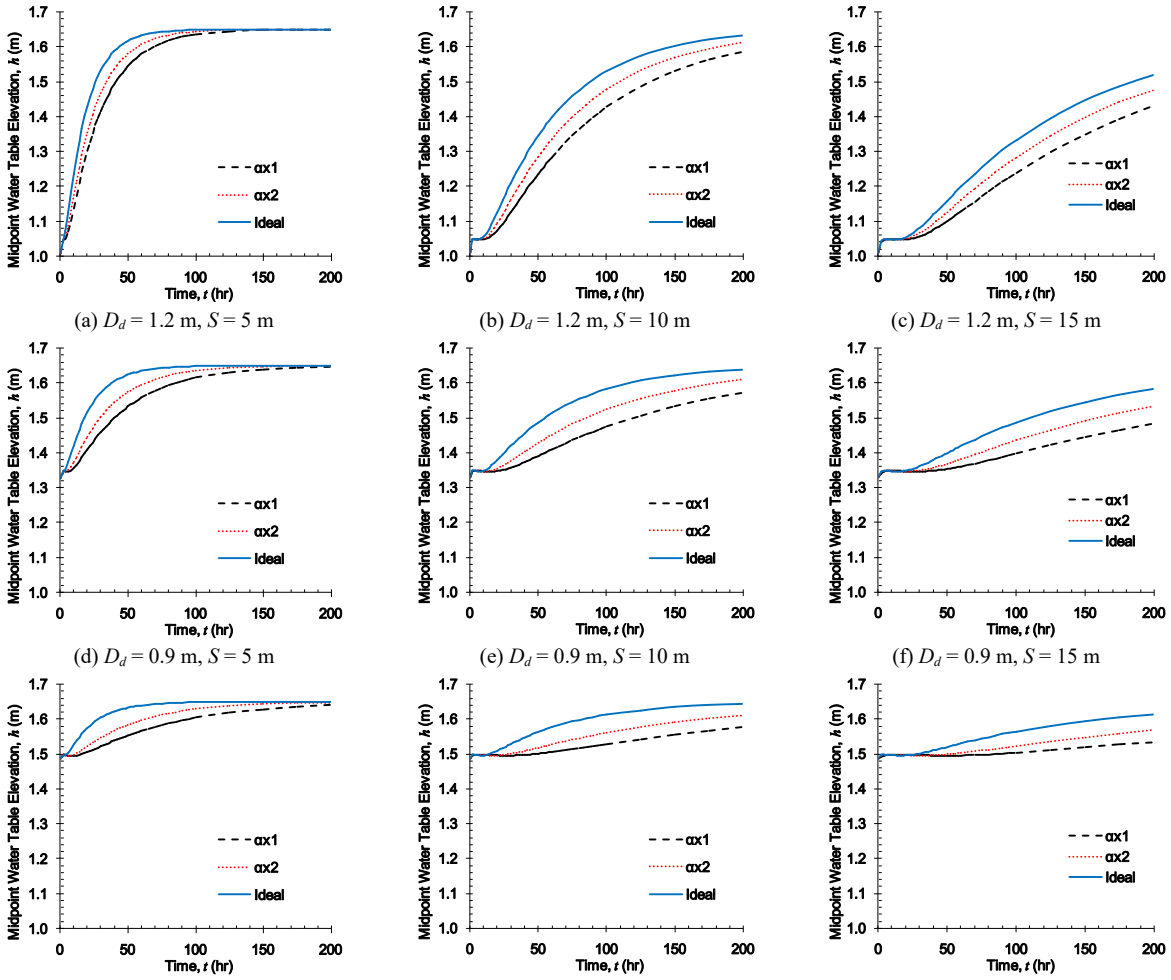

(a) D_d = 1.2 m, S = 5 m (b) D_d = 1.2 m, S = 10 m (c) D_d = 1.2 m, S = 15 m

(d) D_d = 0.9 m, S = 5 m (e) D_d = 0.9 m, S = 10 m (f) D_d = 0.9 m, S = 15 m

(g) D_d = 0.75 m, S = 5 m (h) D_d = 0.75 m, S = 10 m (i) D_d = 0.75 m, S = 15 m

Fig. 6. 5. Water table rise in a Loamy Sand (SM) soil with variable buried depth (D_d) and lateral drain spacings (S).
Note: α_{x1} =sparsely perforated pipe, α_{x2} =densely perforated pipe, and Ideal = fully porous pipe (See Table 6.2).

This disparity in the transient response of the water table due to soil texture can be explained by the variability in the soil's hydraulic properties (k_{sat} and f). The hydraulic conductivity values of the SM and ML soils are one order of magnitude greater than those for the SC and CH soils. As a result, the simulated water table was shown to exceed or approach the predetermined target level at lateral drain spacings as large as 10 m in the medium to coarse-textured soils (SM and ML).

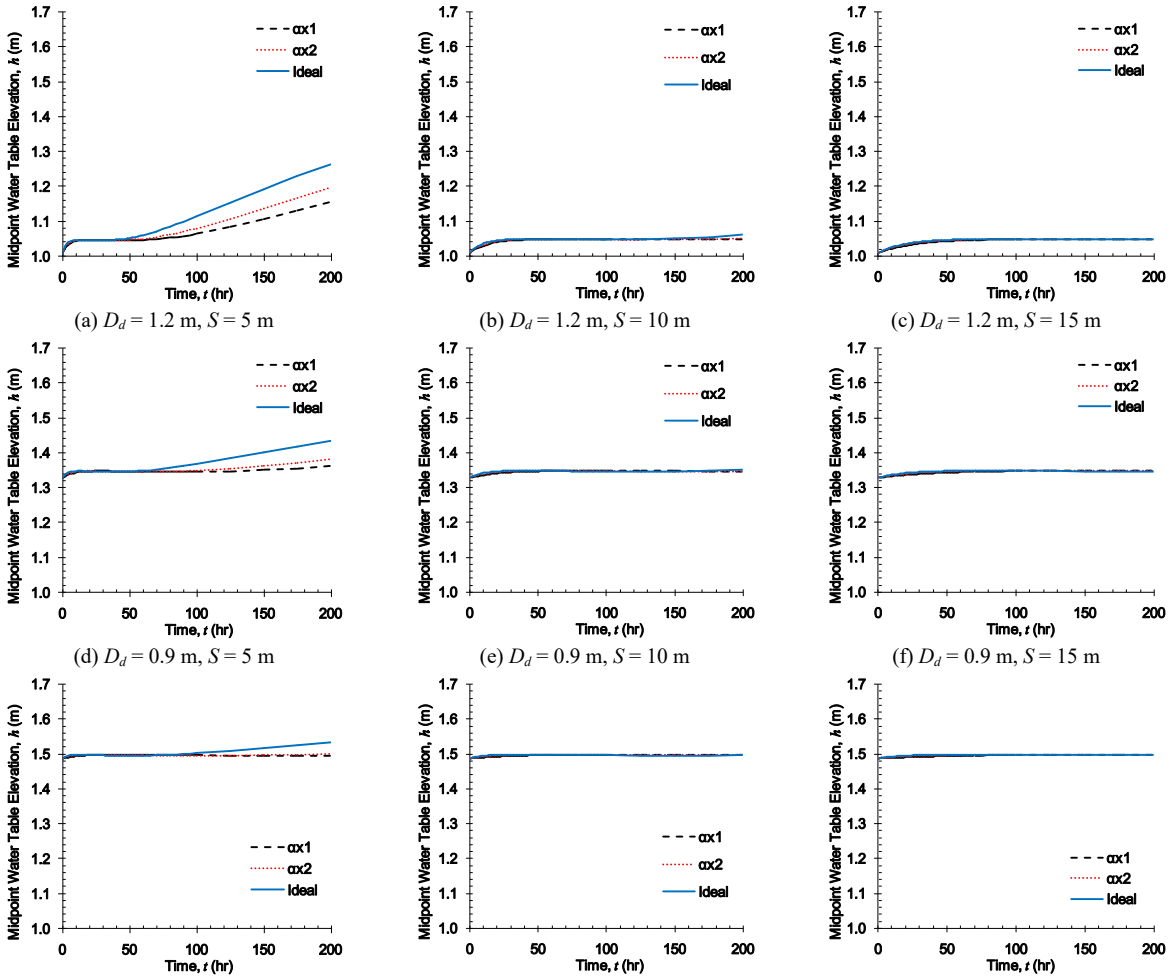

(a) D_d = 1.2 m, S = 5 m (b) D_d = 1.2 m, S = 10 m (c) D_d = 1.2 m, S = 15 m

(d) D_d = 0.9 m, S = 5 m (e) D_d = 0.9 m, S = 10 m (f) D_d = 0.9 m, S = 15 m

(g) D_d = 0.75 m, S = 5 m (h) D_d = 0.75 m, S = 10 m (i) D_d = 0.75 m, S = 15 m

Fig. 6. 6. Water table rise in a Sandy Clay (SC) soil with variable buried depth (D_d) and lateral drain spacings (S).

Note: α_{x1} =sparsely perforated pipe, α_{x2} =densely perforated pipe, and Ideal = fully porous pipe (See Table 6.2).

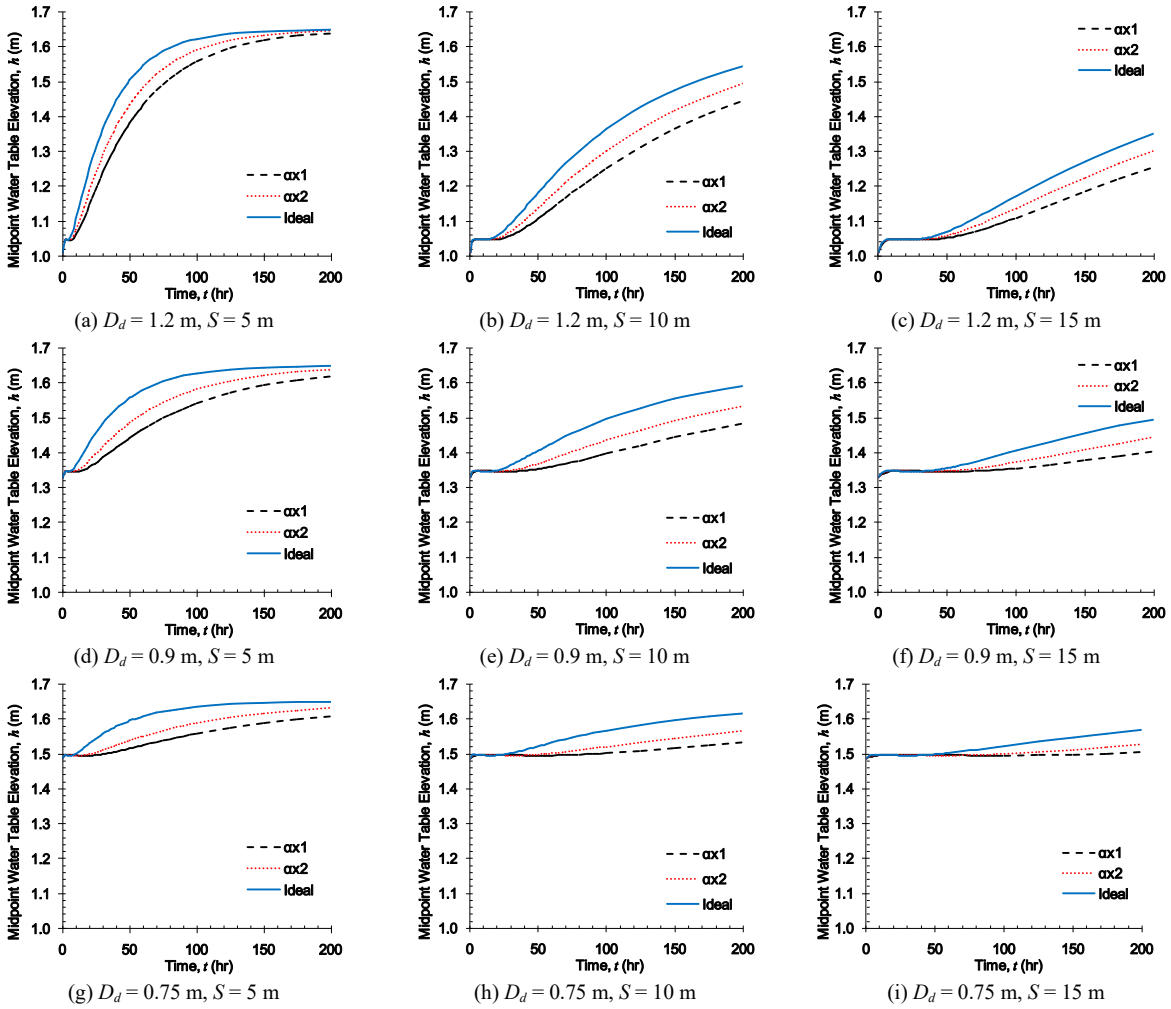

(a) D_d = 1.2 m, S = 5 m (b) D_d = 1.2 m, S = 10 m (c) D_d = 1.2 m, S = 15 m

(d) D_d = 0.9 m, S = 5 m (e) D_d = 0.9 m, S = 10 m (f) D_d = 0.9 m, S = 15 m

(g) D_d = 0.75 m, S = 5 m (h) D_d = 0.75 m, S = 10 m (i) D_d = 0.75 m, S = 15 m

Fig. 6. 7. Water table rise in a Silt Loam (ML) soil with variable buried depth (D_d) and lateral drain spacings (S).
Note: α_{x1} =sparsely perforated pipe, α_{x2} =densely perforated pipe, and Ideal = fully porous pipe (See Table 6.2).

The water table rise into the unsaturated zone is also a function of drainable porosity, which directly affects the response time to raise the water table to the design target level. Generally, the water table will rise rapidly in fine-textured soils where f is typically less than 0.06 m^3/m^3 (Fouss et al., 1999). The larger drainable porosity values for the SM and ML soil textures (f > than 0.15 m^3/m^3) may explain why the response times exceed 100 hrs when the drain laterals are spaced at 10 m. Nevertheless, these simulated response times are comparable to field observations, which reported response times of 168 hrs to raise the water table by 15 cm in SM soils with a 15 m spacing subsurface irrigation system (Davenport and Skaggs, 1990).

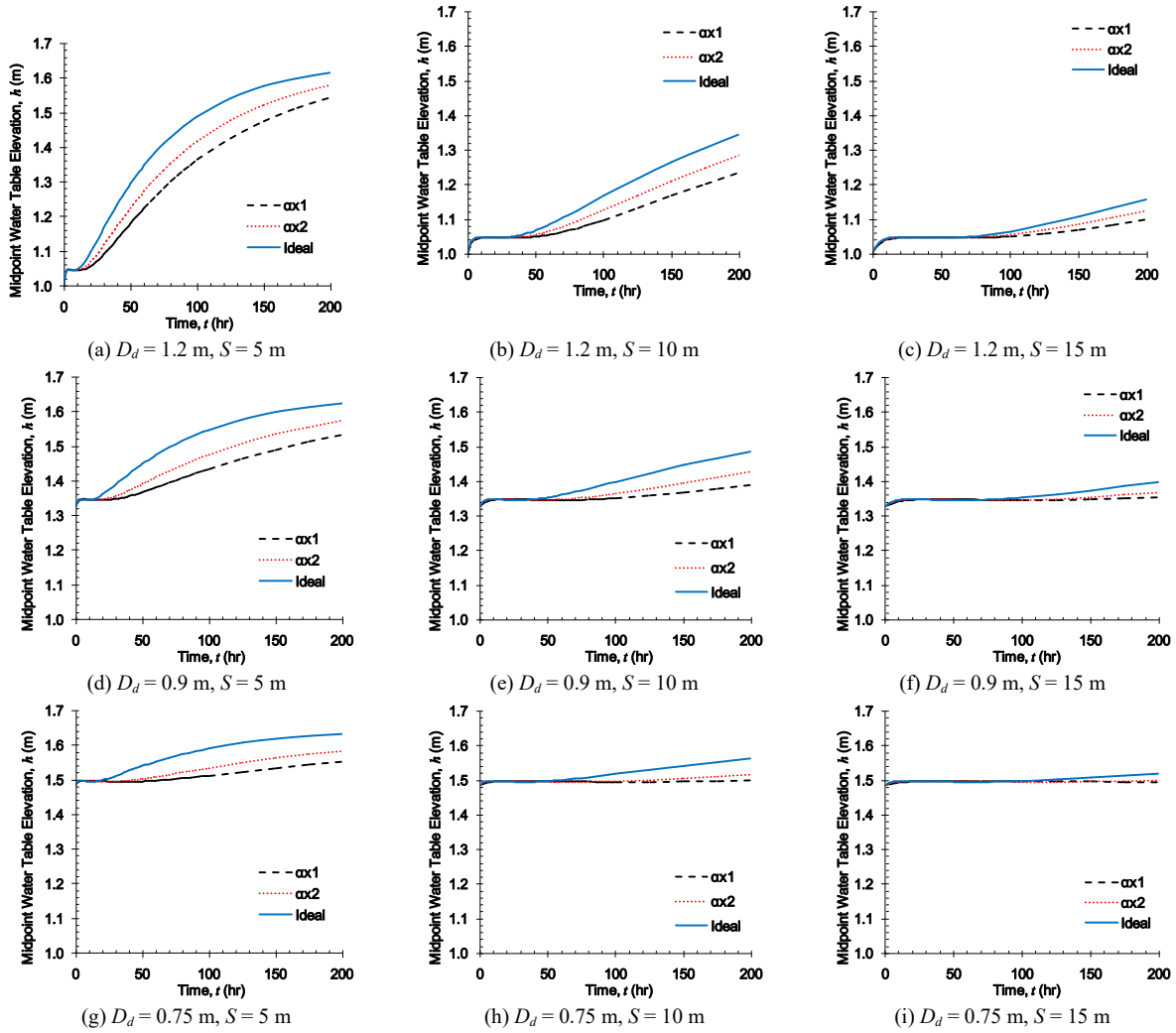

(a) D_d = 1.2 m, S = 5 m (b) D_d = 1.2 m, S = 10 m (c) D_d = 1.2 m, S = 15 m

(d) D_d = 0.9 m, S = 5 m (e) D_d = 0.9 m, S = 10 m (f) D_d = 0.9 m, S = 15 m

(g) D_d = 0.75 m, S = 5 m (h) D_d = 0.75 m, S = 10 m (i) D_d = 0.75 m, S = 15 m

Fig. 6. 8. Water table rise in a Clay (CH) soil with variable buried depth (D_d) and lateral drain spacings (S).
Note: α_{x1} = sparsely perforated pipe, α_{x2} = densely perforated pipe, and Ideal = fully porous pipe (See Table 6.2).

For an ideal pipe (α_x = 0), the general effect of burial depth on the water table rise is that the response time decreases as D_d decreases, which is best demonstrated for the special case of subsurface irrigation pipes buried in a SM soil (Fig. 6.5). The decrease in response time to reach within 5 cm of the target level (i.e. 1.6 m) is 70 hrs as D_d decreases from 1.2 m to 0.75 m when S = 10 m (Figs. 6.5b and 6.5h). This proximity (5 cm) to the target level was primarily chosen to evaluate the decrease in response time because the water table approaches the actual target level asymptotically as S increases. Reductions in the water table

response time as burial depths get shallower is intuitive; the supply pipe (and initial water table level) moves closer to the target level, resulting in a smaller vertical distance for the upward movement of soil-water fluxes into the unsaturated zone. A decrease in response time as D_d decreases from 1.2 m to 0.75 m is also present in other soil textures, varying from 30 hrs in a ML soil (Fig. 6.7) to 65 hrs in a CH soil (Fig. 6.8) when S = 5 m. Notably, the effect is less pronounced with supply pipes buried at a larger drain spacing (greater than 5 m) in the CH and ML soil textures due to their relatively smaller hydraulic conductivities.

6.4.1.2 Response due to perforation characteristics

The impact of the two combinations of perforation characteristics on water table rise is reflected by α_{x1} and α_{x2} in Figs. 6.5-6.8. For context, the water table response for a fully porous buried supply pipe is also shown, representing the case of an ideal pipe with no exit resistance (α_x = 0). Generally, the response time to raise the water table to the target level with buried perforated pipes is larger than the response time with ideal pipes due to the exit resistance of the former. This effect, however, is not clearly exhibited for perforated pipes in SC soils (Fig. 6.6) when the lateral drain spacing is greater than 10 m. As discussed earlier (section 6.4.1.1), the very small conductivity of SC soils (0.25×10^{-6} m/s) results in virtually no water table response at the midpoint between drain pipes. Furthermore, the results show that the water table rise is slower under a sparsely perforated pipe (α_{x1}) as compared to the pipe that was densely perforated (α_{x2}). At a spacing of 5 m and buried depth of 1.2 m, the response times to 1.6 m are 70 and 125 hrs for a sparsely perforated pipe in SM and ML soils, respectively. On the other hand, response times from a densely perforated pipe, simulated by increasing both the number and length of the rectangular slots, is reduced by 14 hrs in SM soils and 15 hrs in ML soils. The reduction in response time due to increased perforation area in CH soils was not evaluated because the midpoint water table rise to 1.6 m exceeds 200 hrs. However, the decrease in response time due to perforations can be as large as 25 hrs for

buried corrugated pipes (S = 5 m and D_d = 1.2 m) in CH soils when evaluated for a water table rise to 1.5 m (Fig. 6.8a).

The water table response from perforated supply pipes is also affected by burial depth. However, unlike the case for ideal pipes (section 6.4.1.1), the response time increases as D_d decreases for both combinations of perforation characteristics (α_{x1} and α_{x2}). For sparsely perforated buried pipes (α_{x1}) in SM soils, the response time to reach 1.6 m is increased from 70 hrs to 95 hrs as D_d decreases from 1.2 m to 0.75 m when S = 5 m (Figs. 6.5a and 6.5g). The corresponding increase in response time for a densely perforated pipe (α_{x2}) is 9 hrs, indicating that the effect of D_d is less severe in pipes a greater perforation area. Similarly, the water table takes 50 hrs and 25 hrs longer to reach 1.6 m in a ML soil for α_{x1} and α_{x2}, respectively (Figs. 6.7a and 6.7g). The relatively larger increases in water table response times for ML soils compared to SM soils, despite the latter having a larger hydraulic conductivity, may be attributed to differences in drainable porosity. The drainable porosity of the ML soil texture in Table 1 is 35% less than that of the SM soil texture. As previously discussed (section 6.4.1.1), the water table will rise faster in soils with a smaller drainable porosity.

The general increase in response time for perforated pipes operated in subsurface irrigation mode can be explained by the increase in exit resistance as D_d decreases (Table 6.2). The increase of α_x is in turn explained by changes in the hydraulic boundary condition at the soil-pipe interface (Gaj and Madramootoo, 2021). The difference in hydraulic head (ΔH) between the constant water level in the control chamber (y_0) and the initial water table level just outside of the supply pipe (H_w) decreases as the buried depth is moved closer to the target elevation. Therefore, less energy is available to overcome the hydraulic resistance of the pipe perforations as irrigation water exits the pipe, resulting in an increase in α_x, and ultimately, increases in water table response times.

A previous field study has suggested that delays in water table response may be responsible for a reduction in corn yields in subsurface irrigation plots (Cordeiro and Sri Ranjan, 2012). In addition to meeting crop water demands, irrigation must be delivered in a timely manner to be most effective. The results from these transient analyses demonstrate that while soil texture and lateral drain spacing are the primary factors governing water table rise into the unsaturated zone, the size and configuration of perforations on the supply pipe can play an important role in reducing response times for subsurface irrigation systems. For dual-purpose drainage and subsurface irrigation systems, decreasing the burial depth of perforated supply pipes will also reduce the discharge capacity when operated under drainage mode. Therefore, subsurface irrigation systems with a shallower buried depth and a constant water level in the control chamber does not appear to be advantageous for agricultural water management.

6.4.2 Steady-state response

6.4.2.1 Soil-water fluxes

Soil-water fluxes (Q_{irr}) through the perforations of buried pipes were computed using Eq. (6.9) to simulate the irrigation supply for the buried pipe system under steady state conditions. Identical soil properties and subsurface irrigation parameters from the transient analysis (section 6.4.1) were used as input for the computations. The results are shown as 3D surfaces for the combined effects of S and D_d on Q_{irr} from buried supply pipes in variable soil textures (Figs. 6.9-6.11). The largest soil-water fluxes were computed for the SM (Fig. 6.9) and ML (Fig. 6.10) soils, corroborating the transient analysis results (Figs. 6.5 and 6.7) that showed discernible water table responses for these medium to coarse-textured soil types.

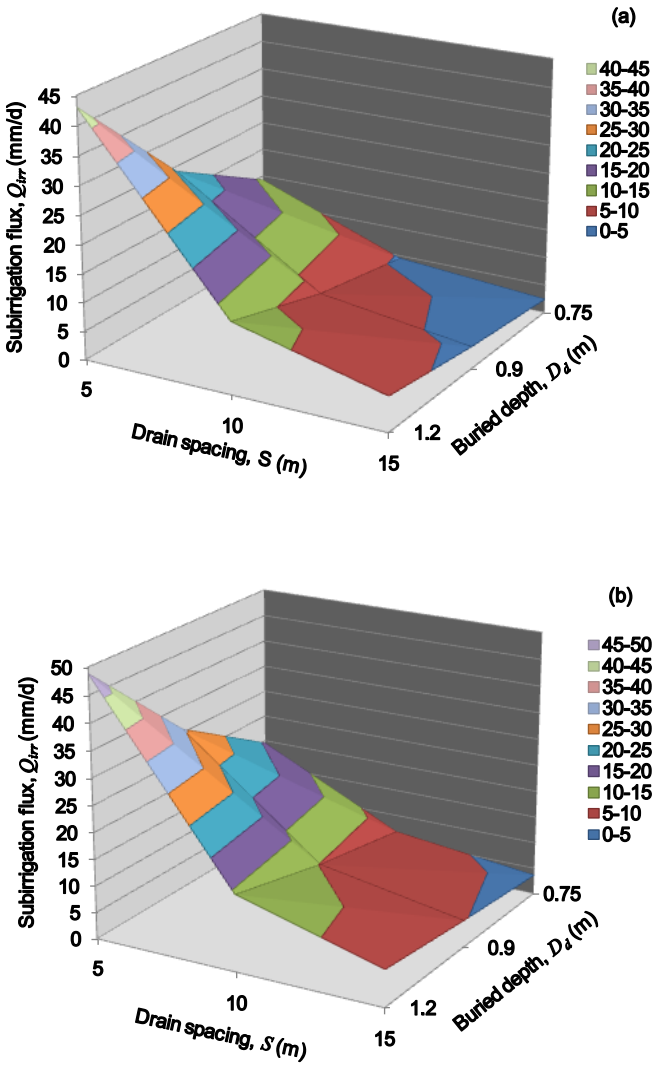

Fig. 6. 9. Soil-water fluxes (Q_{irr}) for variable lateral drain spacings (S) and buried depths (D_d) in a Loamy Sand (SM): (a) α_{x1} (sparsely perforated pipe) and (b) α_{x2} (densely perforated pipe).

Notably, the results indicate that the soil-water flux from pipes with a lateral spacing of 15 m and buried depth of more than 1.0 m in an SM soil will adequately satisfy the water demand for most cereal or grain crops (6 mm/day) across humid regions in North America (Huffman et al., 2013). Fluxes greater than 5 mm/day in a ML soil can be achieved with a closer drain spacing (less than 9 m) and buried depths of at least 1.2 m. In comparison, soil-water fluxes were considerably smaller for the CH soil (Fig. 6.11), falling below 2.1 mm/day even when the laterals were spaced 5 m apart. Smaller soil-water fluxes below irrigation requirements

can induce drought stress in crops, resulting in reduced yields (Ihuoma and Madramootoo, 2019; Singh and Nelson, 2021).

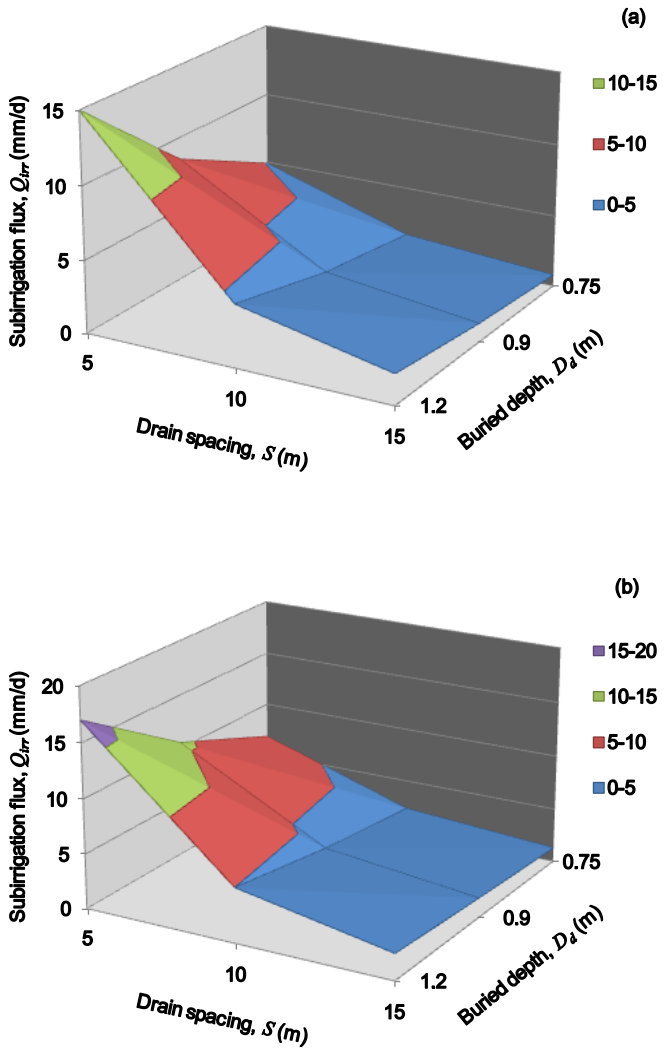

Fig. 6. 10. Soil-water fluxes (Q_{irr}) for variable lateral drain spacings (S) and buried depths (D_d) in a Silt Loam (ML): (a) α_{x1} (sparsely perforated pipe) and (b) α_{x2} (densely perforated pipe).

For the SC soils, negligible soil-water fluxes (less than 1.0 mm/day) were computed for all values of S and D_d (not presented). These findings for steady-state fluxes from buried pipes operated in irrigation mode are also consistent with the transient water table response in fine-textured soils (CH and SC). Consequently, the variability in soil-water fluxes among the soil textures can be explained by differences in k_{sat}.

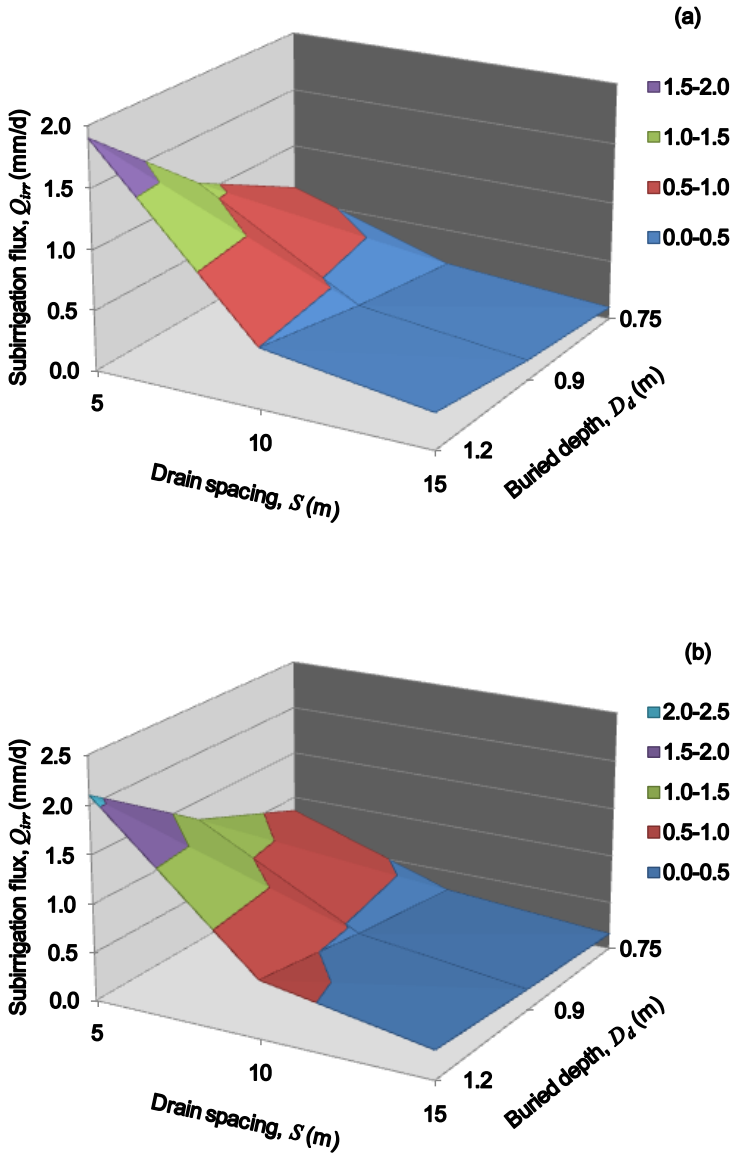

Fig. 6. 11. Soil-water fluxes (Q_{irr}) for variable lateral drain spacings (S) and buried depths (D_d) in a Clay (CH): (a) α_{x1} (sparsely perforated pipe) and (b) α_{x2} (densely perforated pipe).

The effect of perforations on soil-water fluxes for varying drain spacing and buried depth is less perceptible in Figs. 6.9-6.11. The general trend shows an increase in Q_{irr} as α_x decreases. For the coarse-textured SM soils, the fluxes between α_{x1} (sparsely perforated pipe) and α_{x2} (densely perforated pipe) increase by an average of 14% when D_d = 1.2 m. This marginal increase in soil-water flux occurs as the exit resistance of the buried perforated pipe decreases by approximately 59% when D_d = 1.2 m.

The exit resistance under steady-state conditions also changes with D_d when the water level in the control chamber (Fig. 6.1) is constant (section 6.4.1.2). At a shallower buried depth of 0.75 m, the decrease between α_{x1} and α_{x2} is 66%, but the corresponding average increase in Q_{irr} is 45% for SM soils. This sharper increase in soil-water flux is due to a smaller radial divergence near the pipe as the distance from the buried supply pipe to the impermeable layer increases. The same effect is present for the ML soils, where Q_{irr} increases by 15 and 48% due to an increased perforation density for pipes with a buried depth of 1.2 and 0.75 m, respectively.

The soil-water fluxes computed for the fine-textured SC and CH soils are also virtually unaffected by the perforations, but this is most likely as a result of the extremely small magnitude of the fluxes. These results indicate that the soil's hydraulic conductivity, lateral drain spacing, and buried depth have a larger impact on Q_{irr} compared to the pipe's perforation density, which was represented by its exit resistance in the steady-state analysis.

6.4.2.2 Exit head losses

The exit head loss (H_x) can be used to better demonstrate the effects of variable perforations in a subsurface irrigation system operated under steady-state conditions. For simplicity, H_x was computed using Eq. (6.10) for the case when D_d = 1.2 m and Q_{irr} was fixed at 6 mm/day to simulate practical field conditions where the subsurface irrigation system can supply the water demand for cereal and grain crops cultivated in humid regions. The optimum lateral drain spacings required to maintain the steady-state soil-water flux were also computed for each of the four soil textures.

The results presented in Table 6.4 show that H_x for sparsely perforated pipes (α_{x1}) are more than 50% larger than those for densely perforated pipes (α_{x2}). Interestingly, Prasher et al. (1989) reported an exit head loss of 3.67 cm for a corrugated pipe in a sandy soil, which

corresponds to the value reported in Table 6.4 for SM soils and α_{x2}. The pipe used by Prasher et al. (1989) in their sand tank experiments was also densely perforated, having 12 lines of slots in every corrugation valley. These results show that increasing the perforation density on the pipe wall, through N and a_y, are the most effective way to reduce the exit head losses in subsurface irrigation systems.

Table 6.4. Exit head loss (H_x) and optimum lateral spacing (S) for variable perforation

Soil Texture	α_{x1} = 0.8856 (sparsely perforated)		α_{x2} = 0.3664 (densely perforated)	
	H_x (cm)	S (m)	H_x (cm)	S (m)
SM	8.1	15.1	3.6	16.2
SC	44.9	1.8	19.4	1.9
ML	12.8	8.3	5.7	9.0
CH	32.5	2.6	14.2	2.8

Table 6.4 also indicates that the texture of the surrounding soil, as distinguished by its hydraulic conductivity, has a large impact on the exit losses. Larger values of H_x are reported for the fine-grained SC and CH textures. The exit loss can be as large as 19 cm for densely perforated corrugated pipes buried in SC soils. Considering that an optimum spacing of 1.9 m in SC soils would be uneconomical, increasing the water level in the control chamber by 19 cm may incur additional operating costs for subsurface irrigation systems. On the other hand, the head losses due to the perforations may be more manageable in coarse-grained soils, whereby increasing the number of perforations can keep exit losses below 6 cm (SM and ML soils). Ultimately, these results illustrate how the exit head losses can be estimated for variable perforation characteristics, and then incorporated into the analysis and design of buried pipes for subsurface irrigation. Compensation for the head losses can be made through adjustments to the water level in control chambers (Fig. 6.1) during the operation of the subsurface irrigation systems.

6.4.3 Soil-water flux in layered soils

The simulated flow rates exiting the perforated corrugated pipe were used to compare soil-water fluxes between the two-layer heterogeneous and equivalent one-layer homogeneous subsurface irrigation systems. This comparison served as a verification on the accuracy of using the weighted average one-layer $k_{sat\text{-}a}$ to represent field conditions with layered soils. The result for the SM/SC combination is shown in Fig. 6.12, which indicates that Q_{irr} (homogeneous) is underestimated across varying perforation and ΔH combinations. The same trend holds for the other four layer combinations with a $CR_{ks} > 1$ (Table 6.3). The mean percent error between the two soil-water fluxes was largest (19.4%) for the SM/SC arrangement and smallest (8.2%) for the CH/SC arrangement.

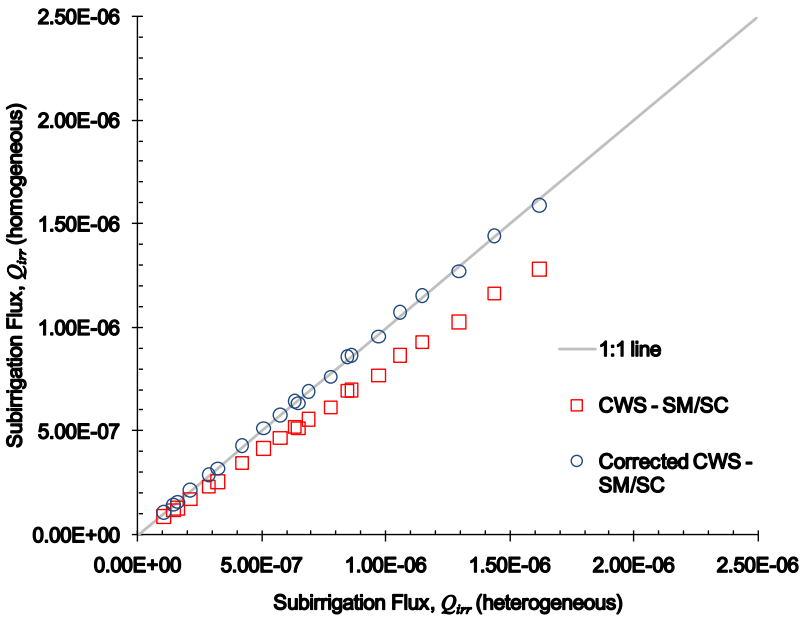

Fig. 6. 12. Comparison of Q_{irr} in a loamy sand on sandy clay (SM/SC) two-layer subsurface irrigation system.

The discrepancy between the two fluxes indicates that the weighted conductivity computed for the homogeneous layer needs a correction in order to reconcile the difference in Q_{irr}. The correction to $k_{sat\text{-}a}$ is warranted since the weighted mean assumes that the flow direction is parallel to the layer, while the flow exiting the perforated pipe is primarily upward and radial

in region close to the pipe (Fig. 6.2). The correction factor (F_{corr}) for $k_{sat\text{-}a}$ was computed as Q_{irr} (heterogeneous)/Q_{irr} (homogeneous), and is presented in Fig. 6.13 as a function of the conductivity ratio (CR_{ks}). The appropriate correction to $k_{sat\text{-}a}$ was applied for the SM/SC equivalent one-layer homogeneous case, and the simulations were updated in order to re-compute the soil-water fluxes. The corrected Q_{irr} (homogeneous) values were also plotted in Fig. 6.12, which shows a much better agreement with the soil-water fluxes for the heterogeneous system (percent error less than 1%). It is important to note that correcting the weighted conductivity for the two-layer system does not affect the pipe's exit resistance under subsurface irrigation, because this parameter is independent of k_{sat} (Gaj and Madramootoo, 2021).

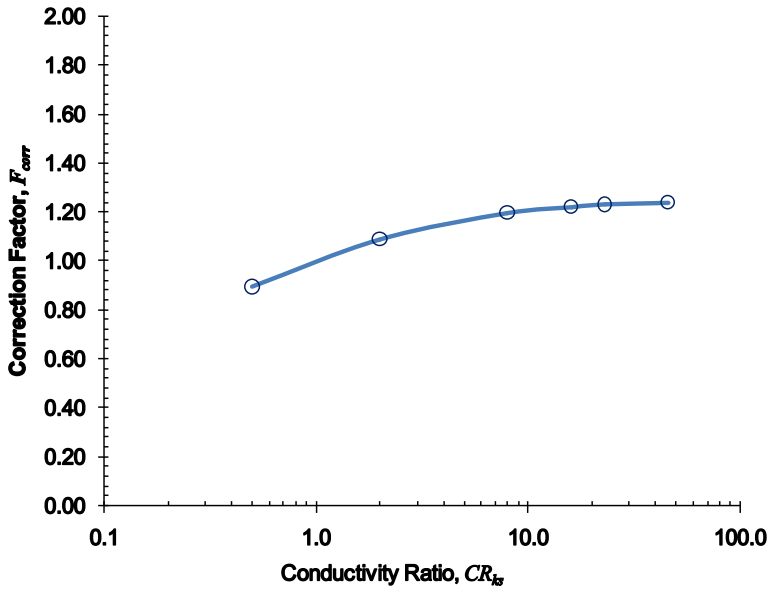

Fig. 6. 13. Correction factor for the weighted $k_{sat\text{-}a}$ as a function of conductivity ratio.

Fig. 6.13 also shows that F_{corr} is highly non-linear, since the plotted data points fit a smooth curve on a semi-log scale, and gradually increases as the conductivity ratio between two layers increase. While F_{corr} can be determined graphically from Fig. 6.13, two functions were fitted to the curve in order to establish a predictive relationship with CR_{ks}

$$F_{corr} = 0.109 \ln(CR_{ks}) + 0.983 \;\; ; \;\; CR_{ks} \leq 10 \tag{6.12}$$

$$F_{corr} = 0.016 \ln(CR_{ks}) + 1.176 \;\; ; \;\; CR_{ks} \geq 10 \tag{6.13}$$

where CR_{ks} = 10 was used as the break-point between the two functions based on the change in slope in Fig. 6.13. The goodness-of-fit as measured by the coefficient of determination (R^2) are 97.1% and 98.9% for the relationships given by Eqs. (6.12) and (6.13), respectively. A limiting value of 1.24 can be used for conductivity ratios exceeding 50. On the other hand, the lower limit of 0.9 appears to be practical for two-layer systems where the conductivity ratio is less than 1.0. Such cases arise in field conditions when the bottom layer has a larger conductivity than the top layer, e.g. SC/CH or heavy clays overlying a sandy layer.

Practitioners can use Eq. (6.12) and (6.13) to compute F_{corr} and increase the weighted hydraulic conductivity of heterogeneous soil layers computed with Eq. (6.11). The corrected $k_{sat\text{-}a}$ can then be used to compute lateral drain spacings under steady-state conditions or to simulate the water table rise in the unsaturated zone under transient conditions for subsurface irrigation systems in layered soils. The effects from rectangular slots with variable characteristics can now also be fully integrated into both steady-state and transient analysis of buried corrugated pipes used in subsurface irrigation systems.

6.5 Summary and Conclusions

The transient water table rise into the unsaturated zone was simulated for four soil textures, three lateral drain spacings, and three buried depths in order to demonstrate the effects from variable perforation characteristics in a typical subsurface irrigation system. Soil-water fluxes and exit head losses were also computed for the system operated under steady-state conditions. Finally, a numerical model was used to simulate subirrigation fluxes from buried perforated pipes in various combinations of heterogeneous two-layer soil systems and

compared with their homogeneous one-layer equivalent typically used in drain spacing equations.

The results show that the simulated water table can reach a target level of 1.65 m above the buried pipe at lateral drain spacings as large as 10 m in coarse-textured soils such as loamy sand and silt loams (SM and ML). The water table rises at a faster rate into the unsaturated zone from the buried pipes with a larger perforation density. Increasing both the number and length of rectangular slots on the pipe wall can reduce the response time to reach the target level by 15 hours in a ML soil and up to 25 hrs in a clay soil (CH). Generally, the response time increases as the buried depth of the supply pipes decreases.

Computations for buried perforated pipes under steady-state conditions showed that soil-water fluxes in SM soils can meet the typically specified crop water demand for cereal or grain crops of 6 mm/day in Eastern Canada and mid-west US. Fluxes were considerably smaller (less than 2.1 mm/day) for the fine-textured sandy clay (SC) and CH soils, even for closely buried pipes (5 m apart). The results also showed that increasing the size and number of perforations can reduce the exit head loss by more than 50%. However, exit losses as large as 19 cm were computed for pipes buried in SC soils due to their relatively small hydraulic conductivity.

Numerical simulations indicated the subsurface irrigation fluxes in an equivalent one-layer soil system are consistently underestimated when the conductivity ratio of the two-layer system is greater than one. A correction factor (F_{corr}) should be applied to the weighted average conductivity of the two-layer system in order to reconcile the soil-water fluxes from perforated pipes located at the layer interface.

Although soil texture and drain spacing are major factors affecting the water movement in subsurface irrigation systems, the size and number of perforations on buried pipes were

shown to have an impact on the water table response and soil-water flux. This study has demonstrated that variable perforation characteristics can be included in the analysis and design of agricultural water management systems to consider the transient water table rise into the unsaturated zone or to estimate the lateral drain spacing under steady state conditions. Water requirements for subsurface irrigation can therefore be optimized with these improvements through better control of automated water table triggers.

6.6 Acknowledgements

This research was funded by the Natural Science and Engineering Research Council of Canada (NSERC) and the James McGill Professor research award held by C.A. Madramootoo.

6.7 References

Amoozegar, A., & Wilson, G. N. (1999). Methods for Measuring Hydraulic Conductivity and Drainable Porosity. In R. W. Skaggs & J. van Schilfgaarde (Eds.), *Agricultural Drainage* (Vol. 38, pp. 1149-1205). Wisconsin, USA: Madison Publishers.

Childs, E. C., & Youngs, E. G. (1958). The Nature of the Drain Channel as a Factor in the Design of a Land-Drainage System. *Journal of Soil Science, 9*(2), 316-331. doi: 10.1111/j.1365-2389.1958.tb01923.x

COMSOL Multiphysics. (2017a). COMSOL Multiphysics v. 5.3a Reference Manual. Stockholm, Sweden: COMSOL AB, www.comsol.com.

COMSOL Multiphysics. (2017b). COMSOL Multiphysics v. 5.3a: Subsurface Flow Module - User's Guide. Stockholm, Sweden: COMSOL AB. www.comsol.com.

Cordeiro, M. R., & Sri Ranjan, R. (2012). Corn Yield Response to Drainage and Subirrigation in the Canadian Prairies. *Transactions of the ASABE, 55*(5), 1771-1780.

Davenport, M. S., & Skaggs, R. W. (1990). Effects of Drain Envelope and Slope on Performance of a Drainage-Subirrigation System. *Transactions of the ASAE, 33*(2), 493-0500. doi: https://doi.org/10.13031/2013.31356

Dierickx, W. (1999). Non-Ideal Drains. In R. W. Skaggs & J. van Schilfgaarde (Eds.), Agricultural Drainage (Vol. 38, pp. 297-330). Wisconsin, USA: Madison Publishers.

Ernst, L. F. (1975). Formulae for groundwater flow in areas with subirrigation by means of open conduits with a raised water level (pp. 33). Wageningen, The Netherlands: Institute for Land and Water Management Research.

Evans, R. O., & Skaggs, R. W. (1996). Operating Controlled Drainage and Subirrigation Systems. NC: North Carolina State University.

Fouss, J. L., Evans, R. O., Thomas, D. L., & Belcher, H. W. (1999). Operation of Controlled-Drainage and Subirrigation Facilities for Water Table Management. In R. W. Skaggs & J. Van Schilfgaarde (Eds.), *Agricultural Drainage* (Vol. 38, pp. 743-763). Wisconsin, USA: Madison Pubilsers.

Gaj, N., & Madramootoo, C. A. (2020). Effects of Perforation Geometry on Pipe Drainage in Agricultural Lands. *Journal of Irrigation & Drainage Engineering, 146*(7), 12. doi: 10.1061/(ASCE)IR.1943-4774.0001482.

Gaj, N., & Madramootoo, C. A. (2021). Simulating upward soil-water flow from buried pipes with variable hydraulic characteristics. *Manuscript to be submitted*.

Garcia-Gaines, R. A., & Frankenstein, S. (2015). USCS and the USDA Soil Classification System: Development of a Mapping Scheme (pp. 46). Hanover, NH: US Army Engineer Research and Develpoment Center (ERDC).

Gunn, K. M., Baule, W. J., Frankenberger, J. R., Gamble, D. L., Allred, B. J., Andresen, J. A., & Brown, L. C. (2016). *Corn yield under subirrigation and future climate scenarios in the Maumee River Basin.* Paper presented at the 2016 10th International

Drainage Symposium Conference, 6-9 September 2016, Minneapolis, Minnesota, St. Joseph, MI.

Huffman, R. L., Fangmeier, D. D., Elliot, W. J., & Workman, S. R. (2013). Water Table Management. *In Soil and Water Conservation Engineering* (7th ed., pp. 321-349). St. Joseph, Michigan: Amercan Society of Agricultural and Biological Engineers (ASABE). doi:10.13031/swce.2013.14.

Ihuoma, S. O., & Madramootoo, C. A. (2019). Sensitivity of spectral vegetation indices for monitoring water stress in tomato plants. *Computers and Electronics in Agriculture, 163*, 104860. doi: https://doi.org/10.1016/j.compag.2019.104860

Madramootoo, C. A. (1999). Planning and Design of Drainage Systems. In R. W. Skaggs & J. van Schilfgaarde (Eds.), *Agricultural Drainage* (Vol. 38, pp. 871-892). Wisconsin, USA: Madison Publishers.

Marmanilo, M. M., Kulshreshtha, S. N., & Madramootoo, C. A. (2021). Economic analysis of the controlled drainage with sub-irrigation system: a case study of grain-producing farms in Quebec and Ontario. *Canadian Water Resources Journal*. doi: https://doi.org/10.1080/07011784.2021.1874537

McWhorter, D. B., & Marinelli, F. (1999). Theory of Soil-Water Flow. In R. W. Skaggs & J. van Schilfgaarde (Eds.), *Agricultural Drainage* (Vol. 38, pp. 111-143). Wisconsin, USA: Madison Publishers.

Moody, W. T. (1966). Nonlinear Differential Equation of Drain Spacing. *Journal of the Irrigation and Drainage Division, 92*(2), 1-10.

Nieber, J. L., & Feddes, R. A. (1999). Solutions for Combined Saturated and Unsaturated Flow. In R. W. Skaggs & J. van Schilfgaarde (Eds.), *Agricultural Drainage* (Vol. 38, pp. 145-212). Wisconsin, USA: Madison Publishers.

Rawls, W. J., Gimenez, D., & Grossman, R. (1998). Use of Soil Texture, Bulk Density, and Slope of the Water Retention Curve to Predict Saturated Hydraulic Conductivity. *Transactions of the ASAE, 41*(4), 983-988.

Singh, G., & Nelson, K. A. (2021). Long-term drainage, subirrigation, and tile spacing effects on maize production. *Field Crops Res., 262*, 108032.

Skaggs, R. W. (1973). Water Table Movement During Subirrigation. *Transactions of the ASAE, 16*(5), 988-0993. doi: https://doi.org/10.13031/2013.37678

Skaggs, R. W. (1981). Water Movement Factors Important to the Design and Operation of Subirrigation Systems. *Transactions of the ASAE, 24*(6), 1553-1561. doi: https://doi.org/10.13031/2013.34489

Skaggs, R. W. (1991). Modeling Water Table Response to Subirrigation and Drainage. *Transactions of the ASAE, 34*(1), 169-0175. doi: https://doi.org/10.13031/2013.31640

Skaggs, R. W. (1999). Water Table Management: Subirrigation and Control Drainage. In R. Skaggs & J. van Schilfgaarde (Eds.), *Agricultural Drainage* (Vol. 38, pp. 695-718). Wisconsin, USA: Madison Publishers.

Skaggs, R. W., & Tang, Y. K. (1976). Saturated and Unsaturated Flow to Parallel Drains. *Journal of the Irrigation and Drainage Division, 102*(IR2), 221-238.

Smith, M. C., Skaggs, R. W., & Parsons, J. E. (1985). Subirrigation System Control for Water use Efficiency. *Transactions of the ASAE, 28*(2), 489-0496. doi: https://doi.org/10.13031/2013.32284

Stuyt, L. C. P. M., Dierickx, W., & Beltran, J. M. (2005). *Materials for subsurface land drainage systems*. FAO Irrigation and Drainage Paper 60. Rome, Italy.

Tang, Y. K., & Skaggs, R. W. (1977). Experimental evaluation of theoretical solutions for subsurface drainage and irrigation. *Water Resources Research, 13*(6), 957-965. doi: 10.1029/WR013i006p00957

Tang, Y. K., & Skaggs, R. W. (1980). Drain Depth and Subirrigation in Layered Soils. *Journal of the Irrigation and Drainage Division, 106*(2), 113-121.

Yu, F., Frankenberger, J. R., Ackerson, J., & Reinhart, B. (2020). Potential Suitability of Subirrigation for Field Crops in the US Midwest. *Transactions of the ASABE, 63*(5), 1559-1570.

Chapter 7

Summary and Conclusions

7.1 General summary

Buried corrugated pipes used in water management systems have perforations on the pipe wall to allow for water entry or exit. However, variable perforation characteristics such as shape, size, and configuration have not been fully incorporated into the hydraulic and structural design of these corrugated pipes. This is because: 1) the hydraulic entrance resistance of corrugated pipes perforated with circular holes has not been established, 2) the stress concentration around circular holes and rectangular slots in corrugated pipes is unknown, 3) the hydraulic exit resistance due to variable perforation characteristics has not been studied for corrugated pipes under subsurface irrigation conditions, and 4) the transient water table response and soil-water fluxes from subsurface irrigation pipes has not been adequately investigated for varying perforation design parameters. Specifying incorrect perforation characteristics can result in extended waterlogged conditions during drainage, considerably slower water table rise during subsurface irrigation, and/or excessive stress concentrations near perforations in the pipe wall, increasing the risk of failure by ductile yielding. This thesis investigated the effects of perforation shape, size, and configuration on the hydraulic and structural responses of corrugated high-density polyethylene (HDPE) pipes under conditions specific to agricultural fields.

7.1.1 Effect of Perforation Geometry on Drainage

The first study (Chapter 3) investigated the effect of pipe perforation characteristics under drainage conditions using a three-dimensional (3D) finite-element-based numerical model of the radial flow region around buried pipes, calibrated with datasets from sand tank experiments, to simulate the entrance resistance (α_e) and delivery ratio (Q/Q_0) for perforated

pipes. The effects of two perforation shapes (circular holes and rectangular slots) on lateral drain spacing and water table drawdown for buried corrugated pipes were also studied. In general, the configuration of perforations on the pipe wall had the largest effect on α_e, compared to the perforation size (diameter of holes or length of slots). Corrugated pipes with circular holes had a larger entrance resistance than plain wall pipes with the same perforation characteristics, which demonstrated the effect of the pipe wall profile on α_e. It was also shown that the entrance resistance of corrugated pipes with holes was twice as large as the resistance for corrugated pipes with slots. Computations showed that the difference in water table drawdown between corrugated pipes perforated with slots and holes was not significantly different, which indicated that larger holes were not any better at increasing subsurface drainage flow. Overall, rectangular slots were found to increase the performance of buried corrugated pipes under drainage conditions.

7.1.2 Structural Response of Buried Corrugated Pipes

For the second study (Chapter 4), a finite-element-based structural mechanics model of HDPE pipes with an annular corrugation profile was used to simulate the wall stress and vertical deflection under frictional (smooth and bonded) boundary loads from 12 agricultural soil textures, two water table positions, and three agri-machinery wheel loads. In addition, the impact of perforation characteristics on local stress concentrations and deformation of corrugated HDPE pipes were studied. Of the three main types of design loads (soil texture, water table height, agri-machinery), imposed live loads from agri-machinery induced the largest structural response (stress and deformation) of corrugated HDPE pipes. The bonded friction condition at the soil-pipe interface usually resulted in greater pipe wall stresses compared to the smooth friction condition, especially for corrugated pipes buried in a sandy clay loam soil. Shallow burial depths (<0.9 m) can increase the risk of material failure by ductile yielding for corrugated pipes with circular holes.

In contrast to the hydraulic response under drainage conditions, the perforation configuration (axial and circumferential spacings) did not affect the stress distribution in the pipe wall, since there were no discernable stress interactions between perforations. A comparison of the two perforation shapes showed that rectangular slots had a lower risk of failure against ductile yielding compared to circular holes, provided that the slot width is less than half of the corrugation valley width. These findings demonstrated the importance of incorporating perforations into the structural analysis and design of buried corrugated HDPE pipes for land drainage.

7.1.3 Exit Resistance of Perforated Subsurface Irrigation Pipes

The third study (Chapter 5) tested the hypothesis that the exit resistance (α_x) of perforated corrugated pipes operated under subsurface irrigation mode is larger than the entrance resistance of the same pipes when operated under drainage mode. The radial flow drainage model developed in Chapter 3 was modified to simulate upward soil-water flow under varying pressure heads on perforated pipes in a subsurface irrigation system. The findings proved the hypothesis correct, indicating that the exit resistance is larger and statistically different than the entrance resistance.

The effects of variable perforation characteristics on α_x were then investigated and non-linear prediction equations were developed as a function of the difference in hydraulic head between the surrounding water table and water level in the control chamber of the subsurface irrigation system. The results showed that the configuration of rectangular slots on the pipe wall has the largest impact on α_x. Pipes with slots in every corrugation valley (a_y = 1.645 cm) will provide the least resistance compared to those with larger longitudinal spacings.

7.1.4 Water table response and fluxes under Subsurface Irrigation Pipes

Chapter 6 of this thesis used the hydraulic exit resistance relationships developed in Chapter 5 as an input to simulate the transient water table response and steady soil-water fluxes from buried pipes with two combinations of perforation characteristics. Design parameters from variable soil textures, lateral drain spacing, and buried pipe depths were used in the simulations to study the effects of increasing the number and length of rectangular slots on the hydraulic response under subsurface irrigation mode. The impact of heterogeneity from layered soils on the soil-water fluxes was also investigated.

The results from the transient analyses demonstrated that while soil texture and lateral drain spacing are the primary factors governing water table rise into the unsaturated zone, the size and configuration of perforations on the supply pipe can play an important role in reducing response times for subsurface irrigation systems. Computations for buried perforated pipes under steady-state conditions showed that the optimum drain spacing needed to maintain a soil-water flux of 6mm/day can be increased in coarse-grained soils (loamy sand and silt loam) by using densely perforated pipes. On the other hand, increasing perforations on buried pipes in fine-grained soils (clays and sandy clays) will have less of an impact on drain spacing increases because of their inherent lower hydraulic conductivity. Overall, this study demonstrated that variable perforation characteristics can be included in the analysis and design of subsurface drainage systems for improving water management.

7.2 Contributions to knowledge

Based on the objectives and findings of this thesis, the contributions to knowledge are as follows:

1. This thesis demonstrated for the first time that rectangular slots were hydraulically more advantageous than circular holes for improving drainage performance of water

management systems with buried corrugated pipes. Manufacturers and practitioners can use the non-linear predictive relationships developed to incorporate variable perforation characteristics into subsurface drainage design.

2. This research proposed a new way of incorporating perforations into the structural analysis and design of buried corrugated HDPE pipes. Incorporating shape, dimension, and configuration of the perforations allowed for an improved appraisal of the pipe's structural performance.
3. This study proposed a new dimensionless parameter to compute the hydraulic exit resistance of buried corrugated pipes with variable perforation characteristics when operated under the subsurface irrigation mode. Water managers can use exit head losses to set better target water levels in control chambers in aid of water conservation.
4. This thesis demonstrated that the size and configuration of perforations on subsurface irrigation pipes can play an important role in reducing the response time for water table rise into the unsaturated zone. Manufacturers, land owners, and crop producers can improve the design and operation of subsurface irrigation systems through the integration of this parameter into water management simulation models.

7.3 Recommendations for future research

1. This study investigated buried corrugated pipes operated under drainage and subsurface irrigation modes. Future studies should incorporate thin synthetic envelopes around perforated corrugated pipes under subsurface irrigation conditions to assess its effect on exit resistance using finite-element-based numerical approaches.
2. Future research should measure the strain and deflection of smaller diameter (<150-mm) single-wall corrugated pipes with variable perforation characteristics embedded

in agricultural soils, to provide further validation of the structural response using numerical approaches.

3. Complexity can be added to porous media flow-based numerical models in order to incorporate three-dimensional unsaturated-saturated flows in the radial zone around perforated corrugated pipes under subsurface irrigation conditions.